U.S. Department
of Transportation
Federal Railroad
Administration

Office of Research,
Development and Technology
Washington, DC 20590

A Feasibility Study on Advanced Nondestructive Evaluation (NDE) Methods to Characterize Weld Defects in Railroad Tank Cars

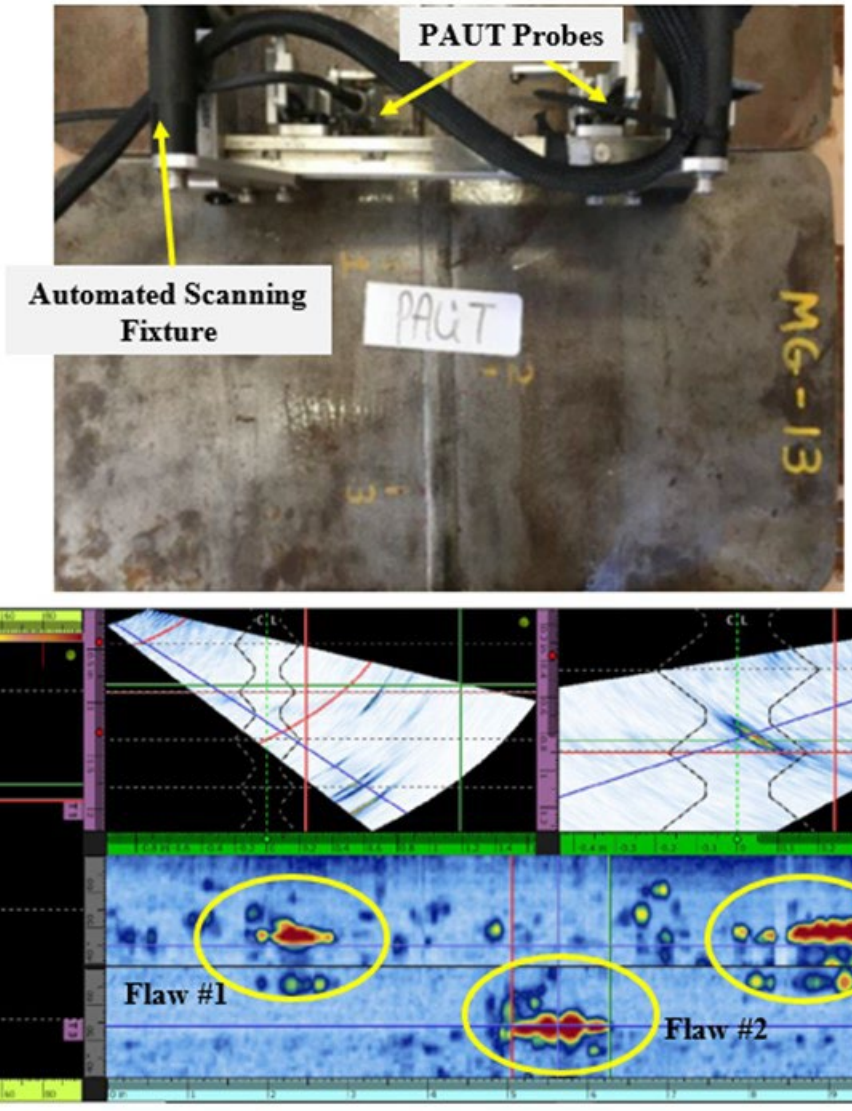

DOT/FRA/ORD-23/02

Final Report | January 2023

REPORT DOCUMENTATION PAGE

Form Approved
OMB No. 0704-0188

1. REPORT DATE *(DD-MM-YYYY*	2. REPORT TYPE	3. DATES COVERED *(From - To)*
01/06/2023	Technical Report	10/01/2018 – 07/30/2022

4. TITLE AND SUBTITLE
A Feasibility Study on Advanced Nondestructive Evaluation (NDE) Methods to Characterize Weld Defects in Railroad Tank Cars

5a. CONTRACT NUMBER
DTFR53-11-D-00008L

5b. GRANT NUMBER

5c. PROGRAM ELEMENT NUMBER

6. AUTHOR(S)
Anish Poudel – 0000-0002-5811-4284
Brian Lindeman – 0000-0003-3903-266X
Survesh Shrestha – 0000-0002-2070-748X
Kenny Morrison – 0000-0003-1382-4175

5d. PROJECT NUMBER

5e. TASK NUMBER
693JJ618F000067

5f. WORK UNIT NUMBER

7. PERFORMING ORGANIZATION NAME(S) AND ADDRESS(ES)
Transportation Technology Center, Inc.
55500 DOT Road
PO BOX 11130
Pueblo, CO 81001-0130

8. PERFORMING ORGANIZATION REPORT NUMBER

9. SPONSORING/MONITORING AGENCY NAME(S) AND ADDRESS(ES)
U.S. Department of Transportation
Federal Railroad Administration
Office of Railroad Policy and Development
Office of Research, Development, and Technology (RD&T)
Washington, DC 20590

10. SPONSOR/MONITOR'S ACRONYM(S)

11. SPONSOR/MONITOR'S REPORT NUMBER(S)
DOT/FRA/ORD-23/02

12. DISTRIBUTION/AVAILABILITY STATEMENT
This document is available to the public through the FRA web site at http://www.fra.dot.gov

13. SUPPLEMENTARY NOTES
COR: Francisco González, III

14. ABSTRACT
Under the sponsorship and support of the Federal Railroad Administration (FRA), Transportation Technology Center, Inc. (TTCI), with participation from the original equipment manufacturer (OEM) of advanced nondestructive evaluation (NDE) equipment, NDE service providers, and other research institutions, conducted a feasibility study of applying advanced NDE methods to detect and characterize weld defects in railroad tank cars. Researchers evaluated the performance/capability of various state-of-the-art advanced NDE techniques for fatigue crack detection and characterization in railroad tank car butt welds and fillet welds. The team determined that advanced NDE methods could detect toe fatigue cracks with acceptable signal-to-noise ratio (SNR) while demonstrating challenges with accurate flaw sizing. Further, based on the false positive results obtained from this study, the team found that detailed attention and efforts are required to reduce the false positive rate.

15. SUBJECT TERMS
Code of federal regulation (CFR), Railroad tank cars, DOT-111, DOT-117, butt weld, fillet weld, weld defect, fatigue cracks, nondestructive evaluation/testing (NDE/NDT), visual testing (VT), liquid penetrant testing (PT), magnetic particle testing (MT), ultrasonic testing (UT), phased array UT (PAUT), full matrix capture (FMC), total focusing method (TFM), alternating current field measurement (ACFM), tangential eddy current array (TECA), pulsed eddy current infrared thermography (PECT), probability of hits (POH).

16. SECURITY CLASSIFICATION OF:			17. LIMITATION OF ABSTRACT	18. NUMBER OF PAGES	19a. NAME OF RESPONSIBLE PERSON
a. REPORT	b. ABSTRACT	c. THIS PAGE			Anish Poudel, Principal Investigator II - NDE
Unclassified	Unclassified	Unclassified		160	19b. TELEPHONE NUMBER *(Include area code)* +1 719-696-1848

Standard Form 298 (Rev. 8/98)
Prescribed by ANSI Std. Z39.18

METRIC/ENGLISH CONVERSION FACTORS

ENGLISH TO METRIC

LENGTH (APPROXIMATE)

1 inch (in)	=	2.5 centimeters (cm)
1 foot (ft)	=	30 centimeters (cm)
1 yard (yd)	=	0.9 meter (m)
1 mile (mi)	=	1.6 kilometers (km)

AREA (APPROXIMATE)

1 square inch (sq in, in^2)	=	6.5 square centimeters (cm^2)
1 square foot (sq ft, ft^2)	=	0.09 square meter (m^2)
1 square yard (sq yd, yd^2)	=	0.8 square meter (m^2)
1 square mile (sq mi, mi^2)	=	2.6 square kilometers (km^2)
1 acre = 0.4 hectare (he)	=	4,000 square meters (m^2)

MASS - WEIGHT (APPROXIMATE)

1 ounce (oz)	=	28 grams (gm)
1 pound (lb)	=	0.45 kilogram (kg)
1 short ton = 2,000 pounds (lb)	=	0.9 tonne (t)

VOLUME (APPROXIMATE)

1 teaspoon (tsp)	=	5 milliliters (ml)
1 tablespoon (tbsp)	=	15 milliliters (ml)
1 fluid ounce (fl oz)	=	30 milliliters (ml)
1 cup (c)	=	0.24 liter (l)
1 pint (pt)	=	0.47 liter (l)
1 quart (qt)	=	0.96 liter (l)
1 gallon (gal)	=	3.8 liters (l)
1 cubic foot (cu ft, ft^3)	=	0.03 cubic meter (m^3)
1 cubic yard (cu yd, yd^3)	=	0.76 cubic meter (m^3)

TEMPERATURE (EXACT)

[(x-32)(5/9)] °F = y °C

METRIC TO ENGLISH

LENGTH (APPROXIMATE)

1 millimeter (mm)	=	0.04 inch (in)
1 centimeter (cm)	=	0.4 inch (in)
1 meter (m)	=	3.3 feet (ft)
1 meter (m)	=	1.1 yards (yd)
1 kilometer (km)	=	0.6 mile (mi)

AREA (APPROXIMATE)

1 square centimeter (cm^2)	=	0.16 square inch (sq in, in^2)
1 square meter (m^2)	=	1.2 square yards (sq yd, yd^2)
1 square kilometer (km^2)	=	0.4 square mile (sq mi, mi^2)
10,000 square meters (m^2)	=	1 hectare (ha) = 2.5 acres

MASS - WEIGHT (APPROXIMATE)

1 gram (gm)	=	0.036 ounce (oz)
1 kilogram (kg)	=	2.2 pounds (lb)
1 tonne (t)	=	1,000 kilograms (kg)
	=	1.1 short tons

VOLUME (APPROXIMATE)

1 milliliter (ml)	=	0.03 fluid ounce (fl oz)
1 liter (l)	=	2.1 pints (pt)
1 liter (l)	=	1.06 quarts (qt)
1 liter (l)	=	0.26 gallon (gal)
1 cubic meter (m^3)	=	36 cubic feet (cu ft, ft^3)
1 cubic meter (m^3)	=	1.3 cubic yards (cu yd, yd^3)

TEMPERATURE (EXACT)

[(9/5) y + 32] °C = x °F

QUICK INCH - CENTIMETER LENGTH CONVERSION

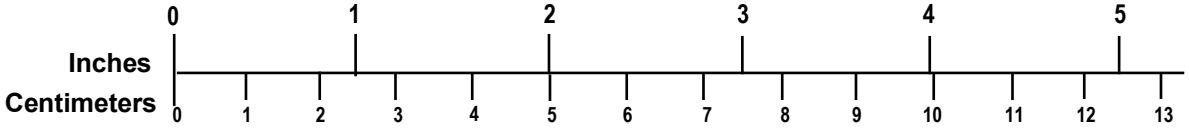

QUICK FAHRENHEIT - CELSIUS TEMPERATURE CONVERSIO

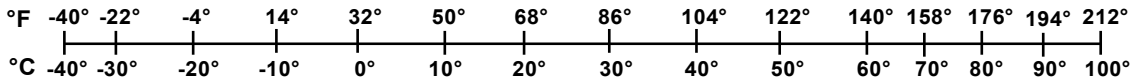

For more exact and or other conversion factors, see NIST Miscellaneous Publication 286, Units of Weights and Measures. Price $2.50 SD Catalog No. C13 10286

Updated 6/17/98

Acknowledgements

Transportation Technology Center, Inc. (TTCI) would like to thank the original equipment manufacturers (OEM) of NDE equipment, NDE service providers, and research institutions who supported this work.

Contents

Illustrations

Tables

Executive Summary

Under the sponsorship and support of the Federal Railroad Administration (FRA), Transportation Technology Center, Inc. (TTCI), with participation from the original equipment manufacturer (OEM) of advanced nondestructive evaluation (NDE) equipment, NDE service providers, and other research institutions, conducted a feasibility study of applying advanced NDE methods to detect and characterize weld defects in railroad tank cars.

Researchers evaluated the performance/capability of various state-of-the-art advanced NDE techniques for fatigue crack detection and characterization in railroad tank car butt welds and fillet welds. These techniques included phased array ultrasonic testing (PAUT), full matrix capture (FMC)/total focusing method (TFM), time of flight diffraction, eddy current testing (ET), tangential eddy current array, alternating current field measurements (ACFM), and pulsed eddy current thermography (PECT). A total of six participants took part in the study, including OEMs of NDE equipment, NDE service providers working with tank car industries, and representatives of other research institutions.

The team used master gauge (MG) test panels that were made from retired tank cars (DOT-111). These included four butt weld MG panels and four fillet weld MG panels. The material for these test panels was close to ASTM A515 grade 70 steel, and contained notches created using electrical discharge machining (EDM) process that simulated fatigue cracks of various sizes. Researchers artificially initiated the fatigue cracks (some tightly spaced closed fatigue cracks) at the toe of the butt welds and at the longitudinal termination of the fillet welds.

The team calculated the probability of correct hits (POH) for each NDE method used by each participant. The PECT method used by Participant F achieved the highest POH of 100 percent while Participant D's ACFM method achieved the lowest POH of 57 percent. It should be noted that during the first trial of PECT technology, the POH obtained was only around 33 percent with one false positive. The team later optimized the system based on the flaw information provided to achieve 100 percent POH. Six out of the 15 advanced NDE methods had an over 80 percent POH. Researchers determined the total false positives for the fillet weld to be 33 percent and the total false positives for the butt weld to be 19 percent. The crack with the highest false negatives was fatigue crack B from MGL-3; however, researchers could not establish a relationship between crack size and false negative. The team also observed differences in crack/notch sizing during the trial for all methods explored by each participant. The median crack/notch length difference for most of the NDE methods that returned crack/notch lengths was within ±0.14 inch. The PAUT and FMC/TFM methods (Participant A) had a median notch length difference outside ±0.14 inch; notably, the given notch lengths were all longer than the MG panel notch length. Overall, 92.3 percent of the notch lengths were equal to or within ±0.50 inch of the MG panel notch lengths. Two NDE methods, ET (Participant C) and PECT (Participant F), were able to score perfect results on a panel with six notches.

Researchers determined that advanced NDE methods could detect toe fatigue cracks with acceptable signal-to-noise ratio (SNR) while demonstrating challenges with accurate flaw sizing. Further, based on the false positive results obtained from this study, the team found that detailed attention and efforts are required to reduce the false positive rate.

Finally, researchers recommended a detailed study be conducted in future to fully understand the extensive capabilities and limitation of the advanced NDE methods explored. The team suggests

the new study use DOT-117 tank car plates, as this material is different than the legacy tank car DOT-111A material used in this study. A wide variety of weld configurations and geometry representative of the actual tank cars must also be considered. Future efforts should explore a robotic automated inspection of the tank car butt welds and longitudinal welds using crawler inspection robot technology designed to be used from the inner diameter of the tank. This will help improve personnel safety associated with confined space.

1. Introduction

In 1995, a rule issued by the Research and Special Programs Administration (RSPA) of the United States Department of Transportation (USDOT) revised federal hazardous materials regulations (HMRs). These revisions were made to improve the safe transportation of hazardous materials in railway tank cars by enhancing their crashworthiness and adopting a damage tolerance philosophy to increase the probability of detecting critical tank car defects. The revised rule, published in the Federal Register, Title 49, Code of Federal Regulation (CFR) Part 180.509, required all facilities that build, repair, and ensure the structural integrity of railway tank cars develop and implement a quality assurance program (QAP) and allow the use of nondestructive evaluation (NDE) techniques[1] in lieu of prescribed periodic hydrostatic pressure testing for fusion welded tank cars [1]. The primary reason for not considering the hydrostatic pressure test as an optimum way to qualify fusion welded tank cars for continued service was its inability to identify and characterize fatigue cracks caused by repeated loading conditions in the principal structural elements (PSE) located within four feet of the bottom longitudinal centerline tank car welds [2-4].

Title 49 CFR Part 179.7 requires all tank car facilities to have a QAP approved by the Association of American Railroads (AAR) and in compliance with AAR specification/ regulations [5, 6]. This includes procedures for quantitatively evaluating inspection and testing, including the accessibility of the area to be inspected, and the sensitivity of the CFR-approved NDE methods. These regulations adopted NDE methods to detect and characterize internal defects/anomalies in the railroad tank car welds consistently, repetitively, and quantitatively. The CFR currently authorizes the following NDE methods for tank car structural integrity inspections:

- Visual testing (VT)
- Liquid penetrant testing (PT)
- Magnetic particle testing (MT)
- Ultrasonic testing (UT)
- Radiographic Testing (RT)
- Acoustic Emissions (AE) (requires special waiver from FRA)

Transportation Technology Center, Inc. (TTCI), under the sponsorship of the Federal Railroad Administration (FRA) and with tank car industry support, conducted studies to analyze the capability of CFR-approved NDE methods and procedures to evaluate butt welds and fillet welds in railroad tank cars.

Results obtained from this research [4] demonstrated that, for the operators that participated in this research, the CFR-approved NDE methods were **NOT** capable of achieving or approaching a 90 percent probability of detection or data (POD) with 95 percent confidence (90/95 POD) for fatigue cracks in the butt weld test panels. Evaluation of the fillet welds data showed mixed

[1] The term NDE is used interchangeably with nondestructive testing (NDT) or nondestructive inspection (NDI).

results with only the MT method reaching 90/95 POD. Researchers observed multiple false positive calls in both butt weld and fillet weld inspection results.

Some of the existing CFR approved NDE methods have limitations. The VT method, which is relatively easy and quick to perform, is not reliable because it is heavily dependent on the operator's eye judgment. The PT method only works when the crack is open to the surface and usually requires the application of penetrants and developers. Other drawbacks to PT include the need for a high degree of smooth, clean surface and the difficulty in removing any excessive penetrant on rough surfaces (e.g., "as-welded" welds), which could result in false positives. The MT techniques have limitations based on the type of electrical current used. (For example, using alternating current (AC) to detect subsurface discontinuities with MT is limited due to the skin effect, where the current runs along the surface of the part, so direct current (DC) is typically used to detect subsurface discontinuities where AC cannot penetrate to magnetize the part at the depth needed; however, the DC approach is limited on very large cross-sectional parts in terms of how effectively it will magnetize the part.) Experience shows that the MT approach is difficult to apply in a complex geometry area (curvature) of the tank cars such as the area close to the front sill pad and head brace region. Traditional RT techniques are usually not possible to perform due to accessibility requirements. The RT method is also highly directional and sensitive to flaw orientation. Further, radiographic inspection can pose a health risk from radiation exposure. Finally, conducting conventional UT requires analysis of continuous signals for each point in the material under consideration. This is tedious and may lead to misinterpretation of data if not performed correctly. Such spurious indications, along with the misreading of signals, can result in unnecessary repairs.

Advanced, reliable, effective, and faster NDE methods are therefore needed to better detect fatigue cracks and other weld related defects in tank cars. This research explored the potential of several advanced NDE techniques for inspecting/characterizing tank car test panels with fatigue cracks to understand and determine their capabilities and limitations. For this study, the team selected several MG test panels (butt welds and fillet welds) with known fatigue crack defects for the feasibility demonstration.

1.1 Objectives

The major objectives of this research were:

- Conduct a feasibility study to evaluate the capabilities and limitations of advanced NDE methods for tank car weld inspection
- Develop recommendations for future work in advancing and adopting these advanced NDE methods for tank car weld inspection

1.2 Scope

Under the sponsorship of FRA, and with participation from the original equipment manufacturers (OEM) of advanced NDE equipment and NDE service providers, researchers evaluated a variety of advanced NDE methods for inspecting fusion-welded tank car butt welds and fillet welds on test panels. Several master gauge (MG) test panels (butt welds and fillet welds) with simulated fatigue cracks created under previous FRA efforts were used for this study. The following seven methods were used: phased array ultrasonic testing (PAUT), full matrix capture (FMC)/total focusing method (TFM), time of flight diffraction (TOFD), eddy

current testing (ET), tangential eddy current array (TECA), alternating current field measurements (ACFM), and pulsed eddy current thermography (PECTA). Six industry participants applied the NDE methods that were available to them. Not every participant reported flaw detection and sizing for all the methods they explored. The main goal of this study was to understand the capabilities and limitations of advanced NDE methods for tank car weld inspection and help the industry achieve higher reliability of railroad tank car structural integrity inspections. This report provides findings of studies conducted at FRA's Transportation Technology Center in Pueblo, CO, and at industry and OEM laboratories.

1.3 Organization of the Report

Section 2 describes the research and test methodology implemented for this study. This section also provides a brief background on the different advanced NDE methods used.

Section 3 presents results obtained from the different NDE methods tested. An effort was also made to calculate the probability of hits (POH) and false calls analysis based on the collected information. Also, defect sizing analysis is presented in this section for each of the individual NDE methods that reported flaw lengths.

Section 4 summarizes the work performed and provides recommendations for further work.

Appendix A provides details of the DOT 111 MG panels.

Appendix B provides a summary of participant findings.

Appendix C provides participant NDE results.

2. Research Methodology

This section describes the research and test methodology used in this study to explore the use of advanced NDE methods for tank car weld inspection.

2.1 Materials and Test Specimens

Under FRA sponsorship, TTCI previously established a defect library containing sample artifacts such as railroad tank cars and sections of railroad tank cars. Samples include tank cars donated by the tank car industry and manufactured artifacts developed at the Transportation Technology Center (TTC) (e.g., blind test panels and MG test panels developed for inspection sensitivity verification). The specimens contain discontinuities developed in service as well as manufactured flaws simulating locations and types of discontinuities expected in service. This study used MGs for feasibility demonstration of various advanced NDE methods.

2.1.1 Master Gauge Test Panels

The MG test panels were made from one of the retired tank cars (DOT-111) donated by tank car industry manufacturers. The material is close to ASTM A515 grade 70 steel. The MG test panels contain notches created using the electrical discharge machining (EDM) process which simulated fatigue cracks of varied sizes. The fatigue cracks (some tightly spaced closed fatigue cracks) were artificially initiated at the toe of the butt welds and at the longitudinal termination of the fillet welds. Details on fatigue crack generation on butt welds and fillet welds can be found in previously published FRA reports [2, 3]. Figure 1 shows the fatigue cracks in the toe of the tank car welds for butt welds (1a) and fillet welds (1b).

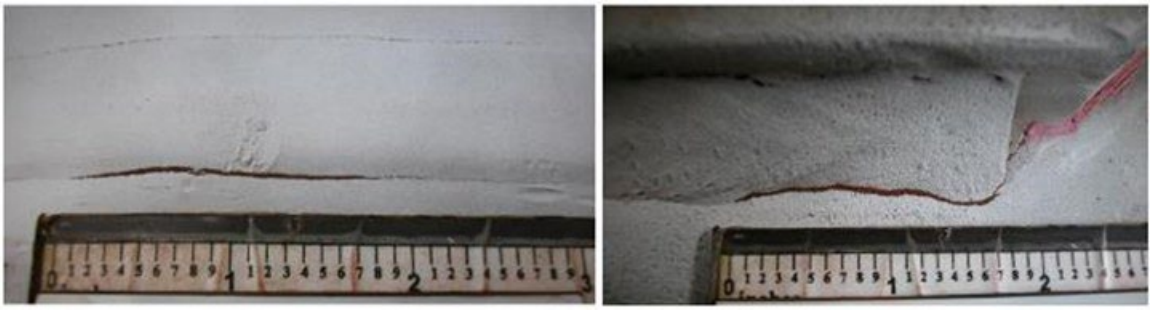

(a) **(b)**

Figure 1. Contrast MT revealing toe cracking in welds of the DOT-111 master gauge test panel: (a) butt welds; (b) fillet welds

These MGs were initially developed as calibration artifacts to assure reproducibility of response linearity during ultrasonic evaluation of the POD test panels and are part of the defect library initiated by TTCI. The primary measure of reliability in NDE are repeatability (obtained through process control) and reproducibility (achieved through rigorous calibration). Unless reproducibility and repeatability are in control, NDE capabilities data (POD) is not in control and data is not representative of the inspection process. For NDE methods, such as PT and MT inspections, both the consistency of the inspection materials used and the sequence of application are critical to process repeatability. Similarly, for inspection methods, such as ET or ultrasound, which involves human pattern recognition and/or signal observation, consistency in the threshold level used in detection (NDE process acceptance criteria) is required.

The MGs developed from the test tank cars are typically used as tools to perform a response comparison to calibration artifacts used in the field. Table 1 and Table 2 lists the butt welds and fillet welds MG test panels crack information used as a part of this study. Appendix A shows the contrast MT and PT characterization results for the butt weld and fillet weld MG panels, respectively.

Table 1. Butt weld master gauge panel flaw description

Master Gauge ID	Location A/1 (in.)	Location B (in.)	Location C/2 (in.)	Location D (in.)	Location E/3 (in.)	Location F (in.)
	Longitudinal	Transverse	Longitudinal	Transverse	Longitudinal	Transverse
TTCI-2 (EDM)	0.50	0.25	0.75	0.75	0.25	0.50
MG-06	0.70		0.70		No Flaw	
MG-13	0.60		0.60		1.00	
MG-16	0.60		No Flaw		0.40	

Table 2. Fillet weld master gauge panel flaw description

Master Gauge ID	Left side (A/C) (in.)	Right side (B/D) (in.)
TTCI-P2 (EDM)	0.30	0.80
MGL-3 A-B	0.80	0.40
MGL-9 A-B	0.60	1.70
MGL-10 C-D	0.50	1.30

2.2 Advanced NDE Methods

This section provides a high-level overview of advanced NDE technologies used in this study.

2.2.1 Phased Array Ultrasonic Testing (PAUT)

This advanced ultrasonic NDE technique uses multiple elements (piezo-composite transducers) packed together in a single probe housing that sends an array of sound in a wide range of angles through the specimen. It works on the wave physics principle of phasing – by pulsing (firing) the elements in programmed delay sequences (different times), ultrasonic beams are controlled to effectively steer (to various angles) and focus (focal distances and focal spot sizes) [7, 8].

Figure 2a illustrates the concept. The phasing is determined by a set of numbers called the focal law. The focal law serves to direct the beam in the intended direction. The returning ultrasonic beam from a reflector (such as defect or anomaly) is received by each element or group of elements in the PA probe at different time. These individual elements returning ultrasonic beams are then time-shifted before being summed up, resulting in a total A-scan signal (response from a desired focal point) as shown in Figure 2b. Instruments for controlling phased array probes are commercially available and these high-speed instruments both trigger the probes and receive data from the probes. When coupled with appropriate computer and control algorithms, the result is to steer the beam to the intended target every time.

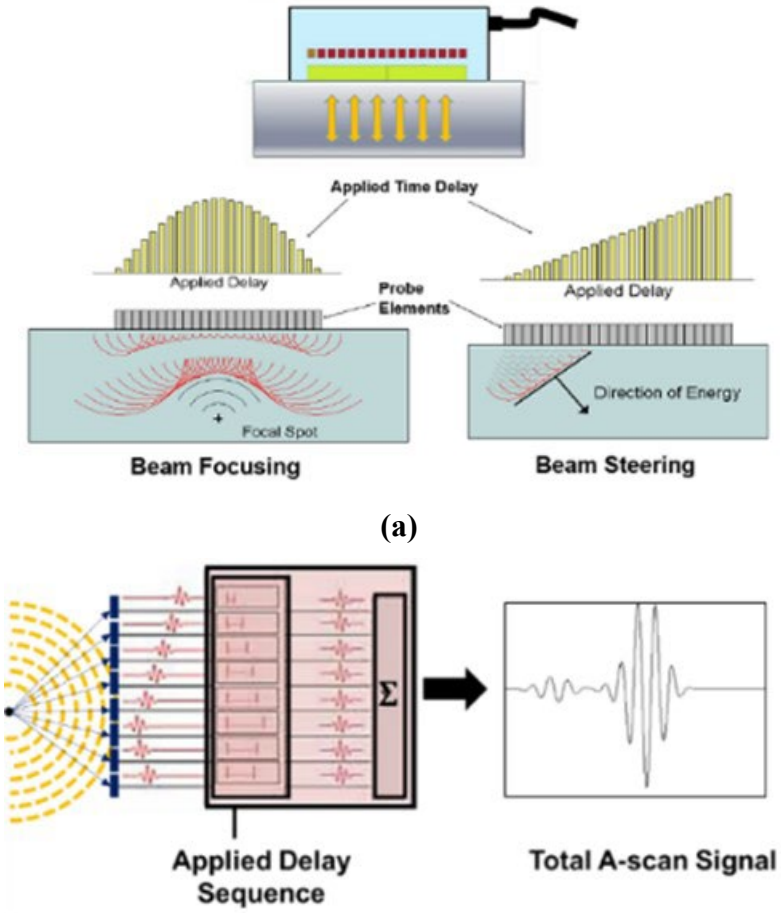

Figure 2. Illustration of PAUT principle: (a) beam focusing and beam steering by phasing element pulses; (b) ultrasonic reception signal [8]

The PAUT approach have rapidly evolved over in the past two decades, offers several operational benefits to weld inspection, and have been widely implemented in various applications [9–14]. The main advantages of PAUT over conventional UT approach are increased inspection sensitivity, coverage, and decreased inspection times. Note that the weld geometry being inspected typically governs what inspection angles are well-suited for that application. However, overall sectorial scanning will allow different ultrasonic inspection angles at the same time to inspect the weld geometry and is particularly useful for inspections with restricted access. A typical sectorial scan involves a stationary PAUT probe, where the ultrasonic beams are made to sweep through a range of angles. Figure 3 shows the sectorial scan setup from 30 degrees to 70 degrees at 1 degree step size using PAUT probe in a 4 inch × 4 inch × 1 inch steel plate with a weld.

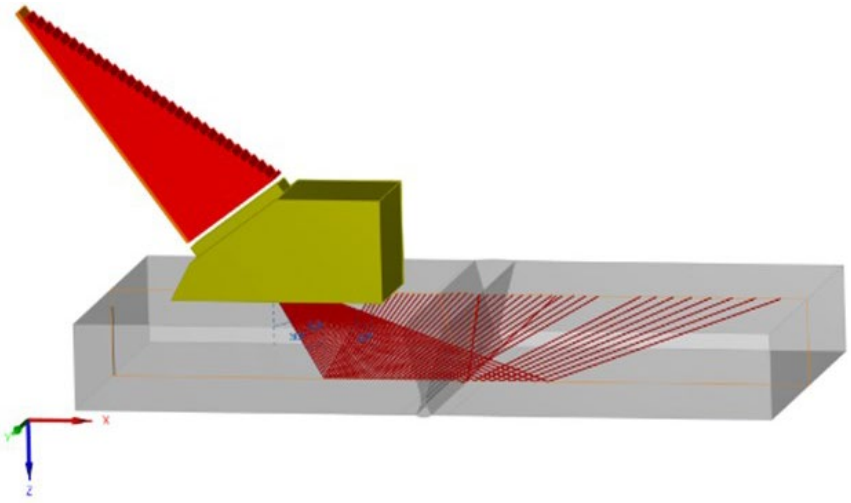

Figure 3. PAUT sectorial scan setup in a steel plate with weld

2.2.2 Full matrix Capture (FMC)/Total Focusing Method (TFM)

Researchers and industry developed and have initiated the use of advanced post-processing PAUT imaging techniques for weld flaw detection and characterization. This approach is often referred to as synthetic aperture focus technique (SAFT) or full matrix capture (FMC)/total focusing method (TFM) [15-21]. FMC is a data acquisition strategy where each individual elements in the array are used as a single emitter in sequence and all array elements are used as receivers creating a matrix of A-scan data. Figure 4 illustrates the FMC concept is demonstrated in which considers an arbitrary four-array probe resulting in 4×4 matrix for collected data. FMC has the capability of acquiring large amounts of data and the collected data can be used in many several ways using different post-processing beamforming techniques.

One of such beamforming technique is referred to as TFM. In this approach, signal processing is applied to produce an image where each pixel is one dedicated and focused law in the region of interest; i.e., it makes coherent summations over all elements to focus on each point of a reconstruction zone [15, 21]. The TFM method is used for reconstructing the data for defect characterization. One of the main advantages of this method is that the acquired FMC data can be used to generate UT images at will for any given focal law and or combination of wave modes through post-processing using TFM.

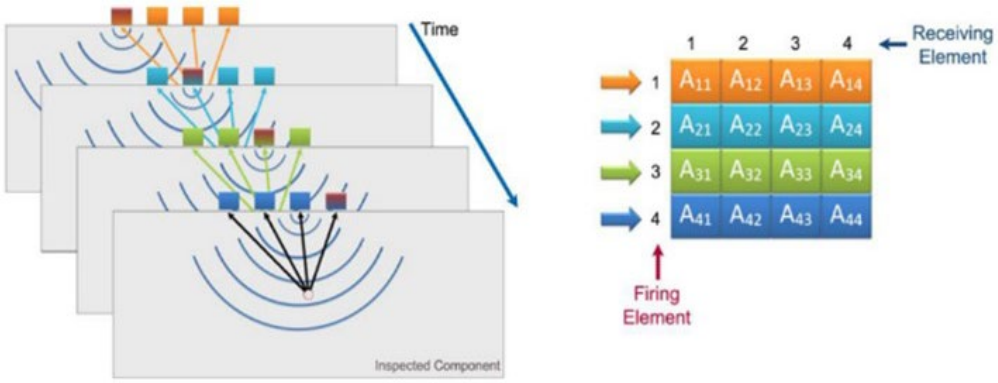

Figure 4. Illustration of data acquisition process using FMC principles [22]

2.2.3 Time of Flight Diffraction (TOFD)

The TOFD is a type of ultrasonic inspection technique that uses the time of flight (TOF) response of the diffracted ultrasonic waves from the tip of an indication. This method uses a pair of ultrasonic probes that are placed on opposite sides of the welds aimed at the same point in the weld volume. One of the ultrasonic probes, the transmitter, sends out an ultrasonic pulse that is picked up by the other ultrasonic probe, the receiver. If there is no flaw present, the ultrasonic signals picked up by the receiver probe are from two wave fronts: one that travels along the surface, known as lateral wave (LW), and one that reflects off the far wall, known as back wall (BW) reflection. If there is a flaw such as crack, there is a diffraction of the ultrasound pulse from the tips of the crack. Figure 5 shows the TOFD setup and illustrates its working principle. TOFD for weld defect detection and sizing is an established and excellent method for quick assessment of the weld quality and is widely used in several applications. Further, the height, length, and position of the flaw can be measured with reasonable accuracy using TOFD, making this method ideal for identifying cracks and lack of fusion located along the fusion line of the weld [23–25].

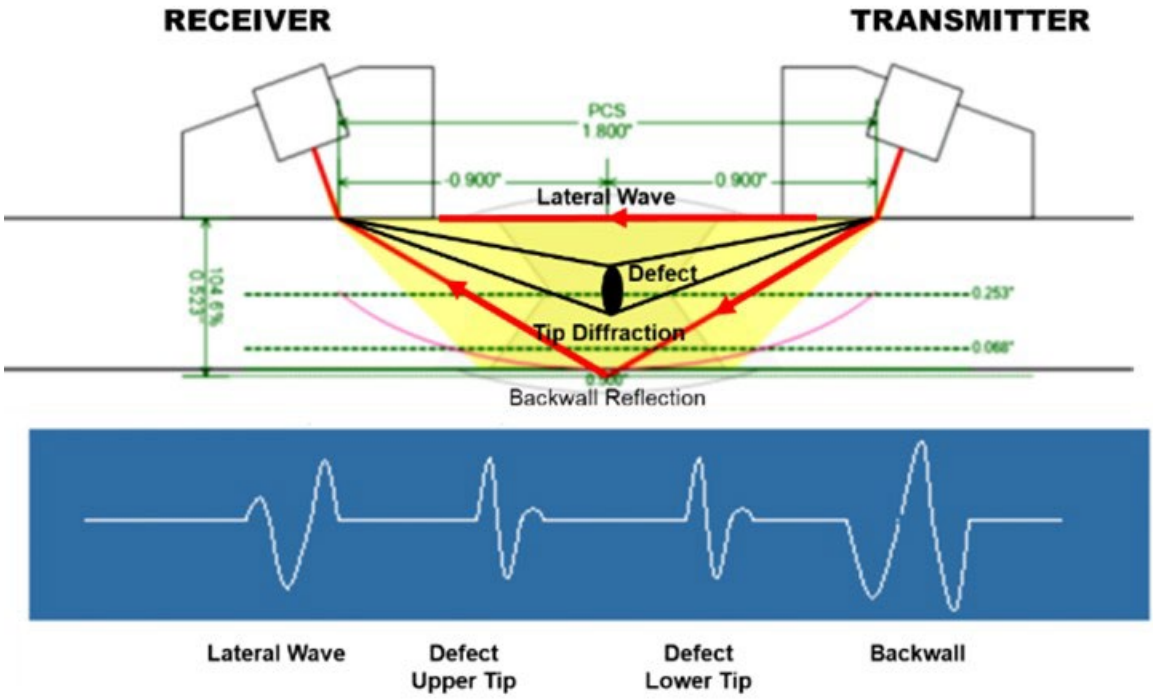

Figure 5. A TOFD setup/configuration and working principle

2.2.4 Eddy Current Testing (ET)

ET is an electromagnetic NDE method that works on electromagnetic induction principles. In this technique, a coil (also called probe or sensor) is usually (but not always) excited with sinusoidal alternating (time-varying) current, and the frequency may range from a few hundred Hz up to a few MHz, typically 100 Hz to 10 MHz [10, 40, 1]. The frequency is selected based on the test material properties and the depth of the defect to be detected. When an electrically conducting material is brought close to this coil, eddy currents are induced in the material. The induced eddy current density depends on the excitation frequency, the material's electrical

conductivity and magnetic permeability, the structure's geometry, and the excitation coil's dimensions and driving current. The amplitude and phase of the eddy currents will change the loading of the coil and its impedance. When the induced current interacts with the surface or sub-surface discontinuity in a material, it disturbs the eddy current flow, weakening its strength and changing the coil impedance. This strength change at crack locations is measured by the EC sensors and helps detect the anomalies in conducting material. Figure 6 shows the basic working principle of the ET method and distortion of eddy current due to crack, edge effect, surface crack, and subsurface void.

Several single-channel/single-frequency, single-channel/dual-frequency, and multi-channel ET instruments are commercially available for NDE measurements. Usually, EC probes are classified according to their configuration and mode of operation. The probe configuration is closely related to how the coils' configuration covers the region of interest in materials being inspected and the probe mode of operation is classified into absolute, differential, reflection, and other hybrid modes. The three major types of EC probes that are commercially available include surface, outside diameter, and inside diameter inspections. These three configurations, as well as some crossover designs, are used for most flaw detection applications. Similarly, absolute probes have a single-coil design and give an "absolute" reading at the flaw. Differential probes use two coils to check for flaws in different areas or to differentiate between two variables. Reflection probes (either absolute or differential) have a primary coil being supplied by the oscillator and at least one coil from the measurement circuit.

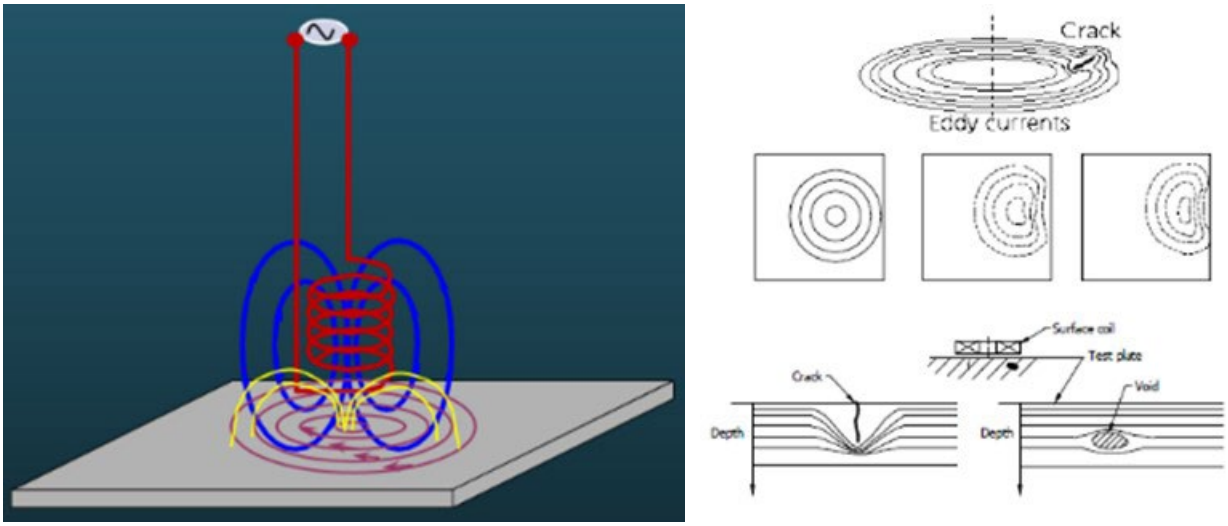

(a) **(b)**

Figure 6. Eddy current testing: (a) principle; (b) distortion of eddy current due to crack, edge-effect, surface crack, and sub-surface void

Advances in the ET have also brought forward other advanced ET technology such as giant magneto resistive/resistance (GMR) sensors [29–31], pulsed eddy current [32–36], and array probe technologies [37, 38].

2.2.5 Tangential Eddy Current Array (TECA)

The TECA is an advanced ET technology that uses combination of multiplexed tangential coils and pancake coils to detect and size cracks that break the rail surface [39, 40]. This approach

eliminates the need for multiple or raster scans as it allows scanning wide surfaces in a single pass, drastically reducing the time needed to perform inspections. Figure 7 illustrates the TECA probe and technology. TECA coil arrangement induces eddy currents that flow perpendicular to the scan direction. As these eddy currents meet with longitudinal cracking, they tend to pass around the crack either by diving underneath it or by flowing around the extremities. It has been reported that TECA offers better overall performances than magnetic particle testing and TECA's probability of detection is significantly higher while the probability of making false calls is much lower [40].

Figure 7. The TECA probe and technology [40]

2.2.6 Alternating Current Field Measurements

The ACFM technique is a non-contact electromagnetic technique used for the detection and sizing of the surface breaking cracks in ferromagnetic and non-ferromagnetic materials. Flaw detection and sizing via ACFM involve scanning the surface of a test object with a pencil probe containing sensors, electronically monitoring the effect of such scanning, and measuring the component of the associated magnetic fields to determine flaw size and depth. The underlying physics or principle lies on the basic concept of inducing locally uniform alternating current into an area of the test component and measuring the magnetic flux density above the test component surface. When a surface-breaking crack is present, the current flows around the ends and down the faces of the crack; hence perturbing the magnetic flux density as shown in Figure 8 [41–43].

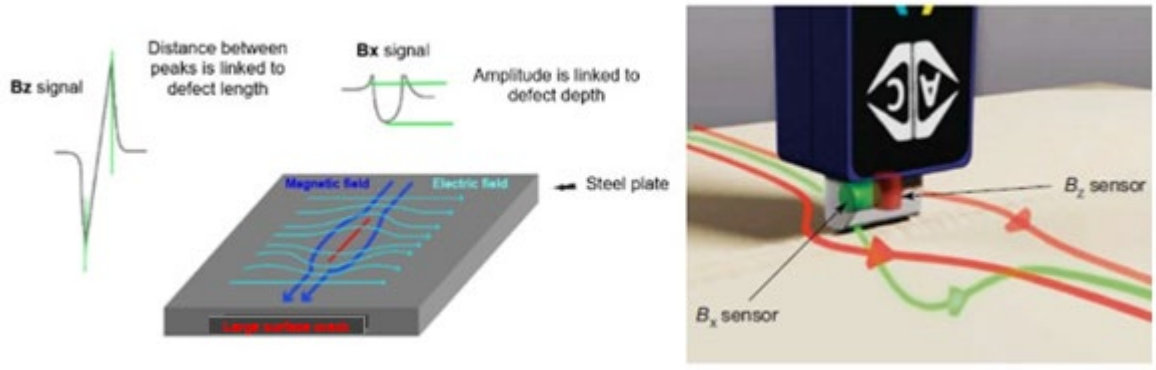

(a) **(b)**

Figure 8. Principle of ACFM: (a) traces produced from the B_X and B_Z sensors as a probe is scanned along the lines of a discontinuity; (b) sensor orientation in pencil probe nose [41].

2.2.7 Pulsed Eddy Current Thermography (PECT)

PECT is hybrid NDE method that uses both eddy current and infrared thermography (IRT) principles to detect and quantify defects surface or subsurface cracks. In this method, test sample is electromagnetically excited using a current carrying coil that causes the material to heat by local induction. In the presence of cracks, it causes localized change in the induced eddy-current flow and the associated Joule heating is imaged at the surface of the part with an infrared camera [44–46]. However, the irregularity of surface emissivity can sometimes produce inhomogeneous temperature results which can provide false indications.

3. Advanced NDE Methods Results and Analysis

This section presents the application of advanced NDE methods for the inspection of fusion welded tank car butt weld and fillet weld MG as presented in Section 2.

3.1 Panels Evaluated by OEM

Table 3 lists the details of the six OEMs of NDE equipment and tank car industry NDE consulting service providers participating in this study. Names of these participants have been anonymized and are represented by the letters A through F. Grouped with each participant is the NDE method(s) they used to evaluate the provided MG panels.

Table 3. Participants and advanced NDE method used

Participant	Method Used
A	PAUT FMC/TFM
B	PAUT FMC/TFM ACFM TECA
C	ET
D	ACFM PAUT FMC/ TFM TOFD
E	PAUT-ID-Line Scan PAUT-ID-Raster PAUT-OD-raster Scan PAUT-OD-Raster TOFD FMC/TFM
F	PECT

Table 4 shows which participants evaluated each MG panel (Table 1 and Table 2). Not all vendors were able to evaluate each panel; those instances were not counted against their probability of hits. Participant A did not evaluate the TTCI-2 panel. Participant B did not evaluate the MGL-10 panel. Participant F did not evaluate any of the panels containing fillet welds.

Table 4. Panel evaluation by OEM

Panel Type	Panel ID	Participants					
		A	B	C	D	E	F
Butt Weld	MG-6	✓	✓	✓	✓	✓	✓
	MG-13	✓	✓	✓	✓	✓	✓
	MG-16	✓	✓	✓	✓	✓	✓
	TTCI-2	✗	✓	✓	✓	✓	✓
Fillet Weld	MGL-3	✓	✓	✓	✓	✓	✗
	MGL-9	✓	✗	✓	✓	✓	✗
	MGL-10	✓	✓	✓	✓	✓	✗
	TTCI-P2	✓	✓	✓	✓	✓	✗

3.2 Advanced NDE Results

This section provides advanced NDE results for the MG tank car panel. For visualization purposes, results are presented for the MG-13 panels as this panel was inspected by all the participants. This panel had three simulated fatigue cracks on the toe of the butt welds as marked by the numbers 1 through 3 in the panel shown in Figure 9. Appendix B and Appendix C provide details of participant findings on the butt welds and fillet welds panels inspected as a part of this trial.

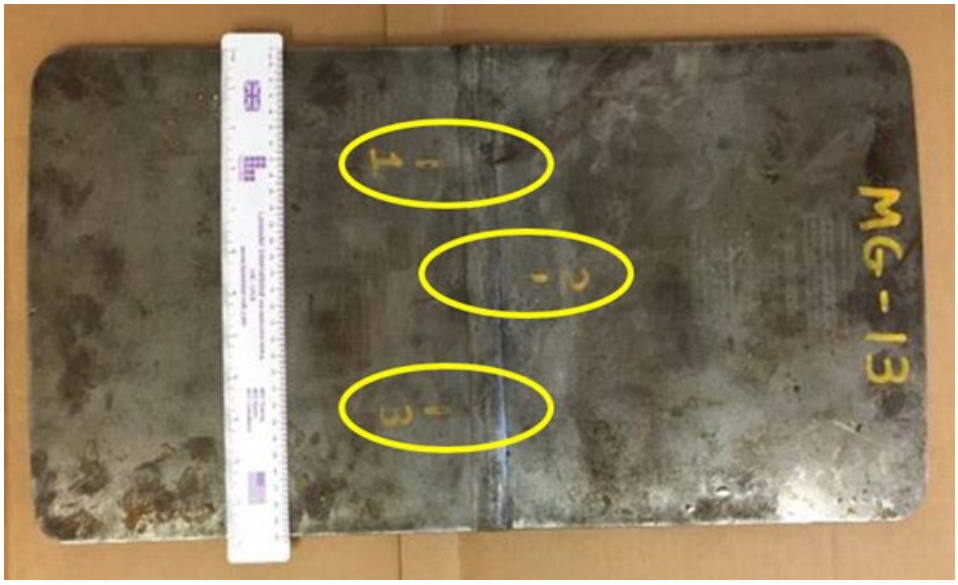

Figure 9. Butt weld master gauge test panel (MG-13)

3.2.1 PAUT

For the automated PAUT, FMC/TFM, and TOFD scans, data was collected from both sides of the weld using an encoded and raster scan. Figure 10 shows one of the test setups used for

encoded testing in the MG plates conducted from the outer diameter. For this setup, a 10 MHz, 32 element PAUT probe with 0.01 inch pitch was used and the sweep angle ranged from 45 to 70 degrees. The scan was conducted at < 6 inches per second for the entire width of the panel (48 inches). The interpretation of the acquisition data was performed automatically using dedicated analysis software. After the defect and the geometric signal were identified, the signal analyzed as the defect or anomaly was evaluated according to the accepted code.

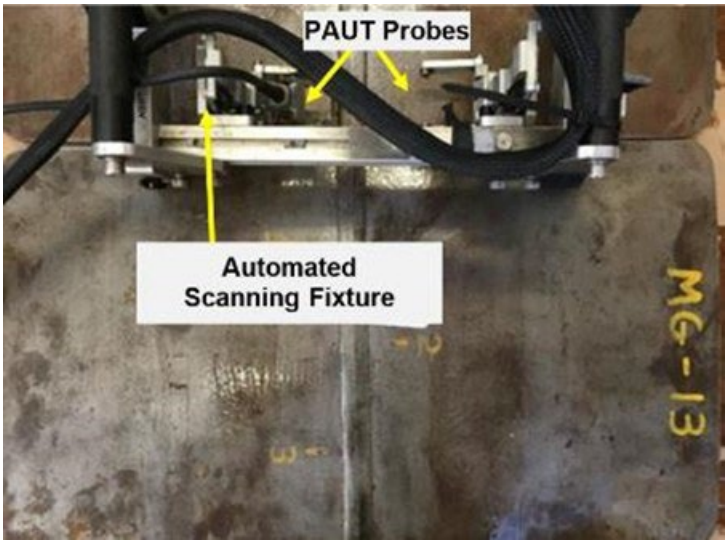

Figure 10. Automated PAUT, FMC/TFM, and TOFD inspection setup

Figure 11 shows the C-scan image with indications of the fatigue cracks identified at locations 1, 2, and 3 on the MG-13 panel using the automated PAUT method.

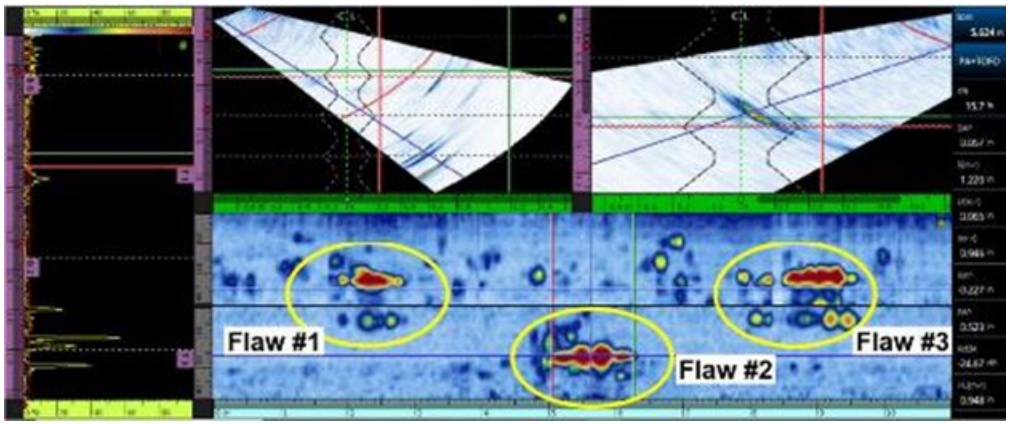

Figure 11. Automated PAUT C-scan results showing flaw indications for MG-13 plate

Defect height and length can be measured using the built-in measurement cursors available in the software. For height measurements, a tip diffraction size was taken by measuring the distance from the corner trap signal of the flaw to the upper most signal that represents, the “tip” of the flaw and for length measurements, cursors were placed on either end of the flaw where signal begins its drop in amplitude from side-to-side. Figure 12b shows an example of the defect length sizing for flaws 1 and 2 in MG-13 panel.

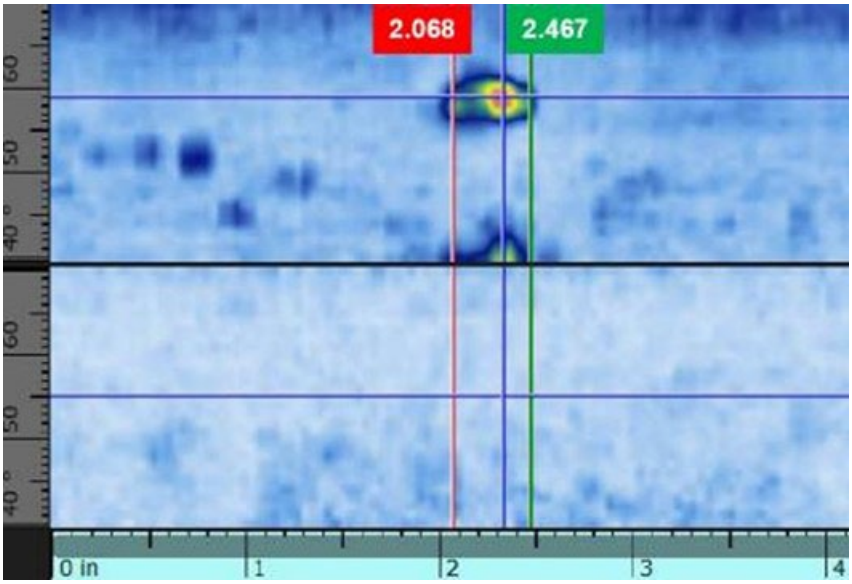

(a)

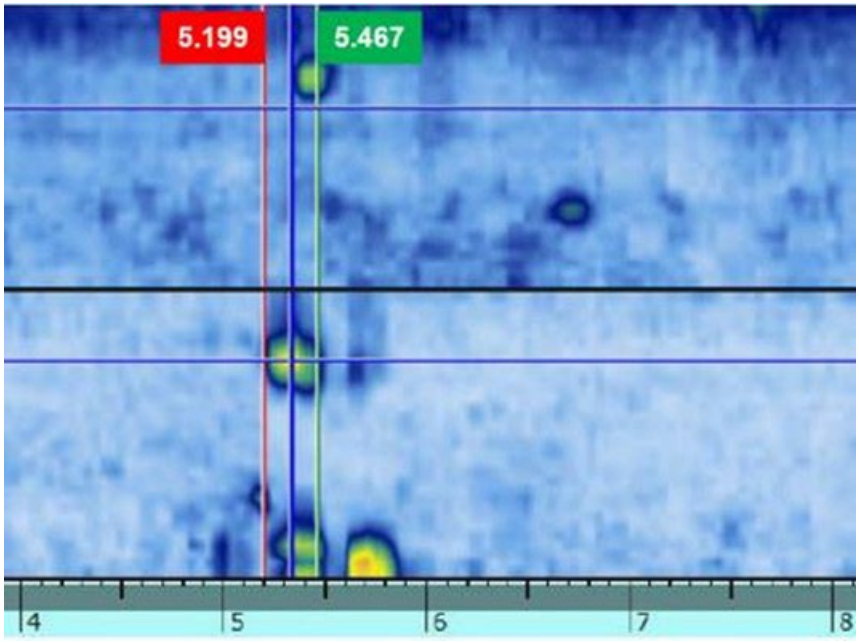

(b)

Figure 12. Defect length sizing in the software: (a) flaw #1; (b) flaw #2

3.2.2 FMC/TFM

In all FMC acquisition, TFM wave modes used in the reconstruction and imaging processes should be indicated. The TTdTT wave mode was defined, which means a refracted shear wave (T) is generated in the specimen Then, the shear wave is reflected from the back wall (TT) and encounters the flaw or defect (TTd). The shear wave is then reflected from the flaw to the backwall surface and is received by the phased array probe (TTdTT). Figure 13 shows the indications of the flaws embedded at locations 1, 2, and 3 on MG-13 panel using PAUT FMC/TFM.

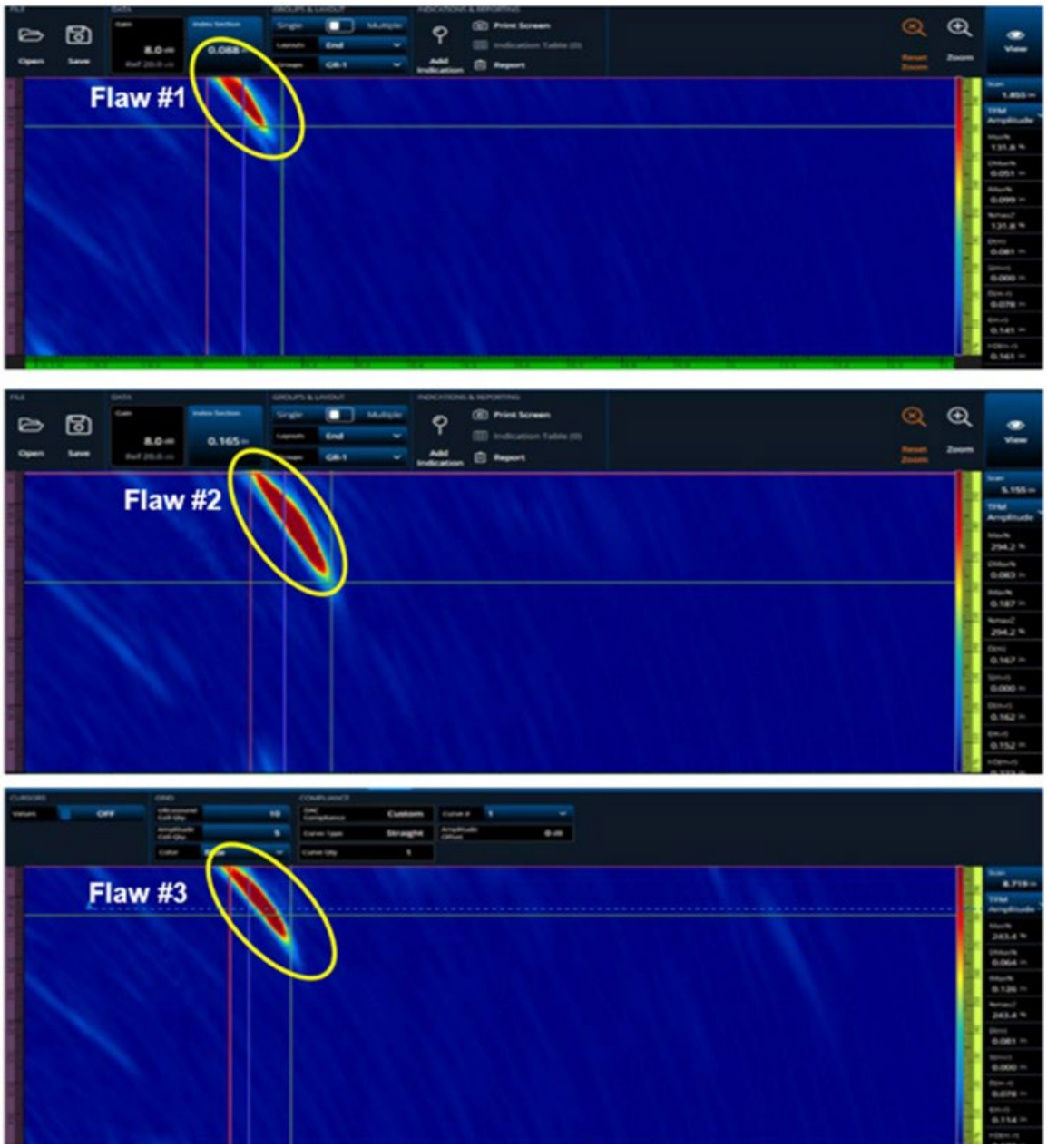

Figure 13. FMC/TFM indication of all three flaws in the MG-13 plates

As demonstrated, the advantages of FMC/TFM are improved resolution and decreased sensitivity for defect orientation. In addition, this method can help reduce operator dependence and increased inspection reliability and performance. Still FMC/TFM should be further explored with different weld configurations and types in the railroad tank cars.

3.2.3 TOFD

TOFD scans were performed concurrently with PAUT from the outer diameter of the panel. Figure 14 shows indications of the flaws detected at locations 1, 2, and 3 on the MG-13 panel

using the TOFD method. Although flaws reported here were detected, these indications were difficult to clearly distinguish as they were hidden within the lateral waves.

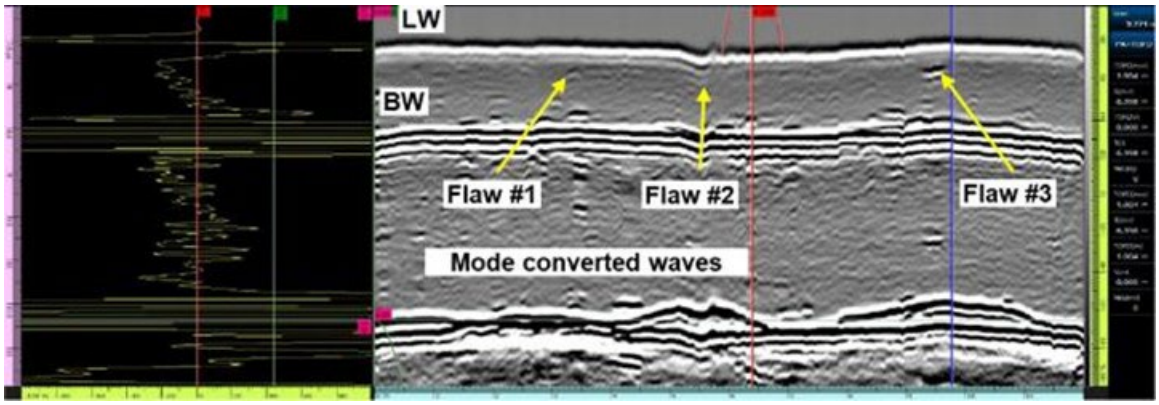

Figure 14. TOFD Indication of all three flaws in MG-13 Plates

Figure 15 shows detailed zoomed in images and corresponding A-scan results for all flaws listed above. The blue vertical cursor shown in the images in Figure 15 show the indication of flaws and corresponding A-scans. The fatigue cracks simulated in this plate were tightly spaced, closed fatigue cracks located at the toe of the welds. Due to a "dead zone" limitation near the surface of material with TOFD (defined at depths up to 0.12 inch), the sizing of these indications presented a significant challenge when dealing with these kinds of cracks. Since, TOFD was run simultaneously with PAUT, it allowed for easy discrimination of these flaws. Otherwise, some of these flaws could be missed if only ran using the TOFD technique. Finally, it should be noted that TOFD is not suitable for providing an accurate depth of flaw but rather is used for quick assessment and to provide a length and height.

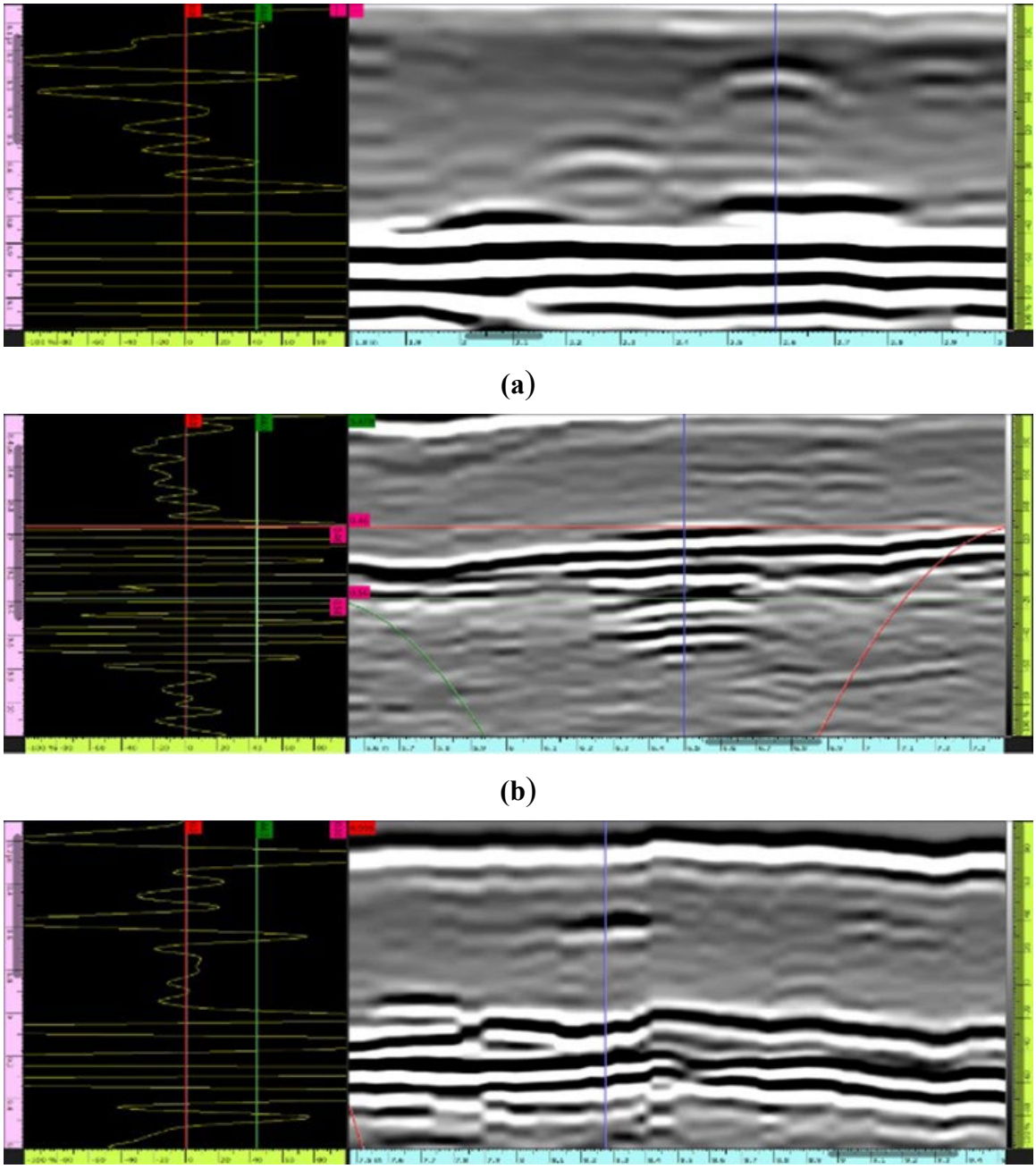

(a)

(b)

(c)

Figure 15. TOFD results for flaws in MG-13 panel: (a) flaw #1; (b) flaw #2; (c) flaw #3

3.2.4 ET

Figure 16 shows the test setup used for ET inspection of the MG plates. Multiple probes were investigated to evaluate different coil configurations to obtain the best results. The configuration that worked best was a pencil probe with a cross-wound coil design that provided directional sensitivity and discrimination in the weld area. A typical carbon steel standard with various notches was used to calibrate the unit. An attempt was also made to use the recorded voltage

measurements on all indications to correlate voltage to depth (mm) and was demonstrated with the simple amplitude curve as shown in Figure 17.

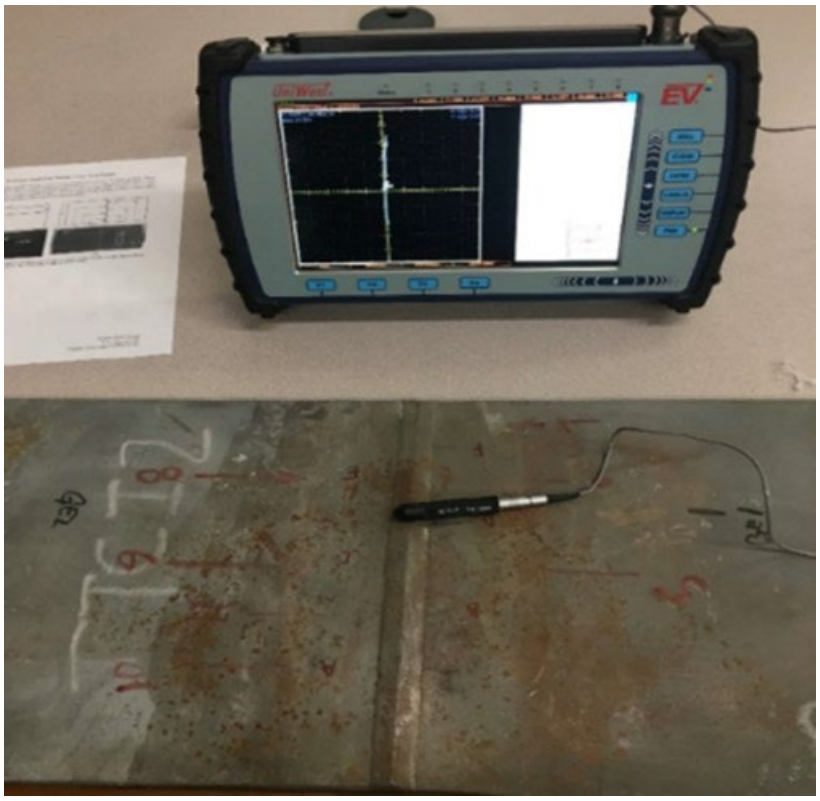

Figure 16. ET inspection setup

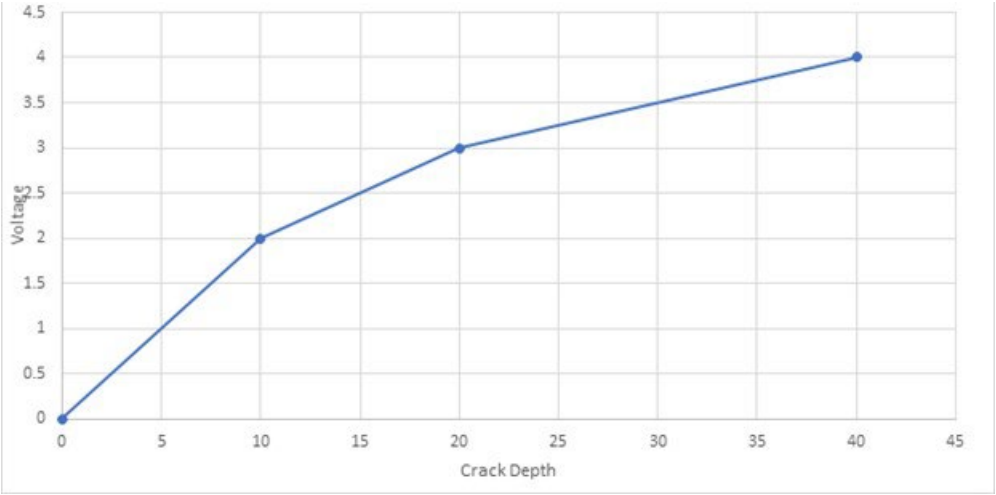

Figure 17. ET amplitude curve for crack depth estimation in the MG plates

Figure 18 shows the indications of the flaws at locations 1, 2, and 3 on panel MG-13 as displayed in the ET impedance plot and A-scan trace.

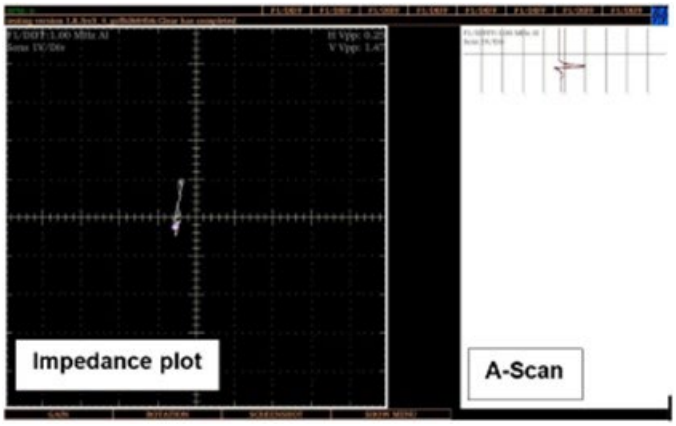

(a)

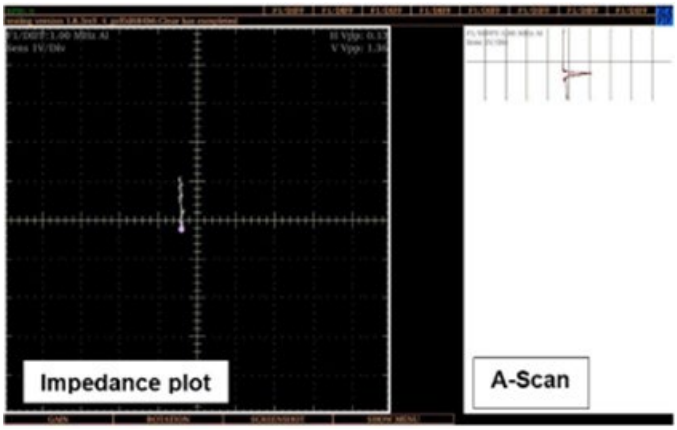

(b)

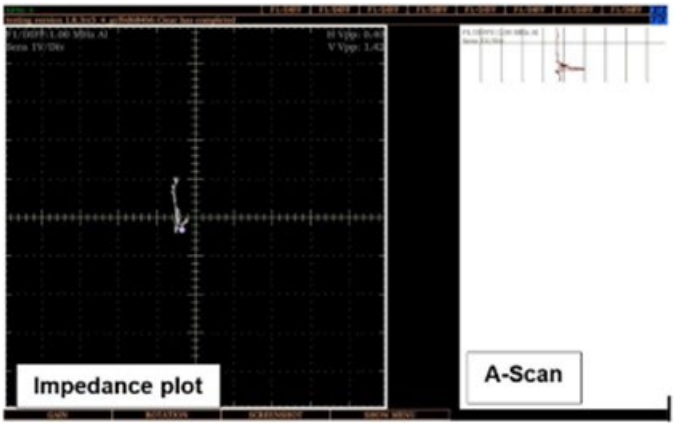

(c)

Figure 18. ET indications on MG-13 panel: (a) location 1; (b) location 2; (c) location 3

3.2.5 TECA

Figure 19 shows the scan plan setup and Figure 20 shows flaw indications using TECA on MG-13 panel.

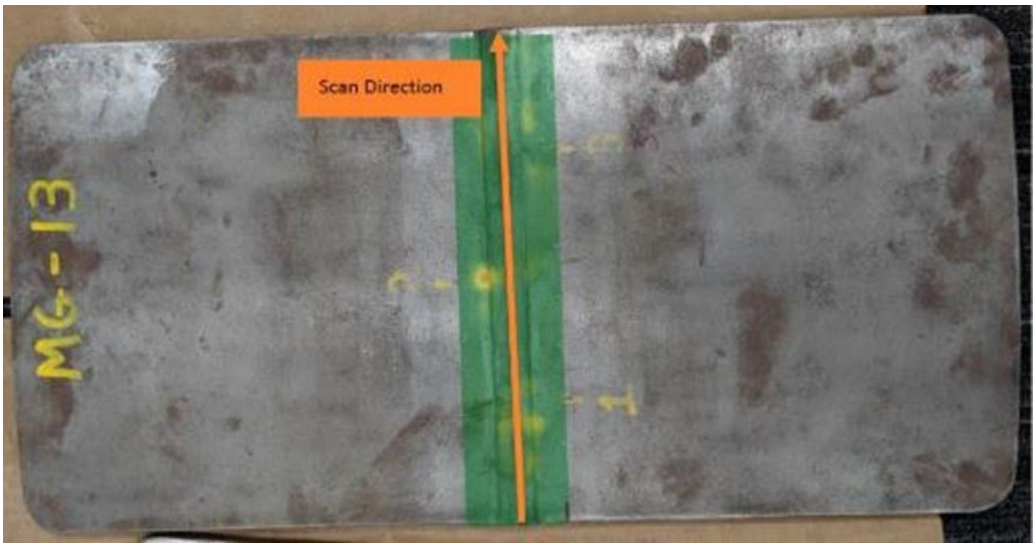

Figure 19. TECA inspection scan plan setup for MG-13 panel

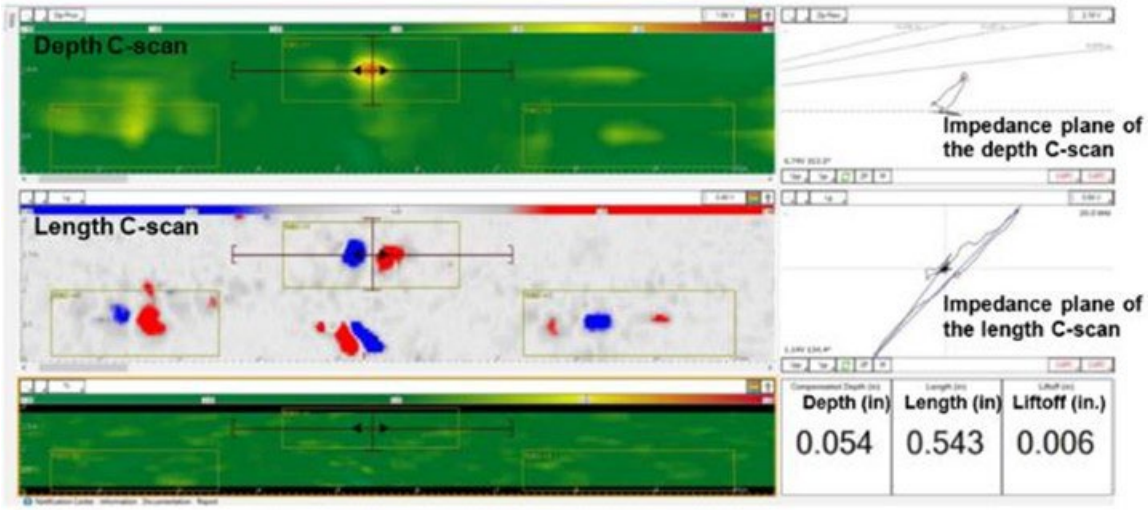

Figure 20. TECA flaw indications on MG-13 panel

The TECA coil design allows for lift-off monitoring and measurement; thus, the defect signal can be adjusted accordingly. The sizing capabilities of this technique rely on multiple depth curves that are dependent on the lift off value associated with the signal response monitored during scanning and are handled automatically by the system. Data is analyzed by reviewing mainly two C-scans, as shown in Figure 20. Flaw-like indications are characterized by the presence of bright spots on the "Depth" C-scan and two aligned spots on the "Length" C-scan. The "Depth" C-scan is used to highlight the depth of surface breaking flaws, while the "Length" C-scan highlights the beginning (blue in the figure) and end of the crack-like indication (red). A defect is made more obvious whenever those patterns are at the same location in both C-Scans (i.e., aligned on both axes of the cursor). When flaw-like indications are detected, they are isolated using the extraction cursor to obtain the sizing information (depth, length, lift off, and position), which are generated automatically displayed to the operator.

Scanning the fillet weld plates using TECA proved challenging; as a result, flaw sizing was not conducted. This issue needs to be further explored in detail in the future.

3.2.6 ACFM

Figure 21 shows the test setups used for automated ACFM inspection of the butt weld and fillet weld MG plates. A 5 kHz straight pencil probe was used during this trial.

Figure 21. ACFM setup for MG plate inspection

The function check plate (supplied with the equipment) was scanned at the beginning of the inspection to ensure the equipment was working correctly. The function check plate is constructed from 0.50 inch thick carbon steel, with a weld running along its length. Semi-elliptical 2.0 inch x 0.20 inch and 0.80 inch x 0.08 inch reflectors are cut into one of the weld toes. If a correctly configured ACFM probe is scanned across the 2.0 inch x 0.20 inch reflector, a butterfly loop appears in the butterfly plot (right) with a visual size of 175 percent of the screen width, and 50 percent of the screen height as shown in Figure 22.

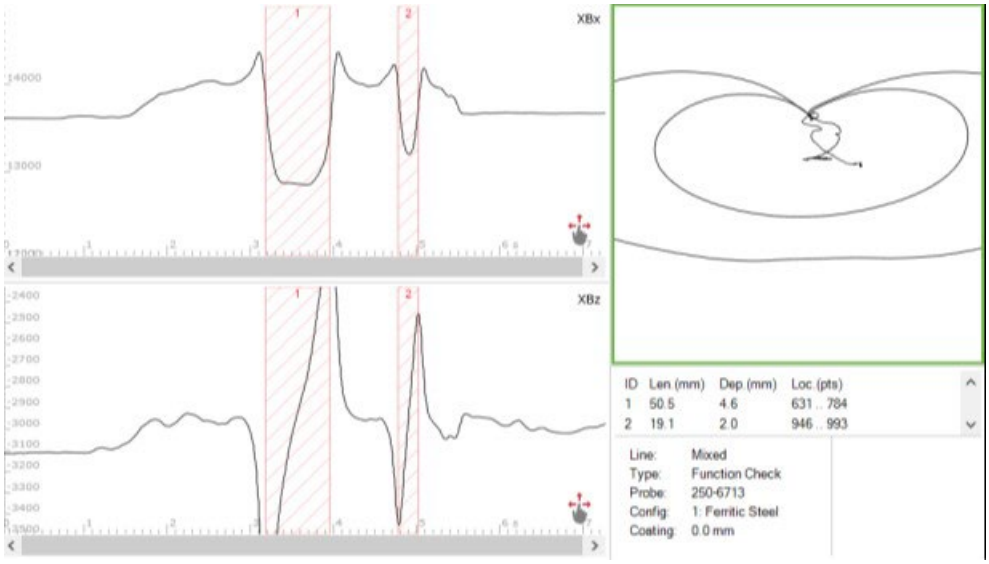

Figure 22. ACFM function check test results

Figure 23 through Figure 25 show ACFM indications and sizes of the flaws detected at locations 1, 2, and 3 on panel MG-13. The length and depth of the flaw 1 were 0.4 inch and 0.01 inch, respectively. The length and depth of the flaw 2 were 0.46 inch and 0.007 inch, respectively. The length and depth of the flaw 3 were 0.70 inch and 0.01 inch, respectively.

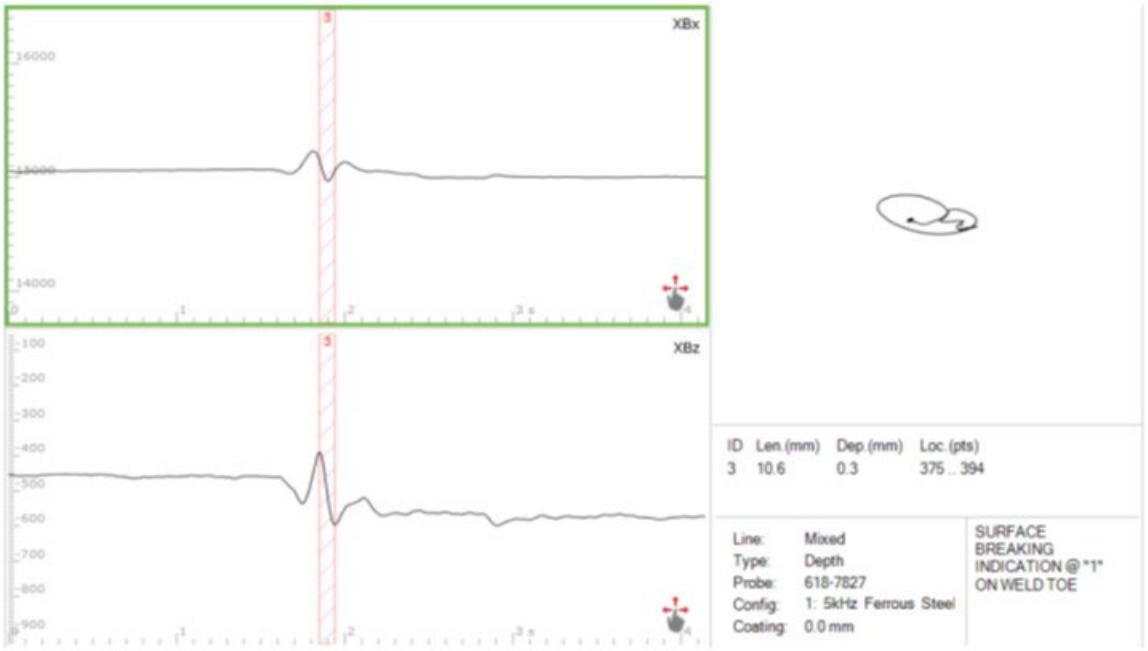

Figure 23. ACFM flaw indication at location 1 on panel MG-13

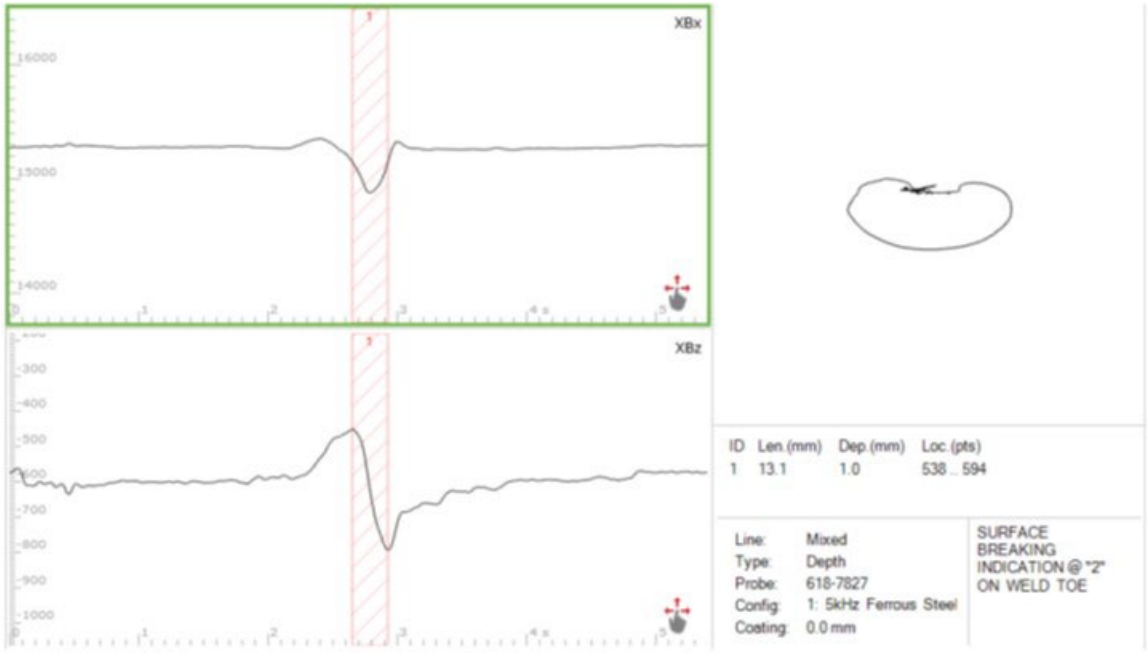

Figure 24. ACFM flaw indication at location 2 on panel MG-13

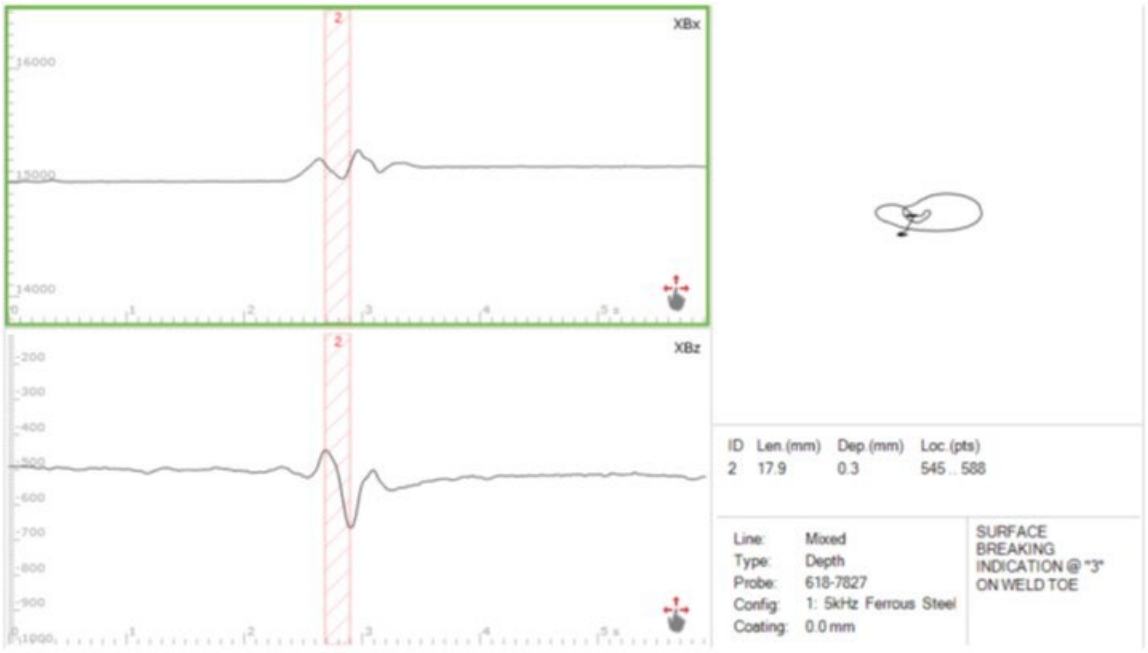

Figure 25. ACFM flaw indication at location 3 on panel MG-13

3.2.7 Pulsed Eddy Current Thermography

Figure 26 shows the ECT inspection setup for the MG test panel. An uncooled Vox microbolometer FLIR IR camera with 640 × 512 array was used. The thermal sensitivity of the camera was less than 40 mK at f/1.0 and a maximum full frame rate of 60 Hz was used. Details on the pulse eddy current excitation (proprietary) was not provided by the participant.

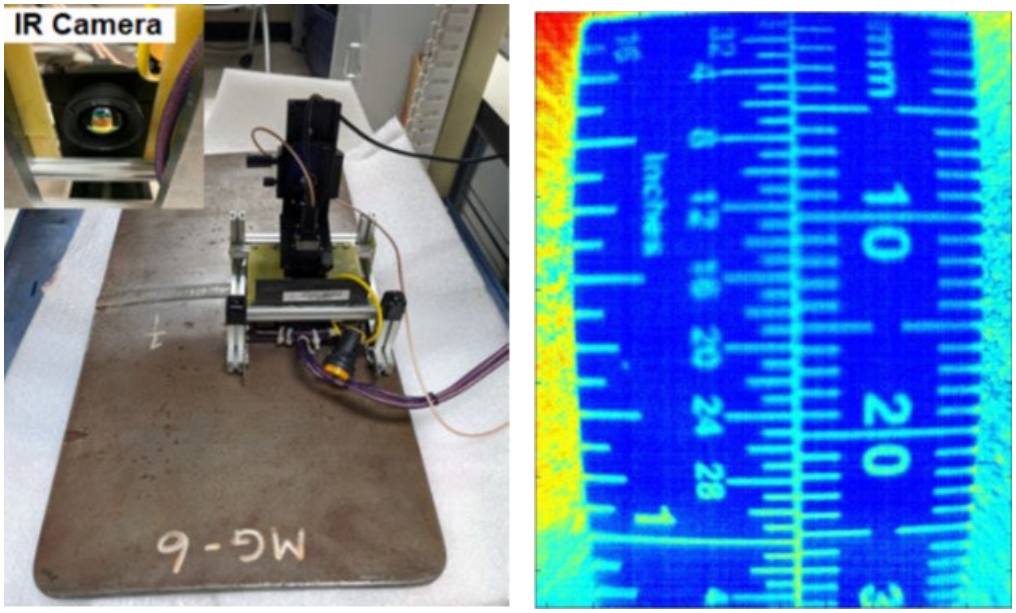

(a) **(b)**

Figure 26. ECT inspection for panel MG-13: (a) experimental setup; (b) FOV

Figure 27 shows indications and sizes of the flaws at locations 1, 2, and 3 using ECT on panel MG-13. The field of view was zoomed to provide a coverage of 30 mm × 22 mm. During the first trial of this technology, the POH was only around 33 percent with one false positive. The system was later optimized based on the flaw information provided to achieve 100 percent POH.

The PECT method, an emerging technique, demonstrated potential for finding fatigue cracks at the toe of the butt welds after a few trials. Following system optimization, EDM notches were easily detected with the heat concentrating at the end of the notch, providing better discrimination for the infrared camera. However, geometry of fillet weld panels was challenging to this method as the coil configuration used was not optimal for inspecting the fillet welds. Further, the geometry of the MG plates (specifically, the weld toe) also interfered with the crack signature at times making detection challenging in one of the panels.

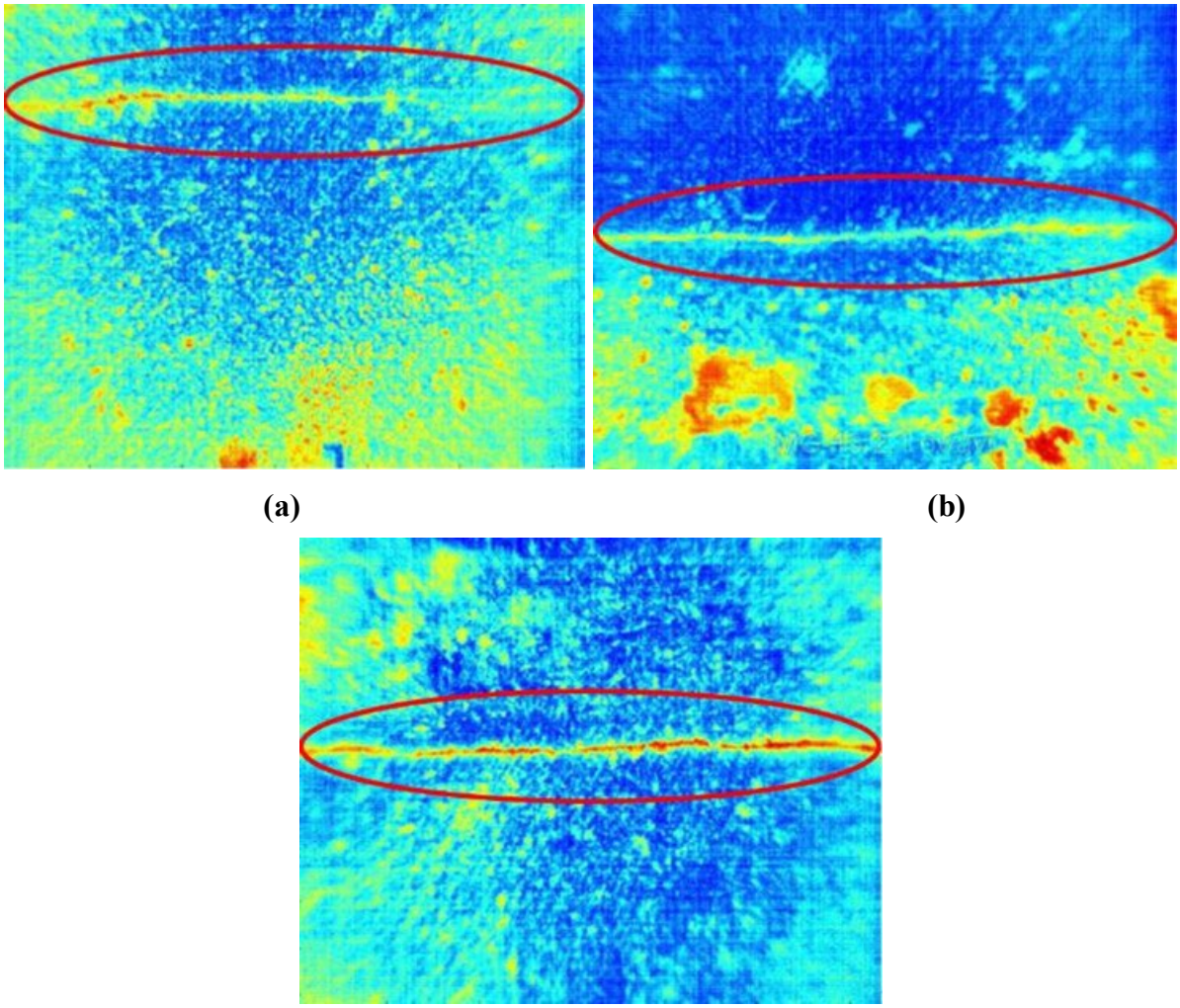

(a) **(b)**

(c)

Figure 27. ECT inspection results for MG-13 panel: (a) location 1; (b) location 2; (c) location 3

3.3 Probability of Hits Analysis

Each evaluation of MG panels was classified into one of the four following groups:

- True positive (TP): The defect was indicated where it was present (hit)
- False negative (FN): The defect was not indicated where it was present (miss)
- True negative (TN): The defect was not indicated where it was not present
- False positive (FP): The defect was indicated where it was not present (false alarm)

For each NDE method used by each participant, the probability of correct hits was calculated. The number of correct evaluations, true positive and true negative, was divided by the total number of defects (cracks/notch) evaluated. Table 5 shows probability of correct detection grouped by participants. Also, included are the full results for each of the four evaluation result categories.

In all cases, there were at most one to two false positive or true negative for the NDE methods. Most of the decrease in probability of correct detection came from false negatives. Results varied between each of the participants even when using similar methods; for example, the ACFM for participants B and D. Each different method for each participant evaluated between 12-23 cracks/notches; crack/notch evaluations varied depending on how many panels were able to be evaluated by the participant. The highest POH achieved was 100 percent and the lowest achieved was 53 percent. Six of the methodologies (out of 15) had over an 80 percent POH.

Table 5. POD grouped by participants

Participants	NDE Method	Evaluation Result					
		True Positive	True Negative	False Positive	False Negative	POH (%)	Total Evaluations
A	PAUT and FMC/TFM	15	N/A	2	N/A	88	17
B	ACFM	16	1	1	3	81	21
	TECA	10	1	1	5	65	17
C	ET	20	2	N/A	1	96	23
D	ACFM	13	N/A	2	8	57	23
	PAUT	10	N/A	2	N/A	83	12
	TOFD	6	2	N/A	7	53	15
	FMC/TFM	10	N/A	2	3	67	15
E	PAUT-ID-Encoded scan	10	N/A	2	5	59	17
	PAUT-ID-Raster scan	14	1	1	5	71	21
	PAUT-OD-Encoded scan	16	N/A	2	5	70	23
	PAUT-OD-Raster	8	1	1	5	60	15
	TOFD	13	N/A	2	N/A	87	15
	FMC/TFM	8	1	1	5	60	15
F	PECT	13	2	N/A	N/A	100	15

Based on this information, the total false positive for the fillet weld was determined to be 33 percent and total false positive for the butt weld was determined to be 19 percent. Table 6 shows the statistics for false negatives grouped by panel to further explain false negatives and their sources. The table is ordered by highest to lowest false negative rate as determined by dividing

the false negative count by the total evaluations. The crack with the highest false negative percent was fatigue crack B from MGL-3. There does not seem to be a relationship with crack size and false negative percent. Most fillet welds are ranked in the top half of the table. There were more evaluations of cracks/notches present in butt welds (186) versus fillet welds (48) panels, but the fillet welds had a higher false negative rate – 33 percent (16 out of 48) versus 19 percent (36 out of 186). Based on this information, the total false positive for the fillet weld was determined to be 33 percent and total false positive for the butt weld was determined to be 19 percent.

Table 6. False negative counts by panel

Weld Type	Panel	Notch/ Crack Marking	Master Crack Length	False Negative Count	Total Evaluations	False Negative
FW	MGL-3	B	0.4	3	6	50%
BW	MG-16	1	0.6	6	15	40%
FW	MGL-10	D	1.3	2	5	40%
FW	MGL-3	A	0.8	2	6	33%
FW	MGL-9	A	0.6	2	6	33%
FW	MGL-9	B	1.7	2	6	33%
FW	TTCI-P2	A	0.3	2	7	29%
FW	TTCI-P2	B	0.8	2	7	29%
BW	MG-13	1	0.6	4	15	27%
BW	MG-13	2	0.6	4	15	27%
BW	MG-13	3	1	4	15	27%
BW	MG-16	3	0.4	4	15	27%
BW	TTCI-2	B	0.25	3	13	23%
BW	TTCI-2	D	0.75	3	13	23%
BW	TTCI-2	F	0.5	3	13	23%
BW	MG-6	1	0.7	3	15	20%
FW	MGL-10	C	0.5	1	5	20%
BW	MG-6	2	0.7	2	15	13%
BW	TTCI-2	A	0.5	0	14	0%
BW	TTCI-2	C	0.75	0	14	0%
BW	TTCI-2	E	0.25	0	14	0%

3.4 Crack/Notch Sizing Analysis

The advanced NDE methods explored in this study identified whether a crack/notch was present as shown by the analysis in the previous section, but they also were tasked with measuring the crack/notch lengths. When a crack/notch was identified where a crack/notch existed (true positive), participants did not always return a length. Table 7 shows the count of crack/notch lengths given by each participant using each NDE method. The possible crack/notch length column represents the number of true positives for each NDE method and participant. The

FMC/TFM used by participant D did not report any crack length. This method was not included in analysis of crack length difference.

Table 7. Count of given crack/notch lengths

NDE Method (Participants)	Number of Notch/ Crack Lengths Measured	Number of Possible Notch/ Crack Lengths	Percent
ACFM (B)	16	16	100
ACFM (D)	10	13	77
ET (C)	20	20	100
PAUT and FMC/TFM (A)	7	15	47
PAUT (D)	10	10	100
PAUT-ID-Encoded scan (E)	10	10	100
PAUT-ID-Raster (E)	14	14	100
PAUT-OD-Encoded scan (E)	16	16	100
PAUT-OD-Raster (E)	8	8	100
PECT (F)	13	13	100
TECA (TECA) (B)	10	10	100
TOFD (E)	10	13	77
TOFD (D)	3	6	50
FMC/TFM (E)	8	8	100
FMC/TFM (D)	0	10	0

The difference from the known MG panel was calculated for each length by taking the NDE method lengths and subtracting the master test panel length. In this manner, the result notch length difference is positive if a length given by an NDE method that is longer than the MG panel notch length. And a notch length difference is negative if a length given by an NDE method is shorter than the MG panel notch length. Figure 28 shows the length results for each NDE method and participants. Results shown only include instances where a notch existed, was identified (true positive), and included a length measurement. From Table 7, the Notch Lengths Given column can be used to understand the underlying number of each data point that makes up each boxplot in Figure 29. For example, PAUT-OD-Raster (participant E) has a total of eight crack/notch lengths given, and there are eight points shown on the plot. The median crack/notch length difference for all NDE methods, except one, that returned crack/notch lengths was within ±0.14 inch. The NDE methods that had a median notch length difference outside ±0.14 inch were PAUT and FMC/TFM (participant A). Notably, the given notch lengths were all longer than the MG panel notch length. Further, 92.3 percent of the notch lengths are equal to or within ±0.50 inch of the MG panel notch lengths. Two NDE methods were able to score perfect results on TTCI-2, which had six notches: ET (participant C) and PECT (participant F).

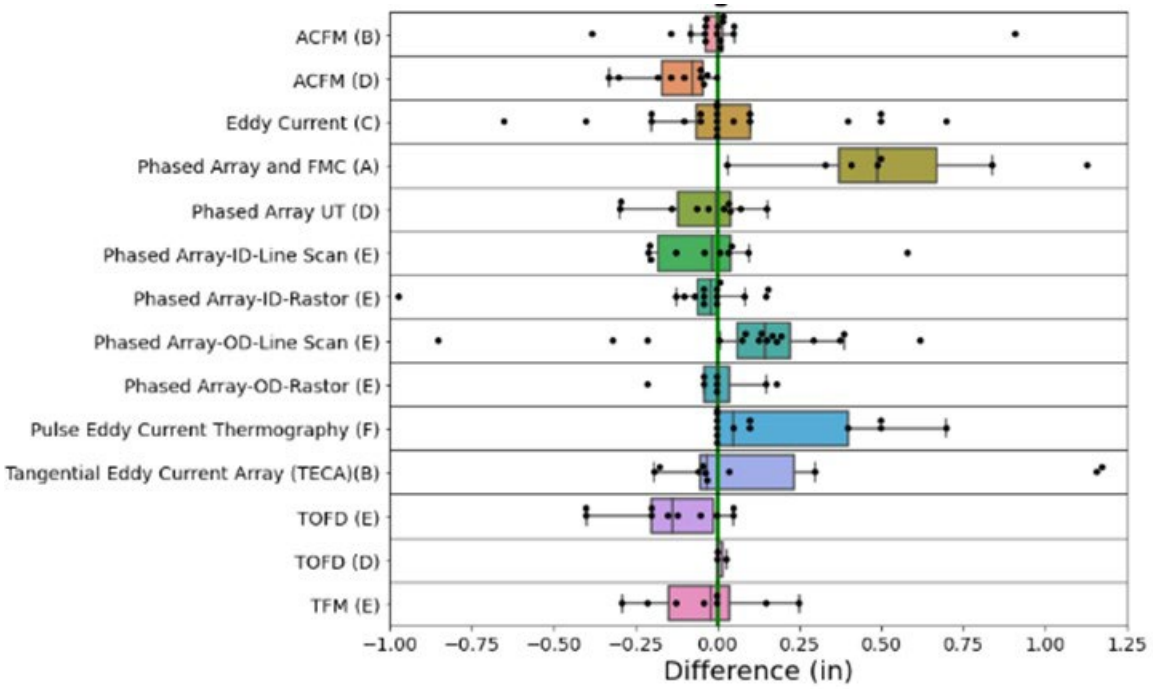

Figure 28. Crack/notch length difference by NDE method (participants)

Figure 29 shows the notch length difference results similar to Figure 28 but grouped instead by MG panel. TTCI-2 had a median closest to zero with most of the data close to the median. Most other MG panels have medians at zero difference but with more variation (larger Q25-Q75 box). The top four MG panels contained butt welds and the bottom four contained fillet welds. The largest differences for NDE methods that measured the crack long (longer than +0.5 inch) occurred for panels with butt welds. The smallest differences for NDE methods that measured the crack short (shorter than -0.5 inch) occurred on the panels with fillet welds.

Finally, Figure 30 shows master notch length versus all notch length differences. The crack size of 0.25 inch were measured longer as most notch length differences are positive. The larger notches measured short (negative notch length difference) but the sample size for them is low.

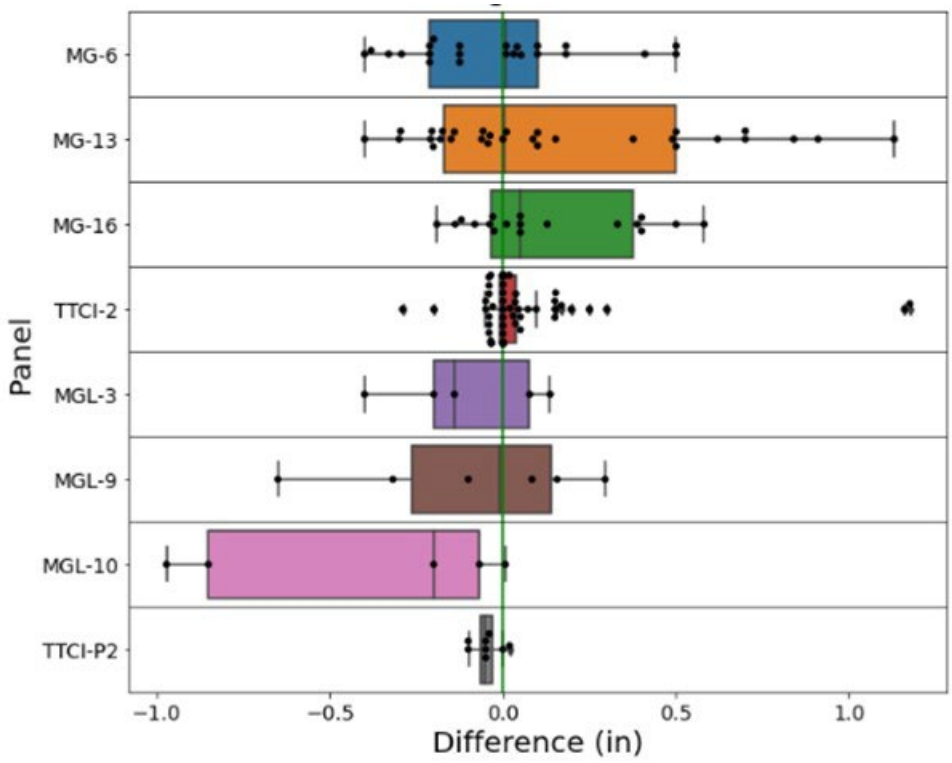

Figure 29. Crack/notch length difference by test panel

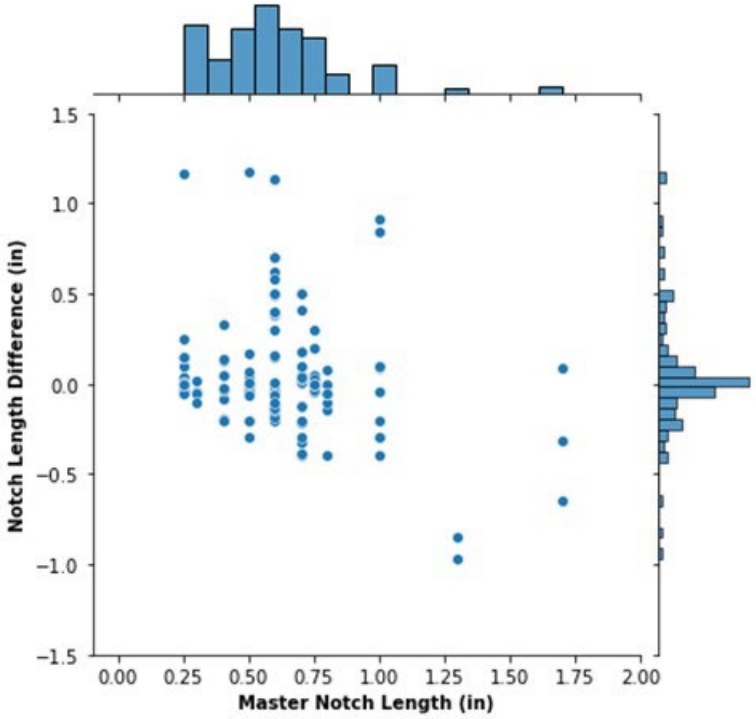

Figure 30. Master crack/notch length versus crack/notch length difference

4. Conclusions and Recommendations

Researchers, with participation from six OEMs of NDE equipment and NDE service providers, performed feasibility demonstrations of various advanced NDE methods on railroad tank car butt and fillet weld master gauge panels. Some of the advanced NDE methods considered included phased array ultrasonic testing (PAUT), full matrix capture (FMC)/ total focusing method (TFM), time of flight diffraction (TOFD), eddy current testing (ET), tangential eddy current array (TECA), alternating current field measurements (ACFM), and pulsed eddy current thermography methods (PECTA).

The team determined that advanced NDE methods could detect toe fatigue cracks with acceptable signal-to-noise ratios while demonstrating challenges in accurate flaw sizing. Researchers found that Participant F (PECT method) achieved the highest POH of 100 percent while Participant D (ACFM method) achieved the lowest POH of 57 percent, and six of the 15 advanced NDE methods had over an 80 percent POH. It should be noted that during the first trial of PECT technology, the POH obtained was only around 33 percent with one false positive. Researchers later optimized the system based on the flaw information provided to achieve 100 percent POH.

The team determined the total false positive for the fillet weld to be 33 percent and total false positive for the butt weld to be 19 percent. Researchers recommended that detailed attention and effort be made in reducing the false positive rate. Finally, the team recommended a detailed study using DOT-117 tank car plates to fully understand the extensive capabilities and limitation of the advanced NDE methods explored. The DOT-117 tank car material properties and thickness are different than the legacy tank car DOT-111A in their material thickness and properties. The team also recommended that a wide variety of weld configurations and geometry representative of the actual tank cars be considered. Exploring a robotic automated inspection of the tank car butt welds and longitudinal welds using crawler inspection robot technology performed from the inner diameter of the tank can help improve personnel safety associated with confined space.

5. References

[1] Crashworthiness Protection Requirements for Tank Cars; Detection and Repair of Cracks, Pits, Corrosion, Lining Flaws, Thermal Protection Flaws and Other Defects of Tank Car Tanks. 60 Fed. Reg. 49048 (September 21, 1995) (pt. 171, 172, 173, 179, and 180).

[2] Garcia, G. (2002). *Railroad Tank Car Nondestructive Methods Evaluation* (Report No. DOT/FRA/ORD-01/04). Federal Railroad Administration.

[3] Garcia, G., Rummel, W. D., & Gonzalez, F. (2016). *Quantitative Nondestructive Testing of Railroad Tank Cars Using the Probability of Detection Evaluation Approach* (Report No. DOT/FRA/ORD-09/1). Federal Railroad Administration.

[4] Poudel, A., Nunez, S. G., & Lindeman, B. (2021). *Analysis of Historical Non-Destructive Evaluation Probability of Detection Data for Railroad Tank Cars* (Report No. DOT/FRA/ORD-21/14). Federal Railroad Administration.

[5] Quality Assurance Program. 60 Fed. Reg. 49076. (September. 21, 1995). (49 CFR pt. 179.7).

[6] Association of American Railroad (1960). *Manual of standards and recommended practices*. AAR.

[7] Olympus (2012). NDT Field Guides: Phased Array Testing – Basic Theory for Industrial Applications, 2nd ed. Waltham, MA: Olympus.

[8] Witte, M. & Poudel, A. (2016). High-Speed Rail Flaw Detection Using Phased Array Ultrasonics. *Technology Digest, TD16-030*. AAR/TTCI.

[9] Roth, D. J., Tokars, R. P., Martin, R. E., Rauser, R. W., & Aldrin, J. C. (2009). Ultrasonic Phased Array Simulations of Welded Components at NASA. *AIP Conference Proceedings, 1096*(1), 1190-1197.

[10] Bokaba, M., Netshidavhini, N., &Mabuza, R. B. (2012) Demonstration of the Capability of Phased Array Technique for Detecting Defects in Thick-section Welds. *18th World Conference on Nondestructive Testing*, *Durban, South Africa*, *2012-07*.

[11] Ghasemi, H. (2014). Development of Phased-Array Ultrasonic Testing Acceptability Criteria (Phase I). *TechBrief-FHWA, HRT-14-074*.

[12] Birring, A. (2021). Optimizing Probe Active Aperture for Phased Array Weld Inspections. *Materials Evaluation, 79*(8), 797-804.

[13] Sundarraj, S. (2021) Advantages of Compound S-scan over Sectorial Scan or E-scan: A Case Study. *Materials Evaluation, 79*(12), 1138-1149.

[14] Diaz, A. A., Cinson, A. D., Crawford, S. L., & Anderson, M. T. (2009). An Evaluation of Ultrasonic Phased Array Testing for Reactor Piping System Components Containing Dissimilar Metal Welds (Report No. JCN N6398, Task 2A). US Nuclear Regulatory Commission/ Department of Energy.

[15] Holmes, C., Drinkwater, B. W., & Wilcox, P. D. (2005). Post-Processing of the Full Matrix of Ultrasonic Transmit–Receive Array Data for Nondestructive Evaluation. *NDT & E International, 38*(8), 701-711.

[16] Drinkwater, B. W. & Wilcox, P. D. (2006). Ultrasonic Arrays for Nondestructive Evaluation: A Review. *NDT & E International, 39*(7), 525-541.

[17] Painchaud-April, G., Badeau, N., & Lepage, B. (2018). Total Focusing Method (TFM) Robustness to Material Deviations. *AIP Conference Proceedings, 1949*(1), 200007.

[18] Spencer, R., Sunderman, R., & Todorov, E. (2018). FMC/TFM Experimental Comparisons. *AIP Conference Proceedings, 1949*(1), 020015.

[19] Ginzel, E. A., Volf, O., & B. Brown (2015). Next Generation Technology for Pipeline AUT TFM/FMC. The e-Journal of Nondestructive Testing (NDT), *20*(8).

[20] Stepinski, T. (2007). An Implementation of Synthetic Aperture Focusing Technique in Frequency Domain. *IEEE Transactions on Ultrasonics, Ferroelectrics, and Frequency Control, 54*(7), 1399-1408.

[21] Hunter, A. J., Drinkwater, B. W., & Wilcox, P. D. (2008). The Wavenumber Algorithm for Full-Matrix Imaging Using an Ultrasonic Array. *IEEE Transactions on Ultrasonics, Ferroelectrics, and Frequency Control, 55*(11), 2450-2462.

[22] Zetec Inc. (2017). Fundamental Principles of FMC and TFM Technologies in Ultrasonic Inspection. Snoqualmie, WA: Zetec Inc. (pp. 1-35).

[23] Kamalahasan, M., Vijayarekha, K., Balasubramaniam, V., & Karthik, D. (2012). Ultrasonic Time of Flight Diffraction Technique for Weld Defects: A Review. *Research Journal of Applied Sciences, Engineering and Technology, 4*(24), 5525-5533.

[24] Sania S., Ismail, M. P., Mohd, S., Masenwat, N. A., Amran, T., Amin, M., Ahmad, M. R. (2017). Design and Development of PC-based TOFD Ultrasonic Scanning System for Welds Inspection. *AIP Conference Proceedings, 1799*(1), 050015.

[25] Nath, S. K., Balasubramaniam, K., Krishnamurthy, C. V., & Narayana, B. H. (2010). Reliability Assessment of Manual Ultrasonic Time of Flight Diffraction (TOFD) Inspection for Complex Geometry Components. *NDT & E International, 43*, 152-162.

[26] Deng, Y. & Liu, X. (2011). Electromagnetic Imaging Methods for Nondestructive Evaluation Applications. *Sensors, 11*(12), 11774-11808.

[27] Tian, G. Y., Sophian, A., Taylor, D. A., & Rudlin, J. R. (2001). Electromagnetic and Eddy Current NDT: A Review. *Insight, 43*(5), 1-5.

[28] AbdAlla, A. N., Faraj, M. A., Samsuri, F,. Rifai, D., Ali, K., & Al-Douri, Y. (2018). Challenges in Improving the Performance of Eddy Current Testing: Review. *Measurement and Control, 52*(1-2), 46-64.

[29] Bailey, J., Long, N., & Hunze, A. (2017). Eddy Current Testing with Giant Magnetoresistance (GMR) Sensors and a Pipe-Encircling Excitation for Evaluation of Corrosion under Insulation. *Sensors (Basel), 17*(10).

[30] N. V. Nair, Melapudi, V. R., Jimenez, H. R., Liu, X., Deng, Y., Zeng, Z., Udpa, L., Moran, T. J., Udpa, S. S. (2006). A GMR-Based Eddy Current System for NDE of Aircraft Structures. *IEEE Transactions on Magnetics,* 42(10),3312-3314.

[31] Du, W., Nguyen, H., Dutt, A., & Scallion, K. (2010). Design of a GMR Sensor Array System for Robotic Pipe Inspection. *Sensors, 2010 IEEE*, *2010*, 2551-2554.

[32] Sambasiva Rao, K., Mahadevan, S., Purna Chandra Rao, B., & Thirunavukkarasu, S. (2018). A New Approach to Increase the Subsurface Flaw Detection Capability of Pulsed Eddy Current Technique. *Measurement, 128*, 516-526.

[33] Tian, G. Y., Sophian, A., Taylor, D., & Rudlin, J. (2005). Multiple Sensors on Pulsed Eddy-Current Detection for 3-D Subsurface Crack Assessment. *IEEE Sensors Journal, 5*(1), 90-96.

[34] Grenier, M., Demers-Carpentier, V., Rochette, M., & Hardy, F. (2016). Pulsed Eddy Current: New Developments for Corrosion Under Insulation Examinations. *19th World Conference on Non-Destructive Testing*, *Munich, Germany*, *2016-07.*

[35] Brett, C. & de Raad, J. (1996). Validation of a Pulsed Eddy Current System for Measuring Wall Thinning Through Insulation. *Proceedings of SPIE, Nondestructive Evaluation Techniques for Aging Infrastructure and Manufacturing, 2947*, 211-222.

[36] Cheng, W. (2012). Pulsed Eddy Current Testing of Carbon Steel Pipes' Wall-thinning Through Insulation and Cladding. *Journal of Nondestructive Evaluation, 31*(3), 215-224.

[37] Goldfine, N., Dunford, T., Washabaugh, A., Chaplan, S., & Diaz, K. (2019). MWM-Array and MR-MWM-Array Eddy Current Testing for Piping and Vessels. *ASNT Research Symposium*, *Los Angeles, CA*.

[38] Grimberg, R., Udpa, L., Savin, A., Steigmann, R., Palihovici, V., & Udpa, S. S. (2006). 2D Eddy Current Sensor Array. *NDT & E International, 39*(4), 264-271.

[39] Repelianto A. S. & Kasai, N. (2019). The Improvement of Flaw Detection by the Configuration of Uniform Eddy Current Probes. *Sensors, 19*(2), 397.

[40] Raude, A., Sirois, M., Lemieux, H., & Crépeau, J. (2016). Advances in Carbon Steel Weld Inspection using Tangential Eddy Current Array. *19th World Conference on Non-Destructive Testing*, *Munich, Germany, 2016-07*.

[41] Lugg M. & Smith, M. (2018). Alternating Current Field Measurement Testing. *Materials Evaluation, 76*(1), 38-47.

[42] Lugg, M. (2011). Applications of ACFM for Weld Inspection by ROV. *Singapore International NDT Conference & Exhibition*, *Singapore*.

[43] Lugg M. & Topp, D. A. (2006). Recent Developments and Applications of the ACFM Inspection Method and ACSM Stress Measurement Method. *ECNDT 2006*, *Berlin, Germany, 2006-11*.

[44] Wilson, J., Tian, G., Mukriz, I., & Almond, D. (2011). PEC Thermography for Imaging Multiple Cracks from Rolling Contact Fatigue. *NDT & E International, 44*(6),505-512.

[45] Weekes, B., Almond, D. P., Cawley, P., & Barden, T. (2012). Eddy-Current Induced Thermography - Probability of Detection Study of Small Fatigue Cracks in Steel, Titanium and Nickel-Based Superalloy. *NDT & E International, 49*, 47-56.

[46] Yin, A., Gao, B., Tian, G. Y., Woo, W. L., & Li, K. (2013). Physical Interpretation and Separation of Eddy Current Pulsed Thermography. *Journal of Applied Physics, 113*(6), 064101.

Appendix A.
DOT 111 Master Gauge (MG) Panels

This section presents the known details of the DOT-111 MG panels that were used for this study. Specifically, MT-contrast findings are presented for each of the butt weld panels and PT findings are presented for the fillet weld panels used for this study.

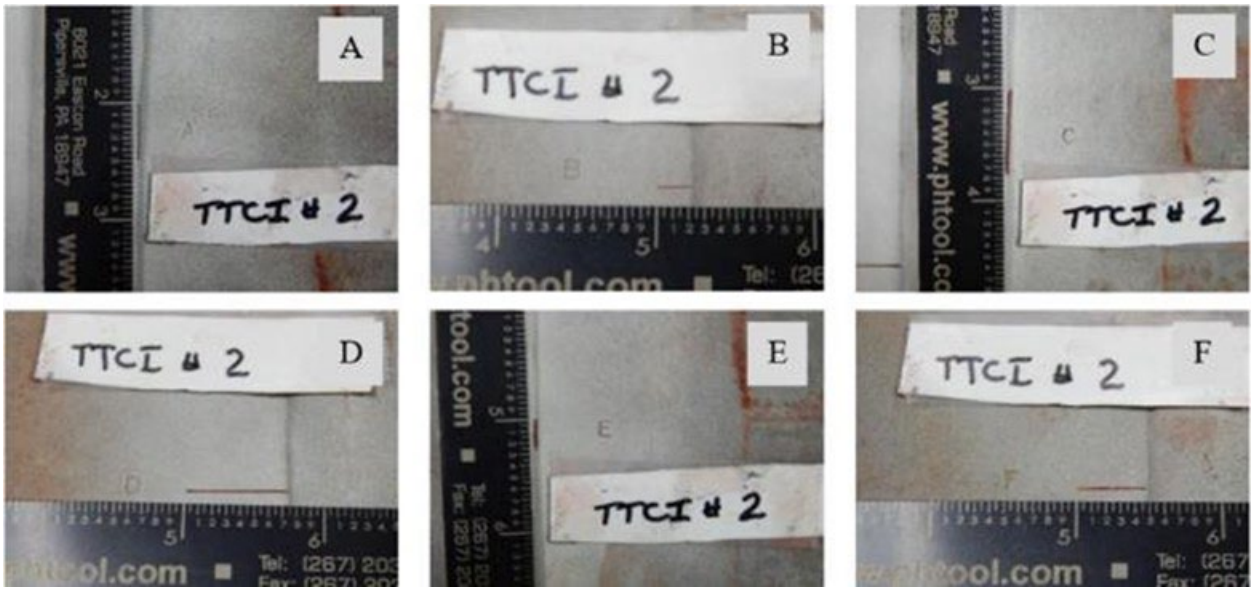

Figure 1. TTCI-2 EDM notch butt weld mg panel

Figure 2. MG-6 simulated fatigue crack butt weld panel

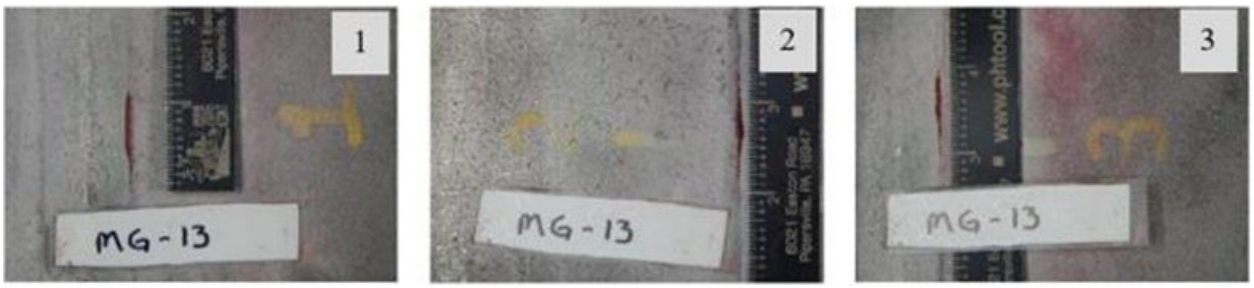

Figure 3. MG-13 simulated fatigue crack butt weld panel

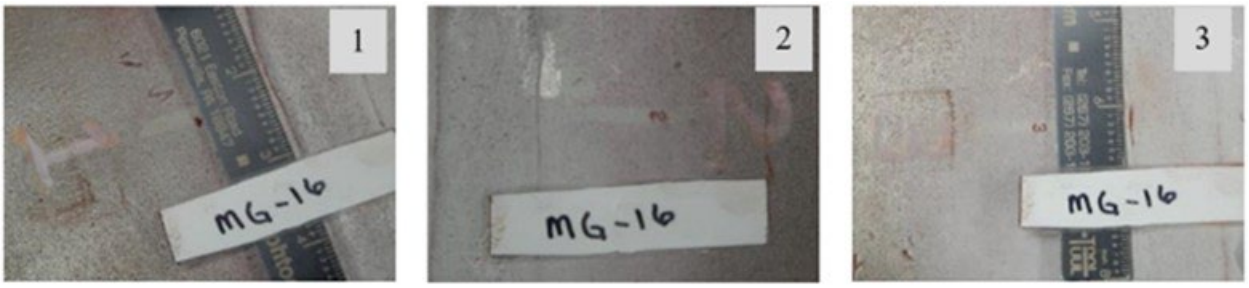

Figure 4. MG-16 simulated fatigue crack butt weld panel

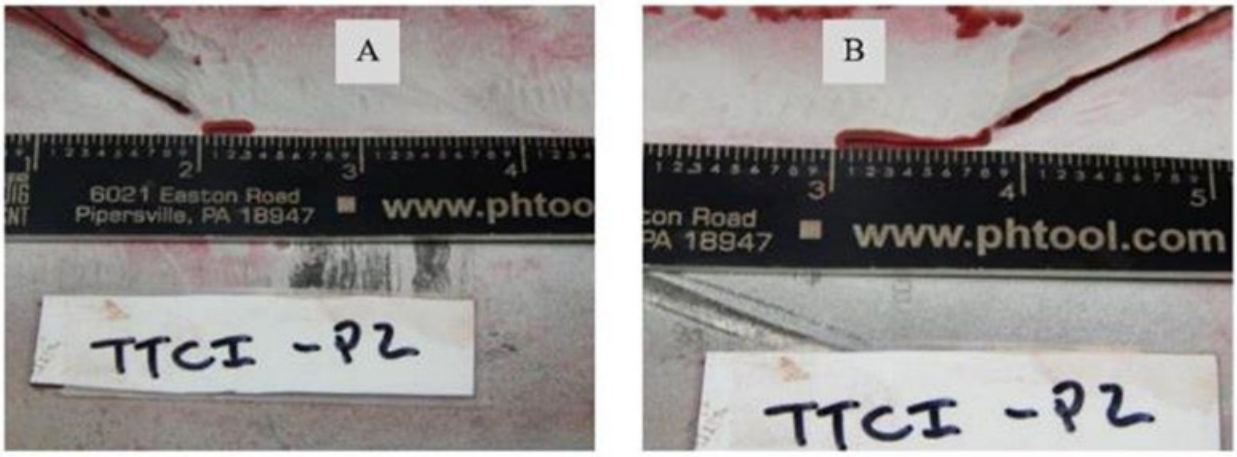

Figure 5. TTCI-P2 EDM notch fillet weld mg panel

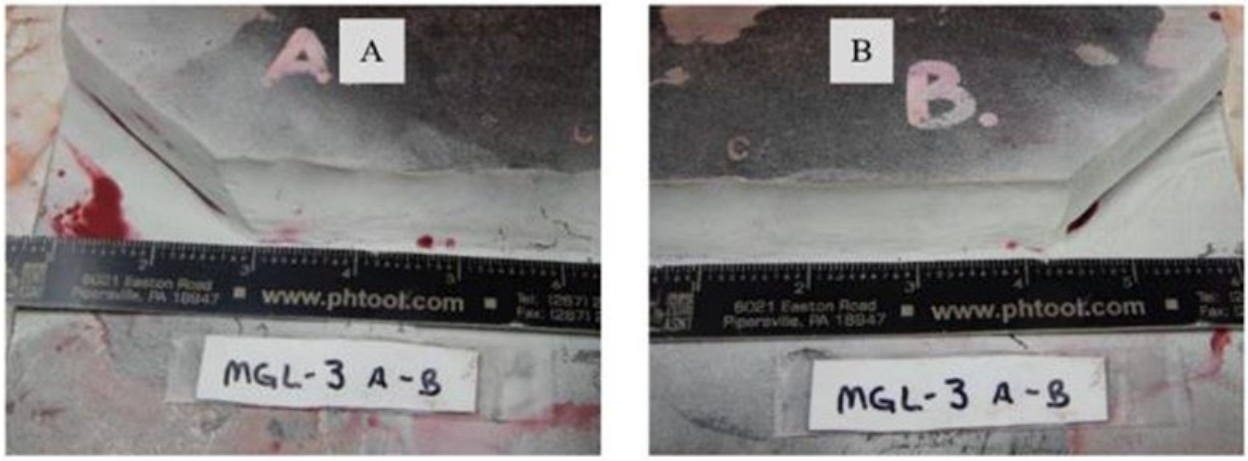

Figure 6. MGL-3-A-B simulated fatigue crack fillet weld MG panel

Figure 7. MGL-9-A-B simulated fatigue crack fillet weld MG panel

Figure 8. MGL-10-C-D simulated fatigue crack fillet weld MG panel

Appendix B.
Participants NDE Findings Summary

This section presents the details of the findings summary for each participant for the DOT-111 MG panels. As previously discussed, not all participants inspected all the fillet weld and butt weld plates. Also, not all participants reported the sizing for all plates.

Table 1. Participant "A" NDE findings summary for MG plates

MG Panel Type	Panel ID	Crack Location	NDE Method	Evaluation Result	Length Measured (in.)	Height (in.)	Master Crack Length (in.)	Difference (in.)
BW	MG-6	1	PAUT and FMC/TFM	True Positive	0.731	0.144	0.7	0.031
BW	MG-6	2	PAUT and FMC/TFM	True Positive	1.11	0.213	0.7	0.41
BW	MG-6	3	PAUT and FMC/TFM	False Positive	0.807	0.285	0	0.807
BW	MG-13	1	PAUT and FMC/TFM	True Positive	1.09	0.226	0.6	0.49
BW	MG-13	2	PAUT and FMC/TFM	True Positive	1.73	0.238	0.6	1.13
BW	MG-13	3	PAUT and FMC/TFM	True Positive	1.84	0.183	1	0.84
BW	MG-16	1	PAUT and FMC/TFM	True Positive	1.1	0.131	0.6	0.5
BW	MG-16	2	PAUT and FMC/TFM	False Negative	0.5	0.246	0	0.5
BW	MG-16	3	PAUT and FMC/TFM	True Positive	0.731	0.109	0.4	0.331
BW	TTCI-3	A	PAUT and FMC/TFM	True Positive	0.821	0.226	0.5	0.321
BW	TTCI-3	C	PAUT and FMC/TFM	True Positive	0.966	0.308	0.75	0.216
BW	TTCI-3	E	PAUT and FMC/TFM	True Positive	0.49	0.204	0.25	0.24
FW	MGL-3	A	PAUT and FMC/TFM	True Positive	Not Reported	1.82	N/A	N/A
FW	MGL-3	B	PAUT and FMC/TFM	True Positive	Not Reported	1.09	N/A	N/A
FW	MGL-9	A	PAUT and FMC/TFM	True Positive	Not Reported	2.52	N/A	N/A
FW	MGL-9	B	PAUT and FMC/TFM	True Positive	Not Reported	1.92	N/A	N/A
FW	MGL-10	C	PAUT and FMC/TFM	True Positive	Not Reported	1.32	N/A	N/A
FW	MGL-10	D	PAUT and FMC/TFM	True Positive	Not Reported	1.82	N/A	N/A
FW	TTCI-P2	A	PAUT and FMC/TFM	True Positive	Not Reported	3.28	N/A	N/A
FW	TTCI-P2	B	PAUT and FMC/TFM	True Positive	Not Reported	3.51	N/A	N/A

Table 2. Participant "B" NDE findings summary for MG plates

MG Panel Type	Panel ID	Crack Location	NDE Method	Evaluation Result	Length Measured (in.)	Master Crack Length (in.)	Difference (in.)
BW	MG-6	1	ACFM	True Positive	0.319	0.7	-0.381
BW	MG-6	2	ACFM	True Positive	0.752	0.7	0.052
BW	MG-6	3	ACFM	False Positive	0.465	0	0.465
BW	MG-6	1	TECA	False Negative		0.7	-0.7
BW	MG-6	2	TECA	False Negative		0.7	-0.7
BW	MG-6	3	TECA	True Negative			
BW	MG-13	1	ACFM	True Positive	0.563	0.6	-0.037
BW	MG-13	2	ACFM	True Positive	0.61	0.6	0.01
BW	MG-13	3	ACFM	True Positive	1.91	1	0.91
BW	MG-13	1	TECA	True Positive	0.425	0.6	-0.175
BW	MG-13	2	TECA	True Positive	0.543	0.6	-0.057
BW	MG-13	3	TECA	True Positive	0.957	1	-0.043
BW	MG-16	1	ACFM	True Positive	0.61	0.6	0.01
BW	MG-16	2	ACFM	True Negative			
BW	MG-16	3	ACFM	True Positive	0.319	0.4	-0.081
BW	MG-16	1	TECA	False Negative		0.6	-0.6
BW	MG-16	2	TECA	False Positive	0.366	0	0.366
BW	MG-16	3	TECA	True Positive	0.209	0.4	-0.191
BW	TTCI-2	A	ACFM	True Positive	0.465	0.5	-0.035
BW	TTCI-2	B	ACFM	True Positive	0.217	0.25	-0.033
BW	TTCI-2	C	ACFM	True Positive	0.752	0.75	0.002
BW	TTCI-2	D	ACFM	True Positive	0.8	0.75	0.05
BW	TTCI-2	E	ACFM	True Positive	0.268	0.25	0.018
BW	TTCI-2	F	ACFM	True Positive	0.465	0.5	-0.035
BW	TTCI-2	A	TECA	True Positive	0.465	0.5	-0.035
BW	TTCI-2	B	TECA	True Positive	1.409	0.25	1.159
BW	TTCI-2	C	TECA	True Positive	0.72	0.75	-0.03
BW	TTCI-2	D	TECA	True Positive	1.049	0.75	0.299
BW	TTCI-2	E	TECA	True Positive	0.287	0.25	0.037
BW	TTCI-2	F	TECA	True Positive	1.675	0.5	1.175
FW	MGL-3	A	ACFM	True Positive	0.66	0.8	-0.14
FW	MGL-3	B	ACFM	False Negative		0.4	-0.4
FW	MGL-3	A	TECA	False Negative		0.8	-0.8
FW	MGL-3	B	TECA	False Negative		0.4	-0.4
FW	MGL-9	A	ACFM	False Negative		0.6	-0.6

MG Panel Type	Panel ID	Crack Location	NDE Method	Evaluation Result	Length Measured (in.)	Master Crack Length (in.)	Difference (in.)
FW	MGL-9	B	ACFM	False Negative		1.7	-1.7
FW	TTCI-P2	A	ACFM	True Positive	0.319	0.3	0.019
FW	TTCI-P2	B	ACFM	True Positive	0.8	0.8	0

Table 3. Participant "C" NDE findings summary for MG plates

MG Panel Type	Panel ID	Crack Location	NDE Method	Evaluation Result	Length Measured (in.)	Master Crack Length (in.)	Difference (in.)
BW	MG-6	1	ET	True Positive	0.8	0.7	0.1
BW	MG-6	2	ET	True Positive	1.2	0.7	0.5
BW	MG-6	3	ET	False Negative			
BW	MG-13	1	ET	True Positive	1.1	0.6	0.5
BW	MG-13	2	ET	True Positive	1.3	0.6	0.7
BW	MG-13	3	ET	True Positive	1.1	1	0.1
BW	MG-16	1	ET	True Positive	1	0.6	0.4
BW	MG-16	2	ET	True Negative			
BW	MG-16	3	ET	True Positive	0.45	0.4	0.05
BW	TTCI-2	A	ET	True Positive	0.5	0.5	0
BW	TTCI-2	B	ET	True Positive	0.25	0.25	0
BW	TTCI-2	C	ET	True Positive	0.75	0.75	0
BW	TTCI-2	D	ET	True Positive	0.75	0.75	0
BW	TTCI-2	E	ET	True Positive	0.25	0.25	0
BW	TTCI-2	F	ET	True Positive	0.5	0.5	0
FW	MGL-3	A	ET	True Positive	0.4	0.8	-0.4
FW	MGL-3	B	ET	True Positive	0.2	0.4	-0.2
FW	MGL-9	A	ET	True Positive	0.5	0.6	-0.1
FW	MGL-9	B	ET	True Positive	1.05	1.7	-0.65
FW	MGL-10	C	ET	True Positive	0.3	0.5	-0.2
FW	MGL-10	D	ET	False Negative		1.3	-1.3
FW	TTCI-P2	A	ET	True Positive	0.25	0.3	-0.05
FW	TTCI-P2	B	ET	True Positive	0.75	0.8	-0.05

Table 4. Participant "D" NDE findings summary for MG plates

MG Panel Type	Panel ID	Crack Location	NDE Method	Evaluation Result	Length Measured (in.)	Master Crack Length (in.)	Difference (in.)
BW	MG-6	1	ACFM	False Negative		0.7	-0.7

MG Panel Type	Panel ID	Crack Location	NDE Method	Evaluation Result	Length Measured (in.)	Master Crack Length (in.)	Difference (in.)
BW	MG-6	2	ACFM	True Positive	0.37	0.7	-0.33
BW	MG-6	3	ACFM	True Positive	0.46	0	0.46
BW	MG-6	1	PAUT	True Positive	0.407	0.7	-0.293
BW	MG-6	2	PAUT	True Positive	0.741	0.7	0.041
BW	MG-6	3	PAUT	True Positive	0.261	0	0.261
BW	MG-6	1	TOFD	False Negative		0.7	-0.7
BW	MG-6	2	TOFD	False Negative		0.7	-0.7
BW	MG-6	3	TOFD	True Negative			
BW	MG-6	1	FMC/TFM	True Positive			
BW	MG-6	2	FMC/TFM	True Positive			
BW	MG-6	3	FMC/TFM	False Positive			
BW	MG-13	1	ACFM	True Positive	0.42	0.6	-0.18
BW	MG-13	2	ACFM	True Positive	0.46	0.6	-0.14
BW	MG-13	3	ACFM	True Positive	0.7	1	-0.3
BW	MG-13	1	PAUT	True Positive	0.539	0.6	-0.061
BW	MG-13	2	PAUT	True Positive	0.752	0.6	0.152
BW	MG-13	3	PAUT	True Positive	0.704	1	-0.296
BW	MG-13	1	TOFD	False Negative		0.6	-0.6
BW	MG-13	2	TOFD	False Negative		0.6	-0.6
BW	MG-13	3	TOFD	False Negative		1	-1
BW	MG-13	1	FMC/TFM	True Positive			
BW	MG-13	2	FMC/TFM	True Positive			
BW	MG-13	3	FMC/TFM	True Positive			
BW	MG-16	1	ACFM	False Negative		0.6	-0.6
BW	MG-16	2	ACFM	False Positive	0.22	0	0.22
BW	MG-16	3	ACFM	True Positive	0.37	0.4	-0.03
BW	MG-16	1	PAUT	True Positive	0.462	0.6	-0.138
BW	MG-16	2	PAUT	False Positive	0.752	0	0.752
BW	MG-16	3	PAUT	True Positive	0.374	0.4	-0.026
BW	MG-16	1	TOFD	False Negative		0.6	-0.6
BW	MG-16	2	TOFD	True Negative			
BW	MG-16	3	TOFD	False Negative		0.4	-0.4
BW	MG-16	1	FMC/TFM	True Positive			
BW	MG-16	2	FMC/TFM	False Positive			
BW	MG-16	3	FMC/TFM	True Positive			
BW	TTCI-2	A	ACFM	True Positive	0.46	0.5	-0.04

MG Panel Type	Panel ID	Crack Location	NDE Method	Evaluation Result	Length Measured (in.)	Master Crack Length (in.)	Difference (in.)
BW	TTCI-2	B	ACFM	True Positive			
BW	TTCI-2	C	ACFM	True Positive	0.75	0.75	0
BW	TTCI-2	D	ACFM	True Positive			
BW	TTCI-2	E	ACFM	True Positive	0.2	0.25	-0.05
BW	TTCI-2	F	ACFM	True Positive			
BW	TTCI-2	A	PAUT	True Positive	0.572	0.5	0.072
BW	TTCI-2	C	PAUT	True Positive	0.771	0.75	0.021
BW	TTCI-2	E	PAUT	True Positive	0.286	0.25	0.036
BW	TTCI-2	A	TOFD	True Positive	0.501	0.5	0.001
BW	TTCI-2	B	TOFD	True Positive			
BW	TTCI-2	C	TOFD	True Positive	0.779	0.75	0.029
BW	TTCI-2	D	TOFD	True Positive			
BW	TTCI-2	E	TOFD	True Positive	0.252	0.25	0.002
BW	TTCI-2	F	TOFD	True Positive			
BW	TTCI-2	A	FMC/TFM	True Positive			
BW	TTCI-2	B	FMC/TFM	False Negative			
BW	TTCI-2	C	FMC/TFM	True Positive			
BW	TTCI-2	D	FMC/TFM	False Negative			
BW	TTCI-2	E	FMC/TFM	True Positive			
BW	TTCI-2	F	FMC/TFM	False Negative			
FW	MGL-3	A	ACFM	False Negative		0.8	-0.8
FW	MGL-3	B	ACFM	False Negative		0.4	-0.4
FW	MGL-9	A	ACFM	False Negative		0.6	-0.6
FW	MGL-9	B	ACFM	False Negative		1.7	-1.7
FW	MGL-10	C	ACFM	False Negative		0.5	-0.5
FW	MGL-10	D	ACFM	False Negative		1.3	-1.3
FW	TTCI-P2	A	ACFM	True Positive	0.2	0.3	-0.1
FW	TTCI-P2	B	ACFM	True Positive	0.75	0.8	-0.05

Table 5. Participant "E" NDE findings summary for MG plates

MG Panel Type	Panel ID	Crack Location	NDE Method	Evaluation Result	Length Measured (in.)	Master Crack Length (in.)	Difference (in.)
BW	MG-6	1	PAUT-OD	True Positive	0.488	0.7	-0.212
BW	MG-6	2	PAUT-OD	True Positive	0.882	0.7	0.182
BW	MG-6	3	PAUT-OD	False Positive	0.68	0	0.68
BW	MG-6	1	PAUT-ID	True Positive	0.575	0.7	-0.125

MG Panel Type	Panel ID	Crack Location	NDE Method	Evaluation Result	Length Measured (in.)	Master Crack Length (in.)	Difference (in.)
BW	MG-6	2	PAUT-ID	True Positive	0.709	0.7	0.009
BW	MG-6	3	PAUT-ID	False Positive	0.354	0	0.354
BW	MG-6	1	PAUT-OD-Raster	True Positive	0.488	0.7	-0.212
BW	MG-6	2	PAUT-OD-Raster	True Positive	0.882	0.7	0.182
BW	MG-6	3	PAUT-OD-Raster	False Positive	0.68	0	0.68
BW	MG-6	1	PAUT-ID-Raster	True Positive	0.575	0.7	-0.125
BW	MG-6	2	PAUT-ID-Raster	True Positive	0.709	0.7	0.009
BW	MG-6	3	PAUT-ID-Raster	False Positive	0.354	0	0.354
BW	MG-6	1	FMC/TFM	True Positive	0.575	0.7	-0.125
BW	MG-6	2	FMC/TFM	True Positive	0.488	0.7	-0.212
BW	MG-6	3	FMC/TFM	False Positive	0.575	0	0.575
BW	MG-6	1	TOFD	True Positive	0.3	0.7	-0.4
BW	MG-6	2	TOFD	True Positive	0.5	0.7	-0.2
BW	MG-6	3	TOFD	False Positive	0.25	0	0.25
BW	MG-13	1	PAUT-OD	True Positive	0.976	0.6	0.376
BW	MG-13	2	PAUT-OD	True Positive	1.22	0.6	0.62
BW	MG-13	3	PAUT-OD	True Positive	1.087	1	0.087
BW	MG-13	1	PAUT-ID	True Positive	0.399	0.6	-0.201
BW	MG-13	2	PAUT-ID	True Positive	0.391	0.6	-0.209
BW	MG-13	3	PAUT-ID	True Positive	0.795	1	-0.205
BW	MG-13	1	PAUT-OD-Raster	False Negative		0.6	-0.6
BW	MG-13	2	PAUT-OD-Raster	False Negative		0.6	-0.6
BW	MG-13	3	PAUT-OD-Raster	False Negative		1	-1
BW	MG-13	1	PAUT-ID-Raster	False Negative		0.6	-0.6
BW	MG-13	2	PAUT-ID-Raster	False Negative		0.6	-0.6
BW	MG-13	3	PAUT-ID-Raster	False Negative		1	-1
BW	MG-13	1	FMC/TFM	False Negative		0.6	-0.6
BW	MG-13	2	FMC/TFM	False Negative		0.6	-0.6
BW	MG-13	3	FMC/TFM	False Negative		1	-1
BW	MG-13	1	TOFD	True Positive	0.45	0.6	-0.15
BW	MG-13	2	TOFD	True Positive	0.6	0.6	0

MG Panel Type	Panel ID	Crack Location	NDE Method	Evaluation Result	Length Measured (in.)	Master Crack Length (in.)	Difference (in.)
BW	MG-13	3	TOFD	True Positive	0.6	1	-0.4
BW	MG-16	1	PAUT-OD	True Positive	0.988	0.6	0.388
BW	MG-16	2	PAUT-OD	False Negative	0.361	0	0.361
BW	MG-16	3	PAUT-OD	True Positive	0.528	0.4	0.128
BW	MG-16	1	PAUT-ID	True Positive	1.181	0.6	0.581
BW	MG-16	2	PAUT-ID	False Negative	0.425	0	0.425
BW	MG-16	3	PAUT-ID	True Positive	0.362	0.4	-0.038
BW	MG-16	1	PAUT-OD-Raster	False Negative		0.6	-0.6
BW	MG-16	2	PAUT-OD-Raster	True Negative			
BW	MG-16	3	PAUT-OD-Raster	False Negative		0.4	-0.4
BW	MG-16	1	PAUT-ID-Raster	False Negative		0.6	-0.6
BW	MG-16	2	PAUT-ID-Raster	True Negative			
BW	MG-16	3	PAUT-ID-Raster	False Negative		0.4	-0.4
BW	MG-16	1	FMC/TFM	False Negative		0.6	-0.6
BW	MG-16	2	FMC/TFM	True Negative			
BW	MG-16	3	FMC/TFM	False Negative		0.4	-0.4
BW	MG-16	1	TOFD	True Positive	0.48	0.6	-0.12
BW	MG-16	2	TOFD	False Positive	0.88	0	0.88
BW	MG-16	3	TOFD	True Positive	0.45	0.4	0.05
BW	TTCI-2	A	PAUT-OD	True Positive	0.669	0.5	0.169
BW	TTCI-2	B	PAUT-OD	False Negative		0.25	-0.25
BW	TTCI-2	C	PAUT-OD	True Positive	0.946	0.75	0.196
BW	TTCI-2	D	PAUT-OD	False Negative		0.75	-0.75
BW	TTCI-2	E	PAUT-OD	True Positive	0.402	0.25	0.152
BW	TTCI-2	F	PAUT-OD	False Negative		0.5	-0.5
BW	TTCI-2	A	PAUT-ID	True Positive	0.535	0.5	0.035
BW	TTCI-2	B	PAUT-ID	False Negative		0.25	-0.25
BW	TTCI-2	C	PAUT-ID	True Positive	0.795	0.75	0.045
BW	TTCI-2	D	PAUT-ID	False Negative		0.75	-0.75
BW	TTCI-2	E	PAUT-ID	True Positive	0.346	0.25	0.096
BW	TTCI-2	F	PAUT-ID	False Negative		0.5	-0.5
BW	TTCI-2	A	PAUT-OD-Raster	True Positive	0.5	0.5	0
BW	TTCI-2	B	PAUT-OD-Raster	True Positive	0.21	0.25	-0.04

MG Panel Type	Panel ID	Crack Location	NDE Method	Evaluation Result	Length Measured (in.)	Master Crack Length (in.)	Difference (in.)
BW	TTCI-2	C	PAUT-OD-Raster	True Positive	0.71	0.75	-0.04
BW	TTCI-2	D	PAUT-OD-Raster	True Positive	0.75	0.75	0
BW	TTCI-2	E	PAUT-OD-Raster	True Positive	0.4	0.25	0.15
BW	TTCI-2	F	PAUT-OD-Raster	True Positive	0.5	0.5	0
BW	TTCI-2	A	PAUT-ID-Raster	True Positive	0.5	0.5	0
BW	TTCI-2	B	PAUT-ID-Raster	True Positive	0.21	0.25	-0.04
BW	TTCI-2	C	PAUT-ID-Raster	True Positive	0.71	0.75	-0.04
BW	TTCI-2	D	PAUT-ID-Raster	True Positive	0.75	0.75	0
BW	TTCI-2	E	PAUT-ID-Raster	True Positive	0.4	0.25	0.15
BW	TTCI-2	F	PAUT-ID-Raster	True Positive	0.5	0.5	0
BW	TTCI-2	A	FMC/TFM	True Positive	0.21	0.5	-0.29
BW	TTCI-2	B	FMC/TFM	True Positive	0.5	0.25	0.25
BW	TTCI-2	C	FMC/TFM	True Positive	0.71	0.75	-0.04
BW	TTCI-2	D	FMC/TFM	True Positive	0.75	0.75	0
BW	TTCI-2	E	FMC/TFM	True Positive	0.4	0.25	0.15
BW	TTCI-2	F	FMC/TFM	True Positive	0.5	0.5	0
BW	TTCI-2	A	TOFD	True Positive	0.3	0.5	-0.2
BW	TTCI-2	B	TOFD	True Positive			
BW	TTCI-2	C	TOFD	True Positive	0.8	0.75	0.05
BW	TTCI-2	D	TOFD	True Positive			
BW	TTCI-2	E	TOFD	True Positive	0.2	0.25	-0.05
BW	TTCI-2	F	TOFD	True Positive			
FW	MGL-3	A	PAUT-OD	True Positive	0.877	0.8	0.077
FW	MGL-3	B	PAUT-OD	True Positive	0.536	0.4	0.136
FW	MGL-9	A	PAUT-OD	True Positive	0.895	0.6	0.295
FW	MGL-9	B	PAUT-OD	True Positive	1.382	1.7	-0.318
FW	MGL-9	A	PAUT-ID-Raster	True Positive	0.756	0.6	0.156
FW	MGL-9	B	PAUT-ID-Raster	True Positive	1.784	1.7	0.084
FW	MGL-10	C	PAUT-OD	True Positive	0.507	0.5	0.007
FW	MGL-10	D	PAUT-OD	True Positive	0.449	1.3	-0.851
FW	MGL-10	C	PAUT-ID-Raster	True Positive	0.432	0.5	-0.068

MG Panel Type	Panel ID	Crack Location	NDE Method	Evaluation Result	Length Measured (in.)	Master Crack Length (in.)	Difference (in.)
FW	MGL-10	D	PAUT-ID-Raster	True Positive	0.328	1.3	-0.972
FW	TTCI-P2	A	PAUT-ID	False Negative		0.3	-0.3
FW	TTCI-P2	B	PAUT-ID	False Negative		0.8	-0.8
FW	TTCI-P2	A	PAUT-OD	False Negative		0.3	-0.3
FW	TTCI-P2	B	PAUT-OD	False Negative		0.8	-0.8
FW	TTCI-P2	A	PAUT-ID-Raster	True Positive	0.26	0.3	-0.04
FW	TTCI-P2	B	PAUT-ID-Raster	True Positive	0.7	0.8	-0.1

Table 6. Participant "F" NDE findings summary for MG plates

MG Panel Type	Panel ID	Crack Location	NDE Method	Evaluation Result	Length Measured (in.)	Master Crack Length (in.)	Difference (in.)
BW	MG-6	1	PECT	True Positive	0.8	0.7	0.1
BW	MG-6	2	PECT	True Positive	1.2	0.7	0.5
BW	MG-6	3	PECT	True Negative			
BW	MG-13	1	PECT	True Positive	1.1	0.6	0.5
BW	MG-13	2	PECT	True Positive	1.3	0.6	0.7
BW	MG-13	3	PECT	True Positive	1.1	1	0.1
BW	MG-16	1	PECT	True Positive	1	0.6	0.4
BW	MG-16	2	PECT	True Negative			
BW	MG-16	3	PECT	True Positive	0.45	0.4	0.05
BW	TTCI-2	A	PECT	True Positive	0.5	0.5	0
BW	TTCI-2	B	PECT	True Positive	0.25	0.25	0
BW	TTCI-2	C	PECT	True Positive	0.75	0.75	0
BW	TTCI-2	D	PECT	True Positive	0.75	0.75	0
BW	TTCI-2	E	PECT	True Positive	0.25	0.25	0
BW	TTCI-2	F	PECT	True Positive	0.5	0.5	0

Appendix C.
Participants NDE Results

This section presents the NDE results of each participant for the DOT-111 MG panels. As previously discussed, not all participants inspected all the fillet weld and butt weld plates. Also, not all participants reported the sizing for all plates.

Participant A

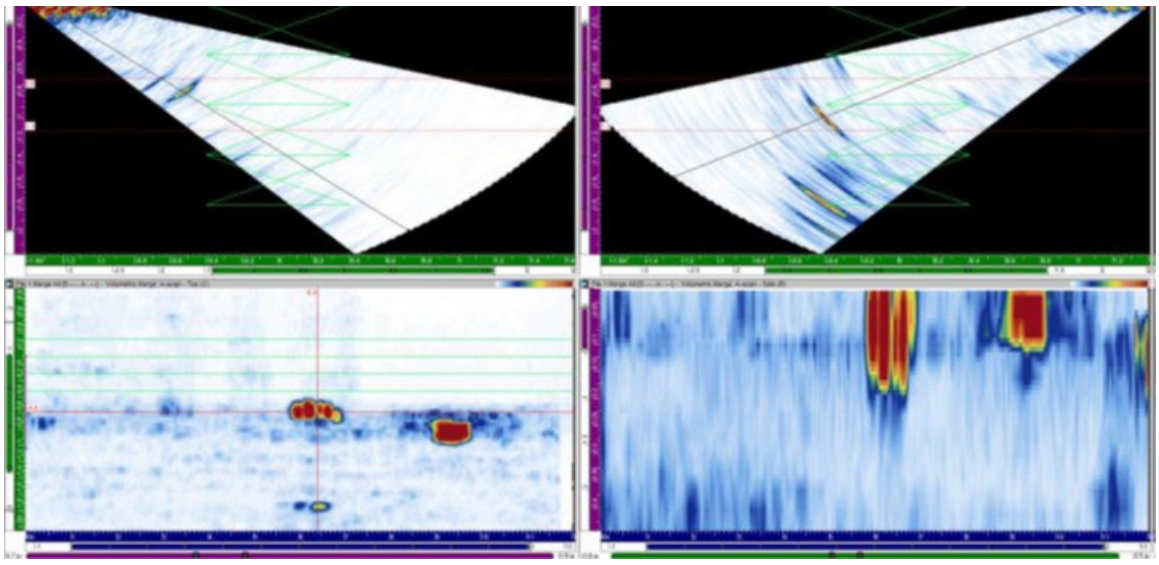

Figure 1. PAUT results showing flaw indications in the MG-6 butt weld test panel

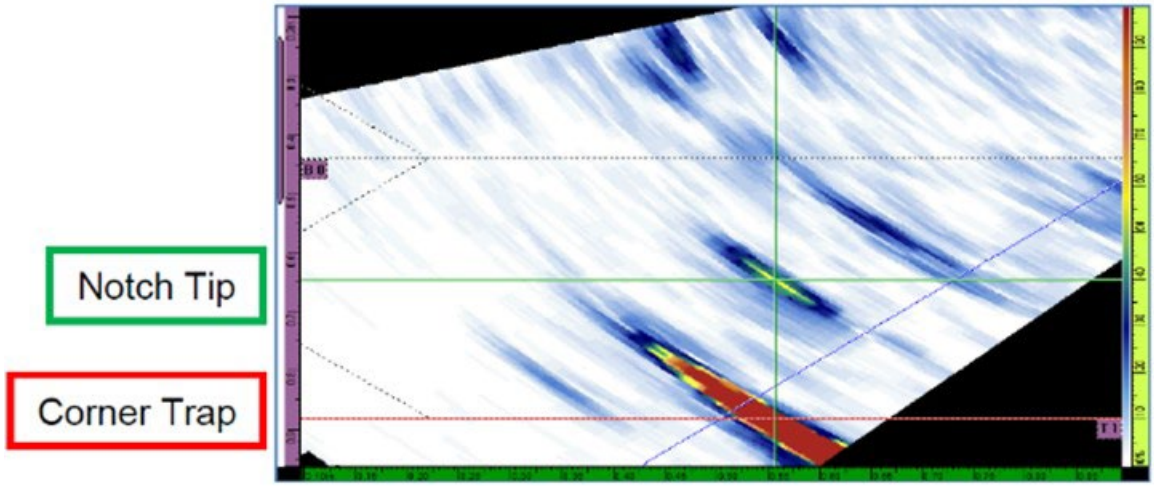

Figure 2. Height measurement of the Flaw D in TTCI-2 MG butt weld test panel

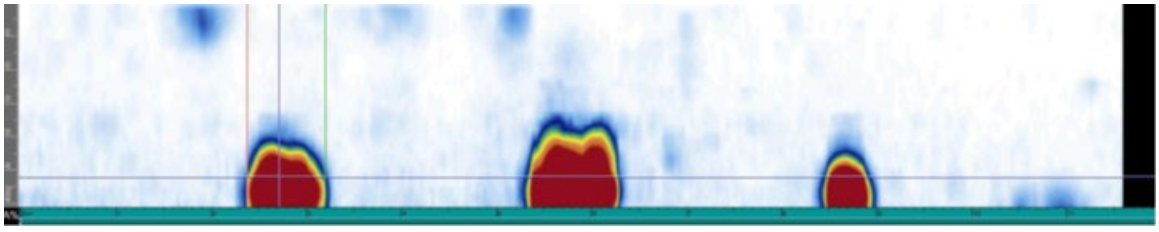

Figure 3. Length measurement of the Flaw D in TTCI-2 MG butt weld test panel

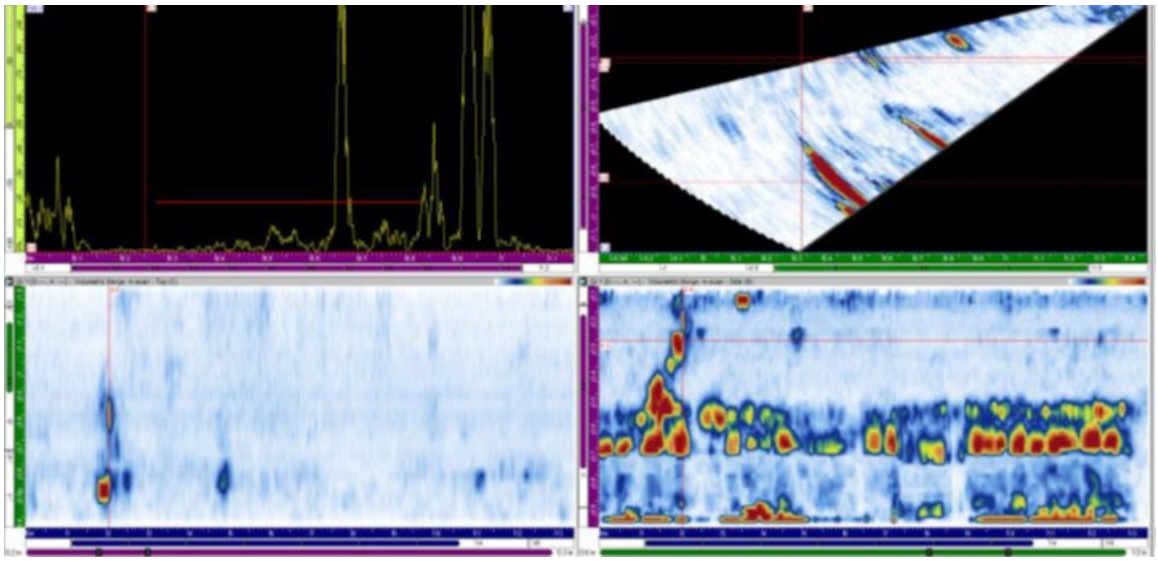

Figure 4. PAUT Results showing flaw indications in the MGL-3 fillet weld test panel

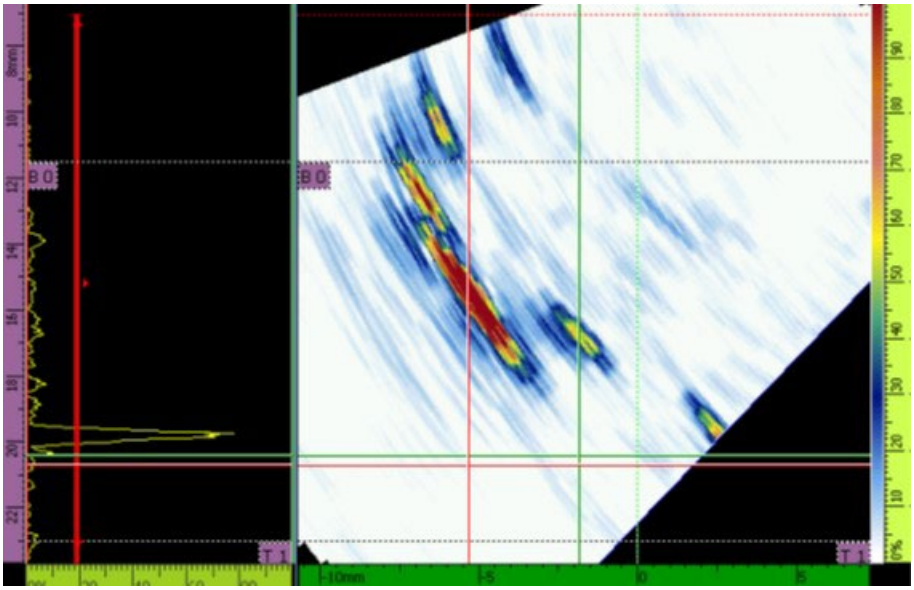

Figure 5. Height measurement of the Flaw B in TTCI P2 fillet weld test panel

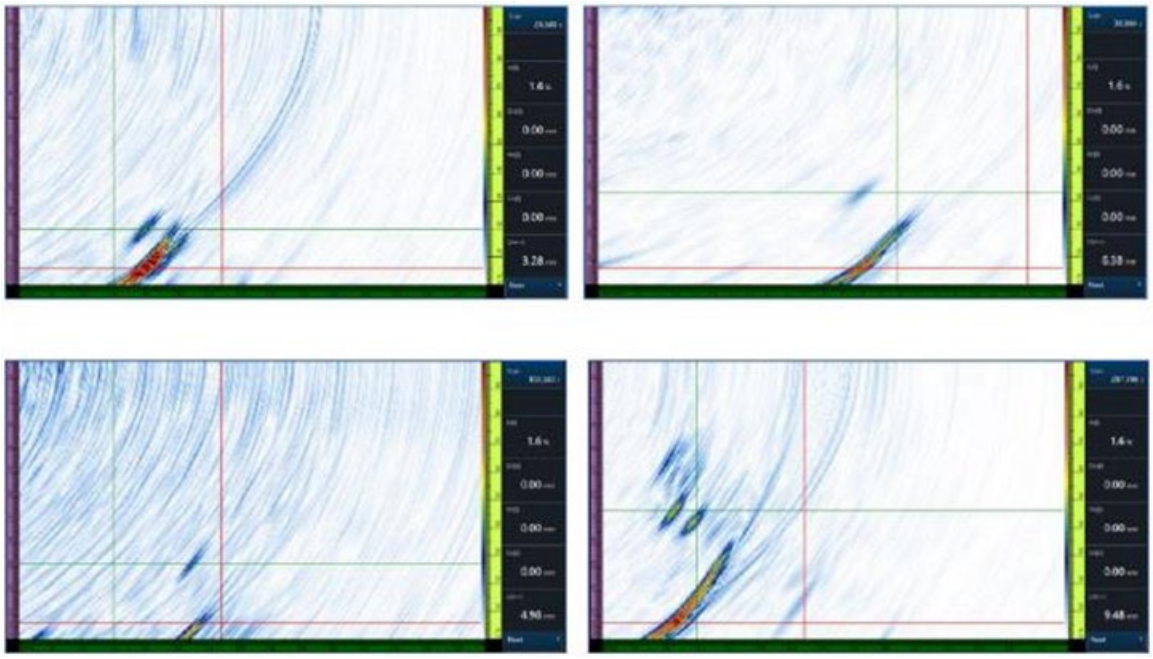

Figure 6. FMC/TFM Results showing the indication of the embedded defects in different test panels

Participant B

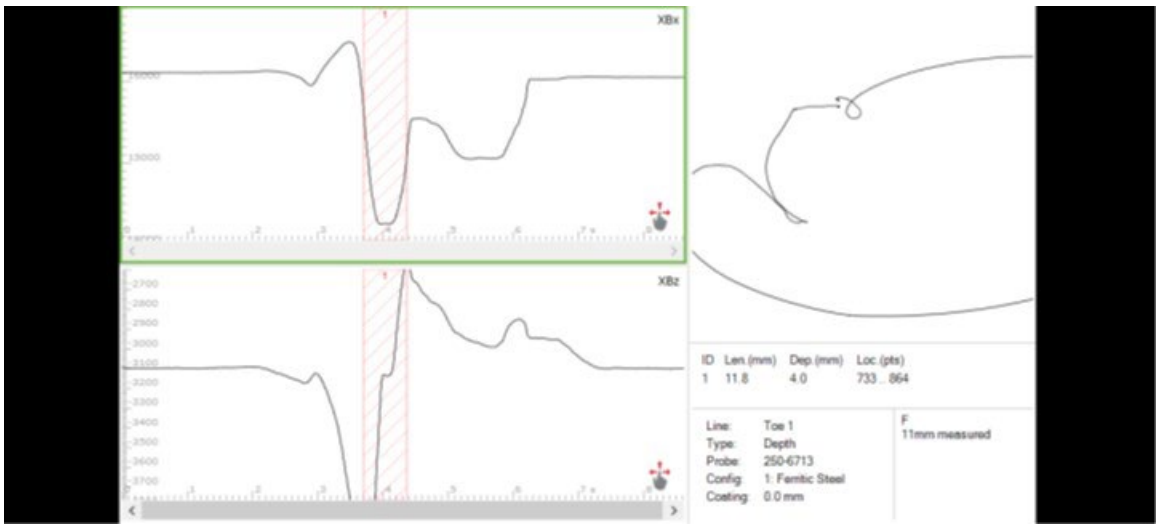

Figure 7. ACFM scan data of Flaw 1 for TTCI-2 butt weld MG panel

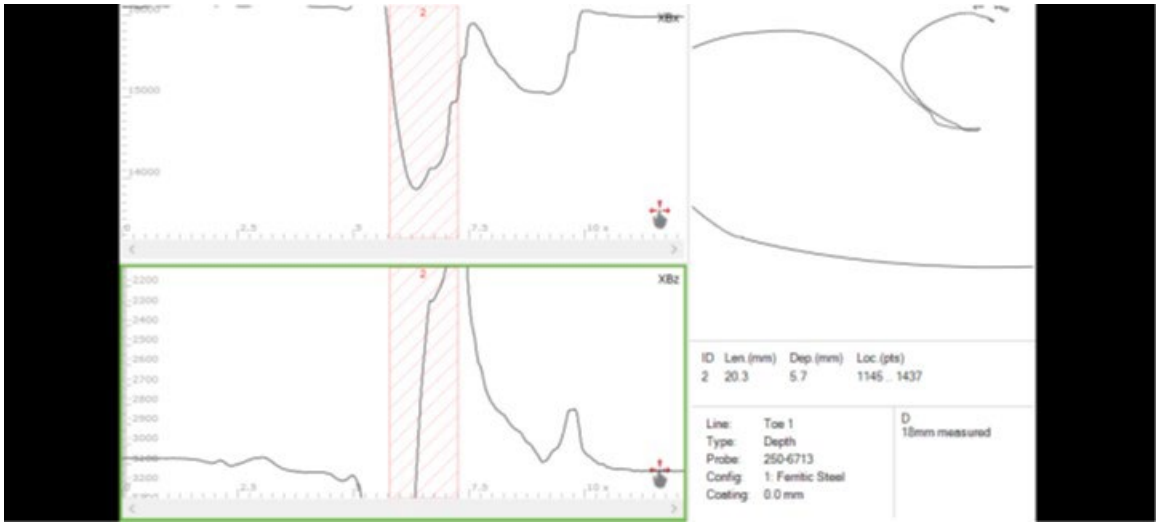

Figure 8. ACFM scan data of Flaw 2 for TTCI-2 butt weld MG panel

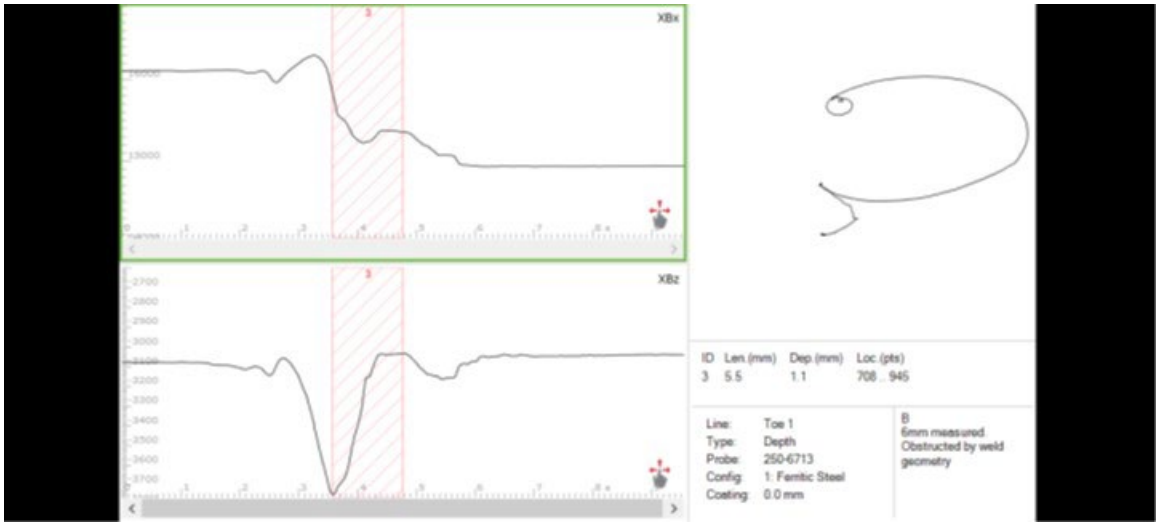

Figure 9. ACFM scan data of Flaw 3 for TTCI-2 butt weld MG panel

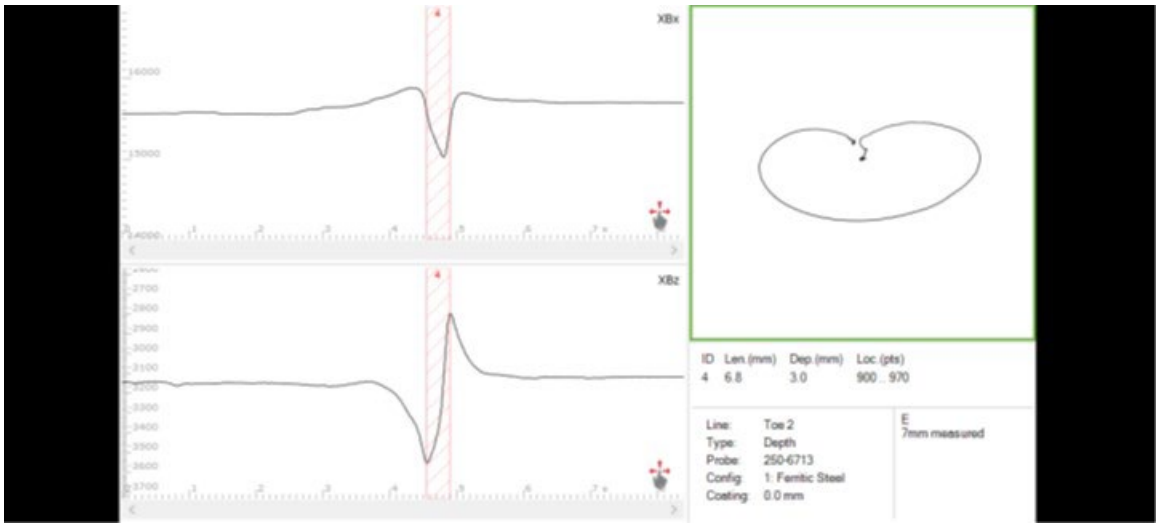

Figure 10. Scan data of Flaw 4 for TTCI-2 butt weld MG panel

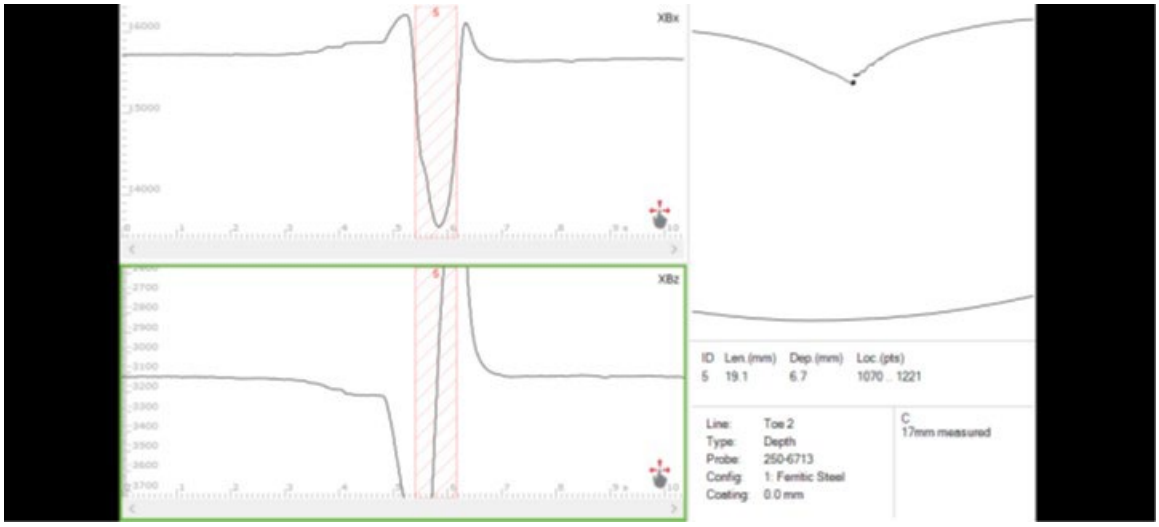

Figure 11. ACFM scan data of Flaw 5 for TTCI-2 butt weld MG panel

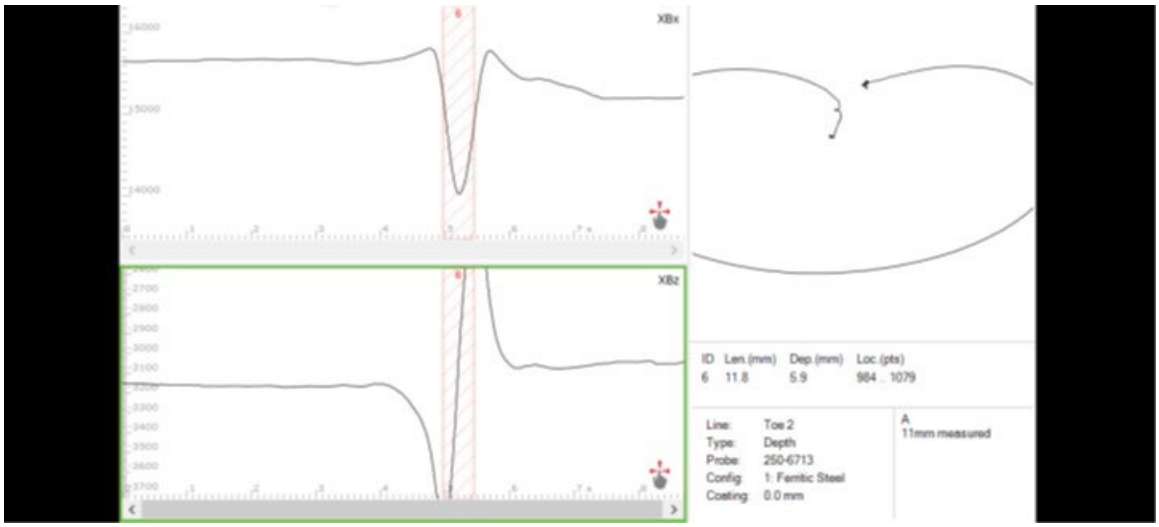

Figure 12. ACFM scan data of Flaw 6 for TTCI-2 butt weld MG panel

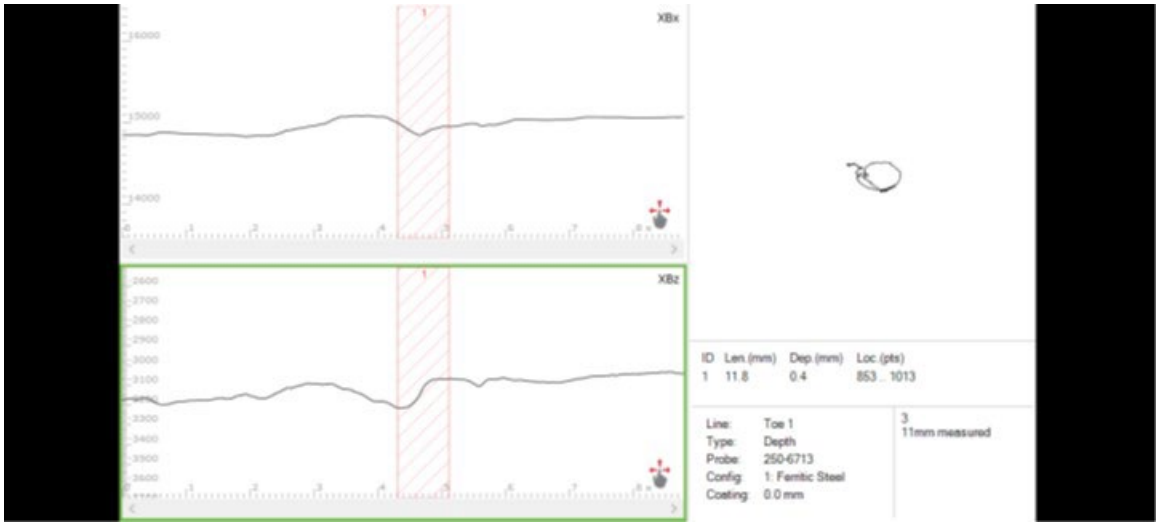

Figure 13. ACFM scan data of Flaw 1 for butt weld MG-6 panel

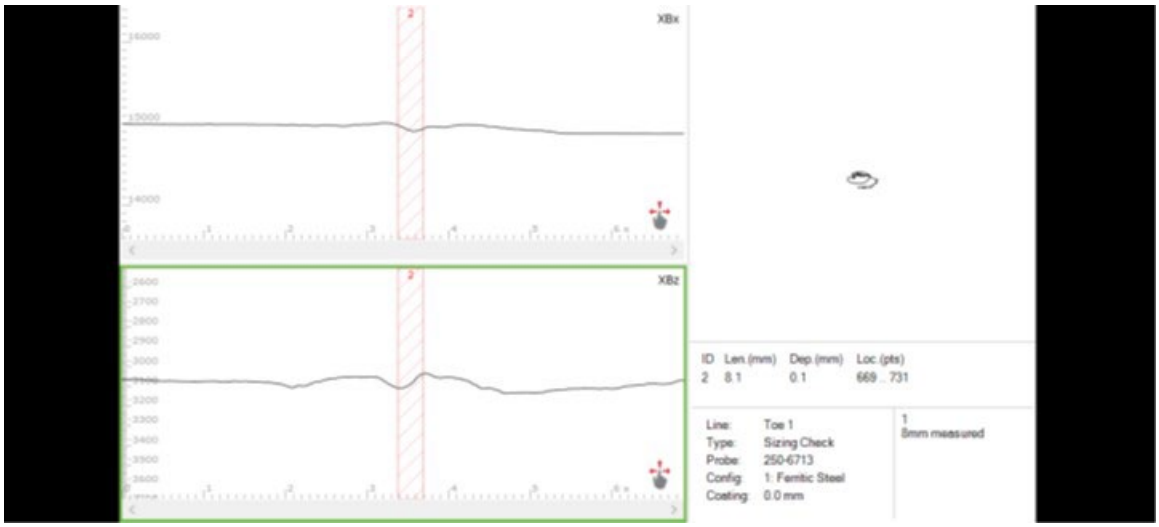

Figure 14. ACFM scan data of Flaw 2 for butt weld MG-6 panel

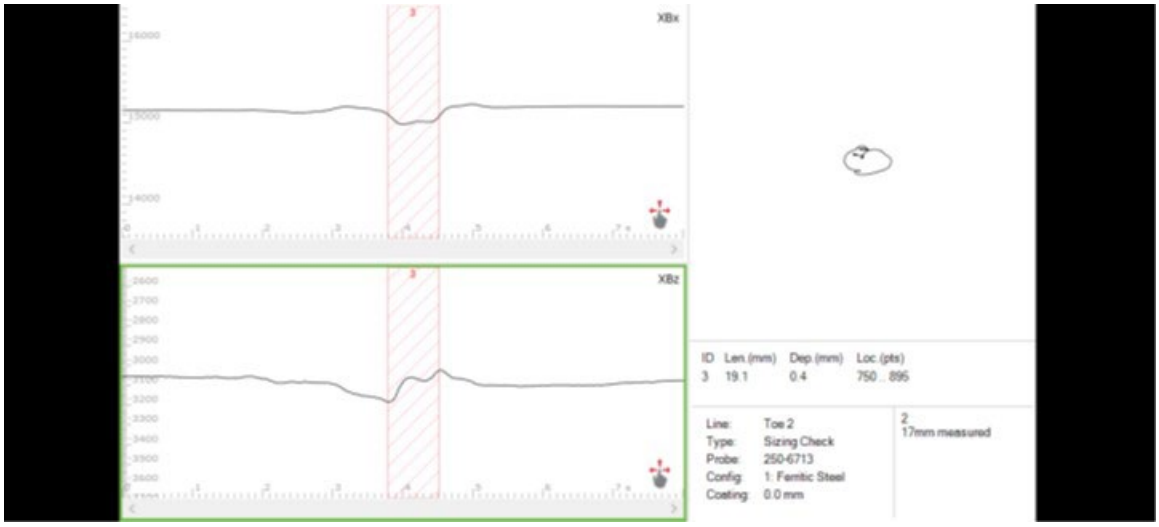

Figure 15. ACFM scan data of Flaw 3 for butt weld MG-6 panel

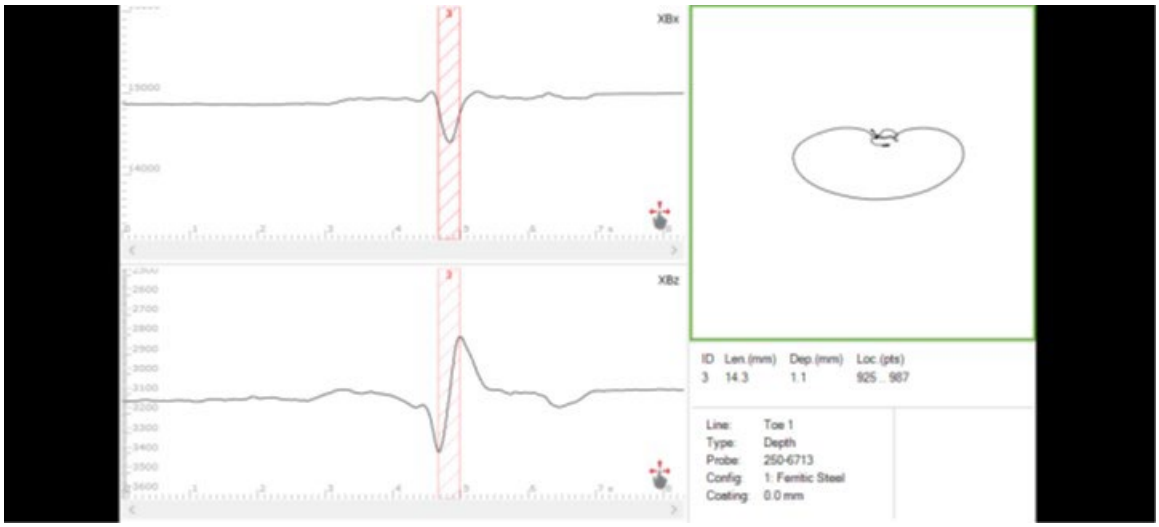

Figure 16. ACFM scan data of Flaw 1 for butt weld MG-13 panel

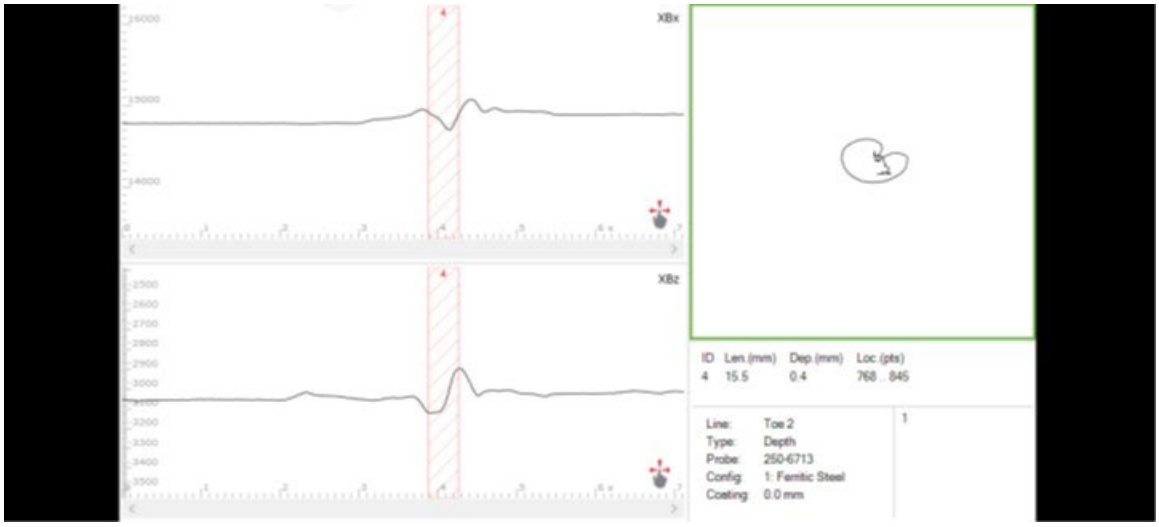

Figure 17. ACFM scan data of Flaw 2 for butt weld MG-13 panel

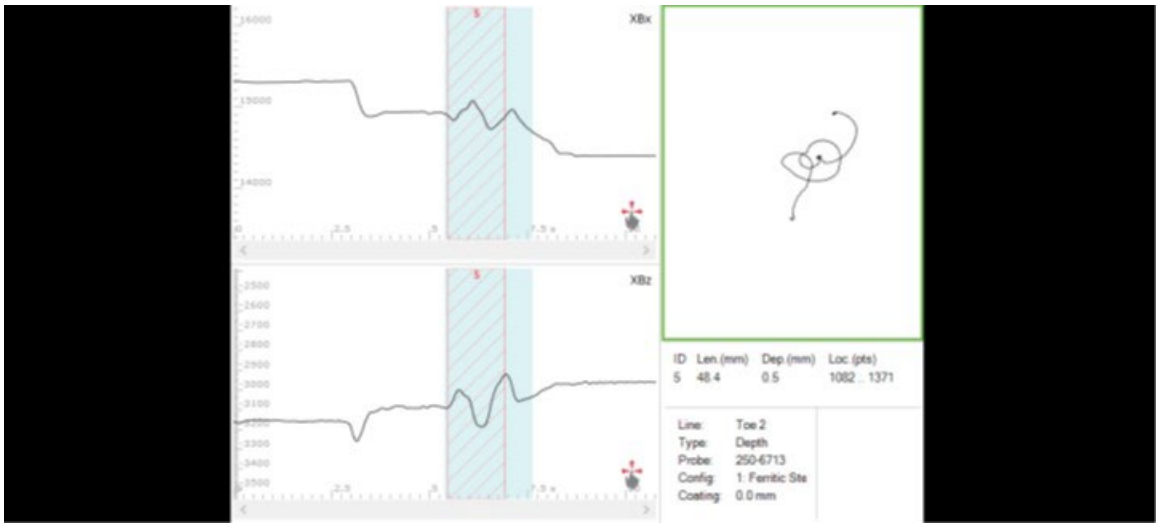

Figure 18. ACFM scan data of Flaw 3 for butt weld MG-13 panel

Figure 19. ACFM scan data of Flaw 1 for butt weld MG-16 panel

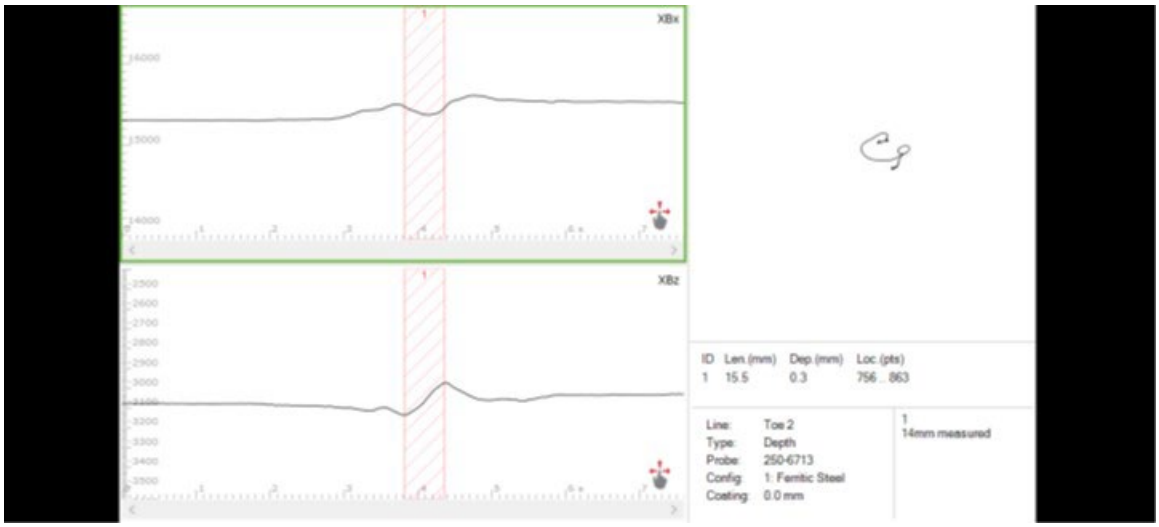

Figure 20. ACFM scan data of Flaw 2 for butt weld MG-16 panel

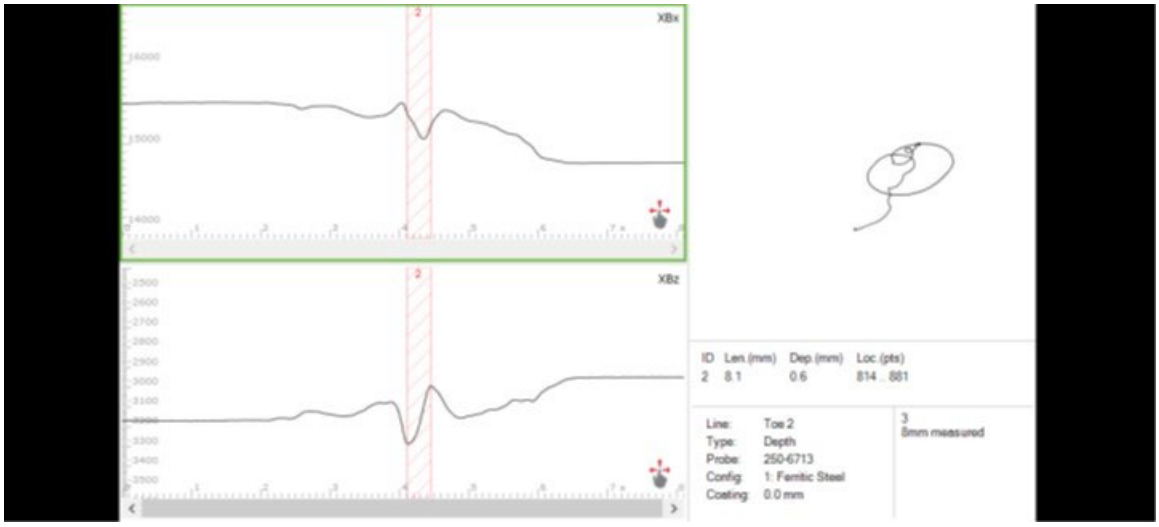

Figure 21. ACFM scan data of Flaw 3 for butt weld MG-16 panel

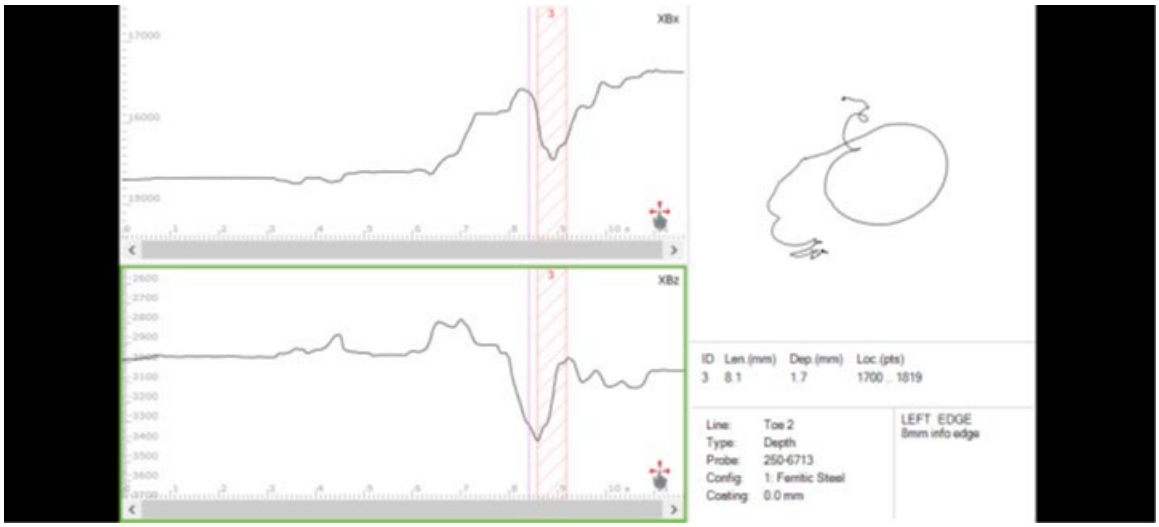

Figure 22. ACFM scan data of Flaw 1 for fillet weld TTCI-P2 panel

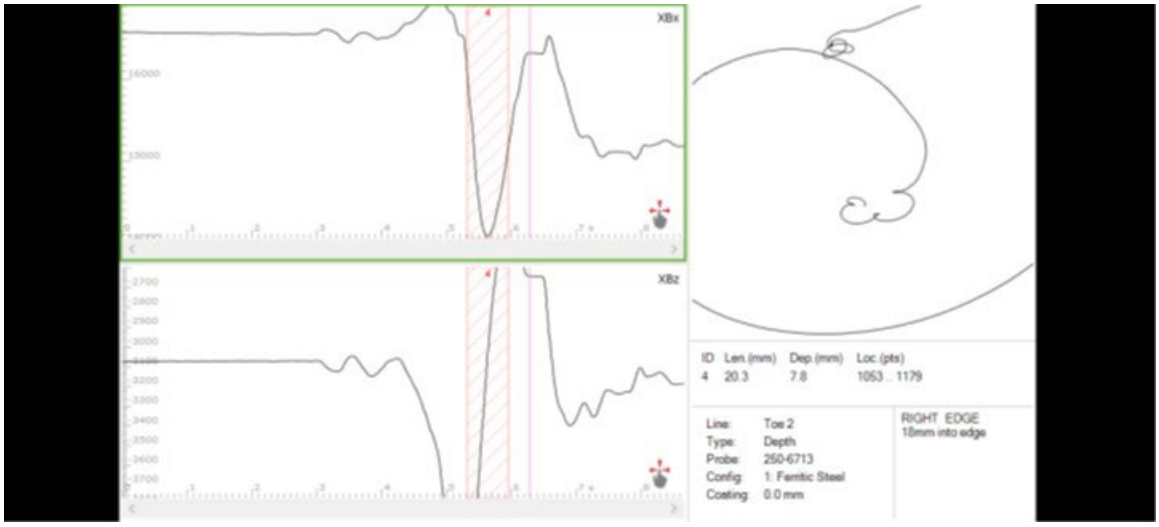

Figure 23. ACFM scan data of Flaw 2 for fillet weld TTCI-P2 panel

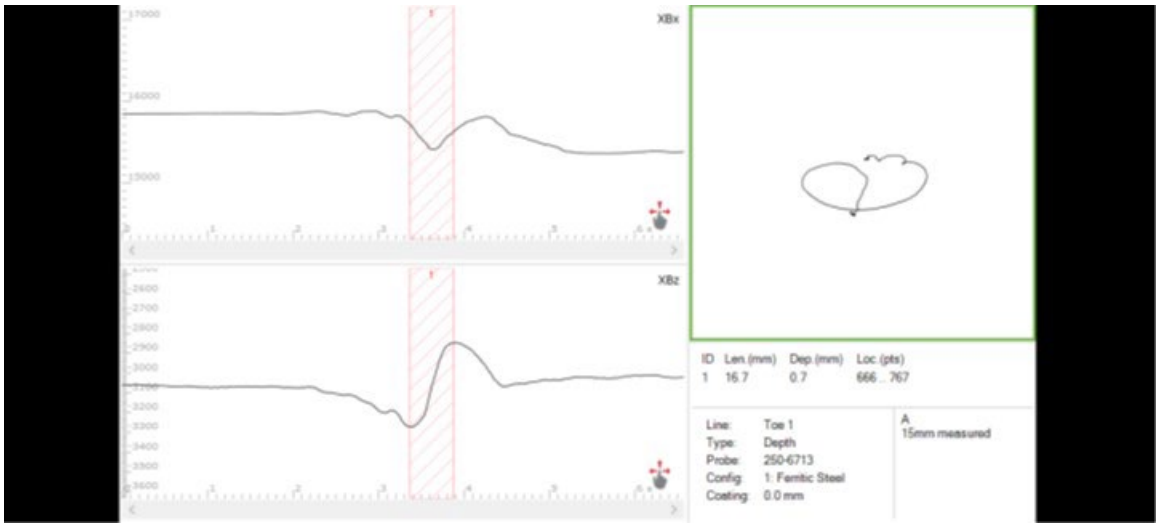

Figure 24. ACFM scan data of Flaw 1 for fillet weld MGL-3 panel

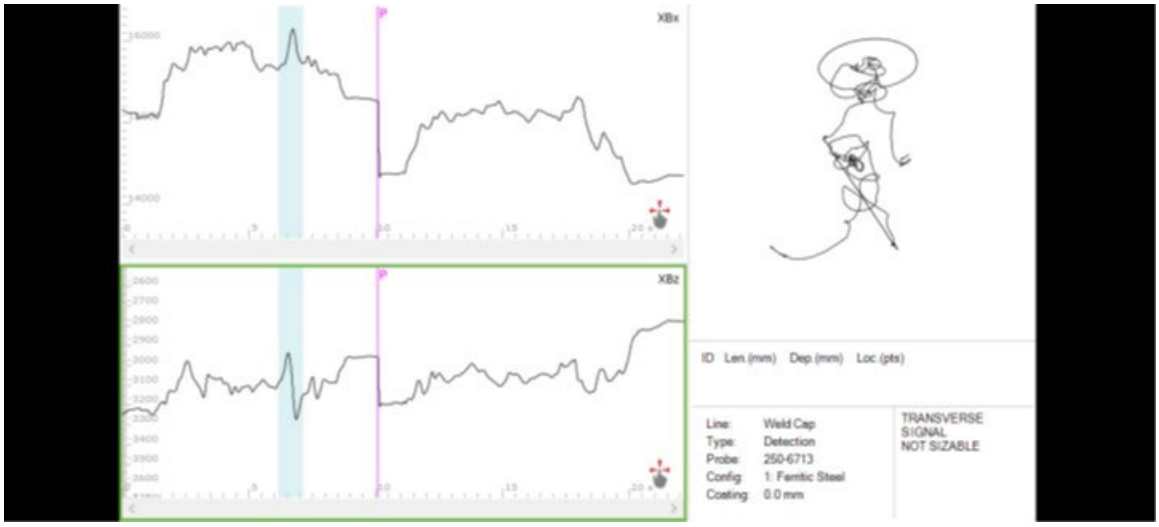

Figure 25. ACFM scan data of Flaw 1 for fillet weld MGL-9 panel

Figure 26. ACFM scan data of Flaw 2 for fillet weld MGL-9 panel

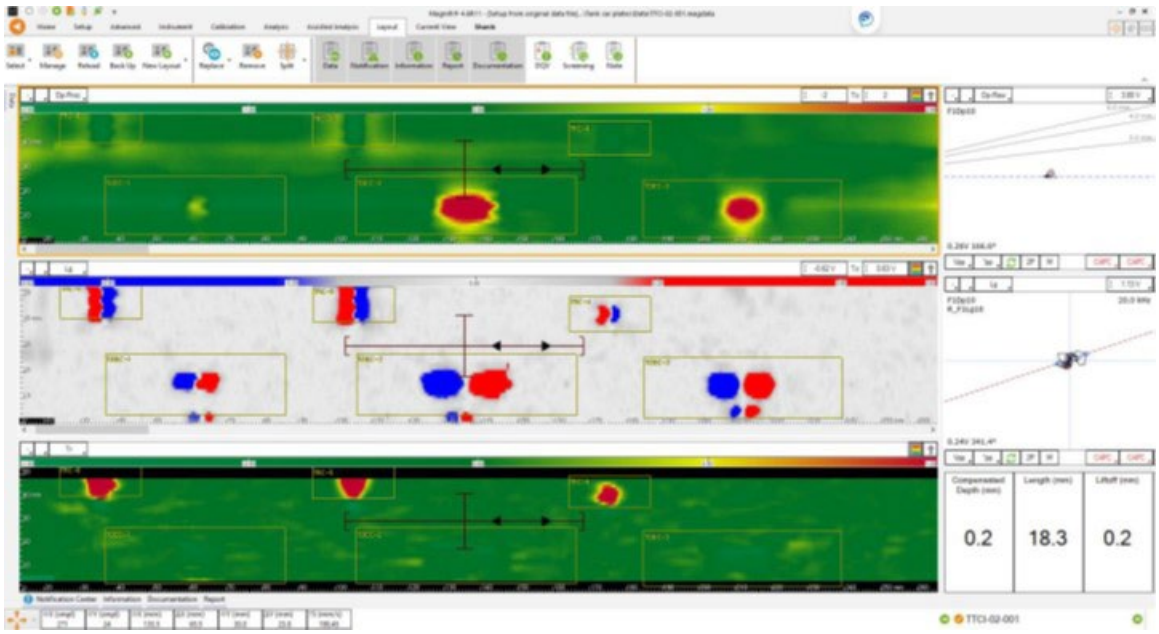

Figure 27. TECA scan results for butt weld TTCI-2 MG panel

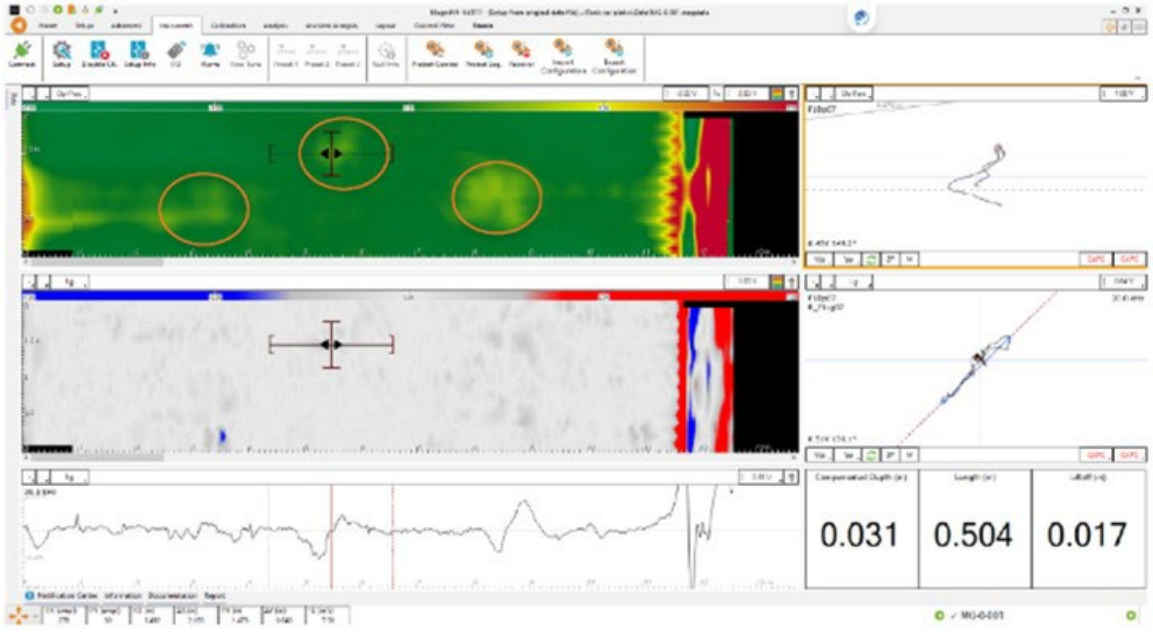

Figure 28. TECA scan results for butt weld MG-6 panel

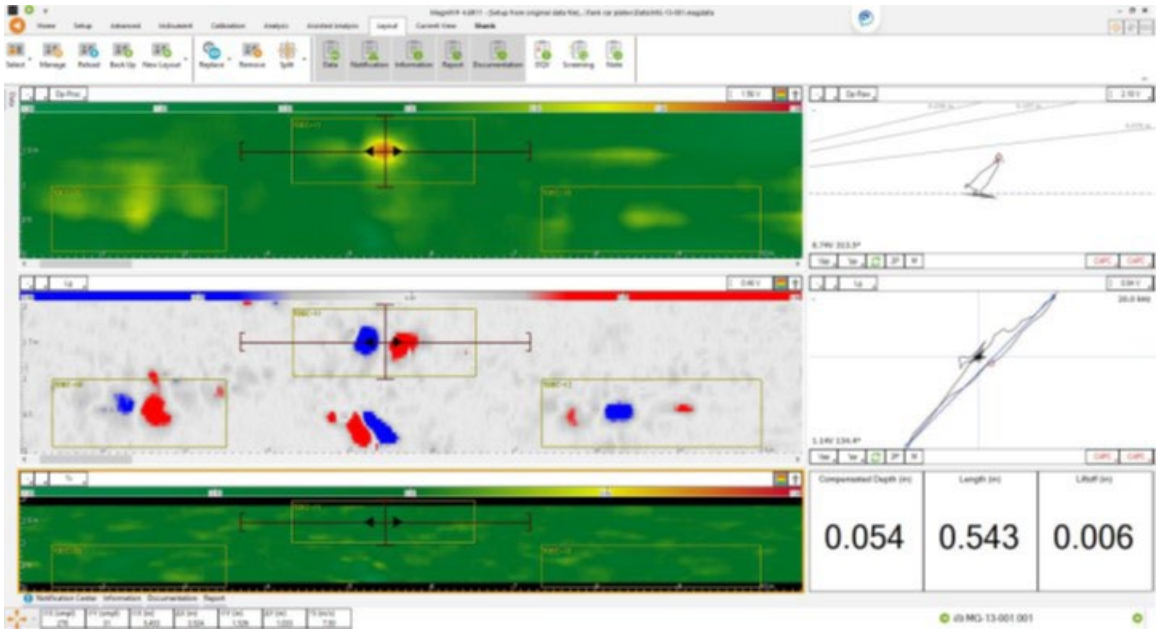

Figure 29. TECA scan results for butt weld MG-13 panel

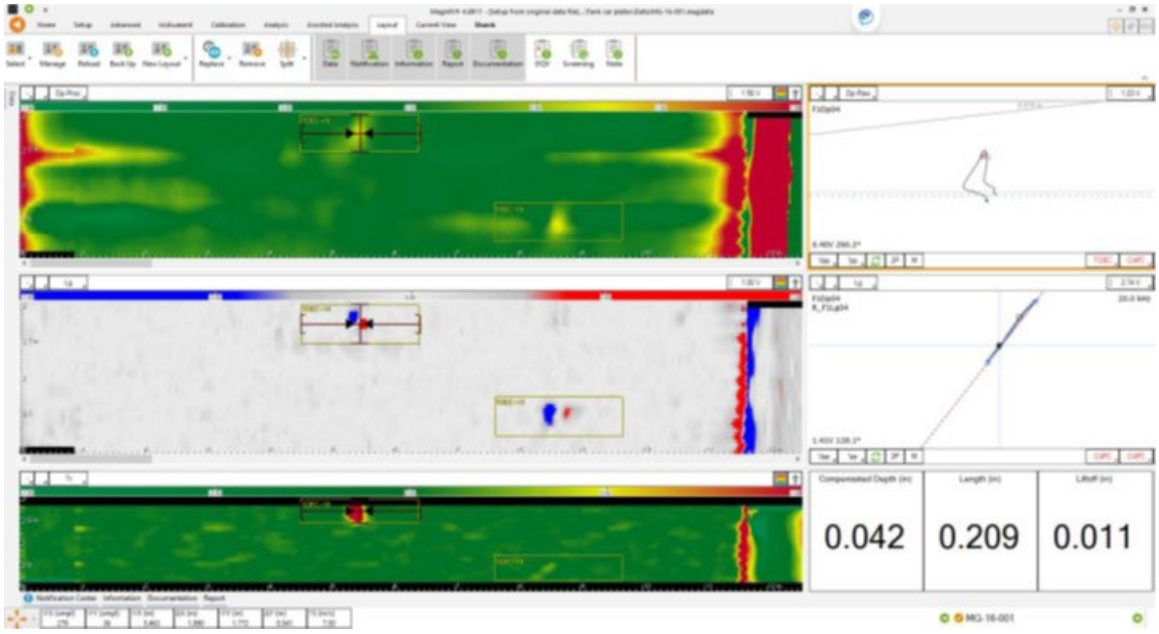

Figure 30. TECA scan results for butt weld MG-16 panel

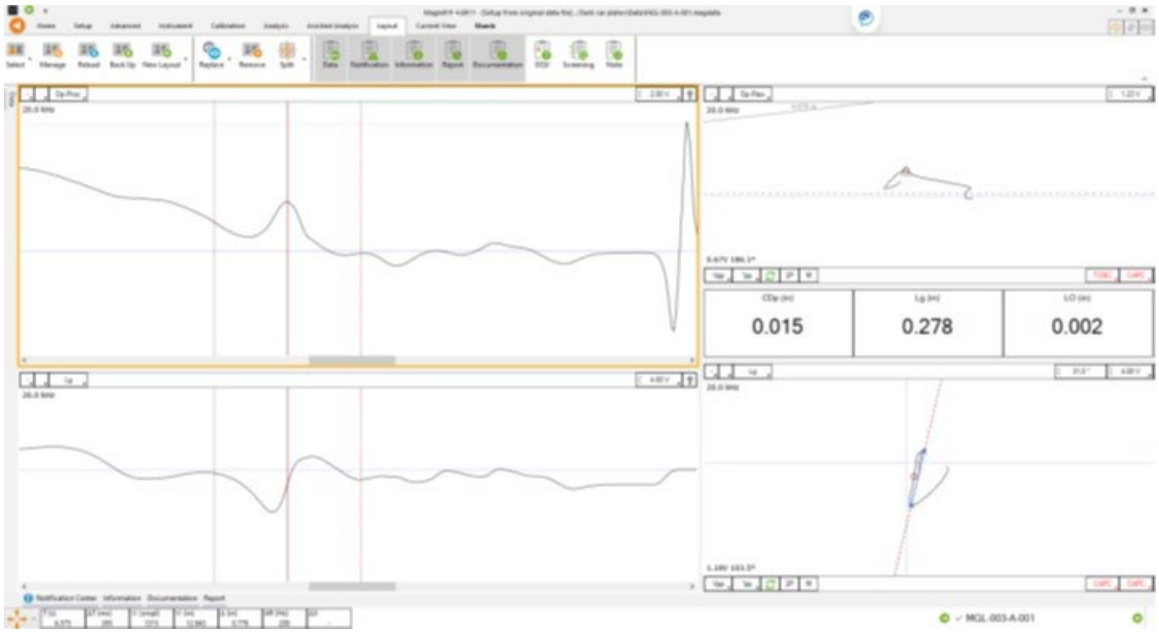

Figure 31. TECA scan results for fillet weld MGL-3 panel

Participant C

Figure 32. ET indication of defect at Location A in butt weld test panel TTCI-2

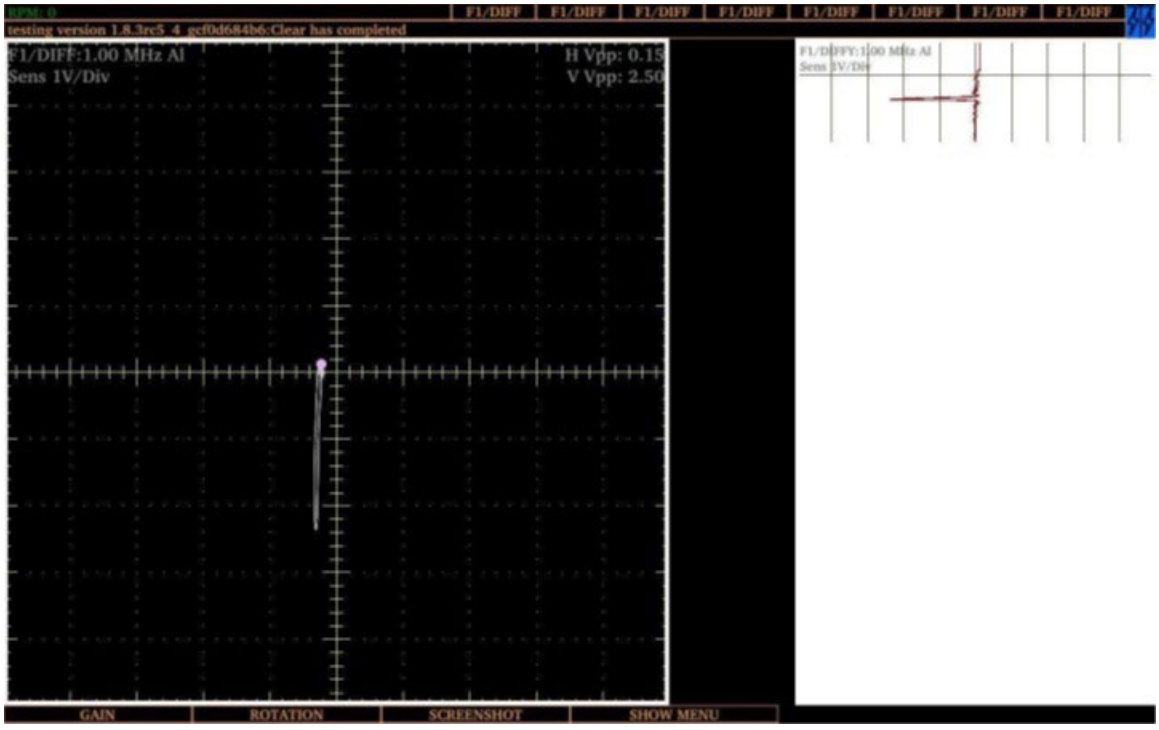

Figure 33. ET indication of defect at Location B in butt weld test panel TTCI-2

Figure 34. ET indication of defect at Location C in butt weld test panel TTCI-2

Figure 35. ET indication of defect at Location D in butt weld test panel TTCI-2

Figure 36. ET indication of defect at Location E in butt weld test panel TTCI-2

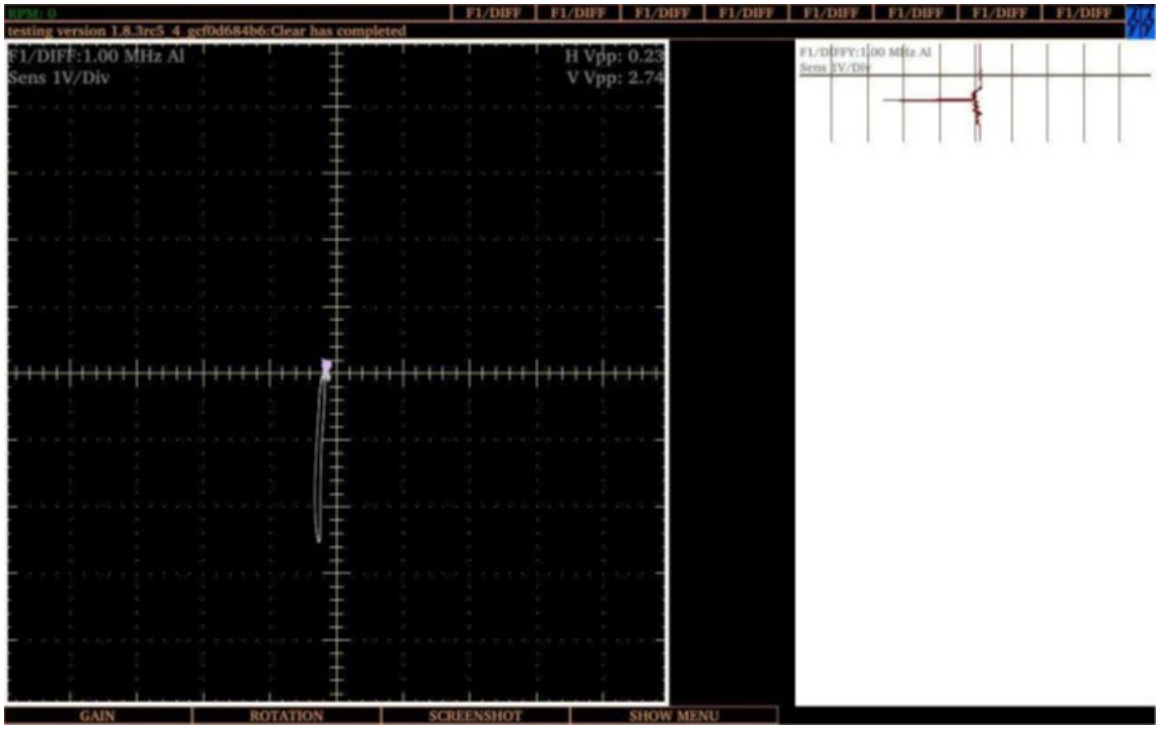

Figure 37. ET indication of defect at Location F in butt weld test panel TTCI-2

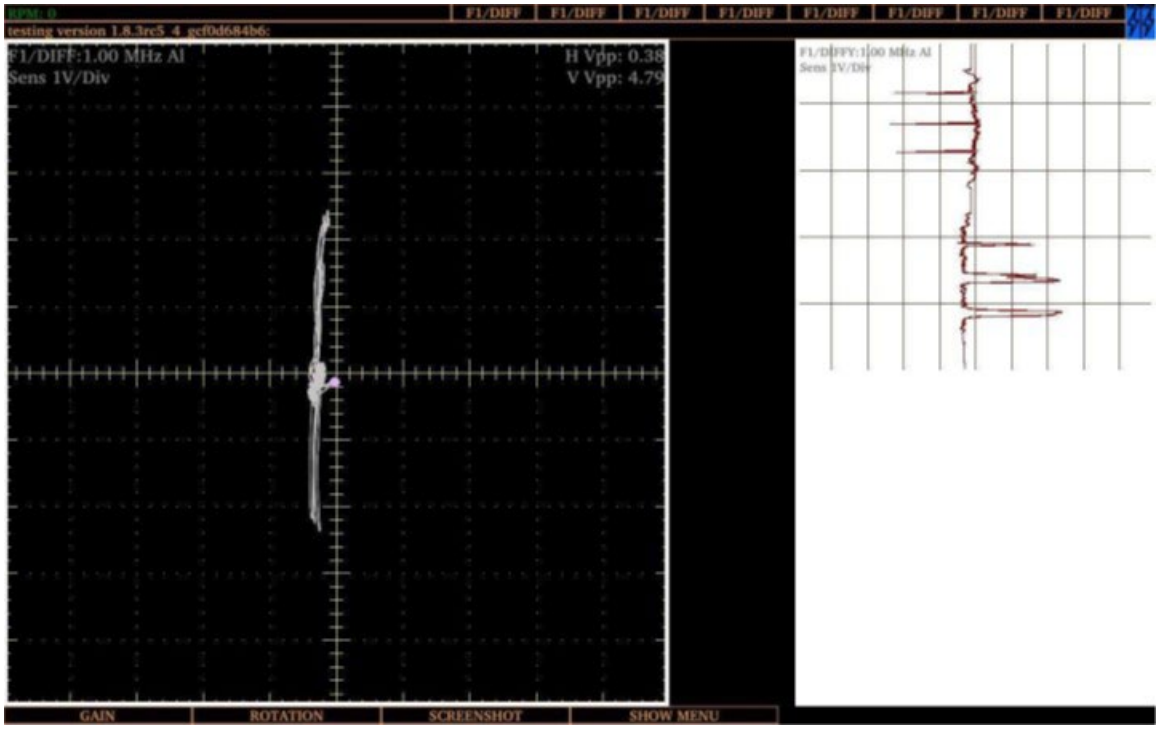

Figure 38. ET indication of all the notches in butt weld test panel TTCI-2

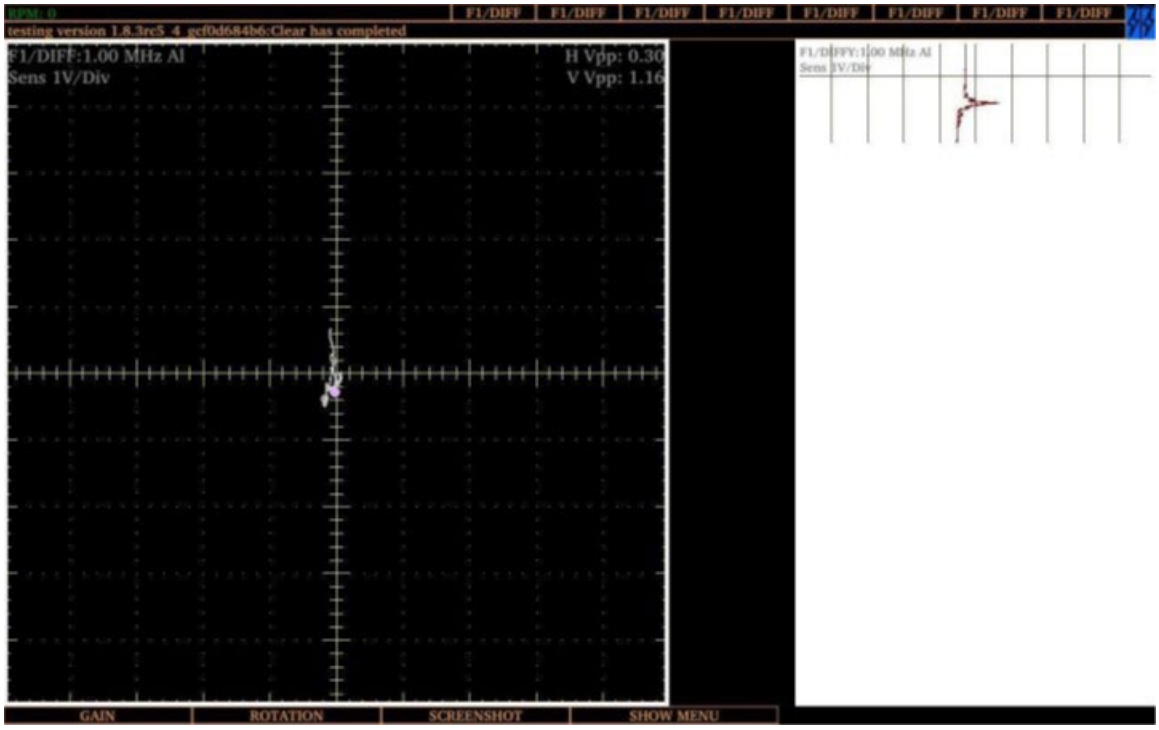

Figure 39. ET indication of defect at Location 1 in butt weld test panel MG-6

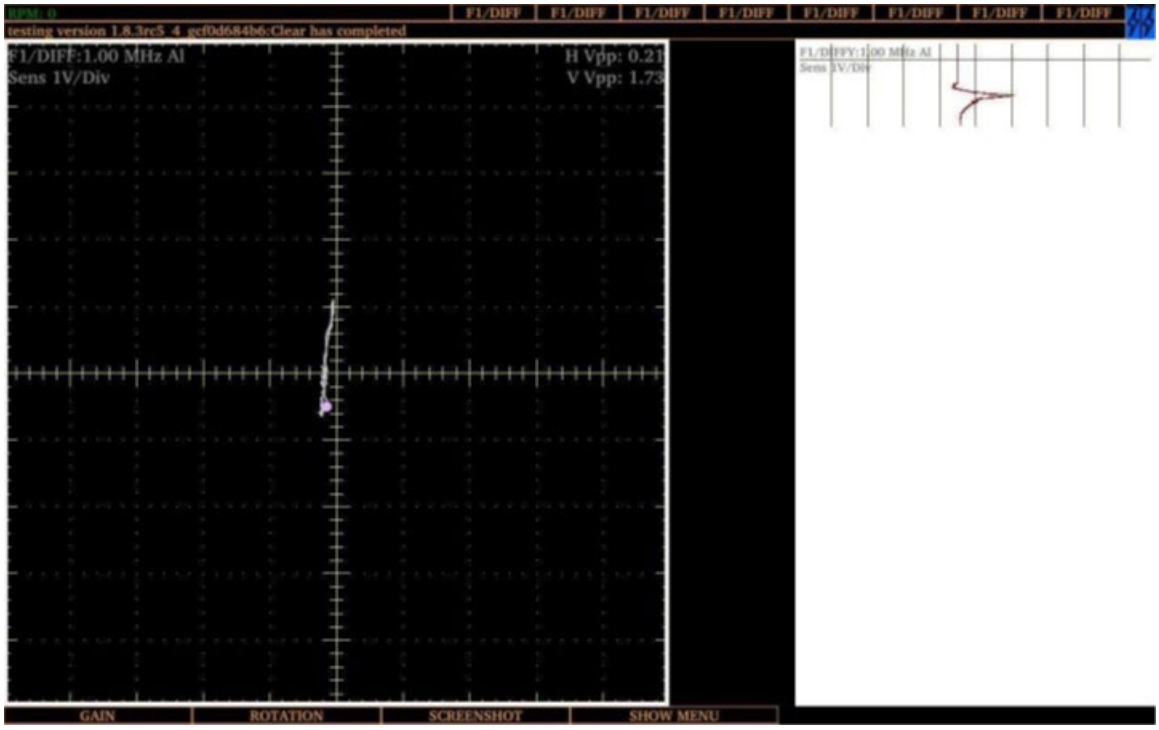

Figure 40. ET indication of defect at Location 2 in butt weld test panel MG-6

Figure 41. ET indication of defect at Location 3 in butt weld test panel MG-6

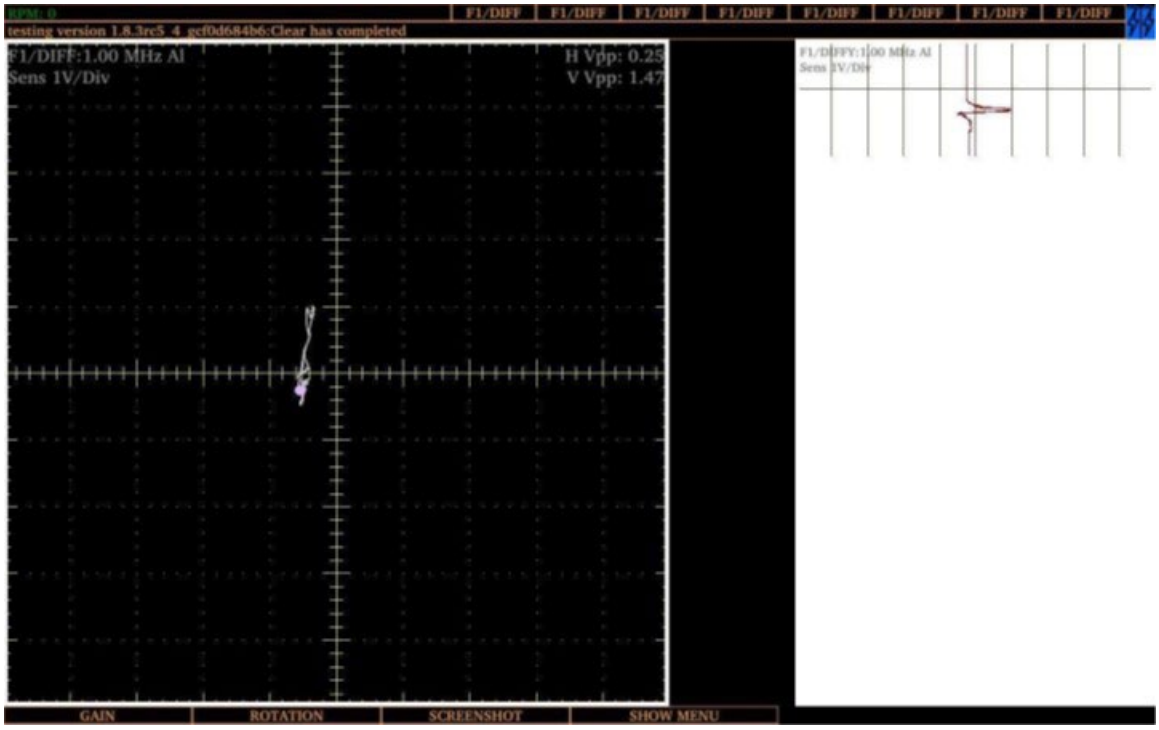

Figure 42. ET indication of defect at Location 1 in butt weld test panel MG-13

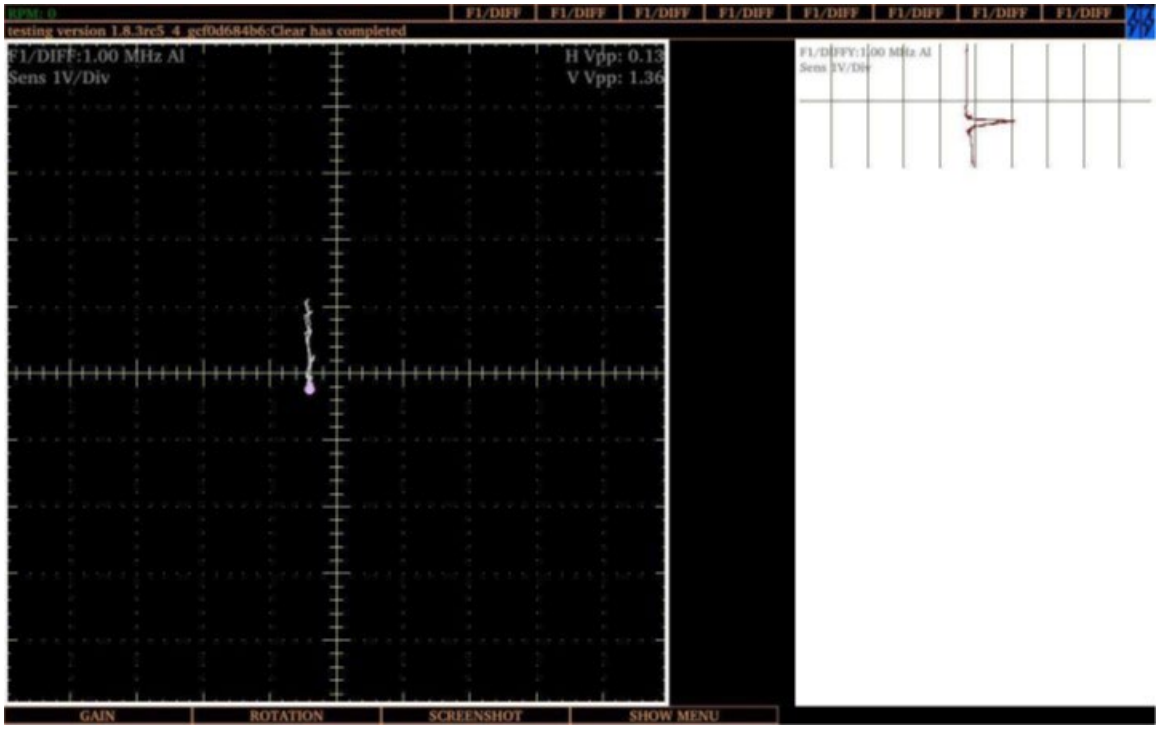

Figure 43. ET indication of defect at Location 2 in butt weld test panel MG-13

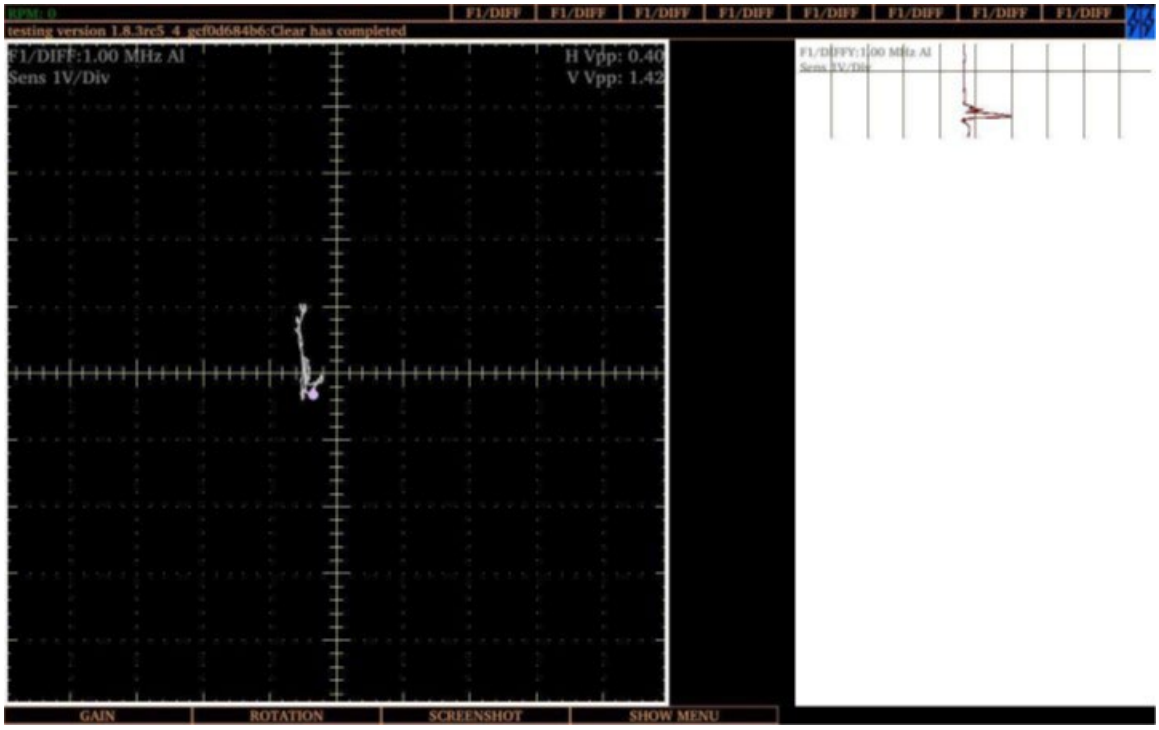

Figure 44. ET indication of defect at Location 3 in butt weld test panel MG-13

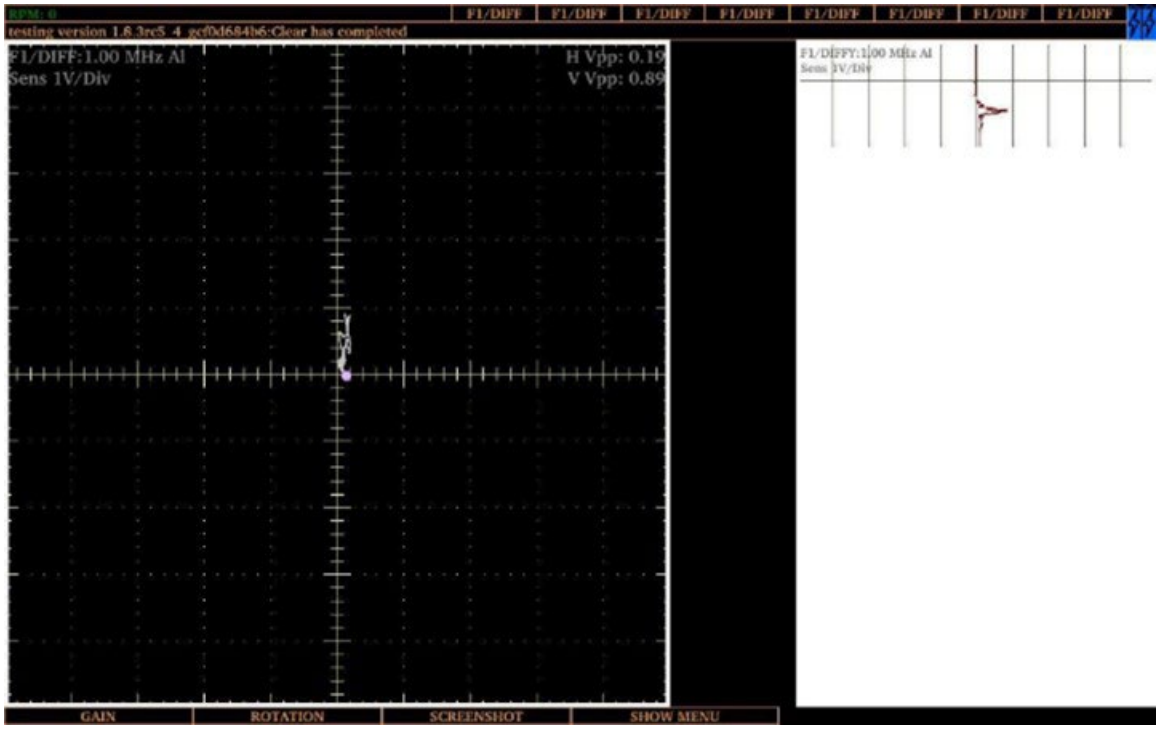

Figure 45. ET indication of defect at Location 1 in butt weld test panel MG-16

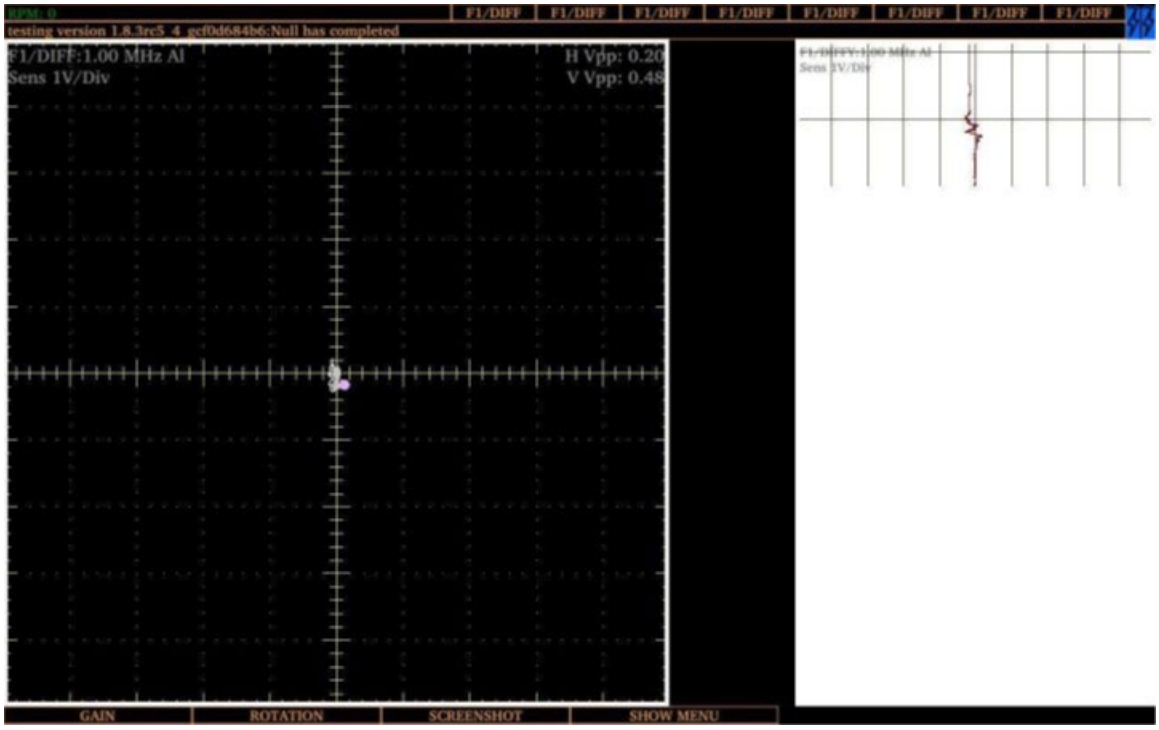

Figure 46. ET indication of defect at Location 2 in butt weld test panel MG-16

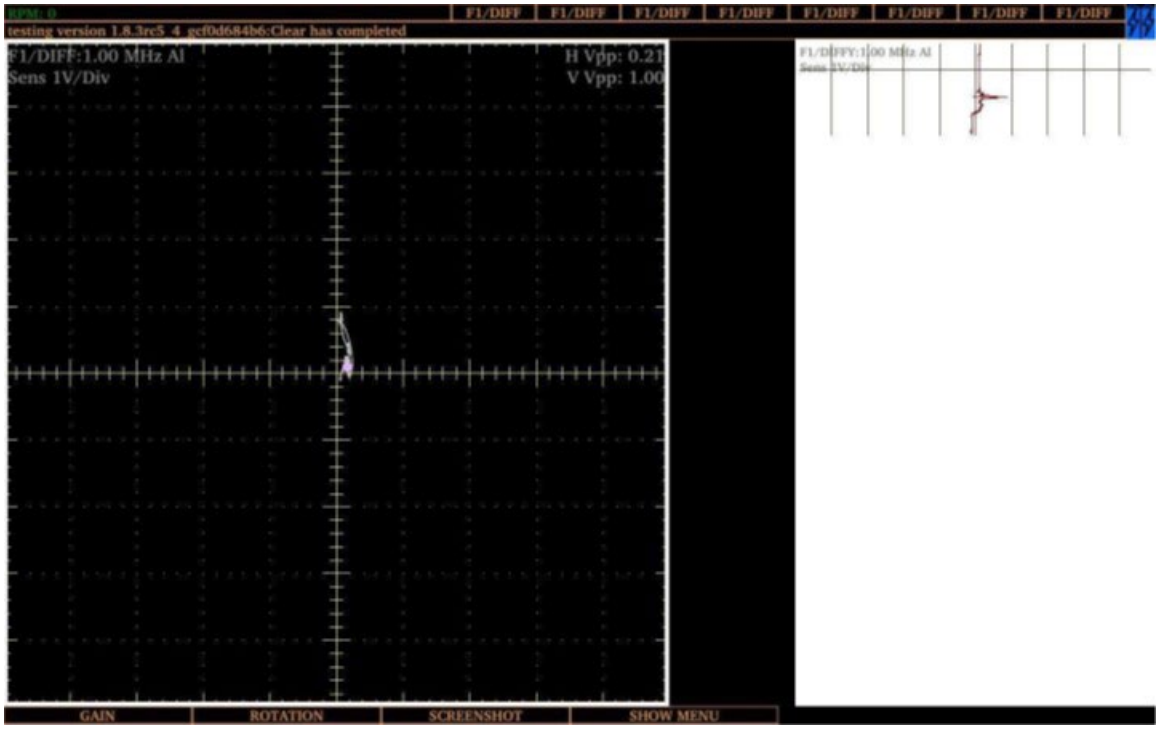

Figure 47. ET indication of defect at Location 3 in butt weld test panel MG-16

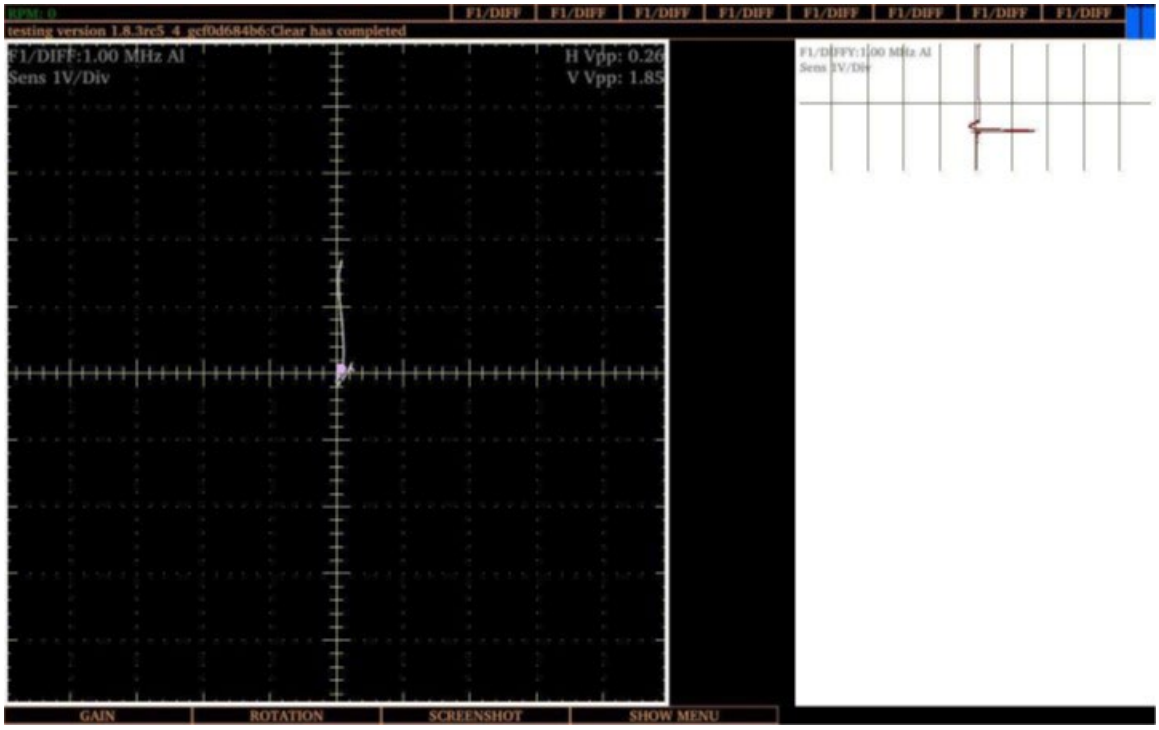

Figure 48. ET indication of defect at Location A in fillet weld test panel TTCI-P2

Figure 49. ET indication of defect at Location B in fillet weld test panel TTCI-P2

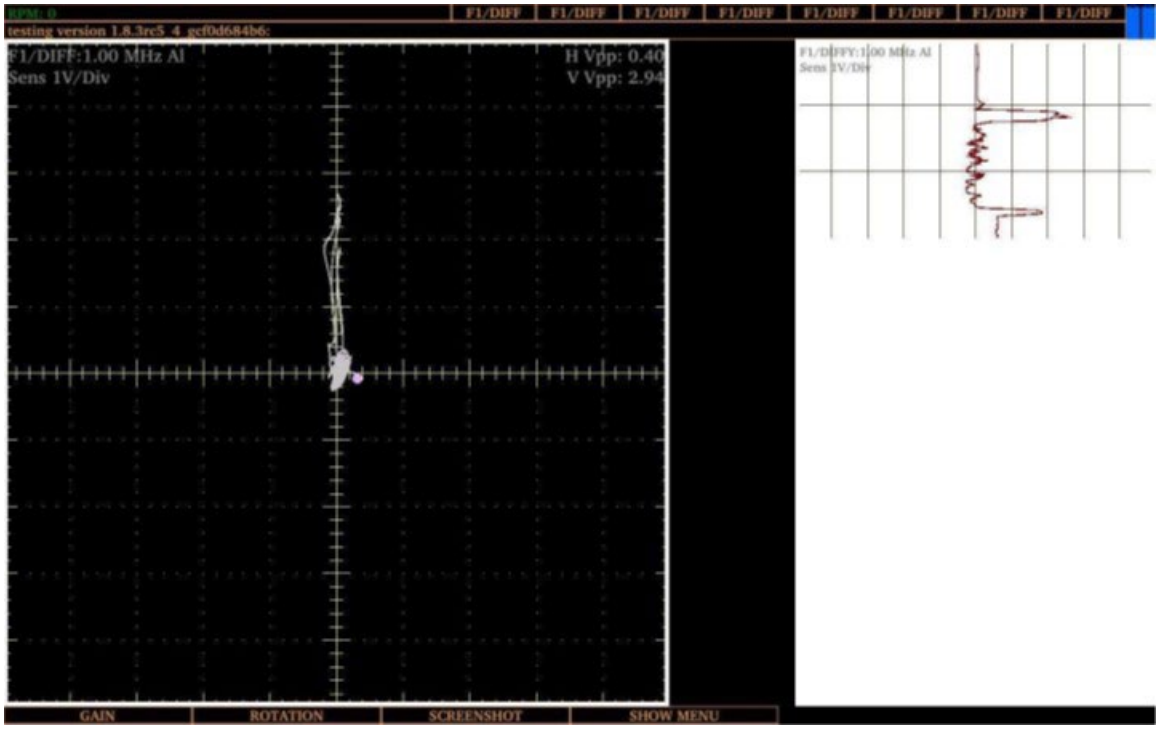

Figure 50. ET indication of defects at Location A and B in fillet weld test panel TTCI-P2

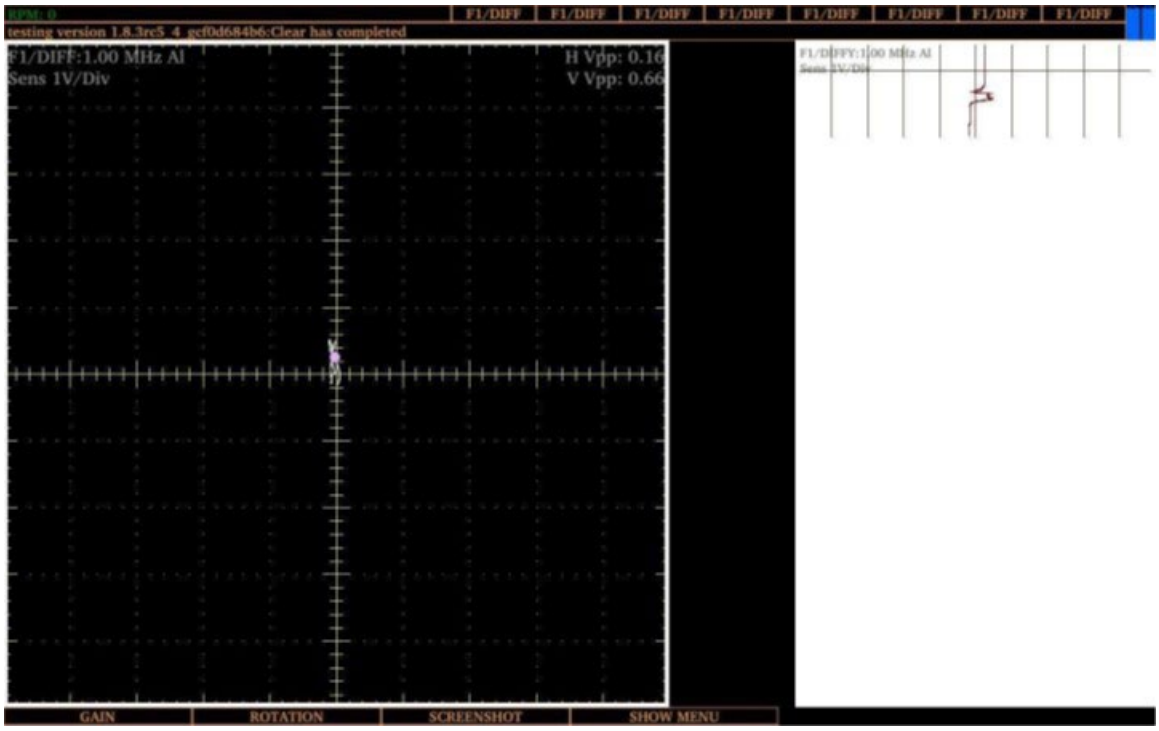

Figure 51. ET indication of defect at Location A in fillet weld test panel MGL-3

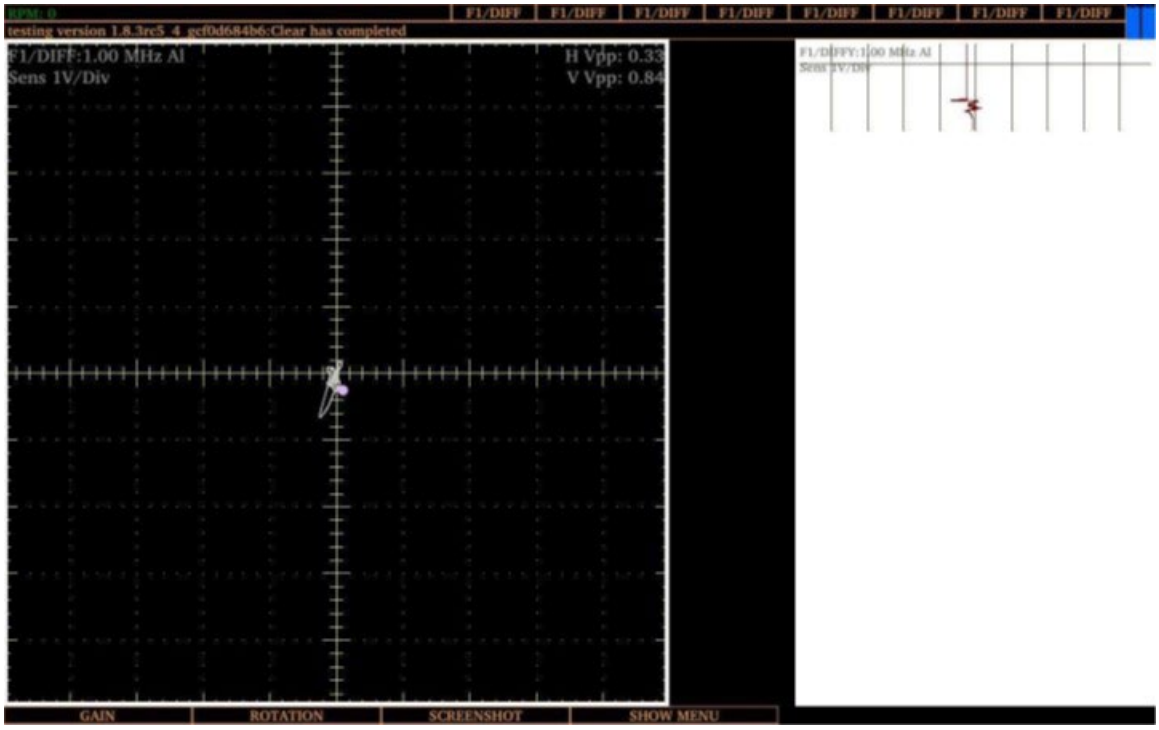

Figure 52. ET indication of defect at Location B in fillet weld test panel MGL-3

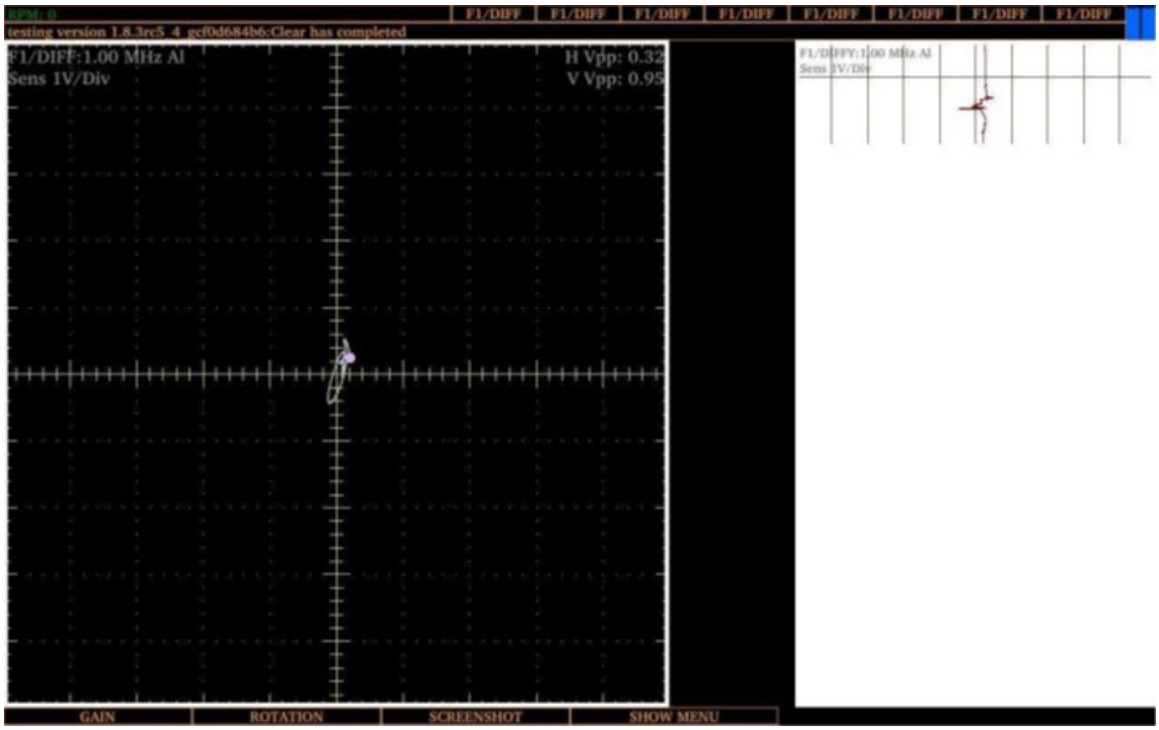

Figure 53. ET indication of defect at Location A in fillet weld test panel MGL-9

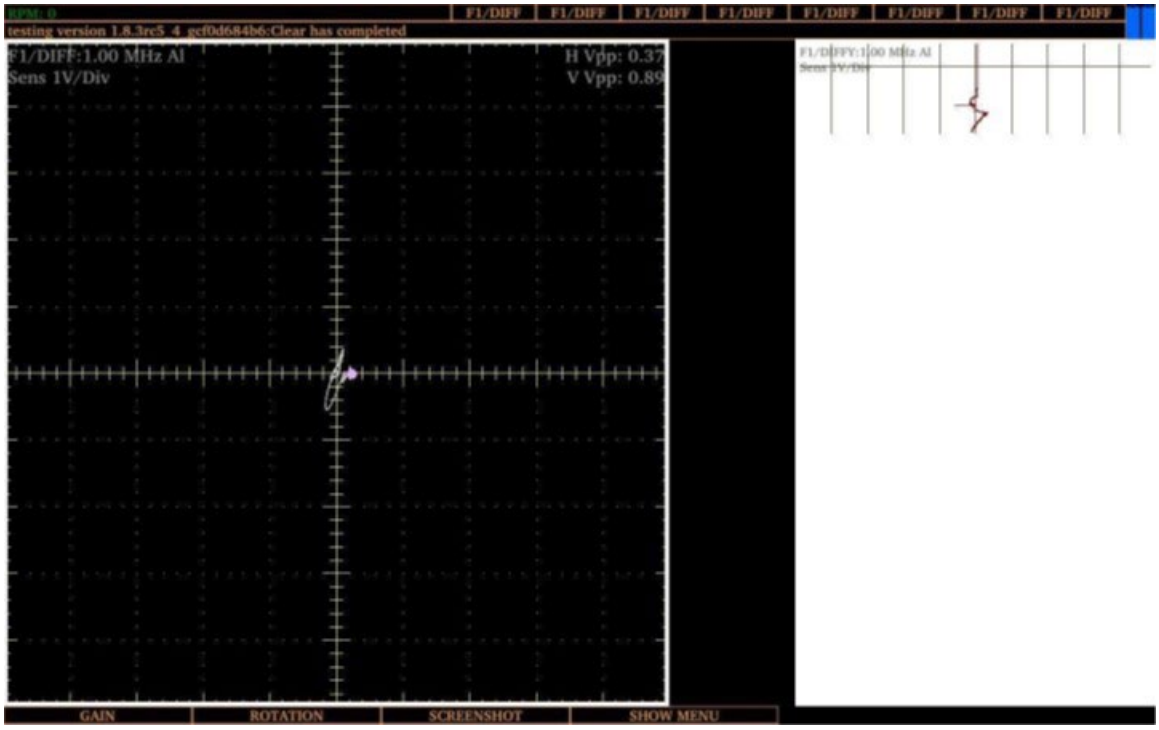

Figure 54. ET indication of defect at Location B in fillet weld test panel MGL-9

Figure 55. ET indication of defect at Location C in fillet weld test panel MGL-10

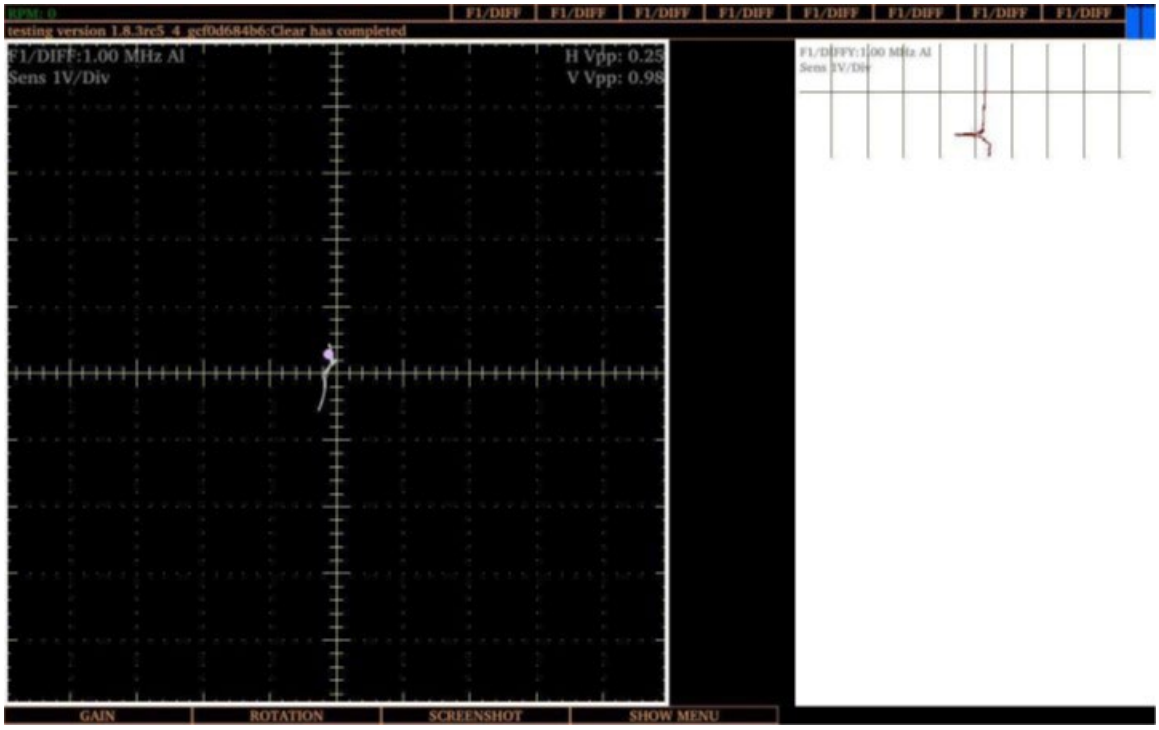

Figure 56. ET indication of defect at Location D in fillet weld test panel MGL-10

Participant D

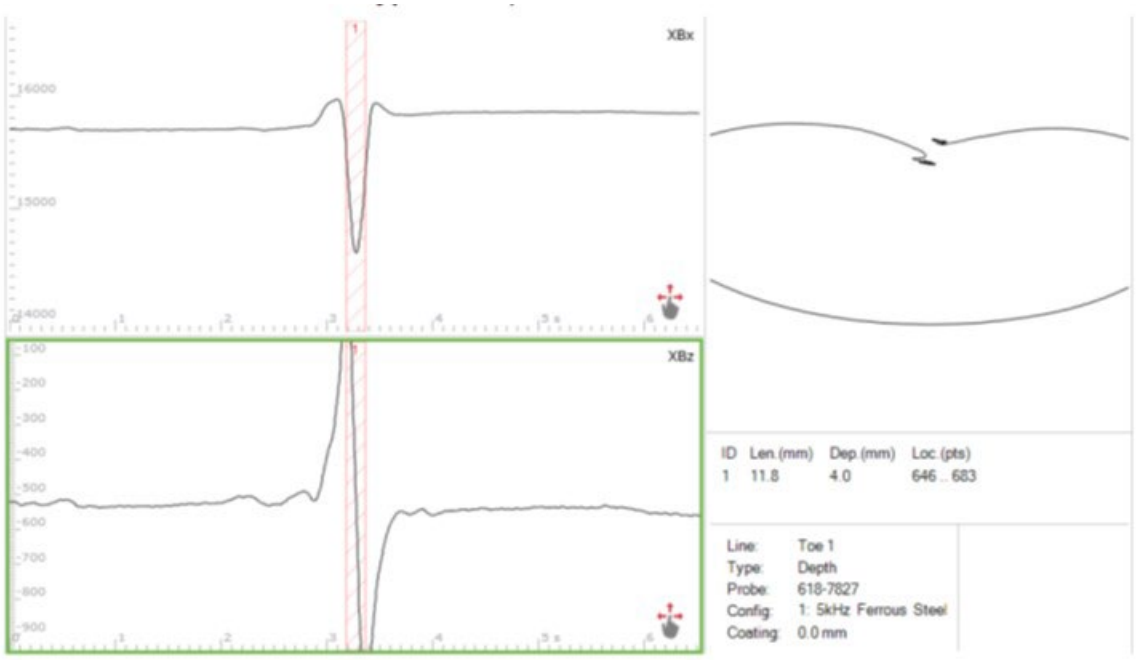

Figure 57. ACFM indication of defect at Location A in test panel TTCI-2

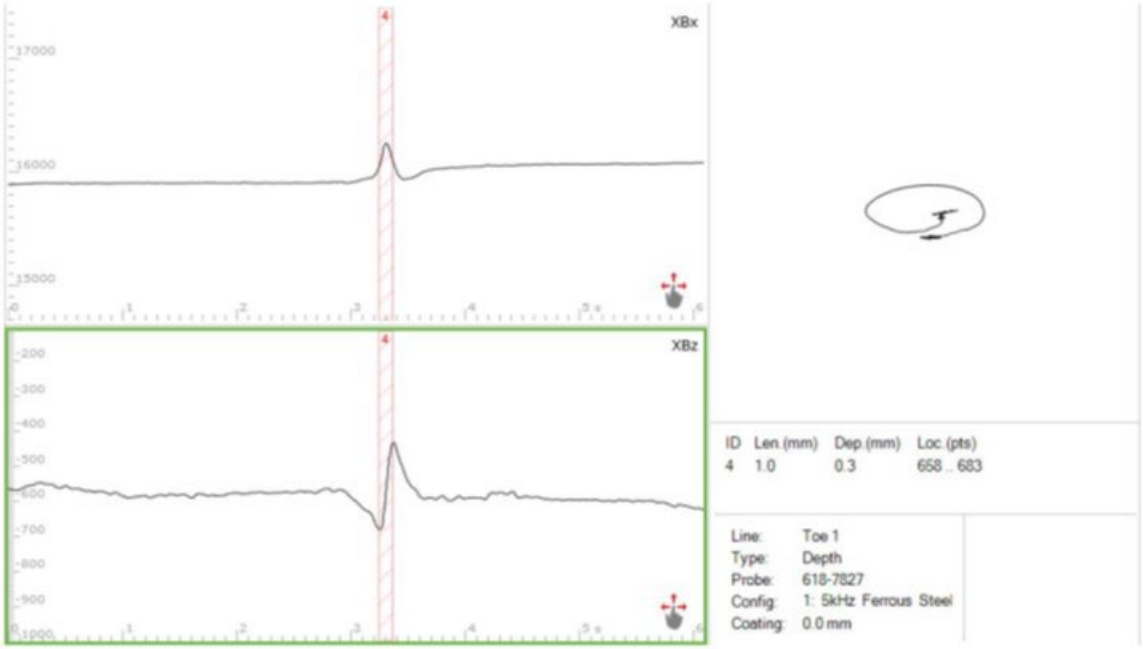

Figure 58. ACFM indication of defect at Location B in test panel TTCI-2

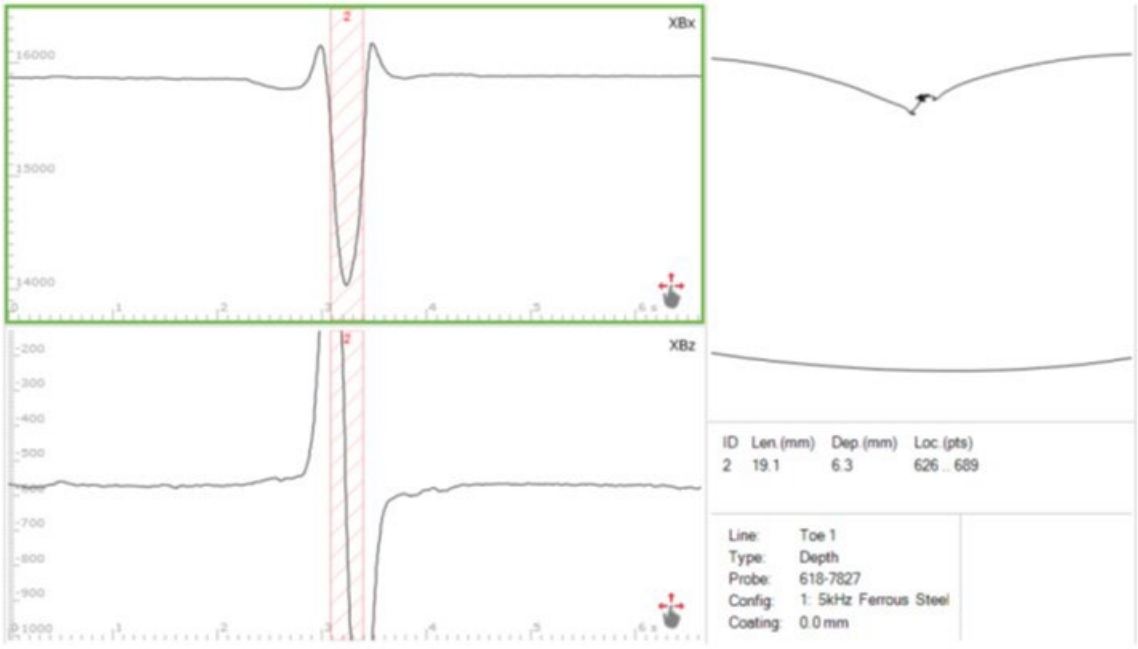

Figure 59. ACFM indication of defect at Location C in test panel TTCI-2

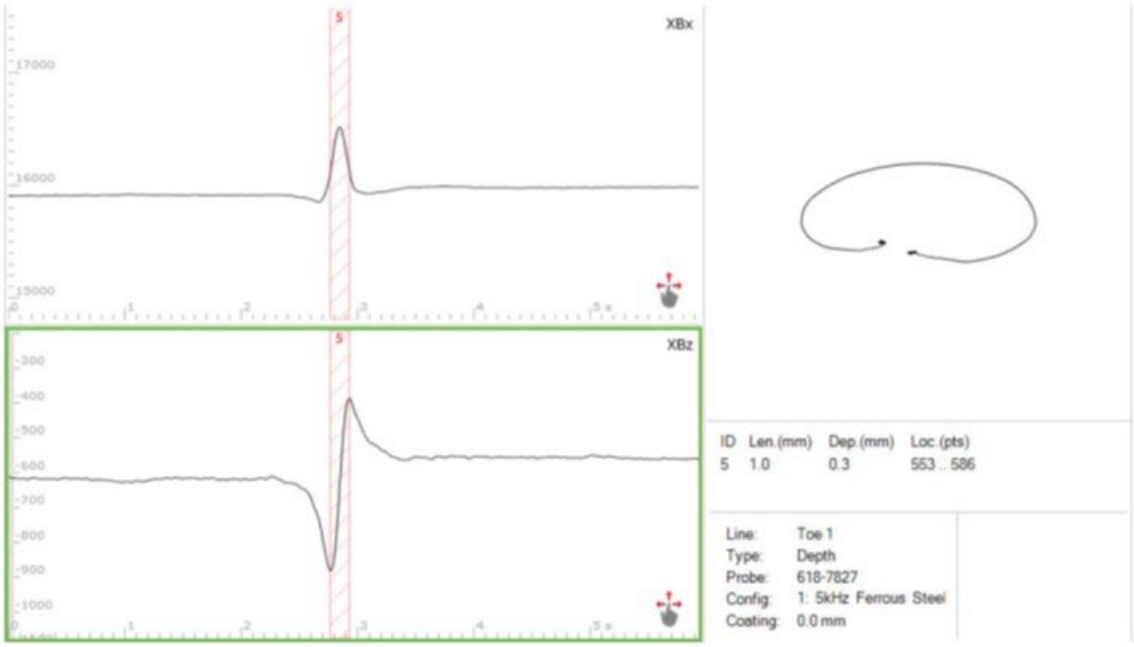

Figure 60. ACFM indication of defect at Location D in test panel TTCI-2

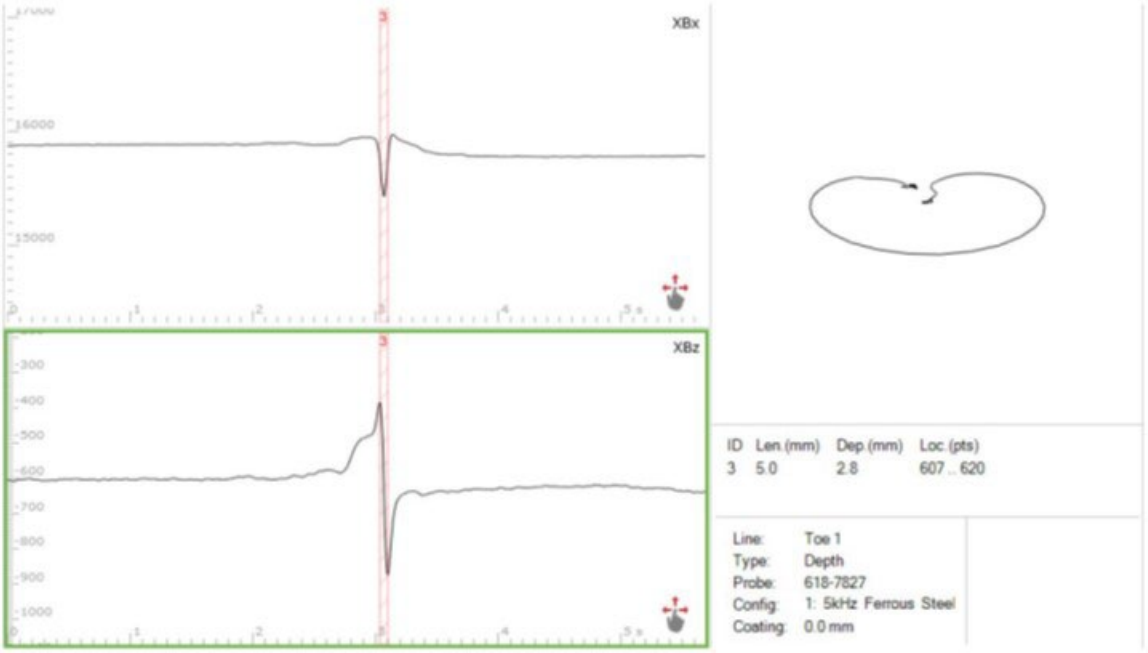

Figure 61. ACFM indication of defect at Location E in test panel TTCI-2

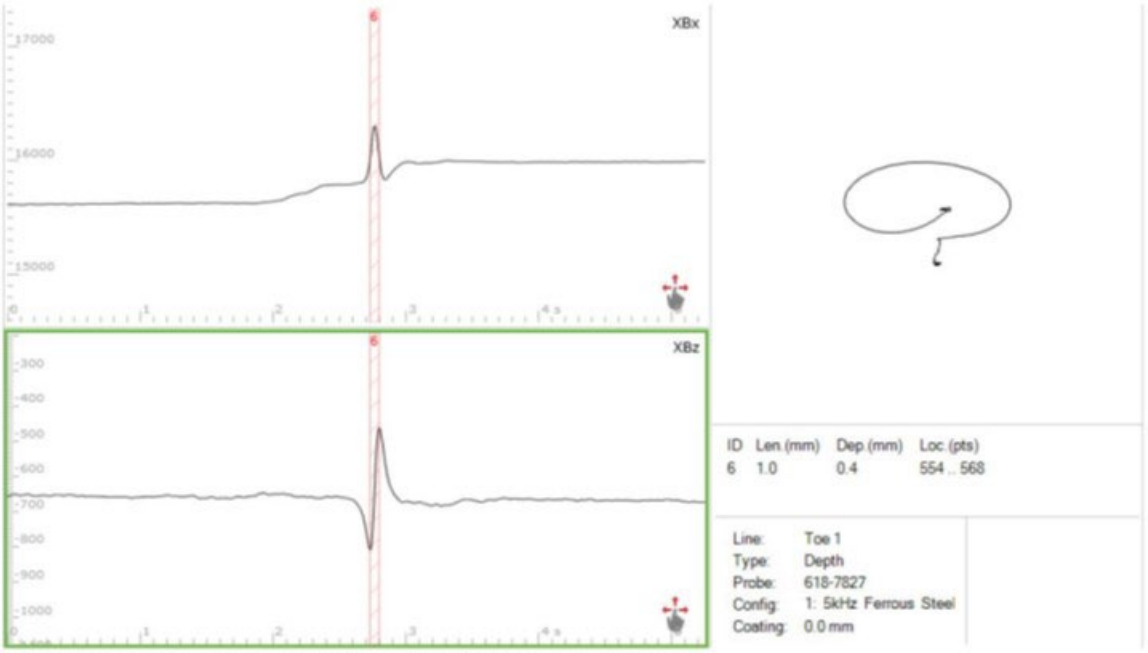

Figure 62. ACFM indication of defect at Location F in test panel TTCI-2

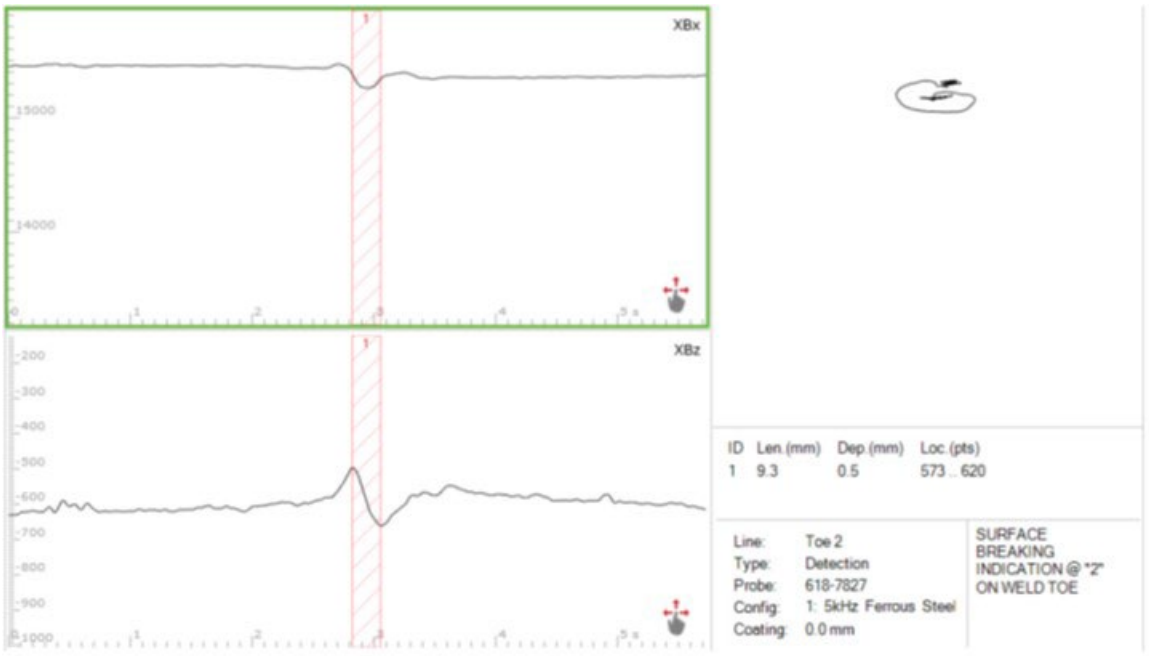

Figure 63. ACFM indication of defect at Location 2 in test panel MG-6

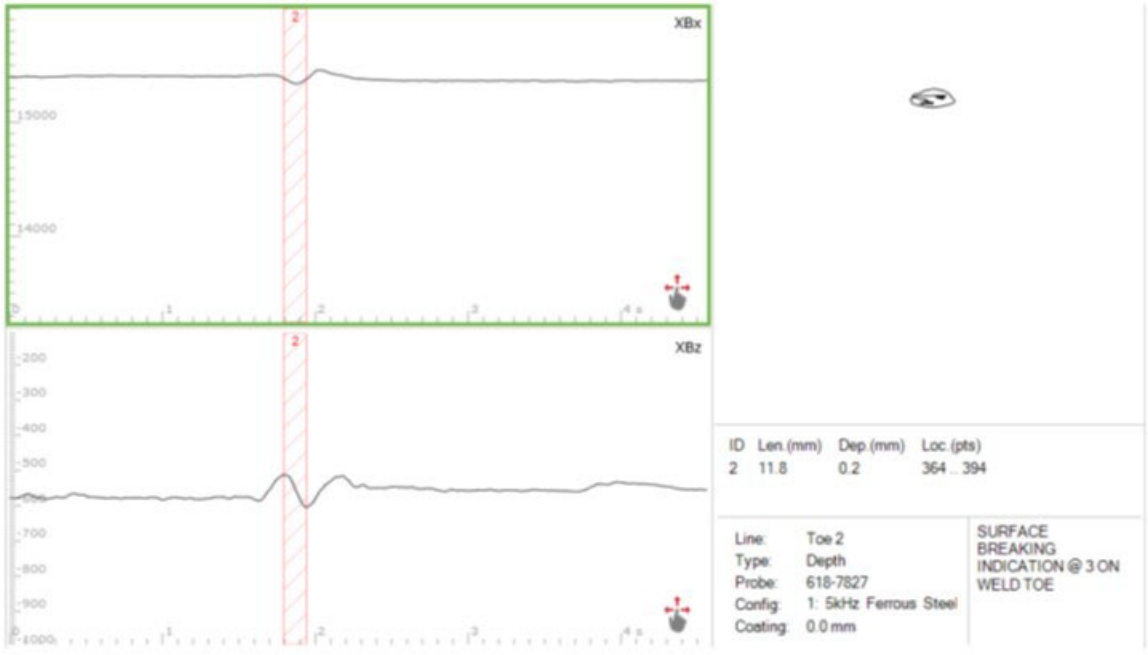

Figure 64. ACFM indication of defect at Location 3 in test panel MG-6

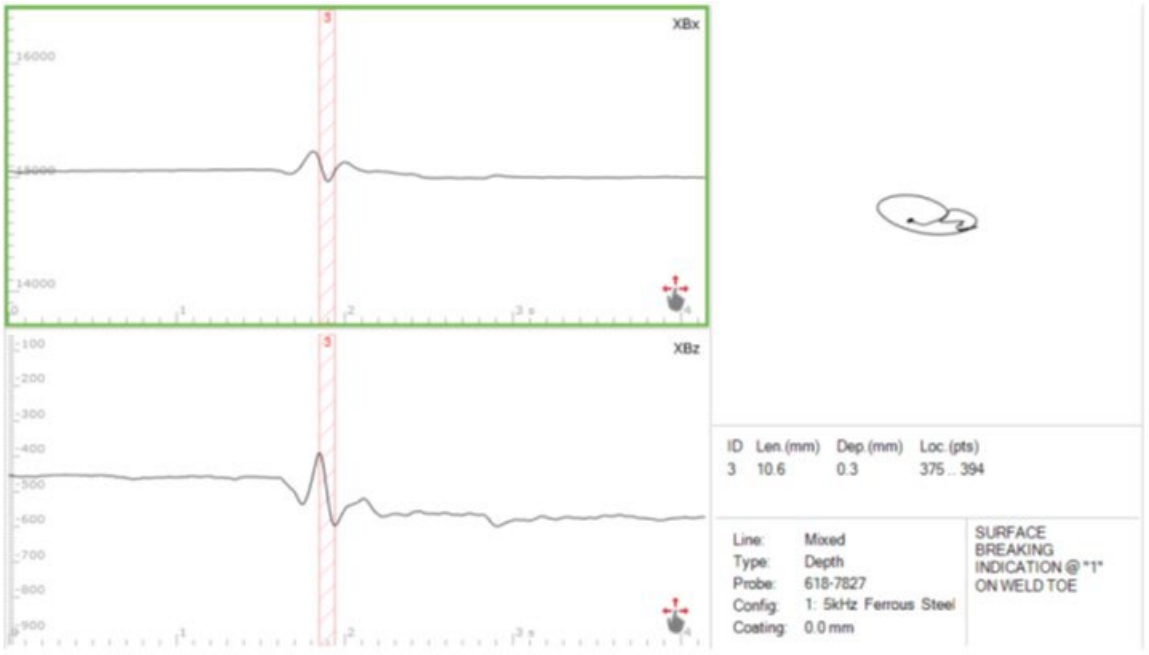

Figure 65. ACFM indication of defect at Location 1 in test panel MG-13

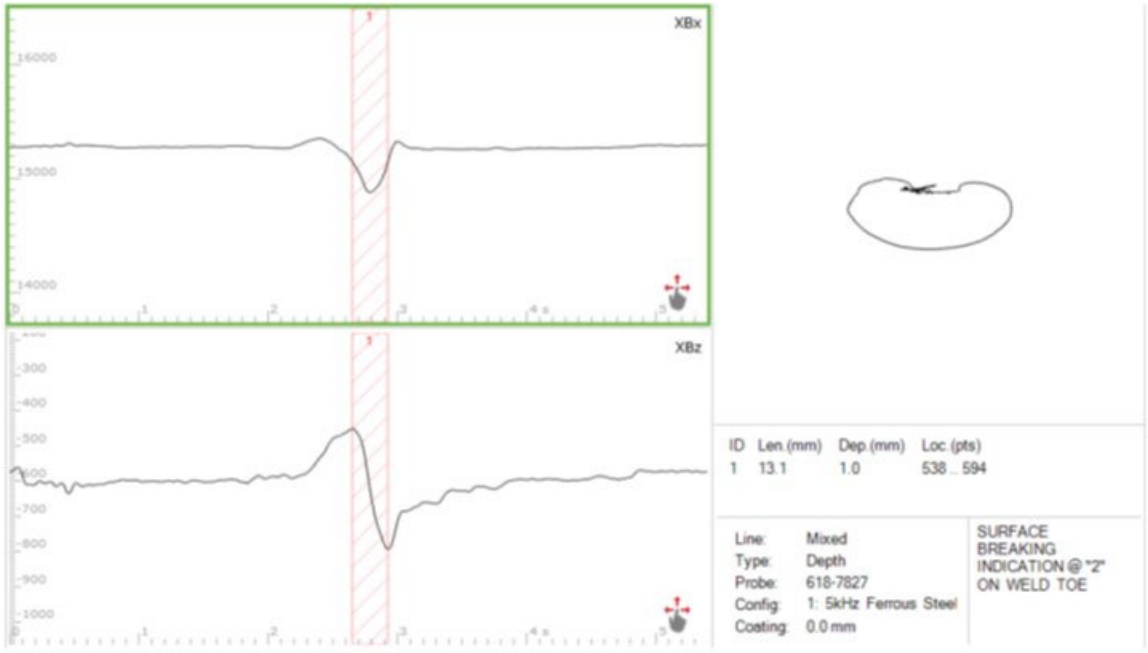

Figure 66. ACFM indication of defect at Location 2 in test panel MG-13

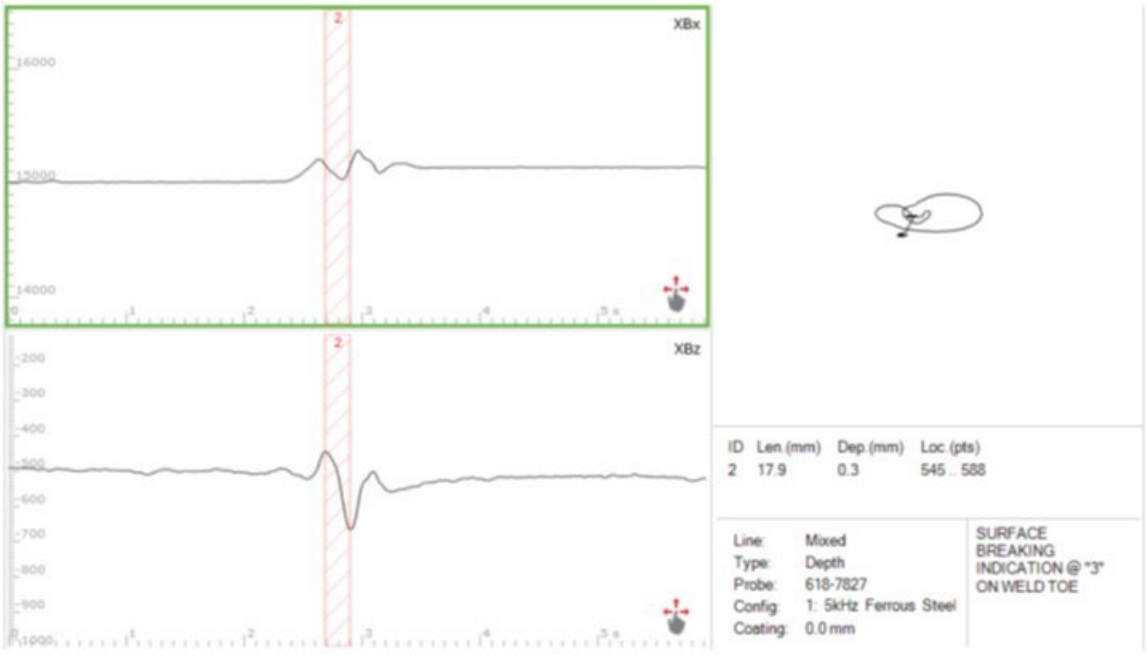

Figure 67. ACFM indication of defect at Location 3 in test panel MG-13

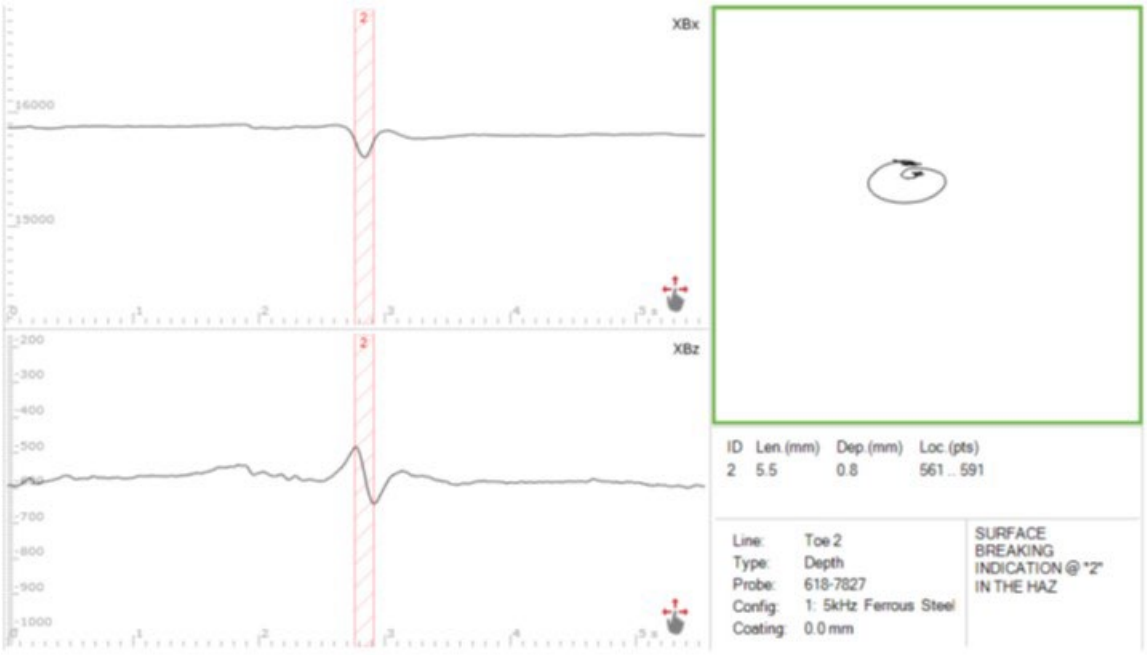

Figure 68. ACFM indication of defect at Location 2 in test panel MG-16

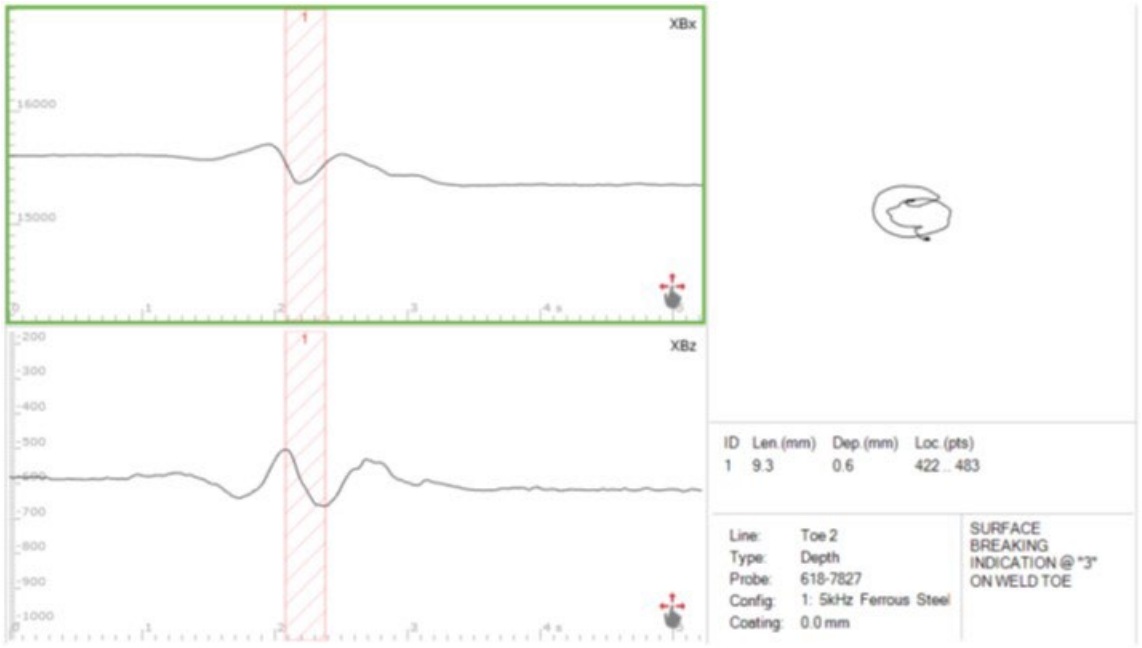

Figure 69. ACFM indication of defect at Location 3 in test panel MG-16

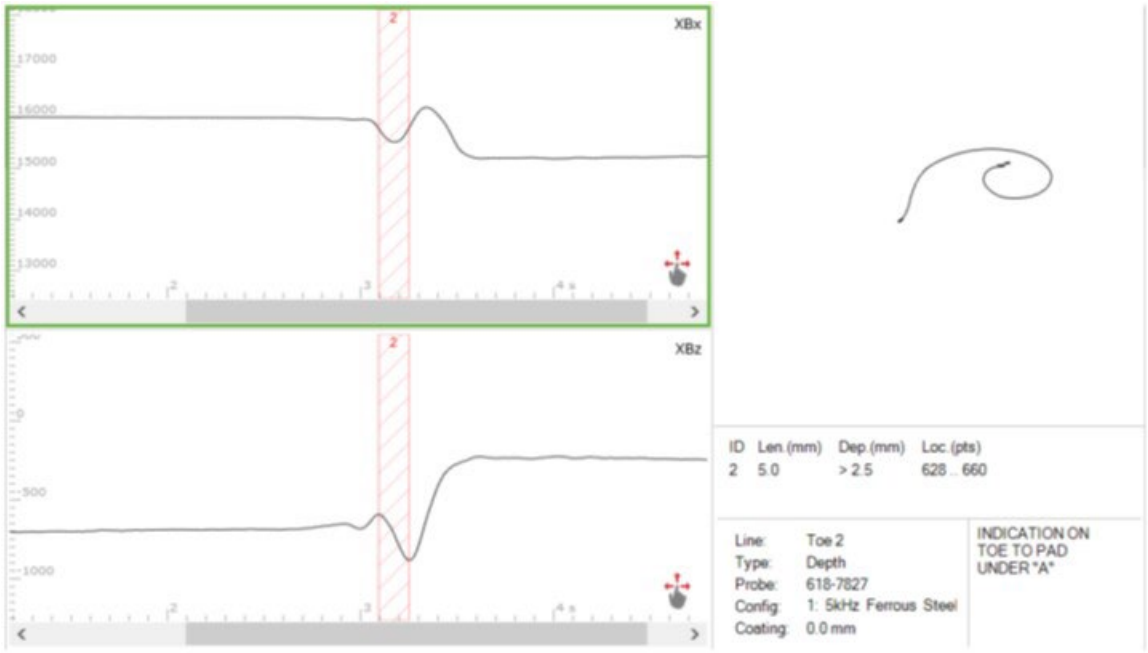

Figure 70. ACFM indication of defect at Location A in test panel TTCI-P2

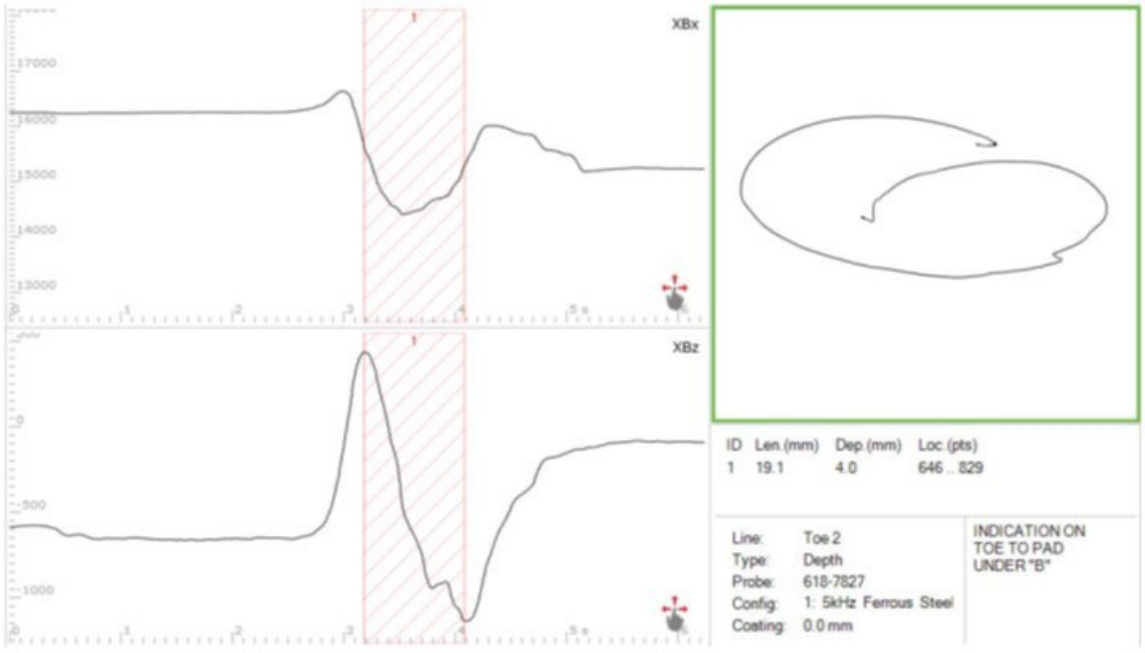

Figure 71. ACFM indication of defect at Location B in test panel TTCI-P2

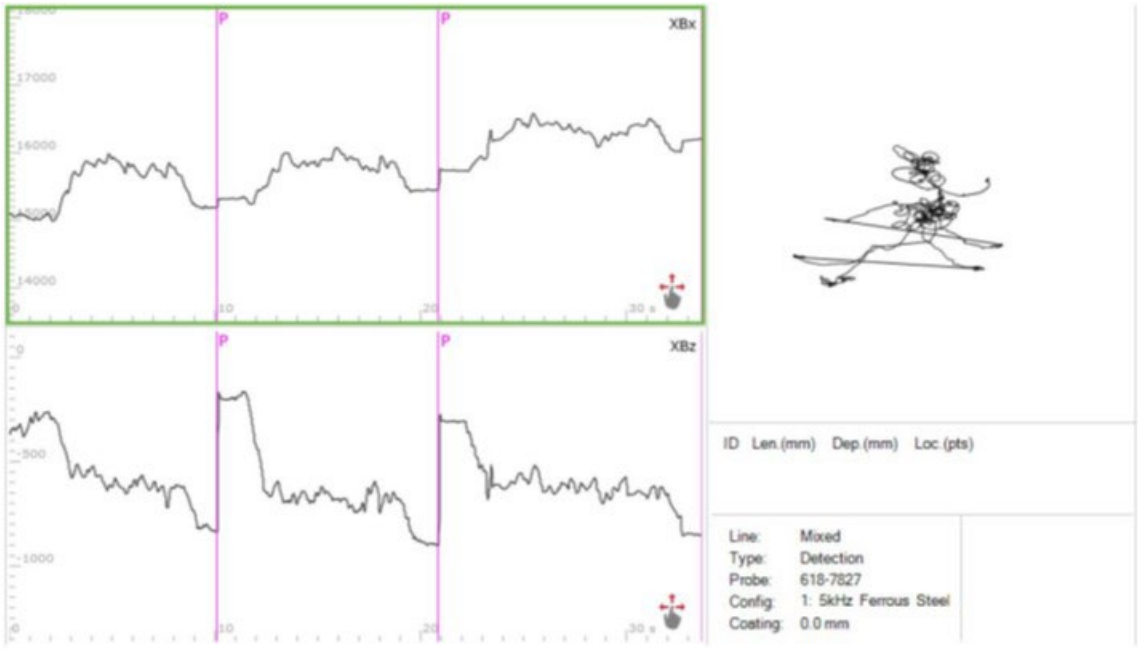

Figure 72. ACFM single probe scan of test panel MGL-3

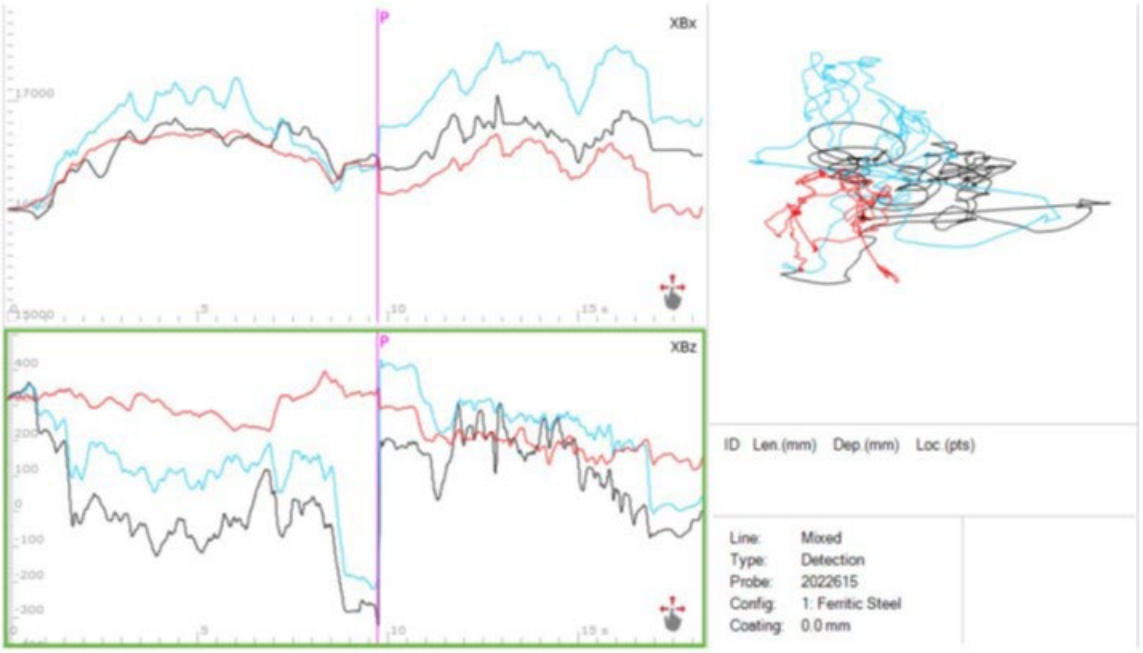

Figure 73. ACFM array probe scan of test panel MGL-3

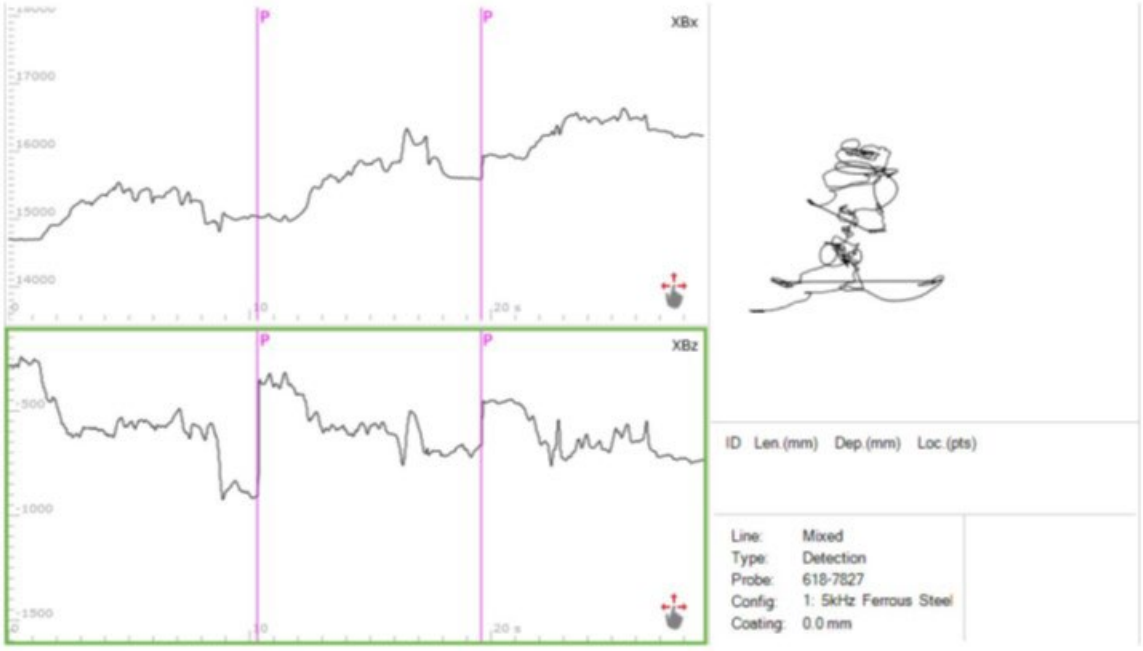

Figure 74. ACFM single probe scan of test panel MGL-9

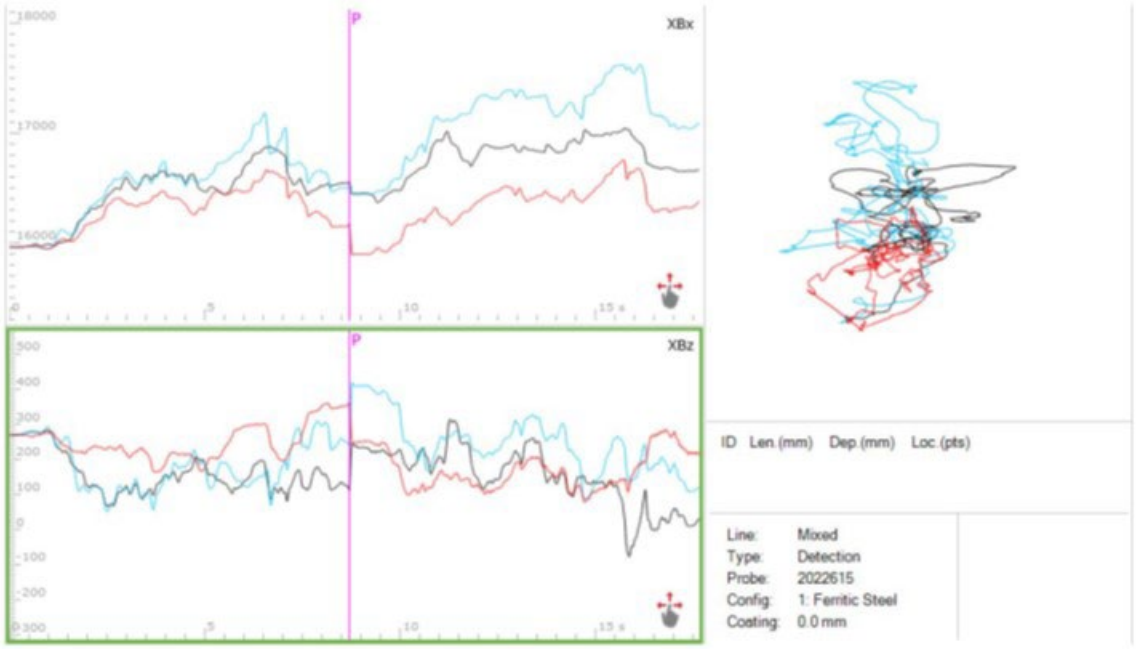

Figure 75. ACFM array probe scan of test panel MGL-9

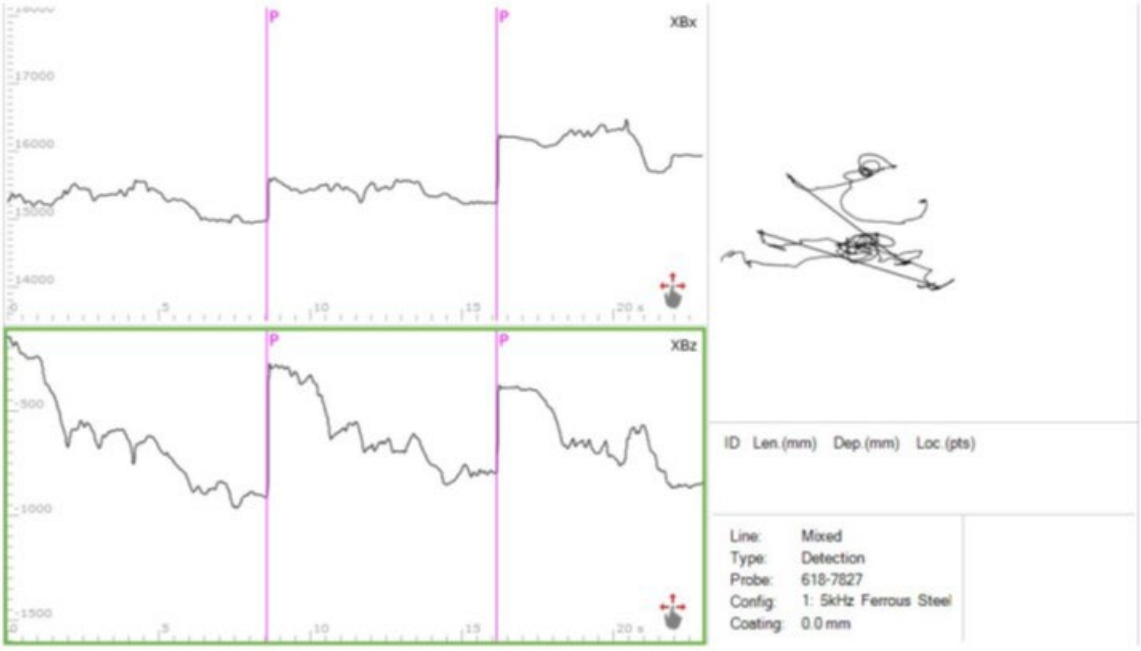

Figure 76. ACFM single probe scan of test panel MGL-10

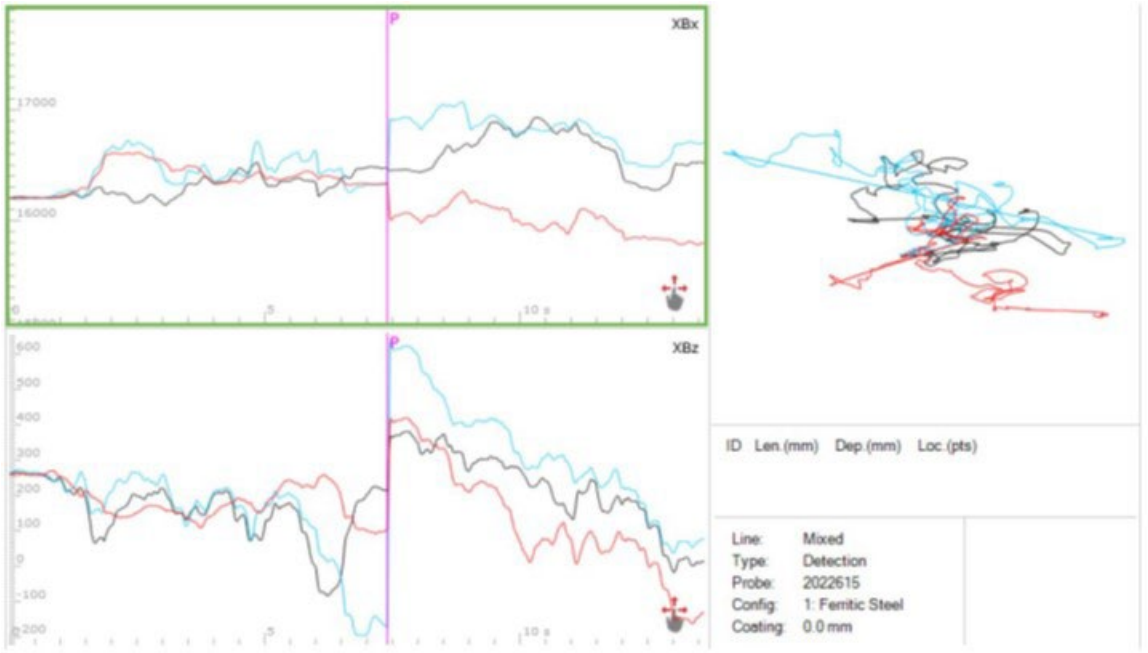

Figure 77. ACFM array probe scan of test panel MGL-10

Figure 78. PAUT indication of defect at Location A in test panel TTCI-2

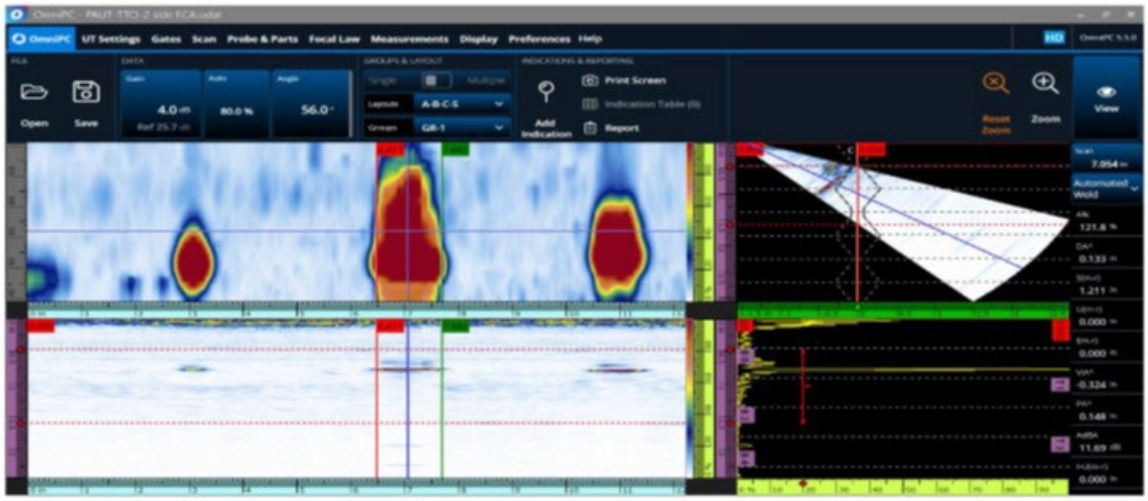

Figure 79. PAUT indication of defect at Location C in test panel TTCI-2

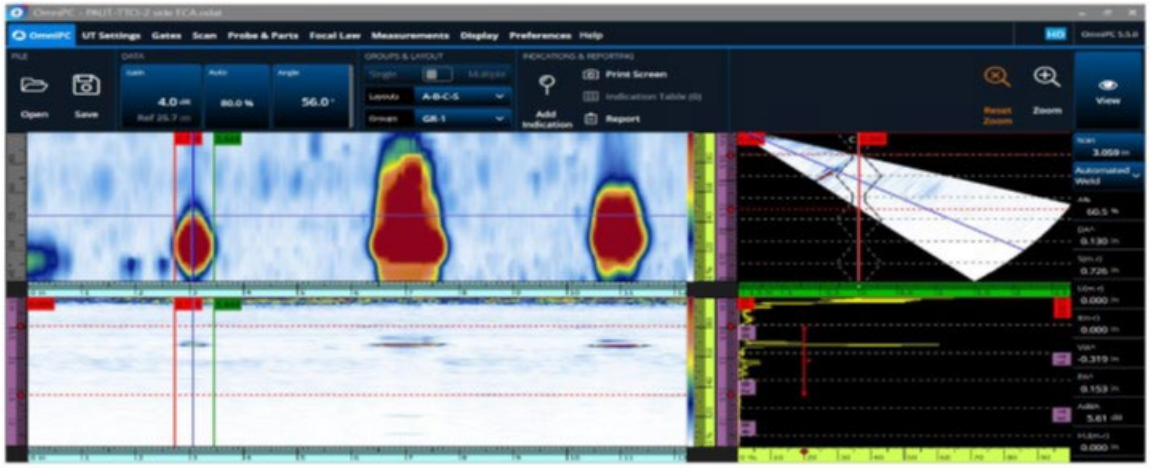

Figure 80. PAUT indication of defect at Location E in test panel TTCI-2

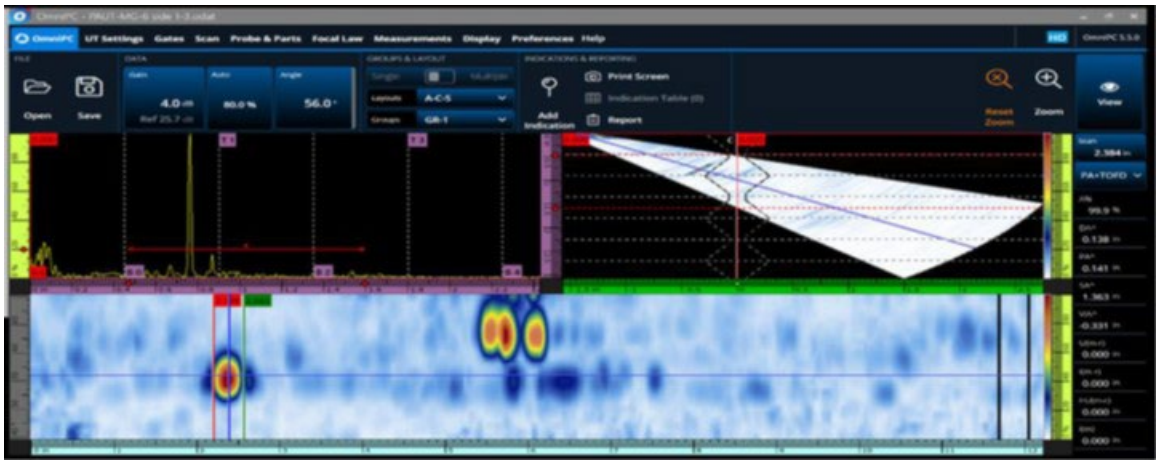

Figure 81. PAUT indication of defect at Location 1 in test panel MG-6

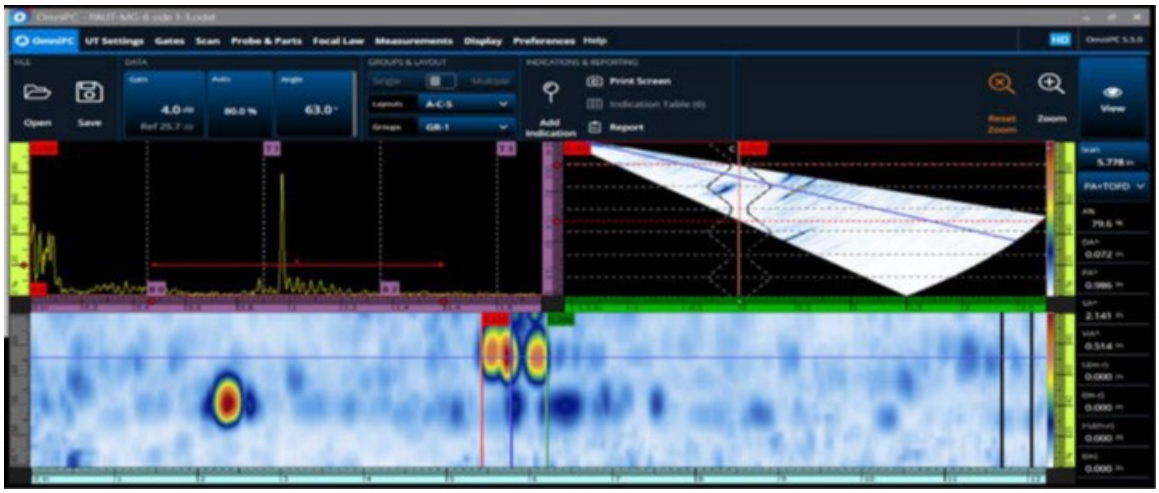

Figure 82. PAUT indication of defect at Location 2 in test panel MG-6

Figure 83. PAUT indication of defect at Location 3 in test panel MG-6

Figure 84. PAUT indication of defect at Location 1 in test panel MG-13

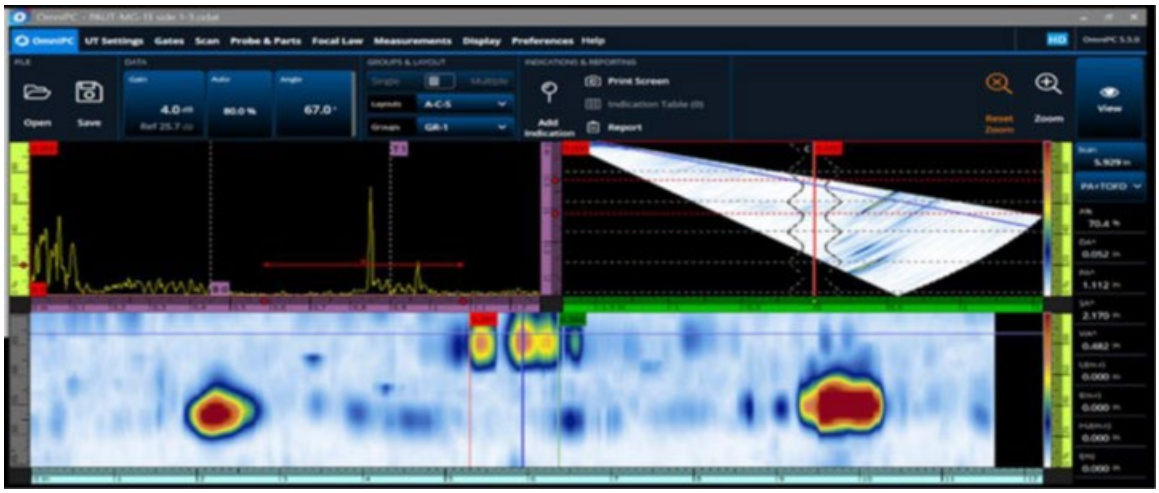

Figure 85. PAUT indication of defect at Location 2 in test panel MG-13

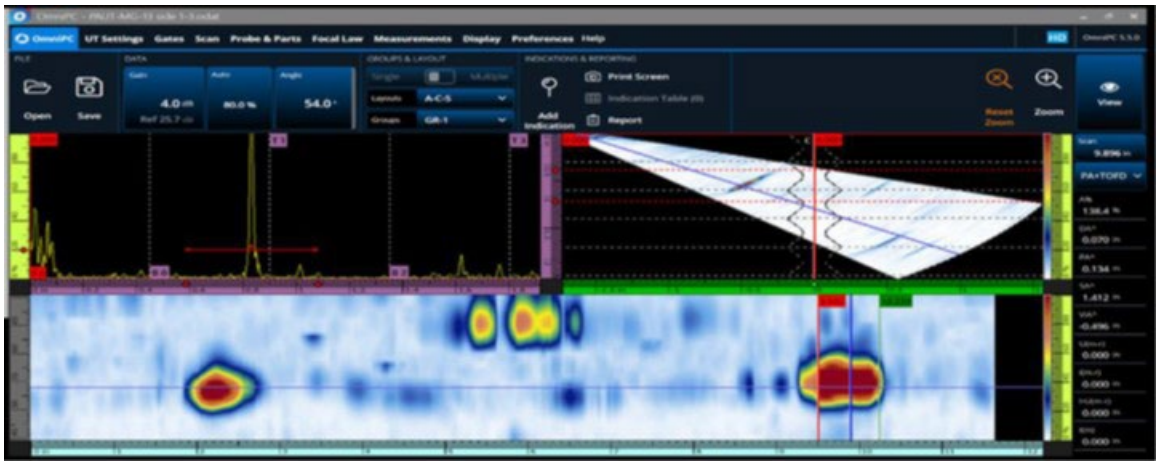

Figure 86. PAUT indication of defect at Location 3 in test panel MG-13

Figure 87. PAUT indication of defect at Location 1 in test panel MG-16

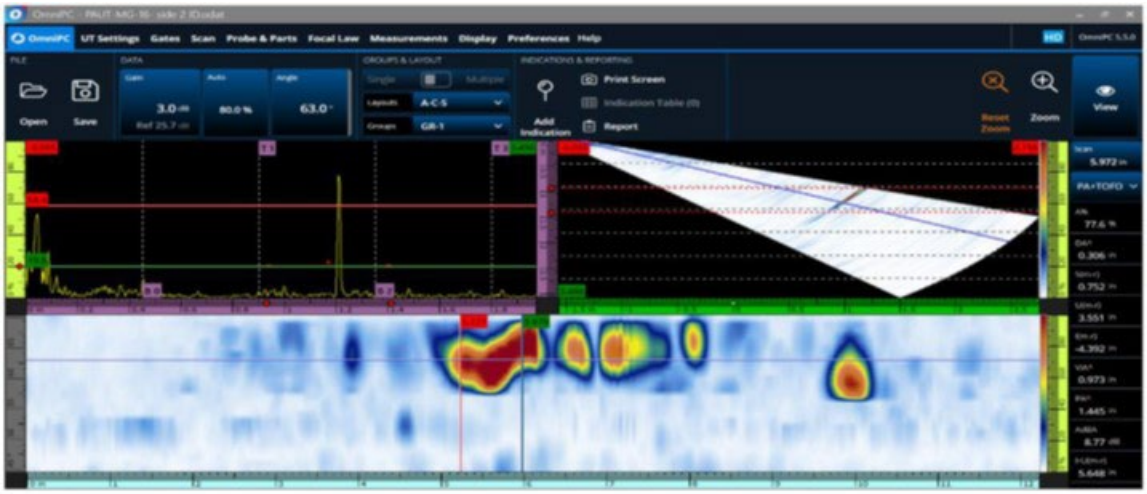

Figure 88. PAUT indication of defect at Location 2 in test panel MG-16

Figure 89. PAUT indication of defect at Location 3 in test panel MG-16

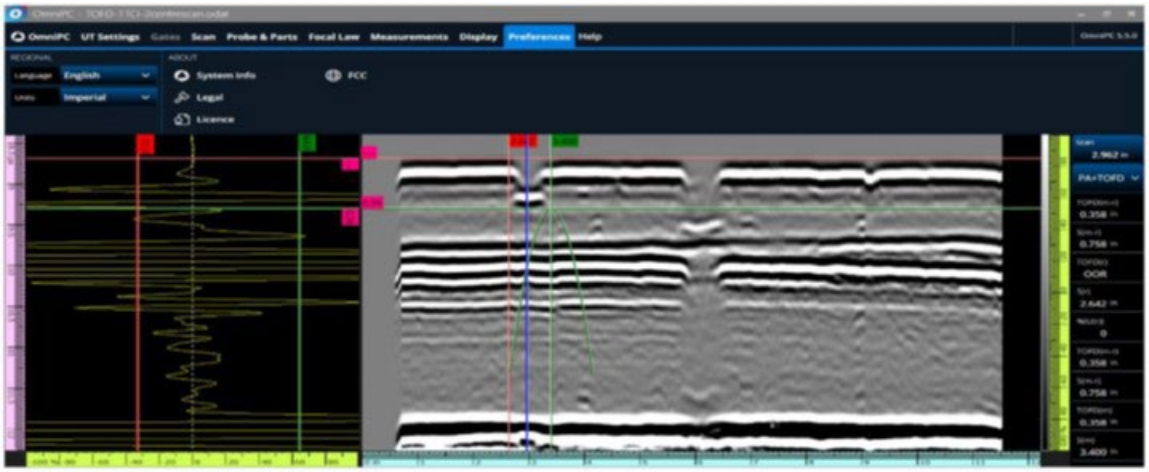

Figure 90. TOFD indication of defect at Location A in test panel TTCI-2

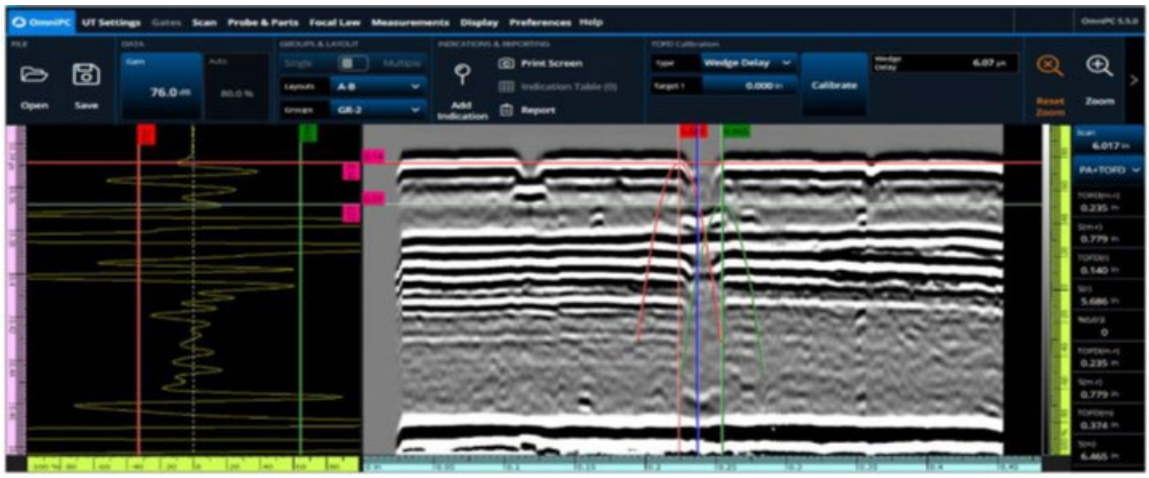

Figure 91. TOFD indication of defect at Location C in test panel TTCI-2

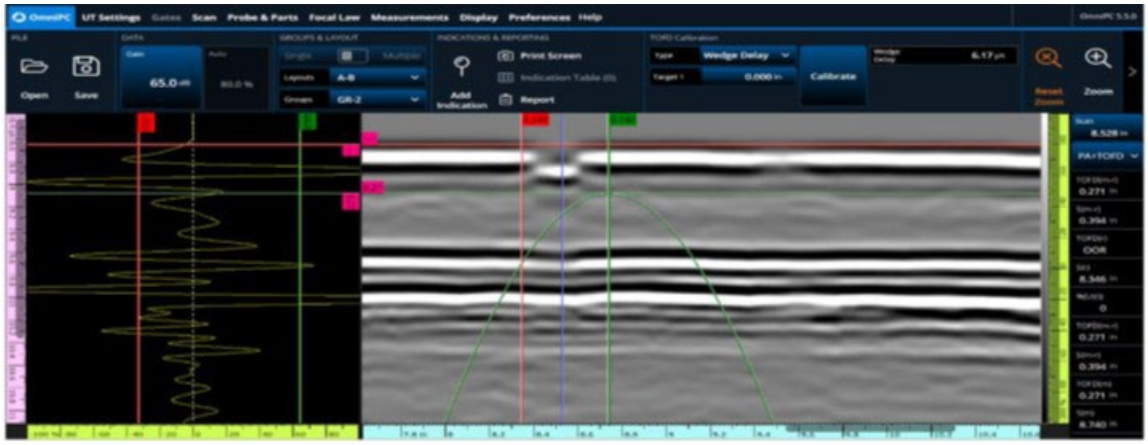

Figure 92. TOFD indication of defect at Location E in test panel TTCI-2

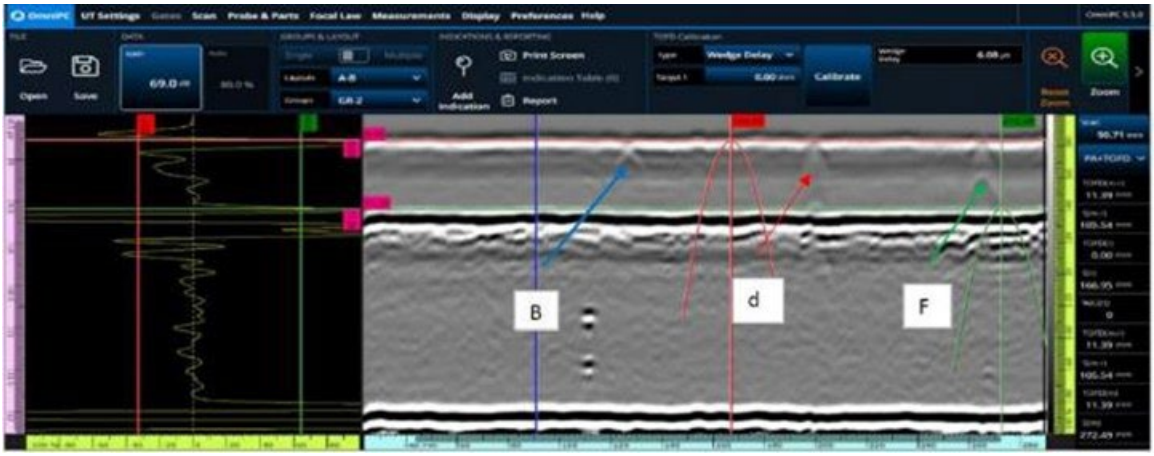

Figure 93. TOFD indications of defect at Location B, D and F in test panel TTCI-2

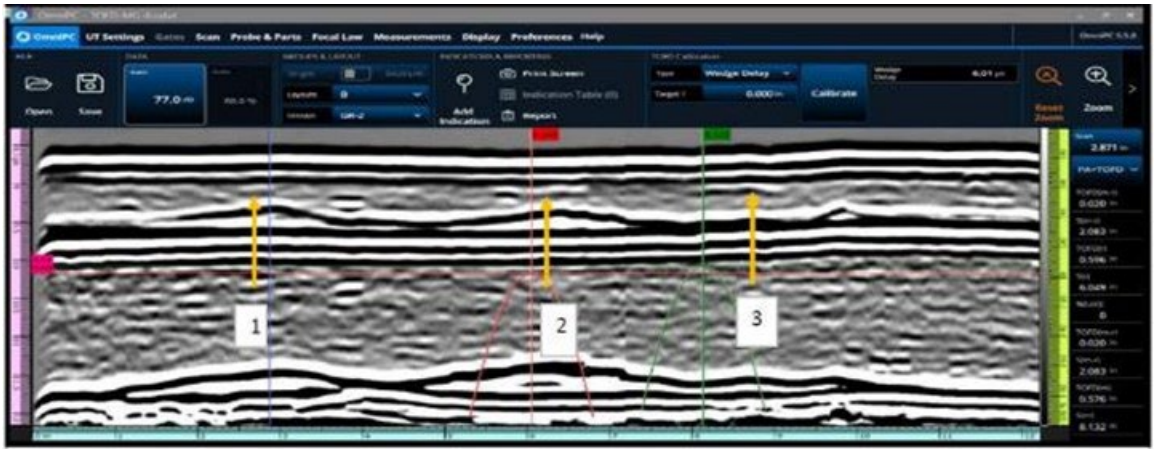

Figure 94. TOFD indication of defect at Location 1, 2 and 3 in test panel MG-6

Figure 95. TOFD indication of defect at Location 1, 2 and 3 in test panel MG-13

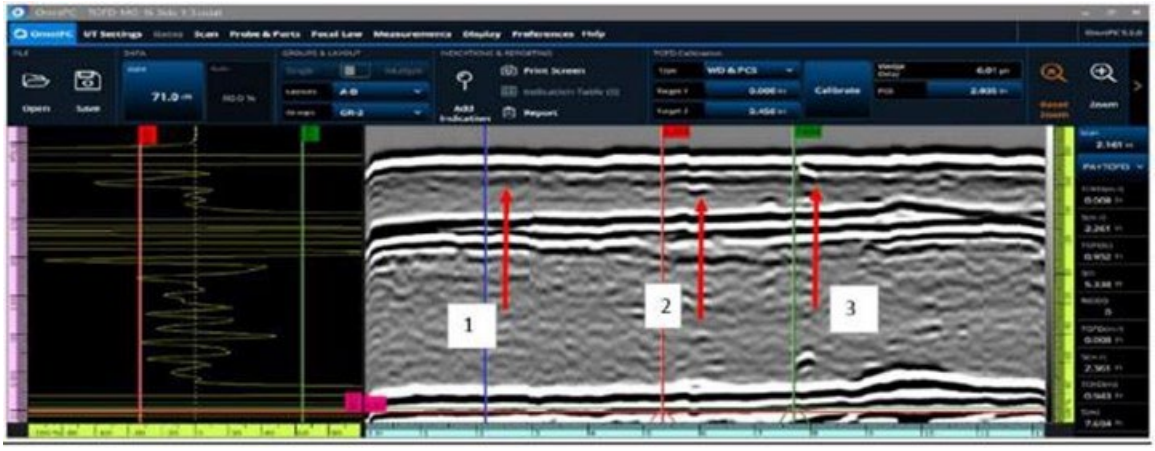

Figure 96. TOFD indication of defect at Location 1, 2 and 3 in test panel MG-16

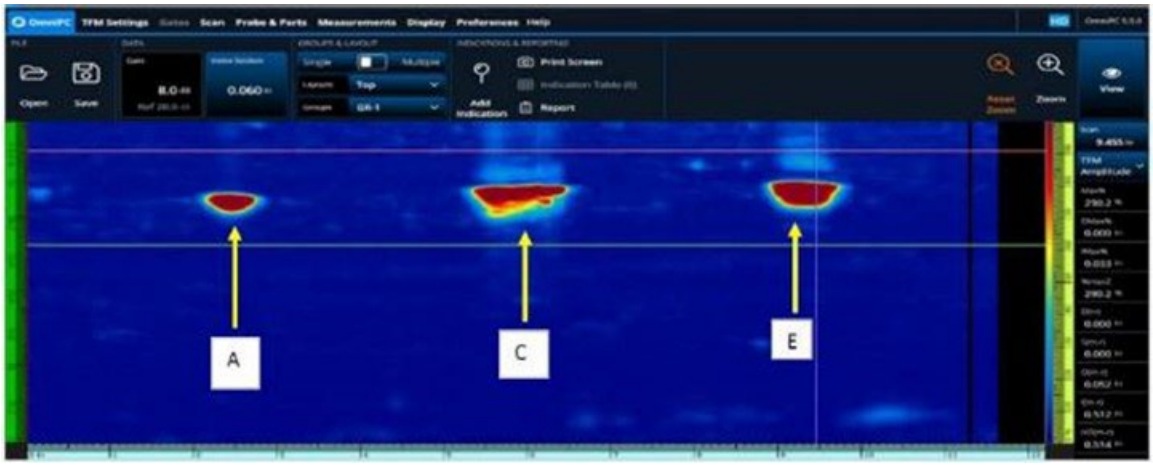

Figure 97. FMC/TFM indication of defect at Location A, C and E in test panel TTCI-2

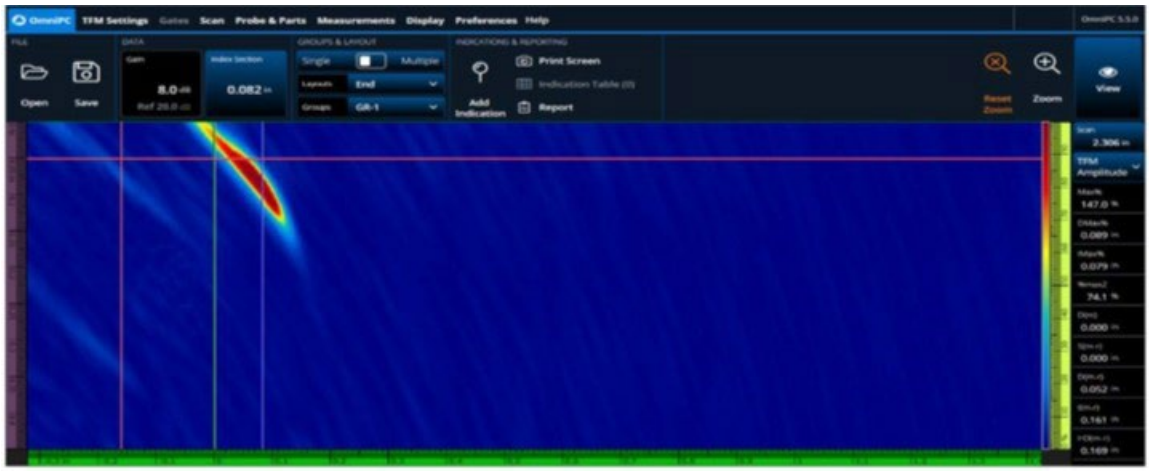

Figure 98. FMC/TFM indication of defect at Location 1 in test panel MG-6

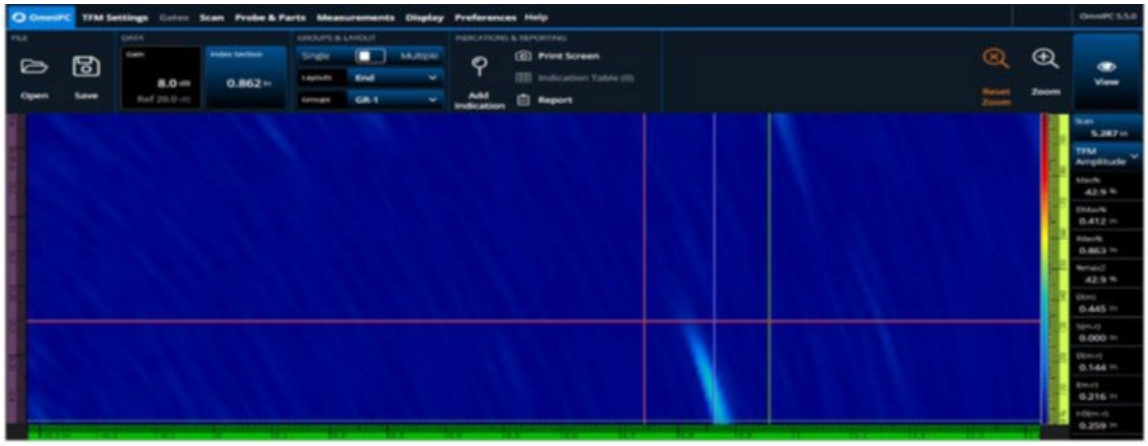

Figure 99. FMC/TFM indication of defect at Location 2 in test panel MG-6

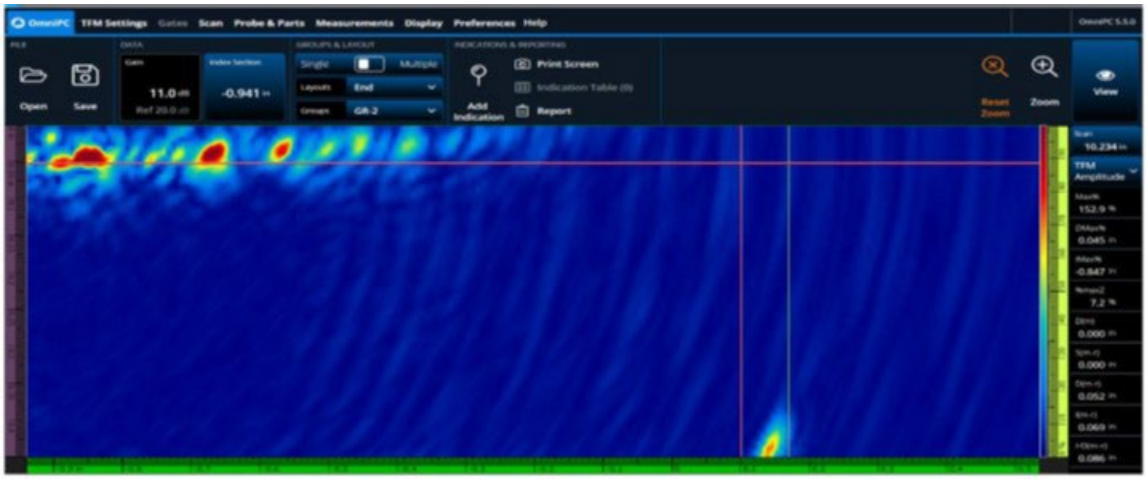

Figure 100. FMC/TFM indication of defect at Location 3 in test panel MG-6

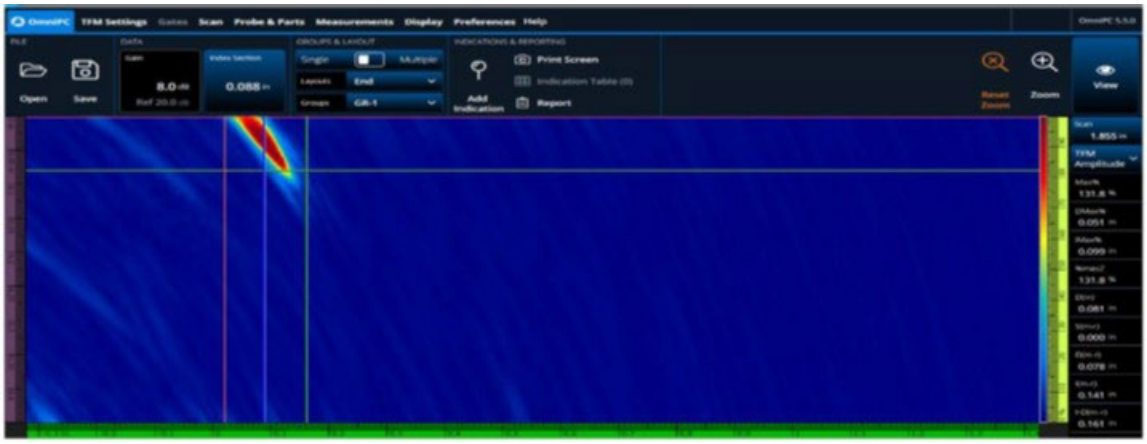

Figure 101. FMC/TFM indication of defect at Location 1 in test panel MG-13

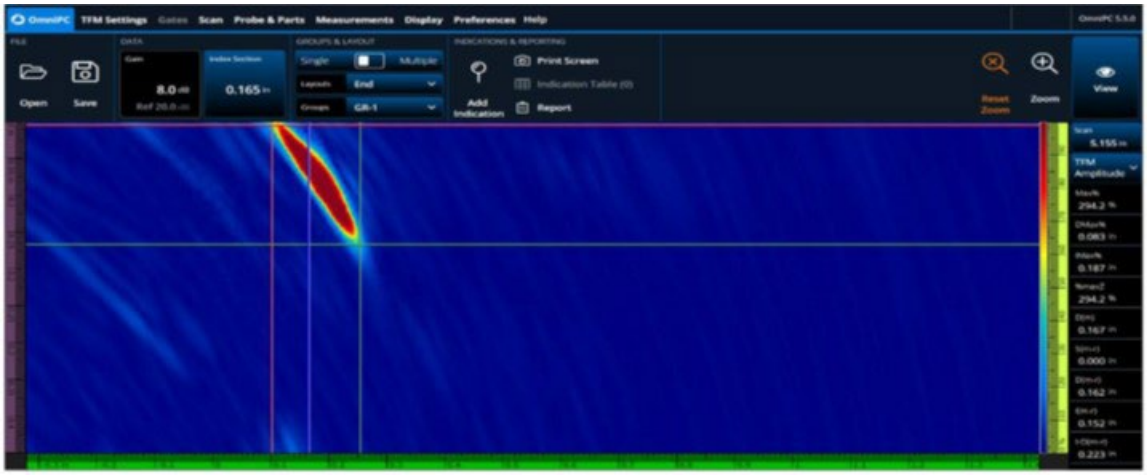

Figure 102. FMC/TFM indication of defect at Location 2 in test panel MG-13

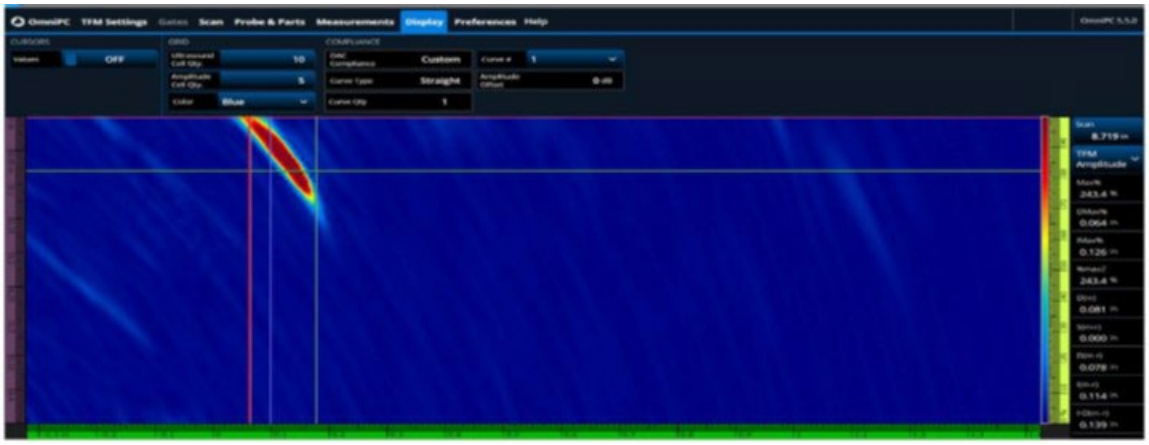

Figure 103. FMC/TFM indication of defect at Location 3 in test panel MG-13

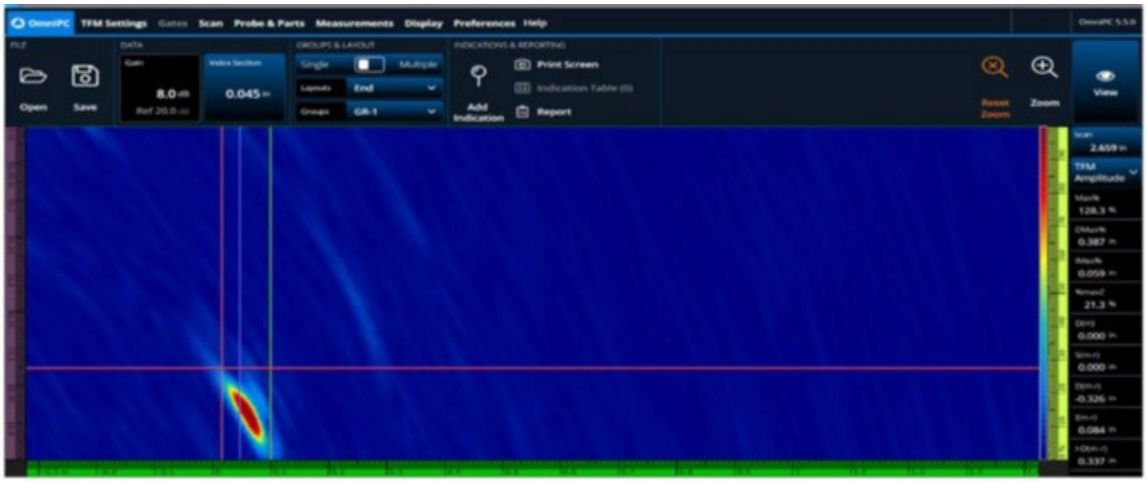

Figure 104. FMC/TFM indication of defect at Location 1 in test panel MG-16

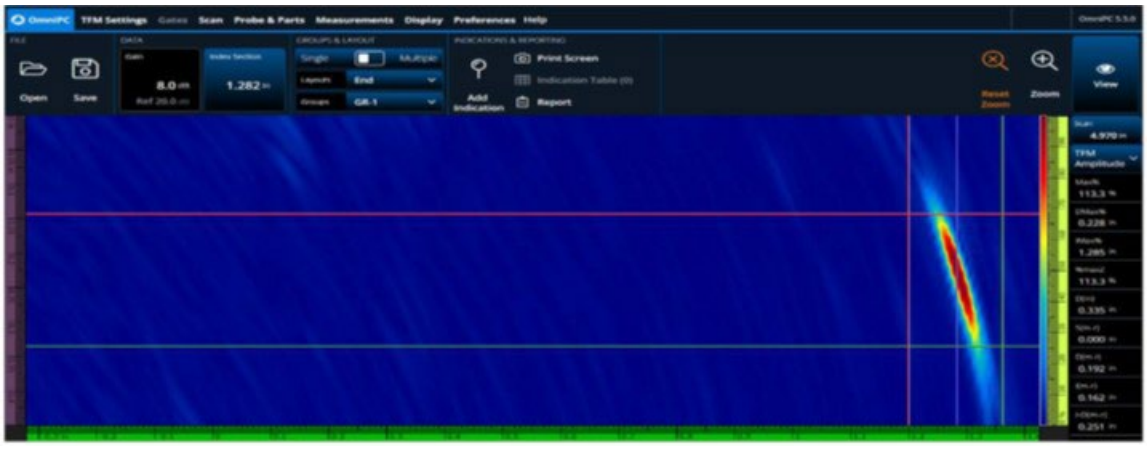

Figure 105. FMC/TFM indication of defect at Location 2 in test panel MG-16

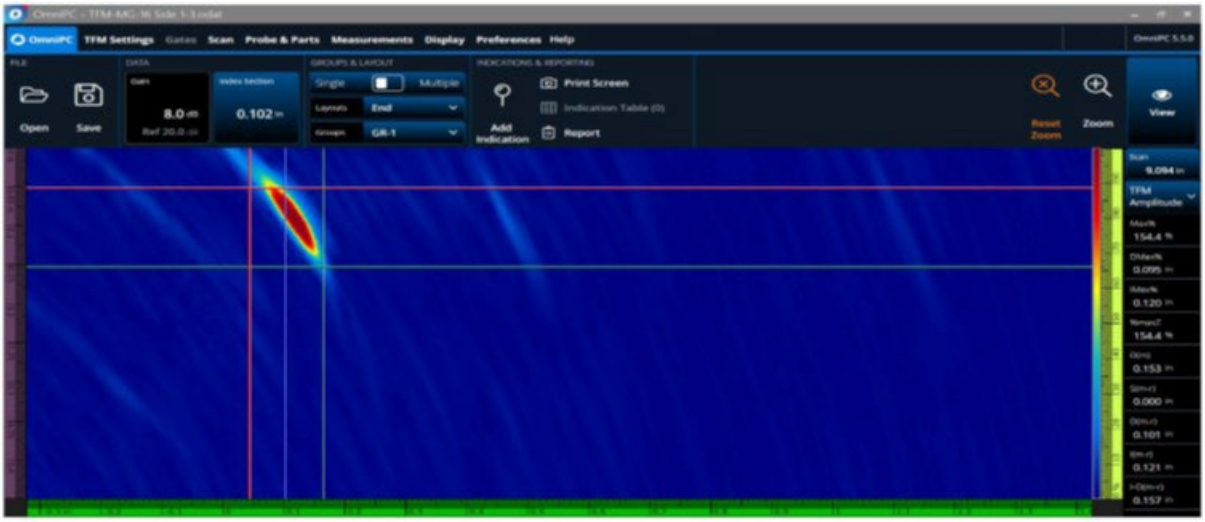

Figure 106. FMC/TFM indication of defect at Location 2 in test panel MG-16

Participant E

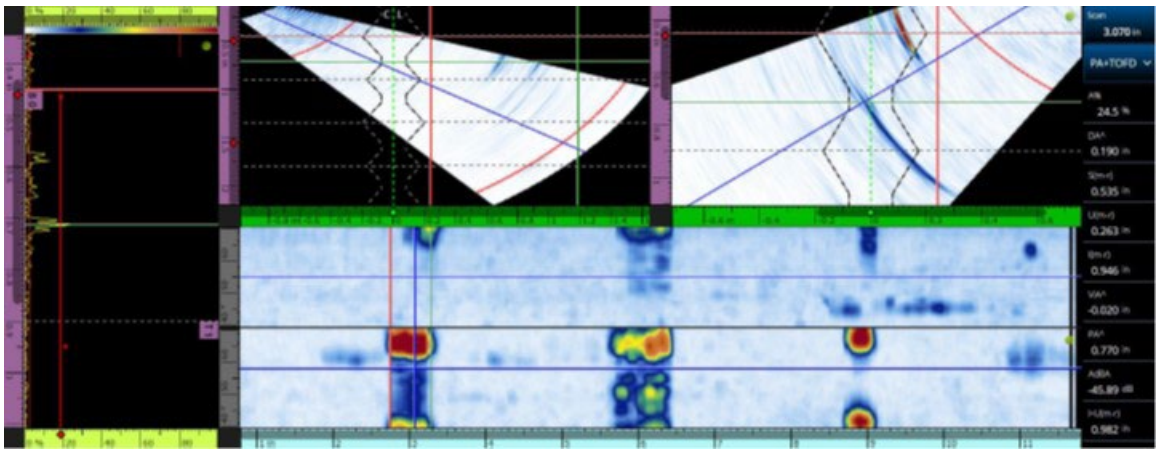

Figure 107. PAUT defect sizing at Location A in test panel TTCI-2 from ID-encoded scan

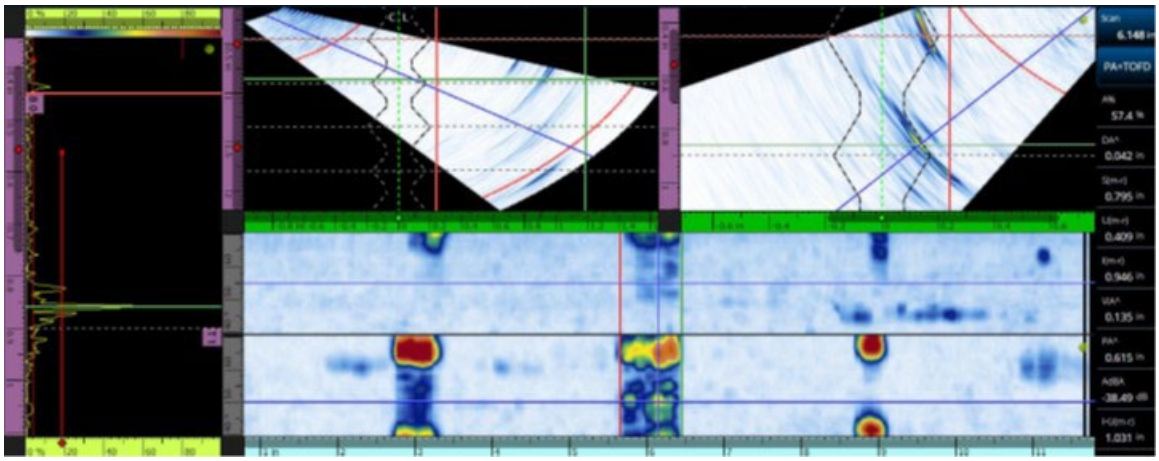

Figure 108. PAUT defect sizing at Location C in test panel TTCI-2 from ID-encoded scan

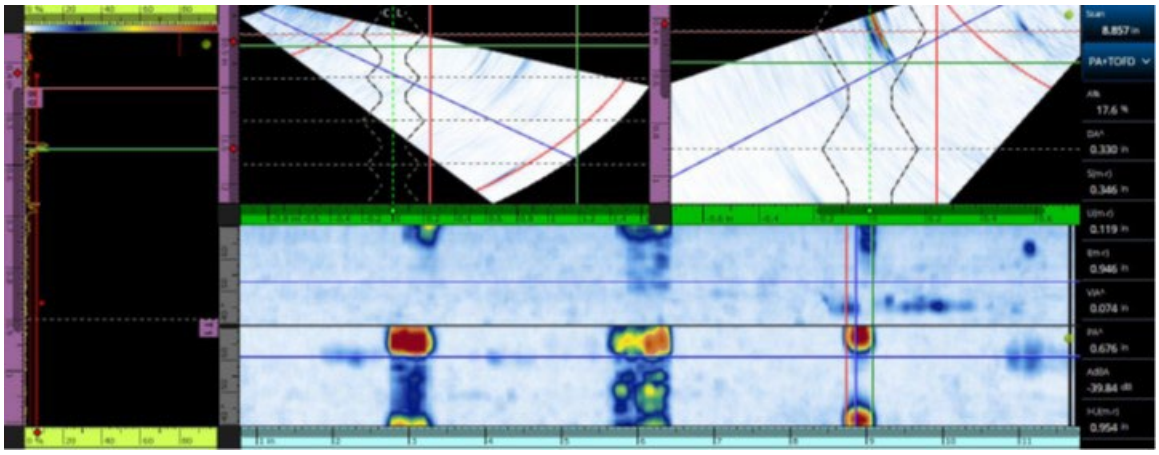

Figure 109. PAUT defect sizing at Location E in test panel TTCI-2 from ID-encoded scan

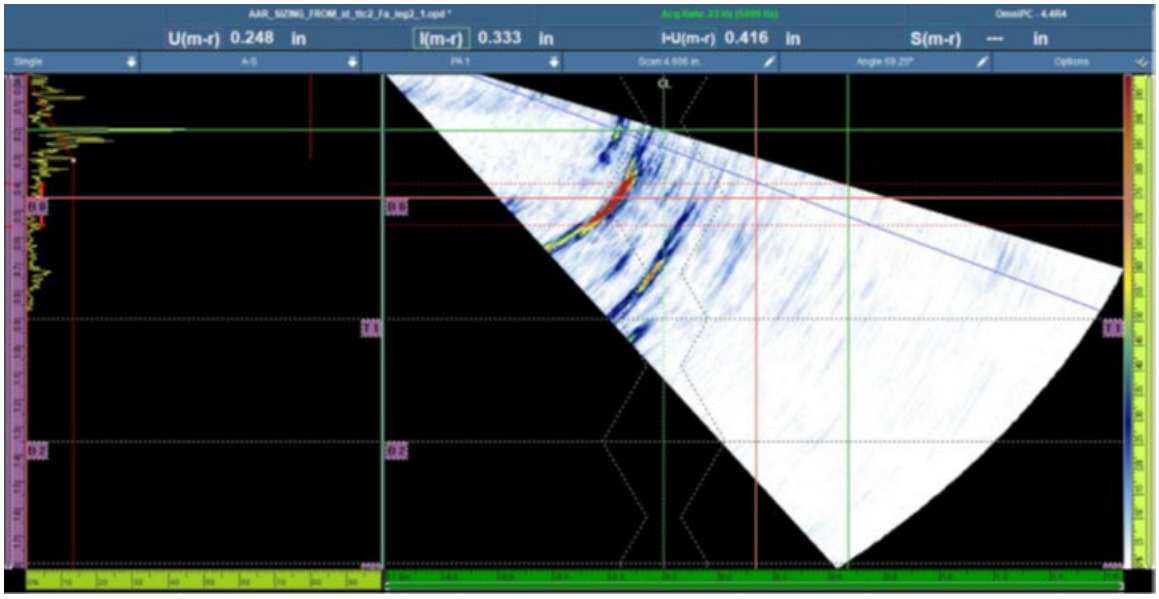

Figure 110. PAUT defect indication at Location A in test panel TTCI-2 from ID-raster scan

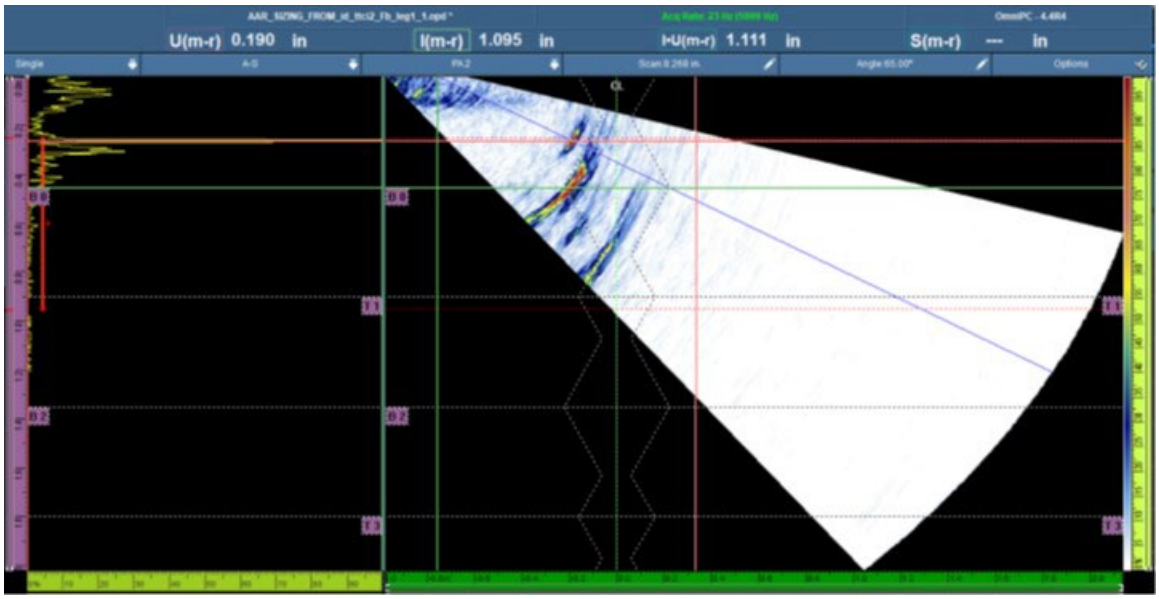

Figure 111. PAUT defect indication at Location B in test panel TTCI-2 from ID-raster scan

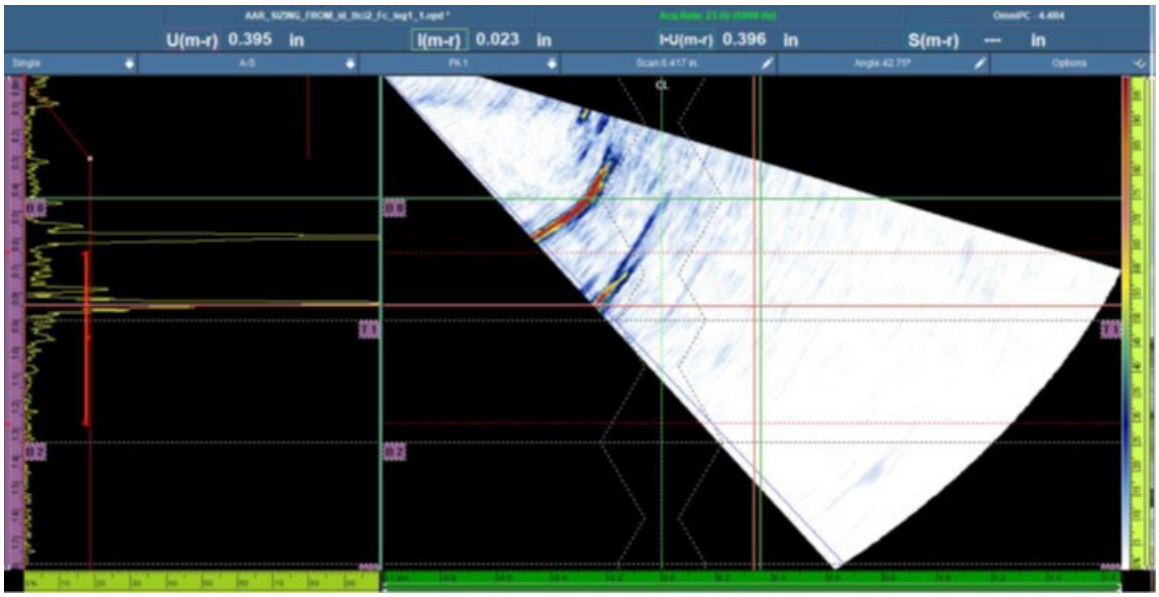

Figure 112. PAUT defect indication at Location C in test panel TTCI-2 from ID-raster scan

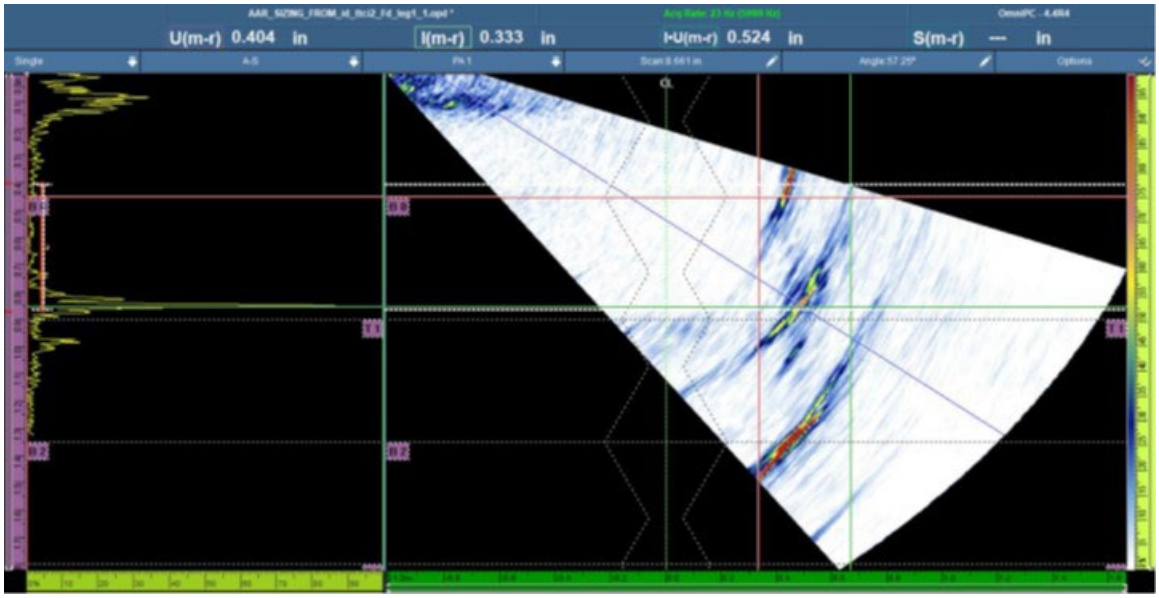

Figure 113. PAUT defect indication at Location D in test panel TTCI-2 from ID-raster scan

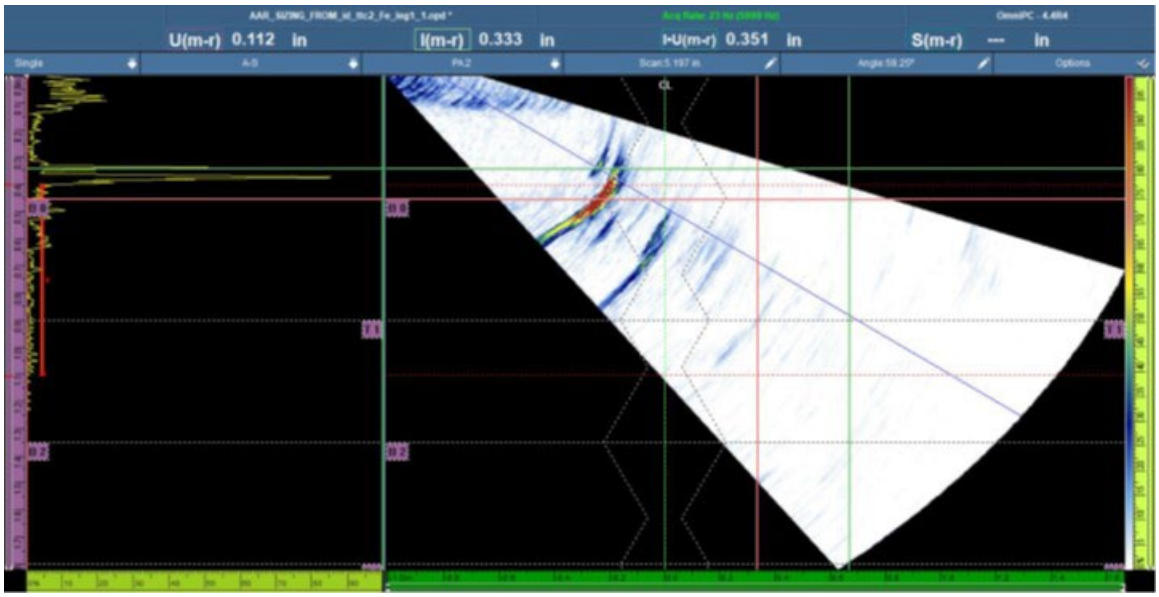

Figure 114. PAUT defect indication at Location E in test panel TTCI-2 from ID-raster scan

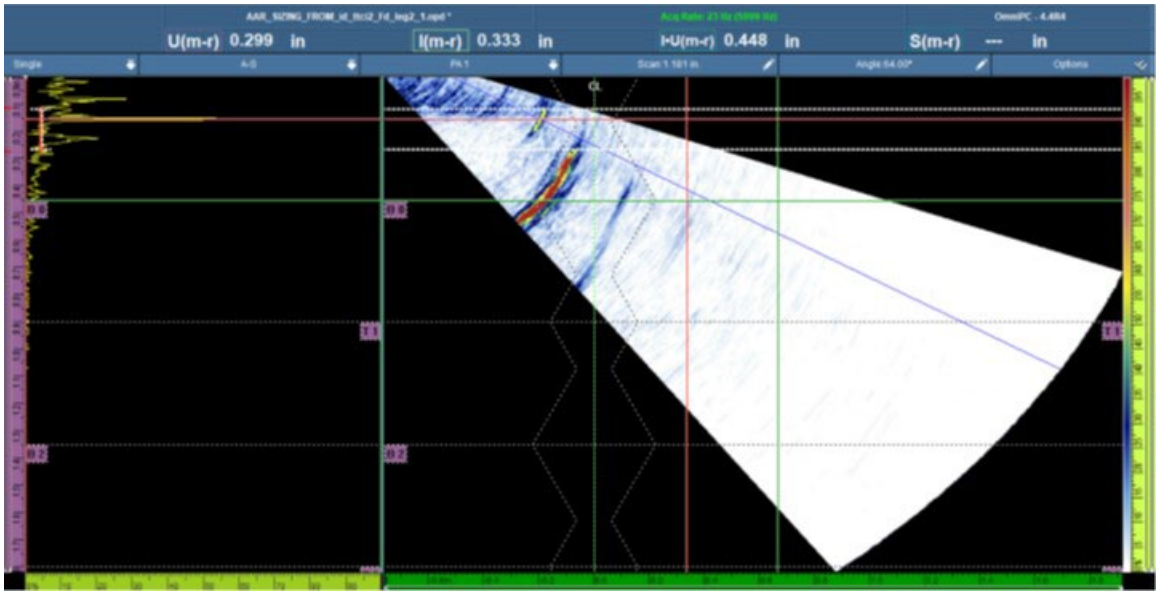

Figure 115. PAUT defect indication at Location F in test panel TTCI-2 from ID-raster scan

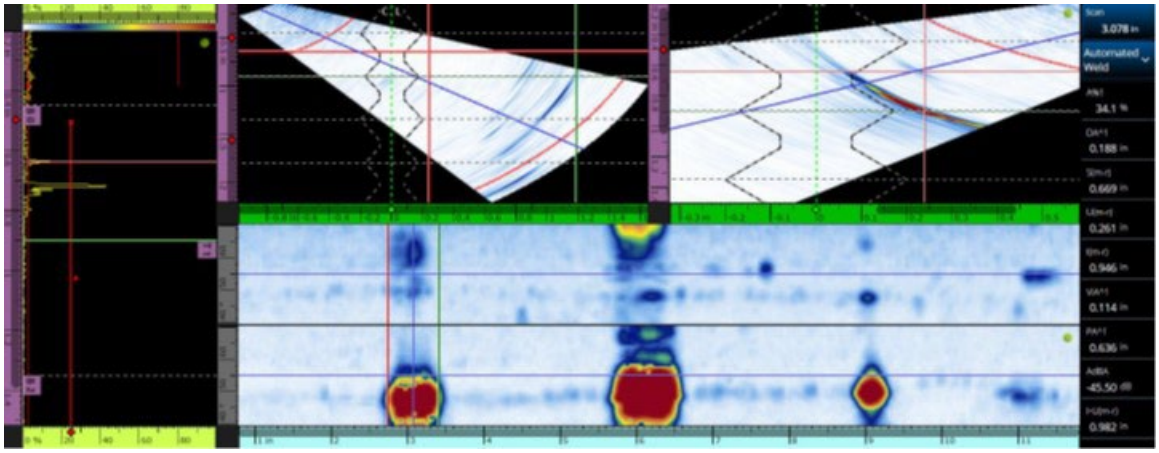

Figure 116. PAUT defect sizing at Location A in test panel TTCI-2 from OD-encoded scan

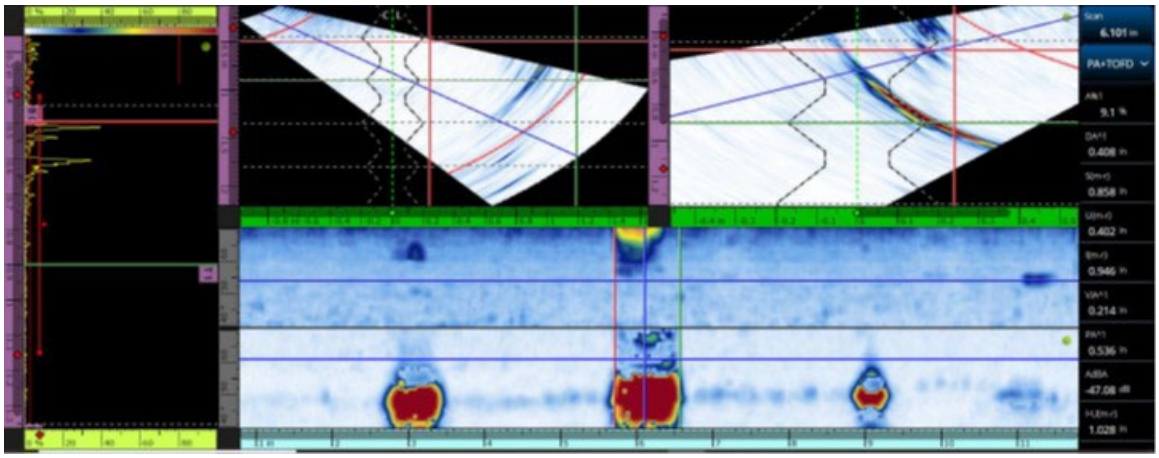

Figure 117. PAUT defect sizing at Location C in test panel TTCI-2 from OD-encoded scan

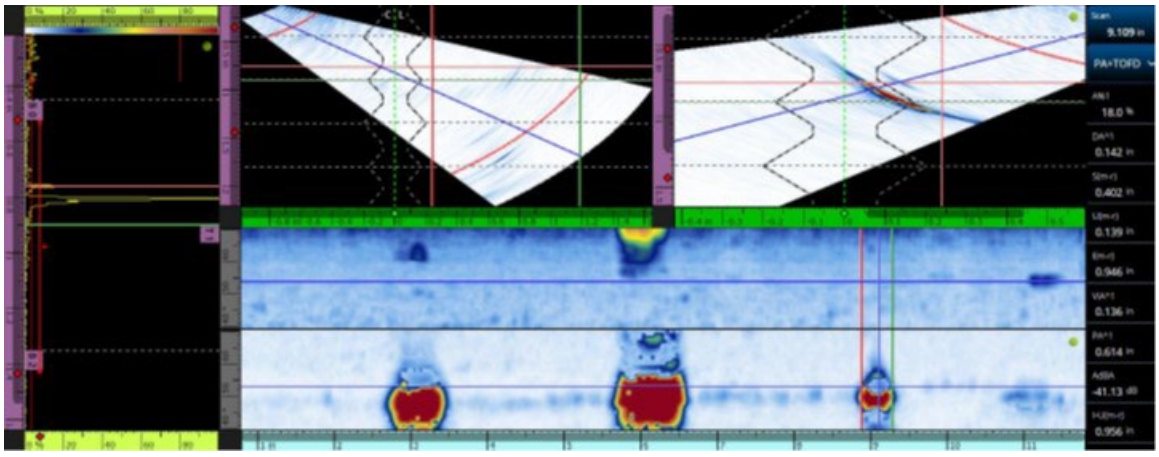

Figure 118. PAUT defect sizing at Location E in test panel TTCI-2 from OD-encoded scan

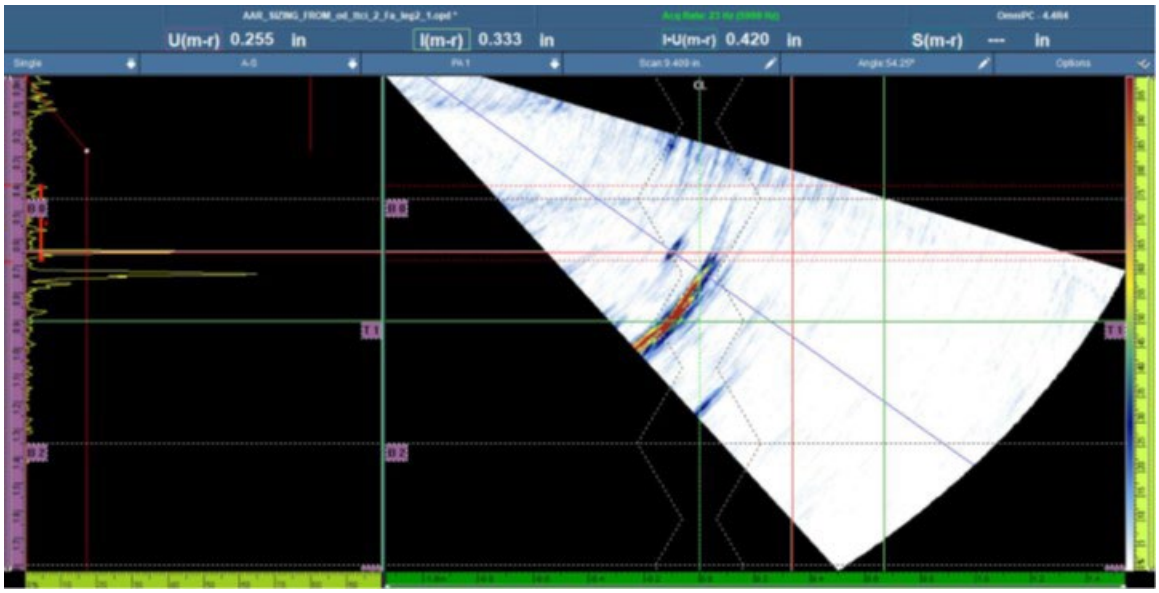

Figure 119. PAUT defect indication at Location A in test panel TTCI-2 from OD-raster scan

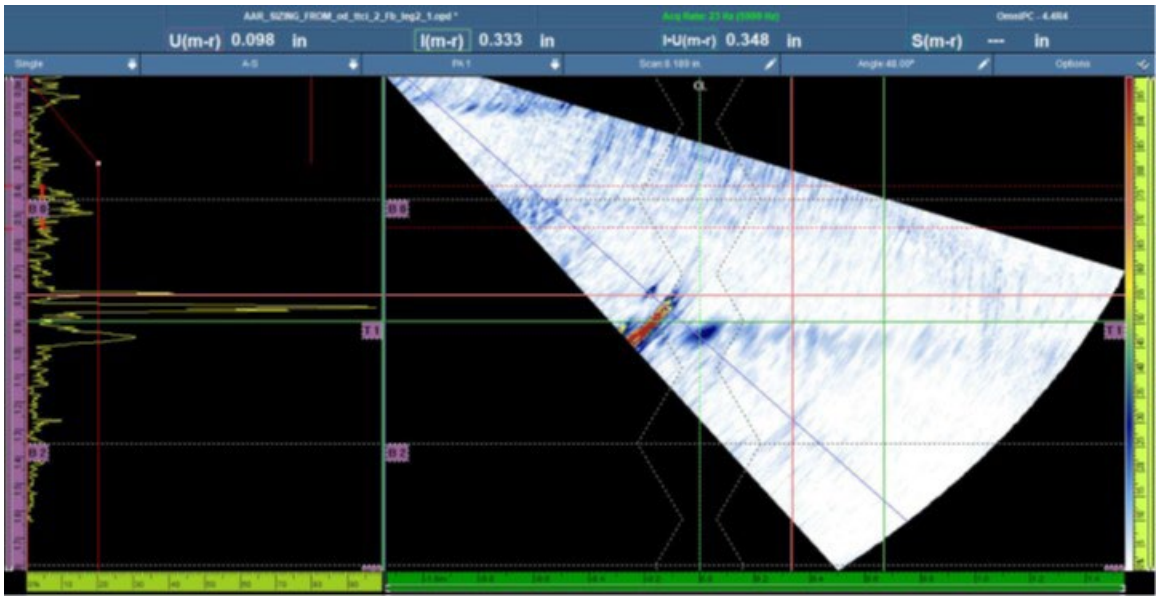

Figure 120. PAUT defect indication at Location B in test panel TTCI-2 from OD-raster scan

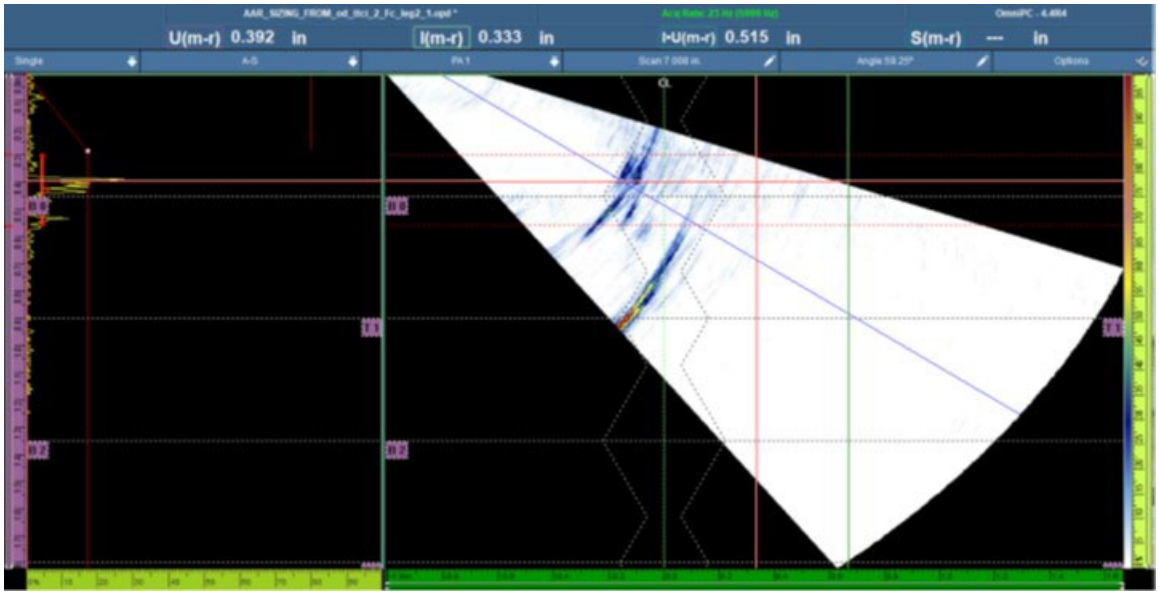

Figure 121. PAUT defect indication at Location C in test panel TTCI-2 from OD-raster scan

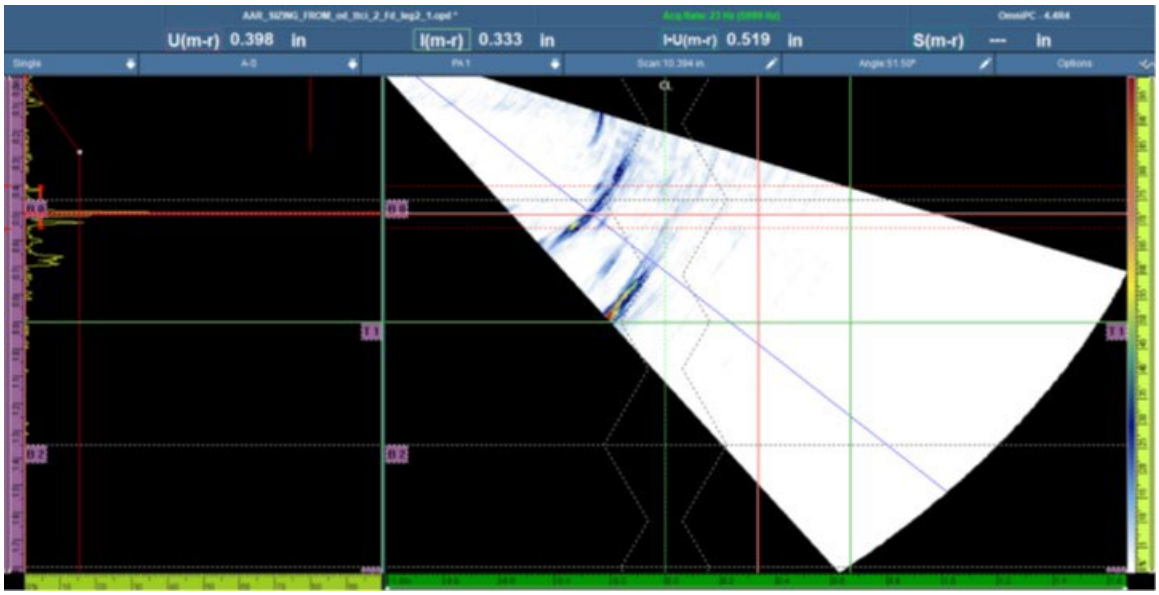

Figure 122. PAUT defect indication at Location D in test panel TTCI-2 from OD-raster scan

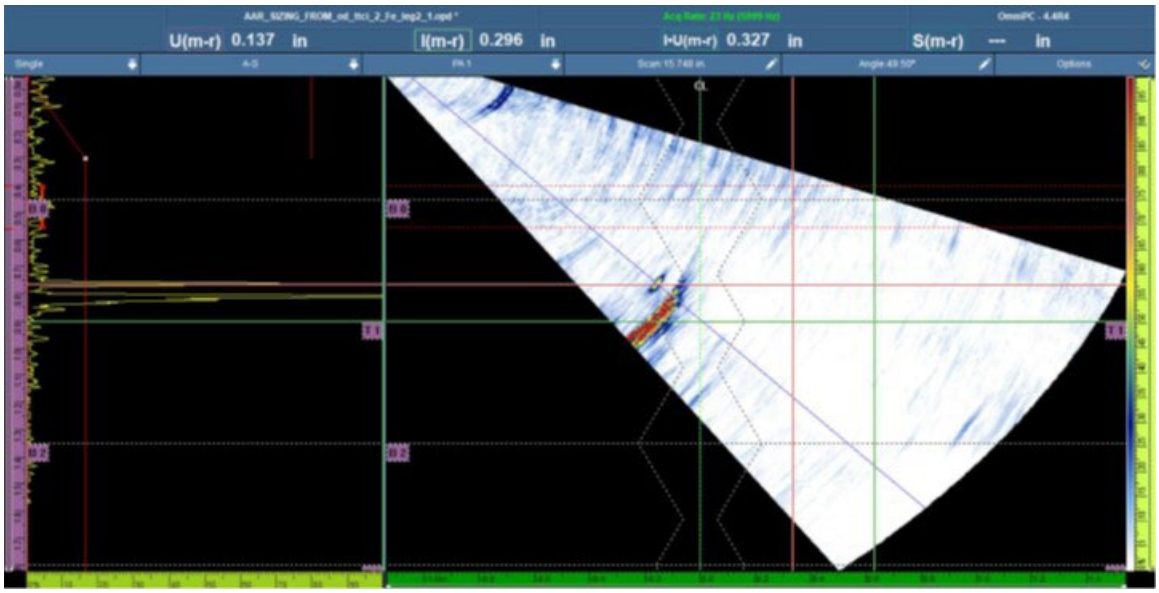

Figure 123. PAUT defect indication at Location E in test panel TTCI-2 from OD-raster scan

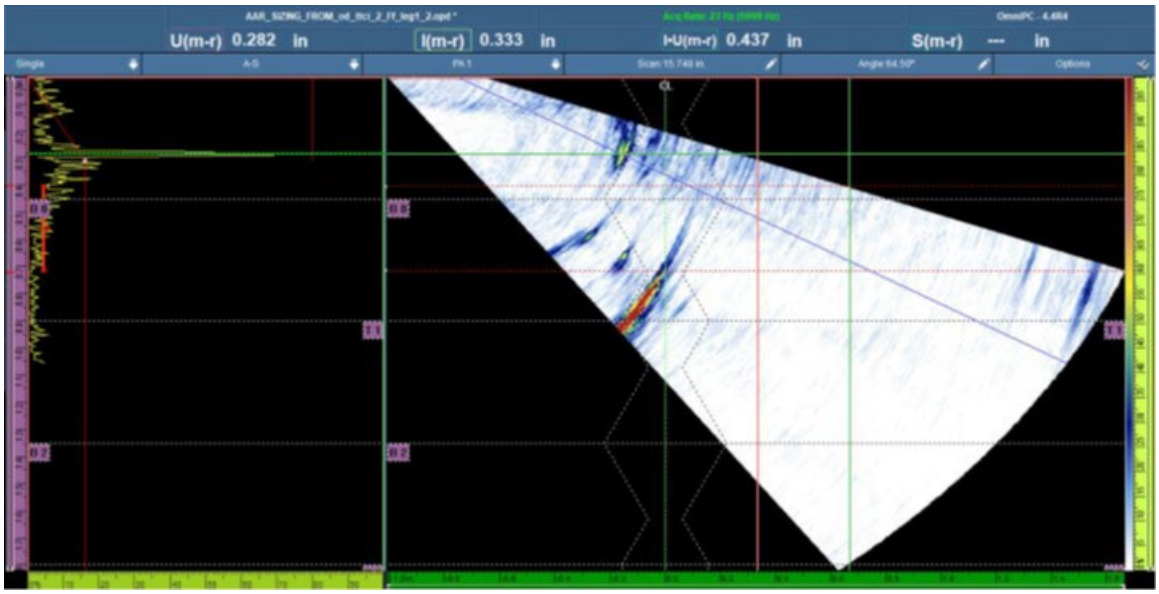

Figure 124. PAUT defect indication at Location F in test panel TTCI-2 from OD-raster scan

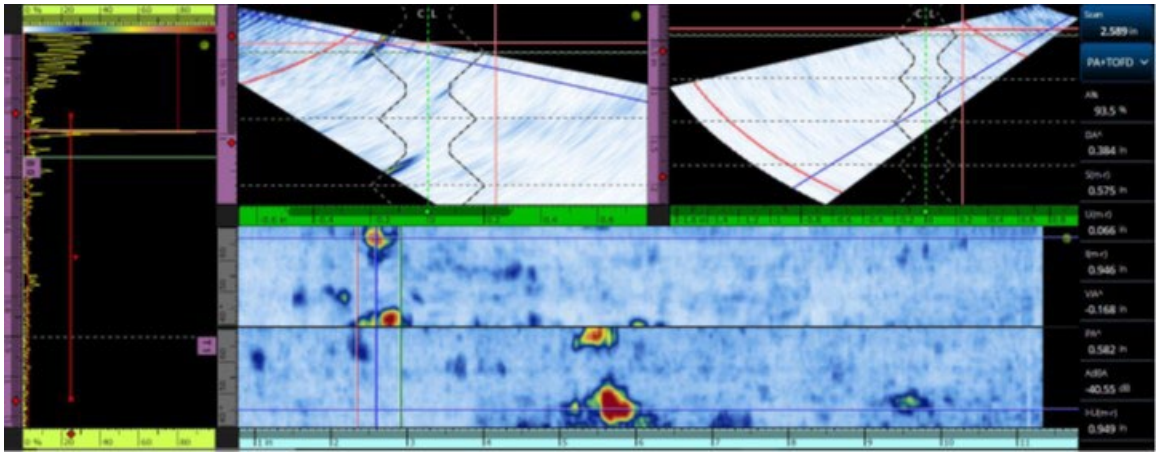

Figure 125. PAUT defect sizing at Location 1 in test panel MG-6 from ID-encoded scan

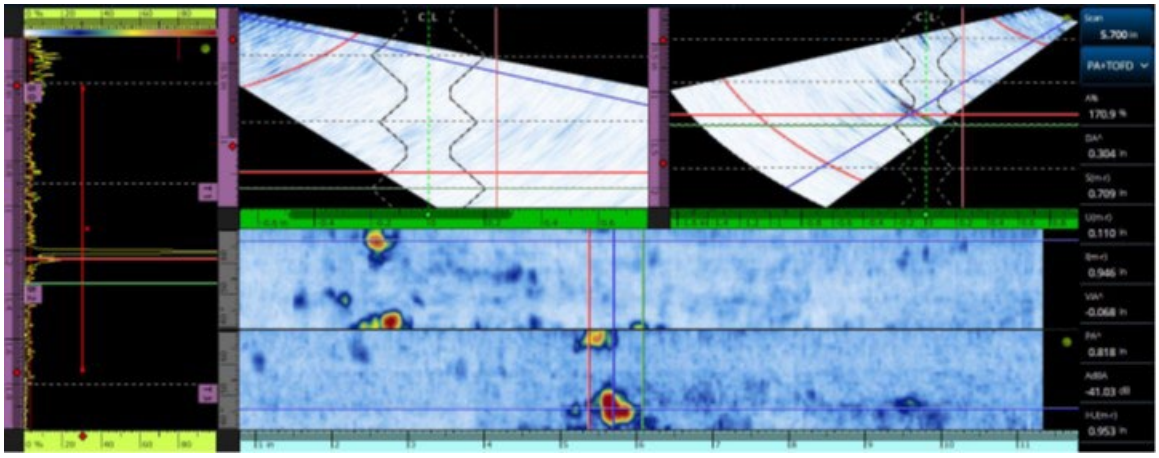

Figure 126. PAUT defect sizing at Location 2 in test panel MG-6 from ID-encoded scan

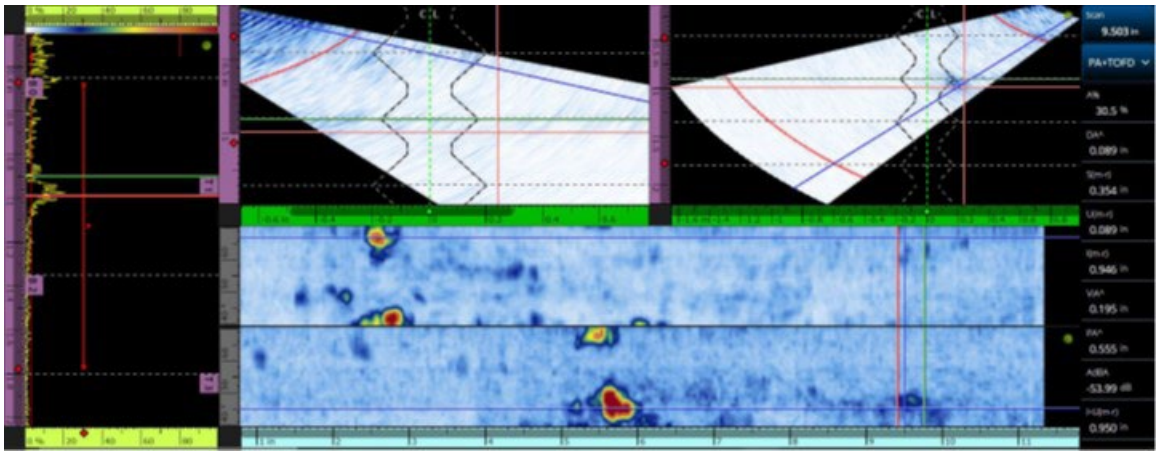

Figure 127. PAUT defect sizing at Location 3 in test panel MG-6 from ID-encoded scan

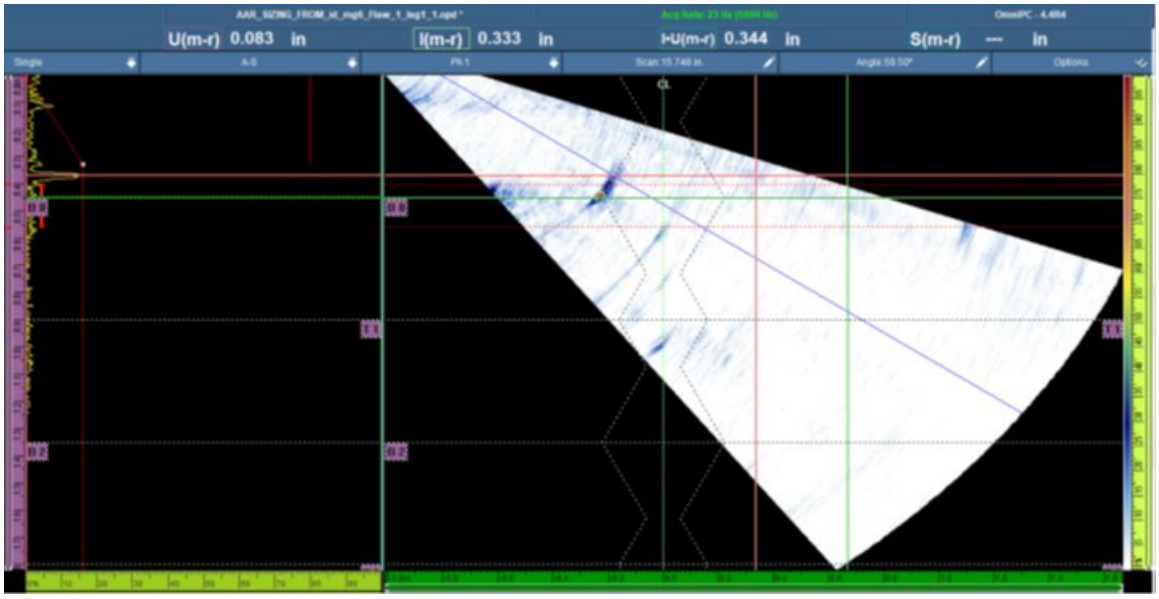

Figure 128. PAUT defect indication at Location 1 in test panel MG-6 from ID-raster scan

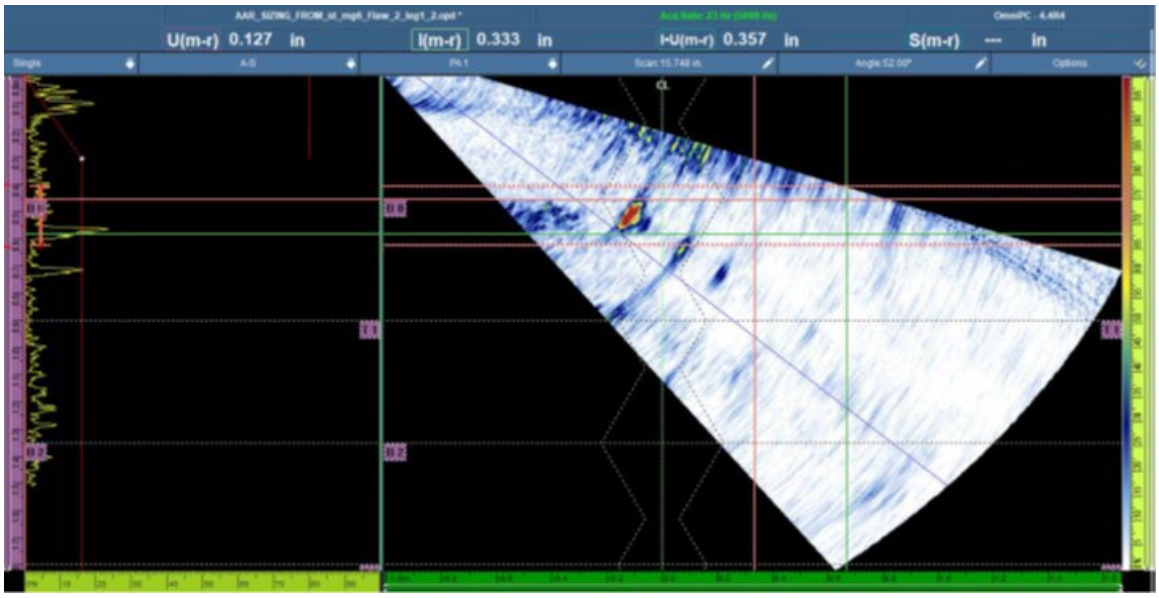

Figure 129. PAUT defect indication at Location 2 in test panel MG-6 from ID-raster scan

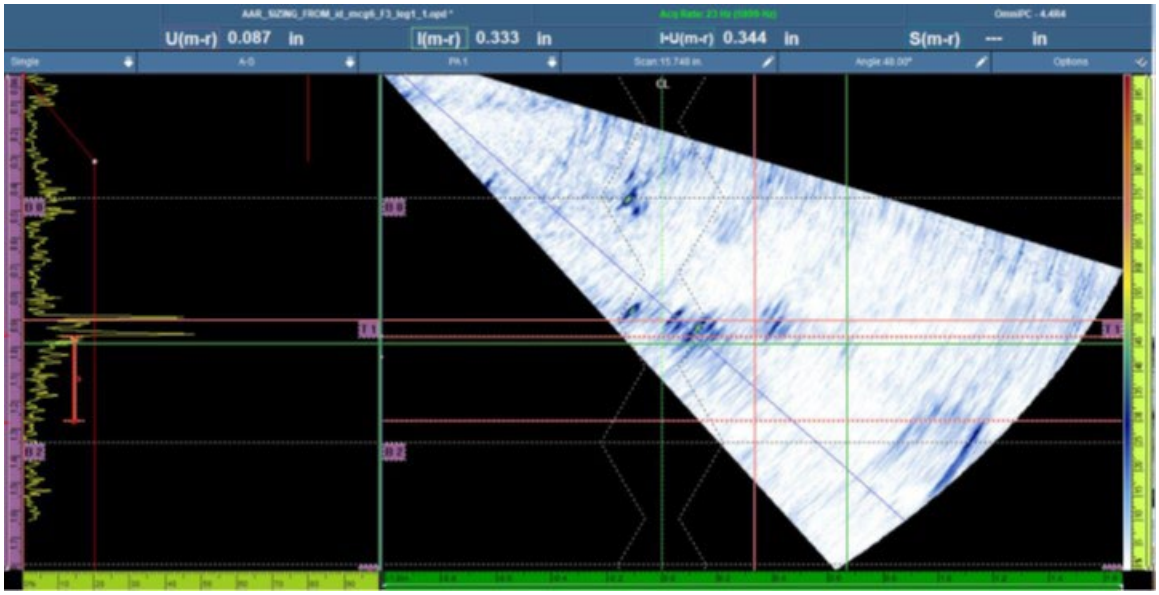

Figure 130. PAUT defect indication at Location 3 in test panel MG-6 from ID-raster scan

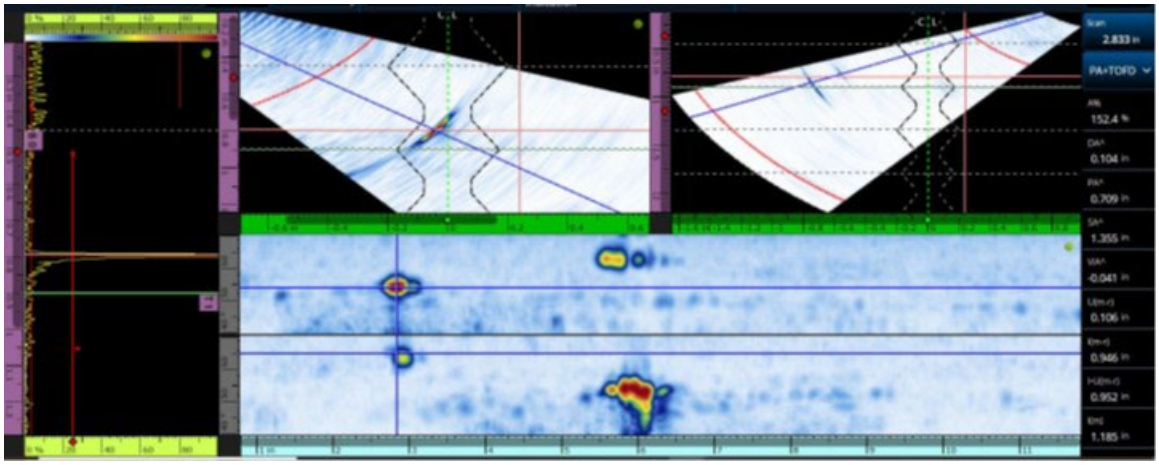

Figure 131. PAUT defect sizing at Location 1 in test panel MG-6 from OD-raster scan

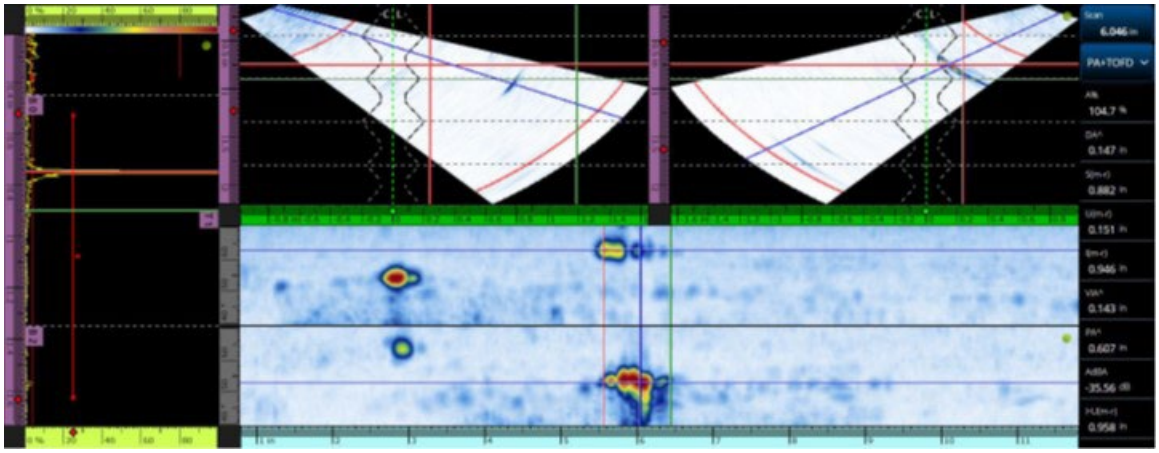

Figure 132. PAUT defect sizing at Location 2 in test panel MG-6 from OD-encoded scan

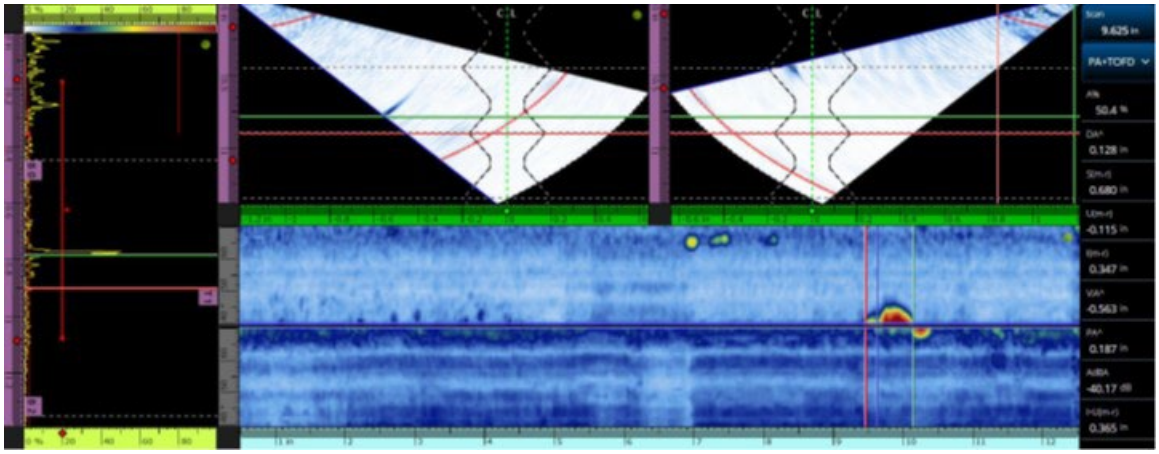

Figure 133. PAUT defect sizing at Location 3 in test panel MG-6 from OD-encoded scan

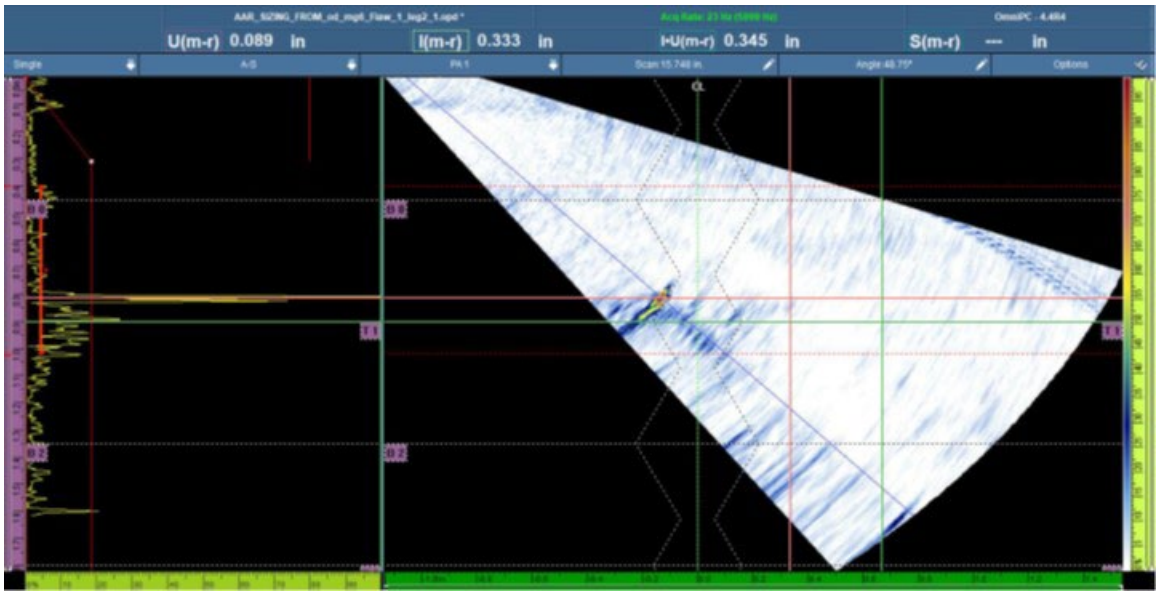

Figure 134. PAUT indication of defect at Location 1 in test panel MG-6 from OD-raster scan

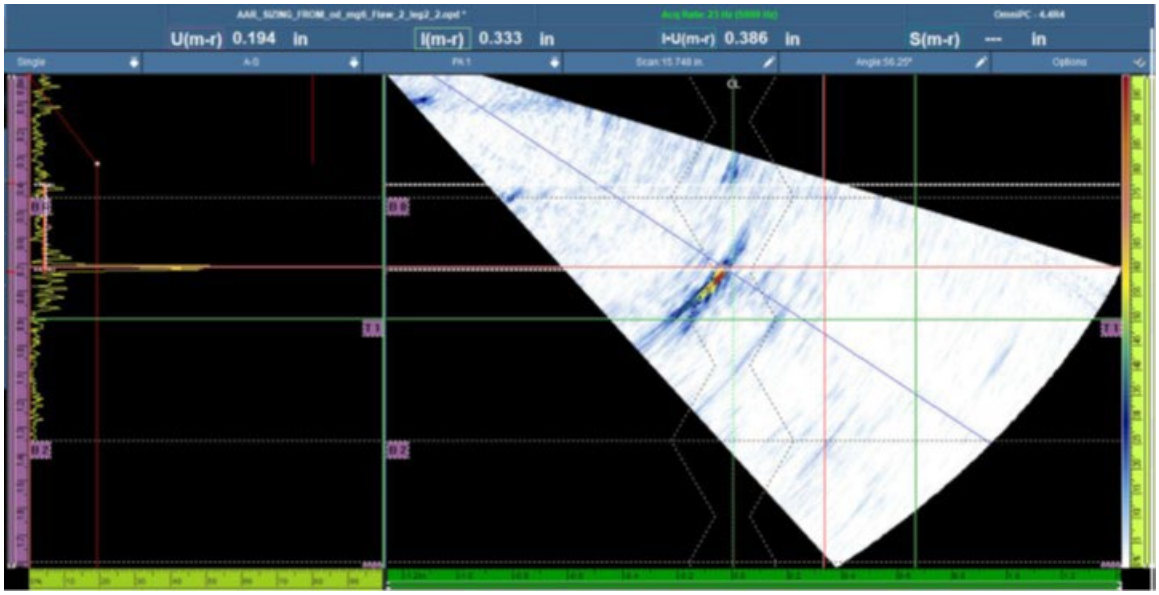

Figure 135. PAUT indication of defect at Location 2 in test panel MG-6 from OD-raster scan

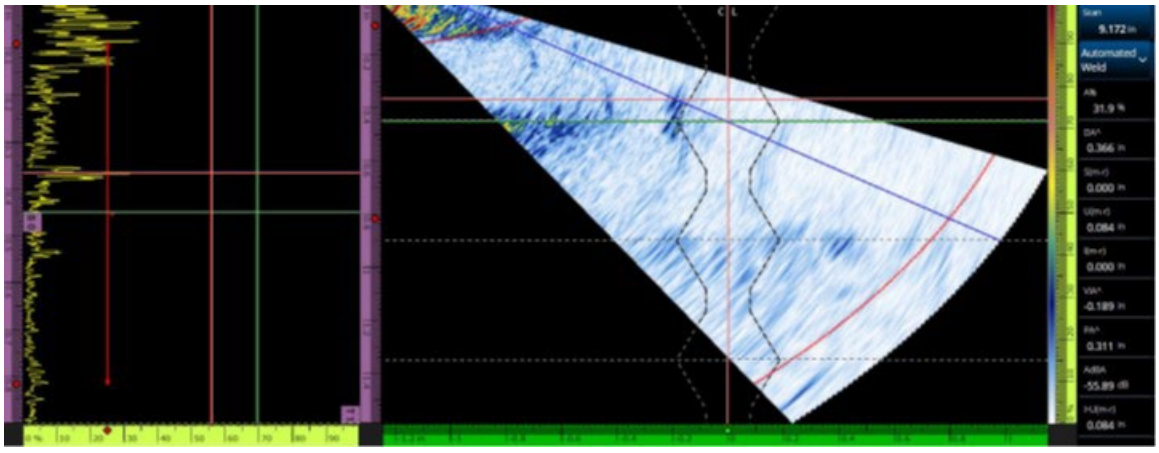

Figure 136. PAUT defect indication at Location 3 in test panel MG-6 from OD-raster scan

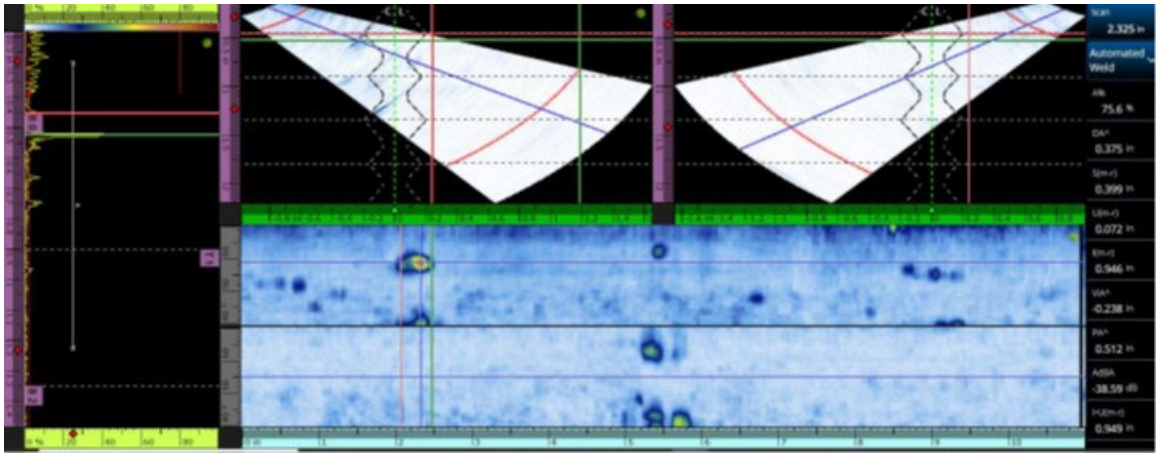

Figure 137. PAUT defect sizing at Location 1 in test panel MG-13 from ID-encoded scan

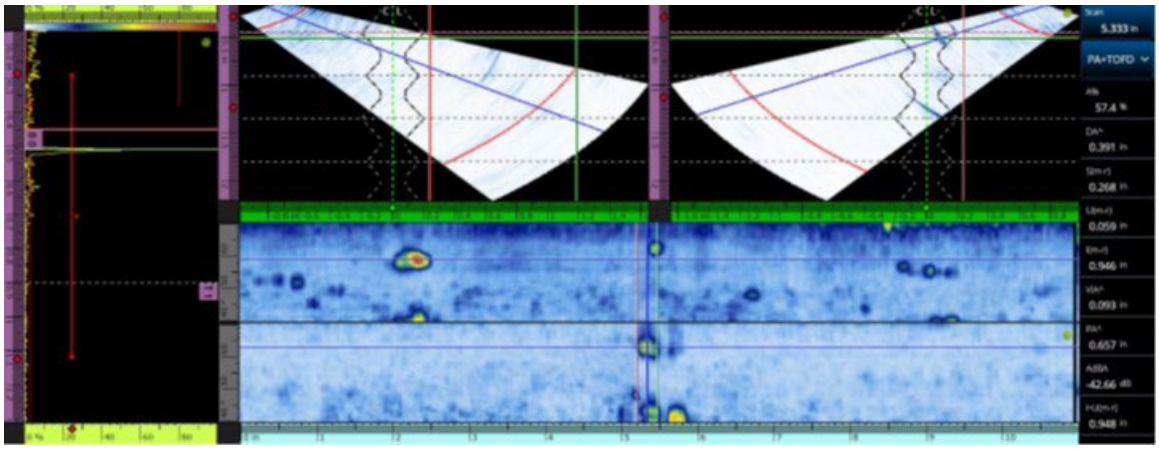

Figure 138. PAUT defect sizing at Location 2 in test panel MG-13 from ID-encoded scan

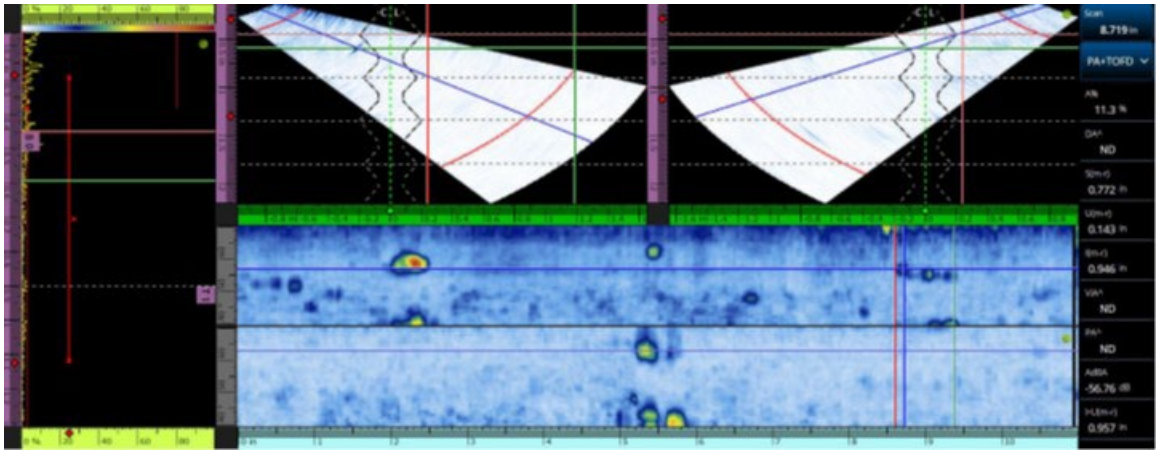

Figure 139. PAUT defect sizing at Location 3 in test panel MG-13 from ID-encoded scan

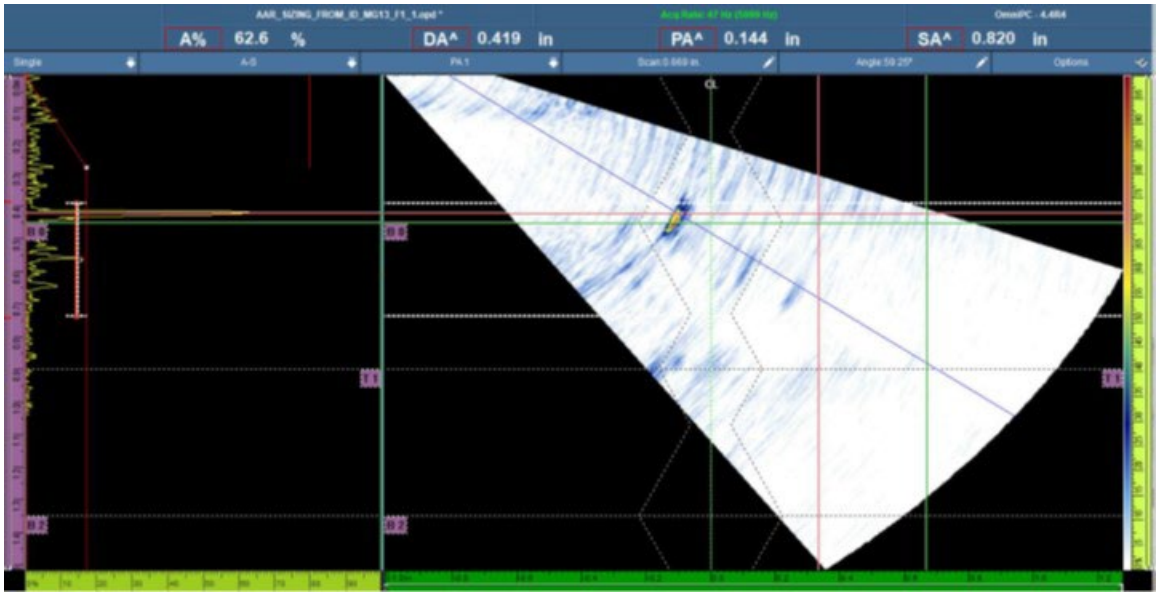

Figure 140. PAUT indication of defect at location 1 in test panel MG-13 from ID-raster scan

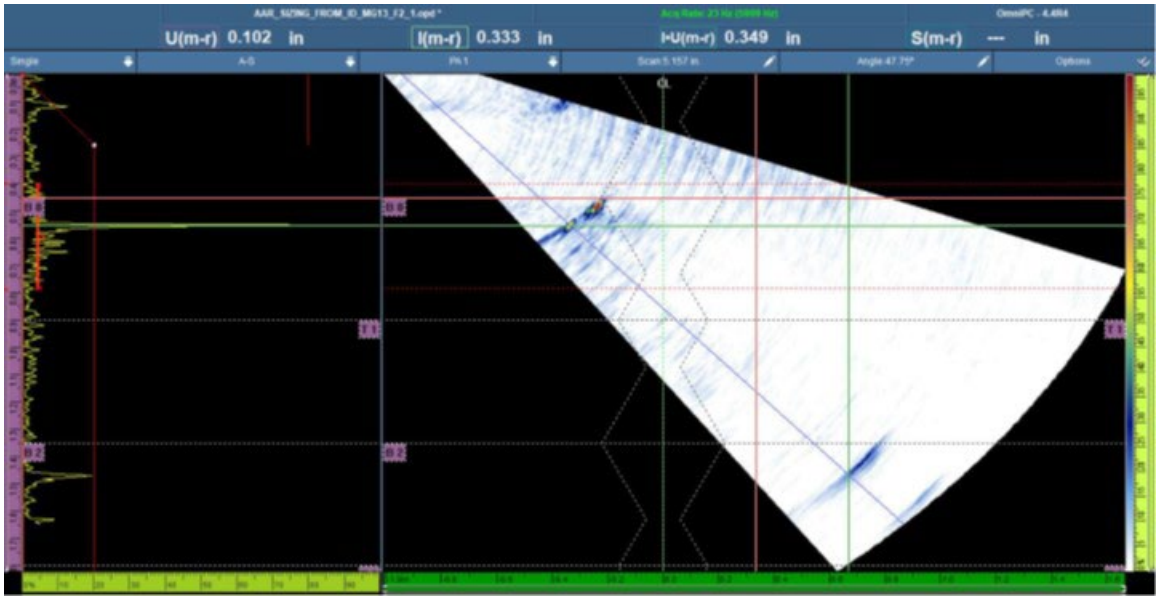

Figure 141. PAUT indication of defect at Location 2 in test panel MG-13 from ID-raster scan

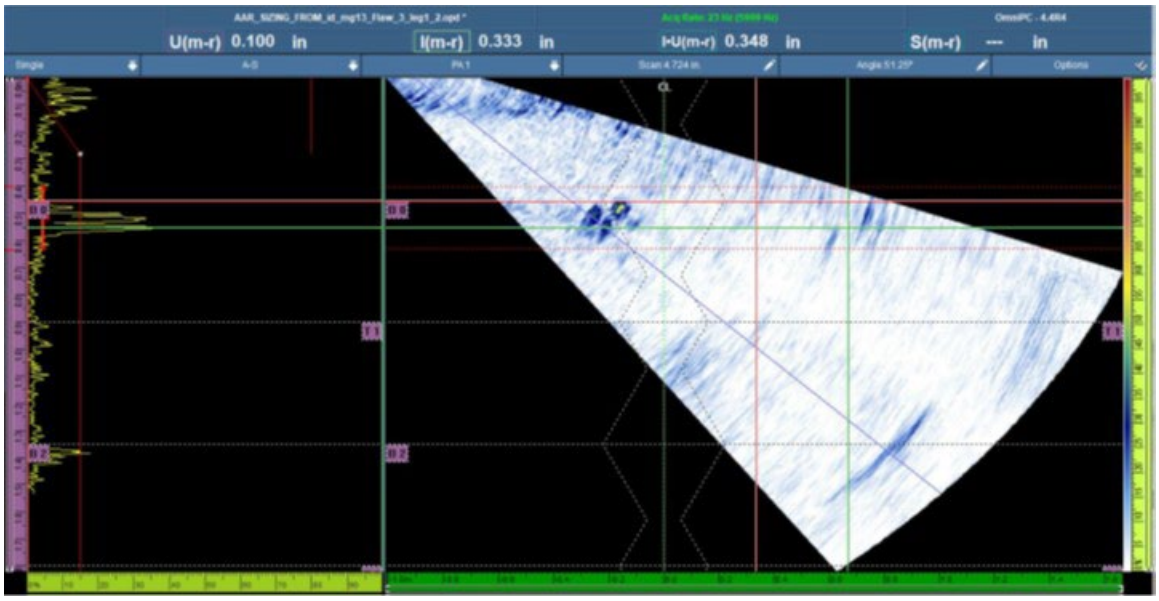

Figure 142. PAUT indication of defect at Location 3 in test panel MG-13 from ID-raster scan

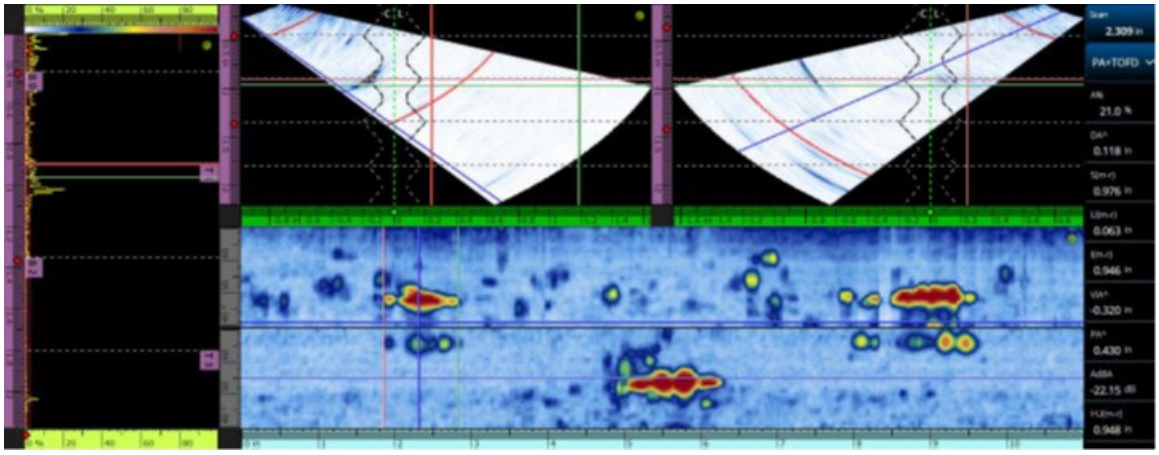

Figure 143. PAUT defect sizing at Location 1 in test panel MG-13 from OD-encoded scan

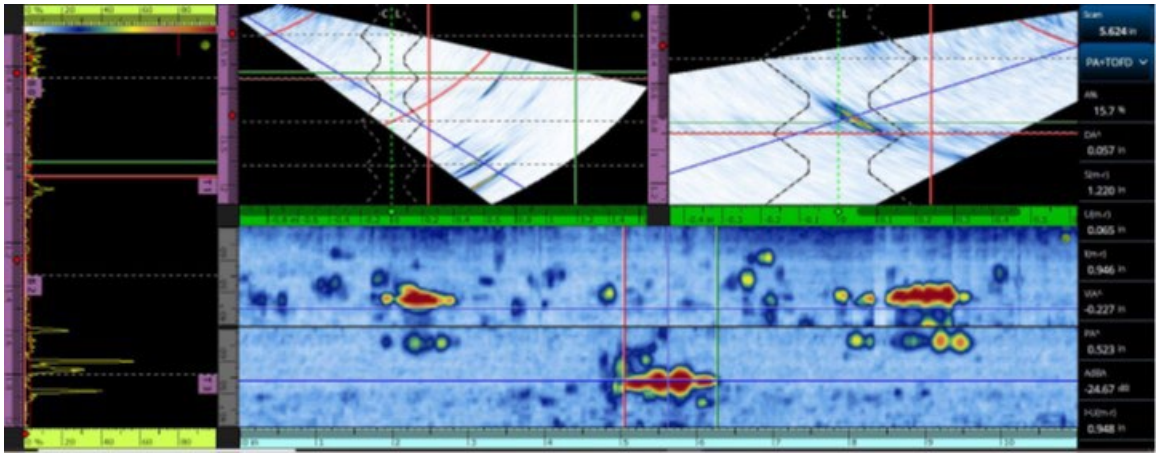

Figure 144. PAUT defect sizing at Location 2 in test panel MG-13 from OD-encoded scan

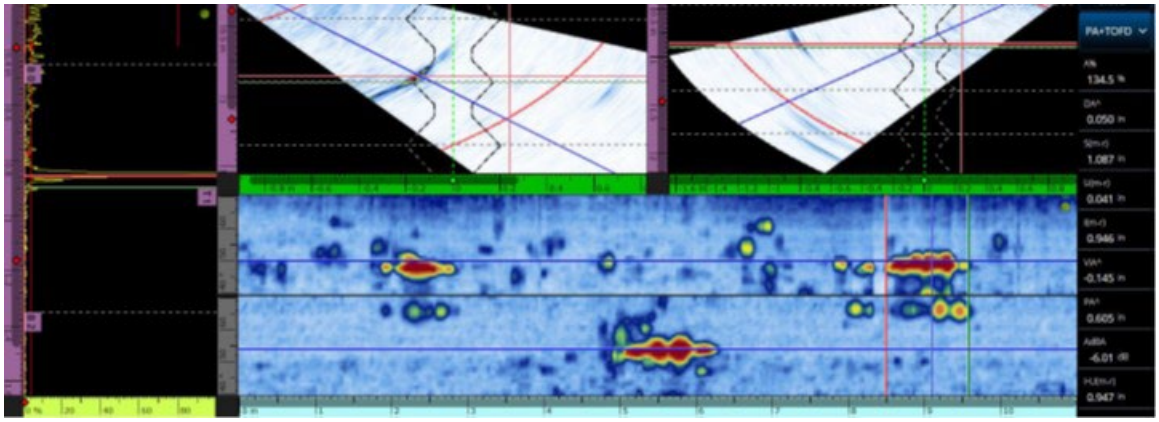

Figure 145. PAUT defect sizing at Location 3 in test panel MG-13 from OD-encoded scan

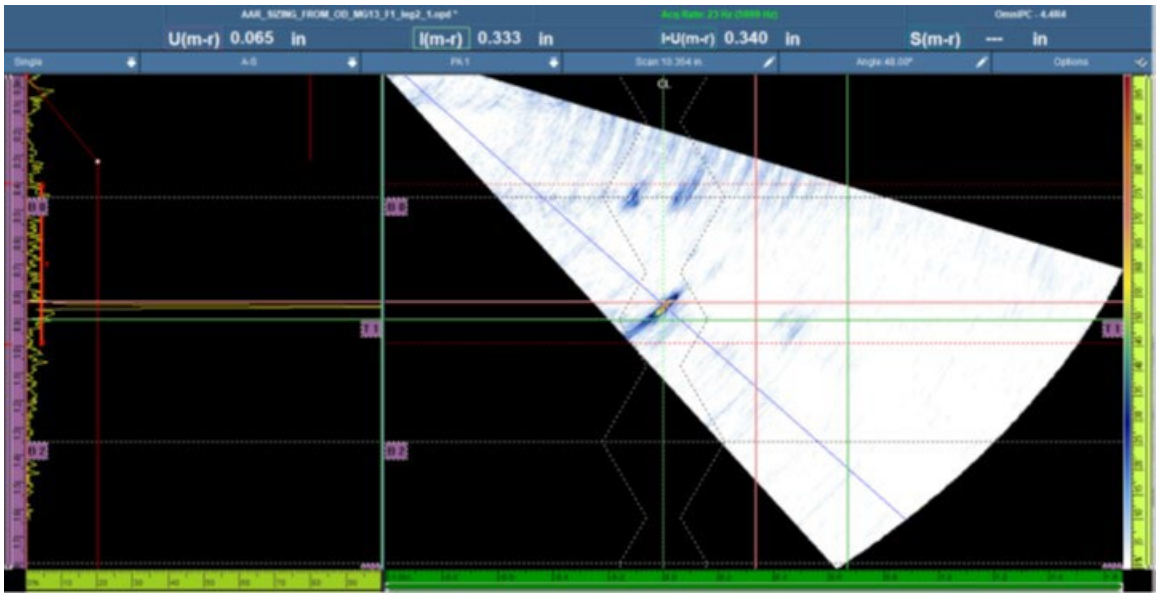

Figure 146. PAUT indication of defect at Location 1 in test panel MG-13 from OD-raster scan

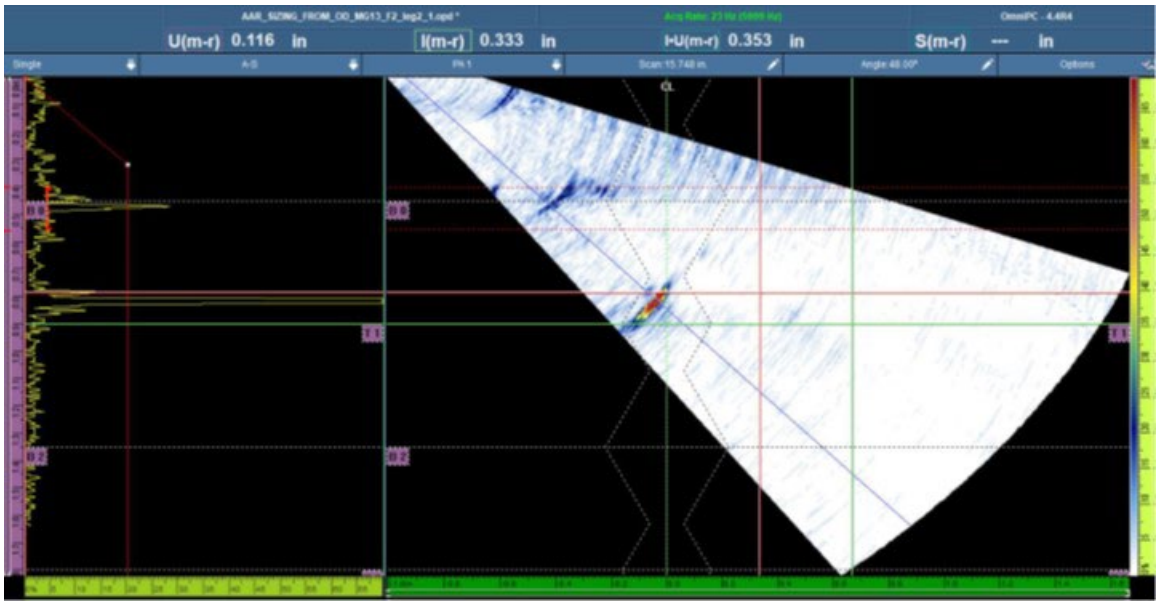

Figure 147. PAUT indication of defect at Location 2 in test panel MG-13 from OD-raster scan

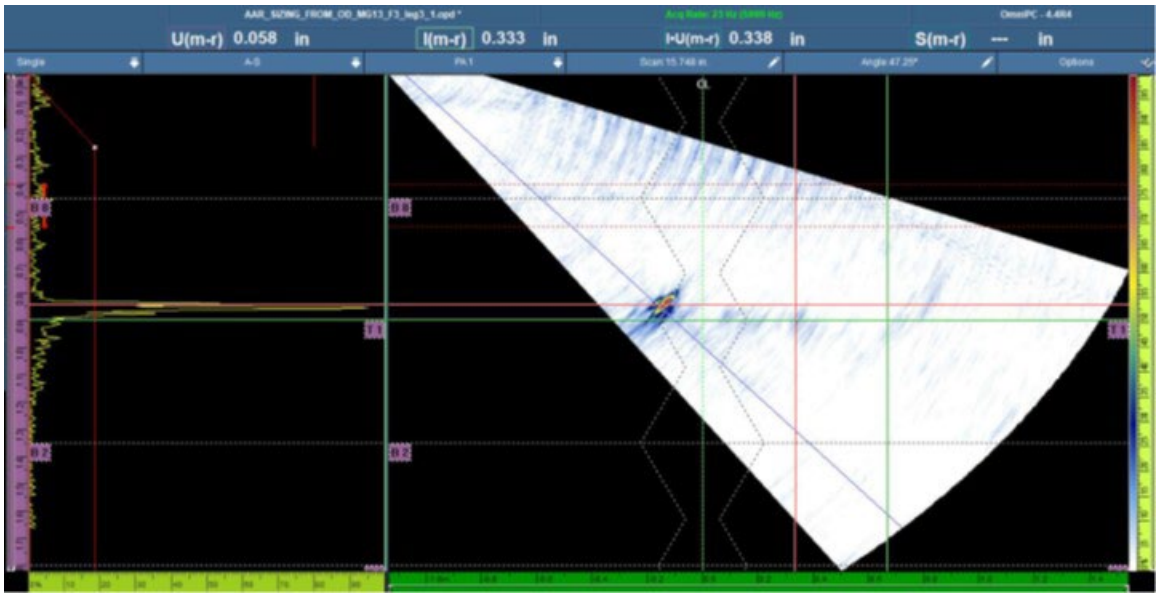

Figure 148. PAUT indication of defect at Location 3 in test panel MG-13 from OD-raster scan

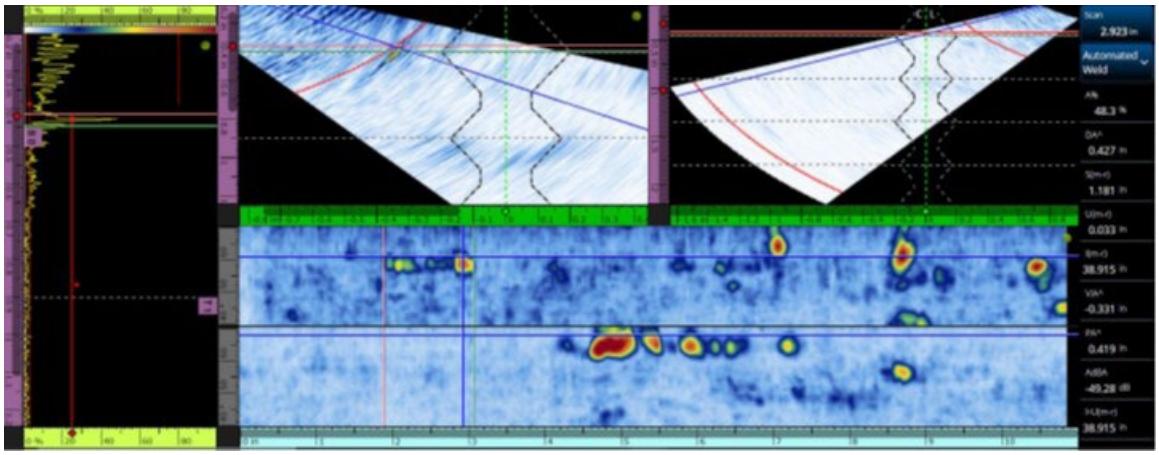

Figure 149. PAUT defect sizing at Location 1 in test panel MG-16 from ID-encoded scan

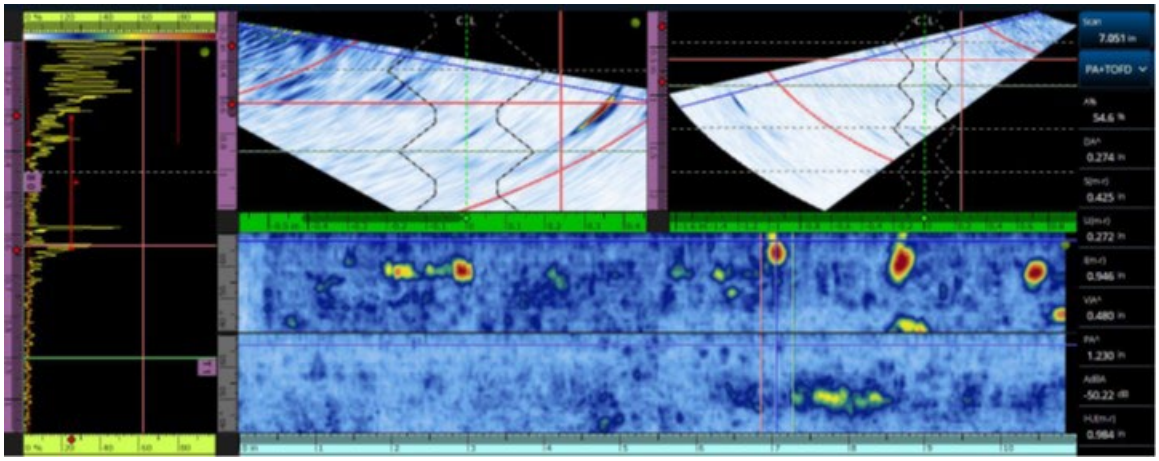

Figure 150. PAUT defect sizing at Location 2 in test panel MG-16 from ID-encoded scan

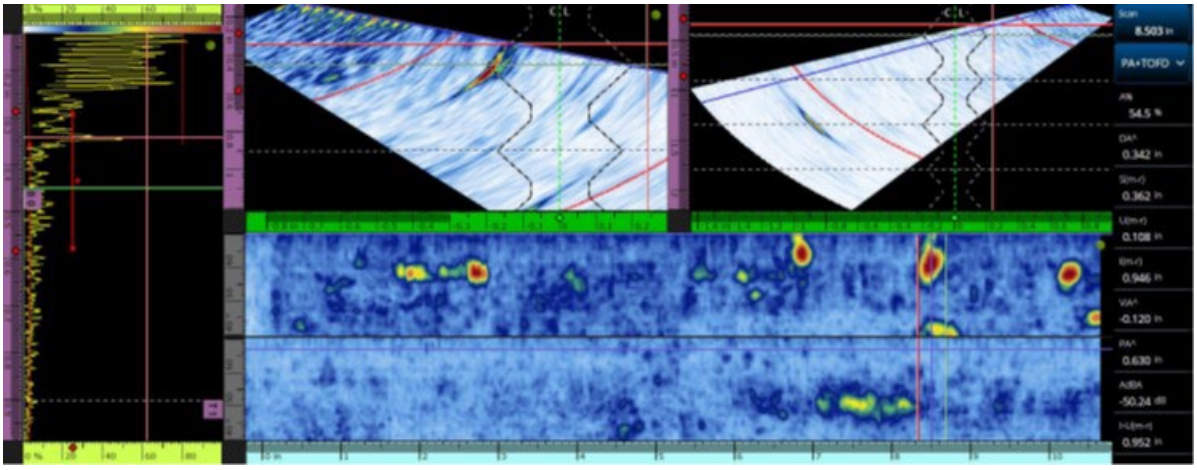

Figure 151. PAUT defect sizing at Location 3 in test panel MG-16 from ID-encoded scan

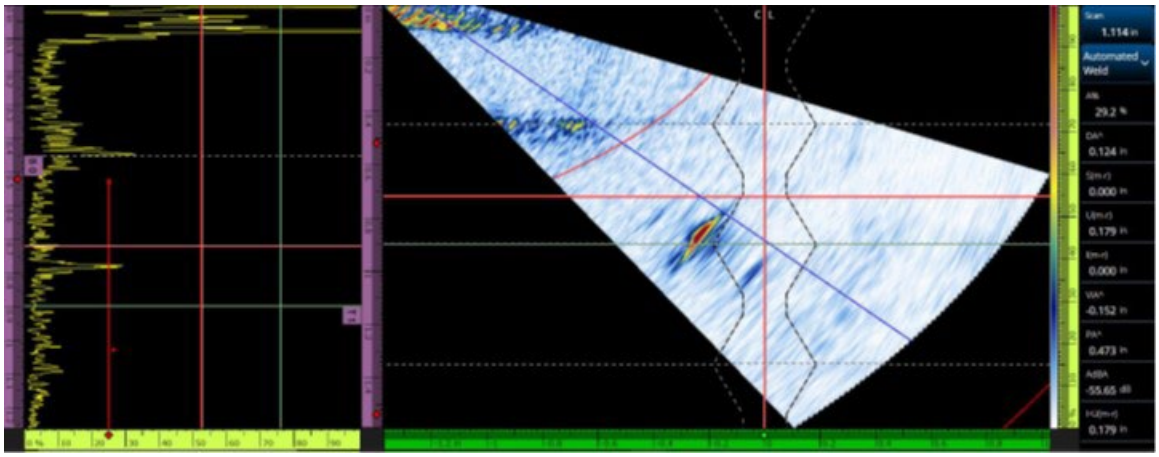

Figure 152. PAUT defect indication at Location 1 in test panel MG-16 from ID-raster scan

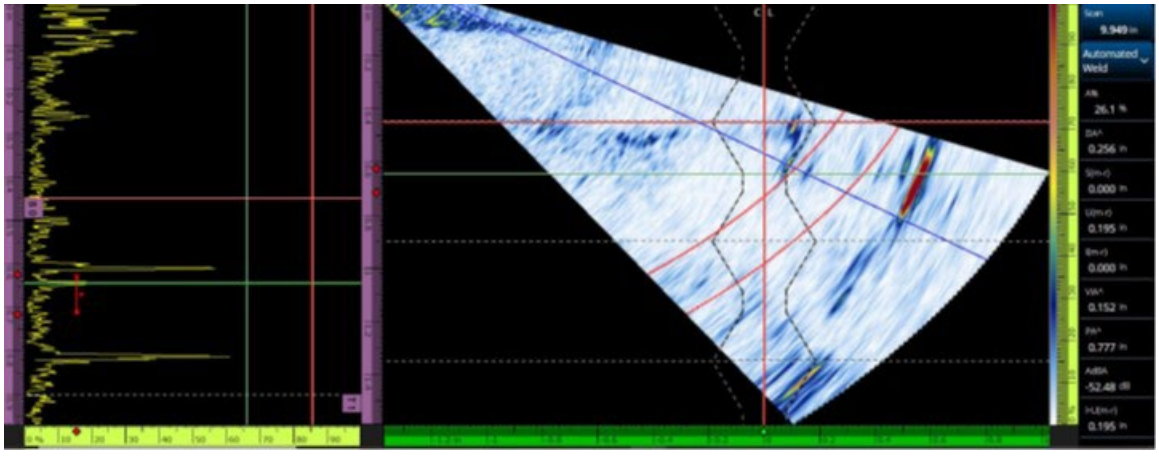

Figure 153. PAUT defect indication at Location 2 in test panel MG-16 from ID-raster scan

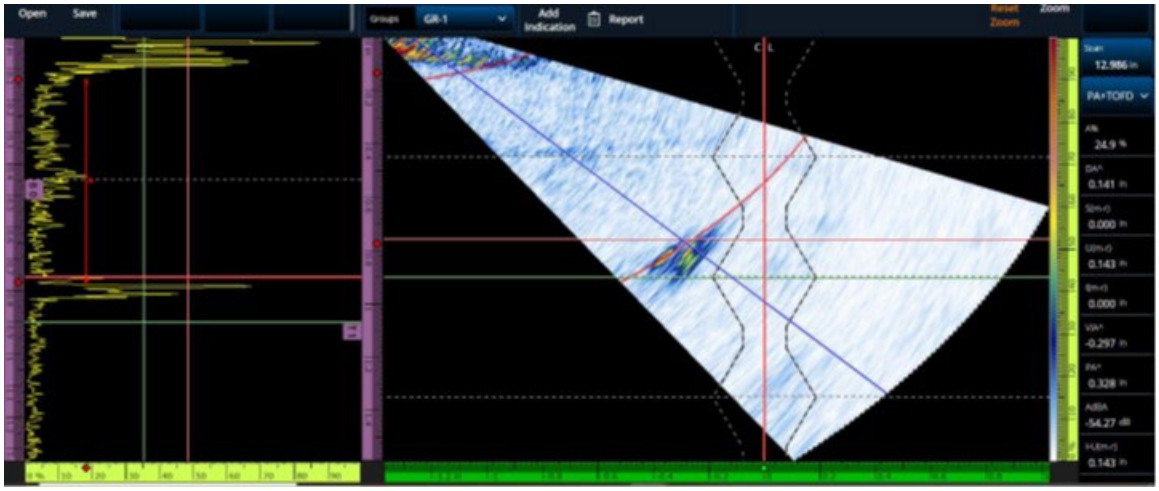

Figure 154. PAUT defect indication at Location 3 in test panel MG-16 from ID-raster scan

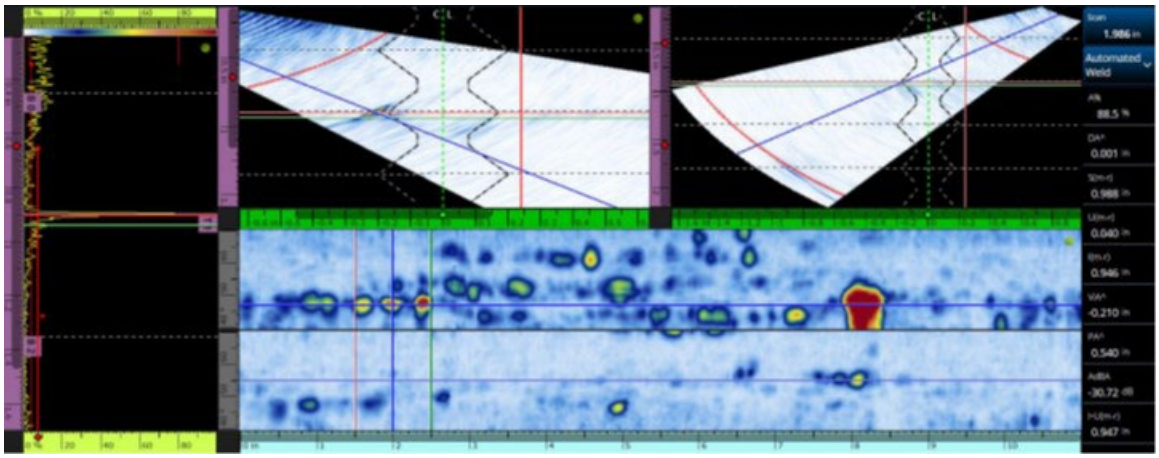

Figure 155. PAUT defect sizing at Location 1 in test panel MG-16 from OD-raster scan

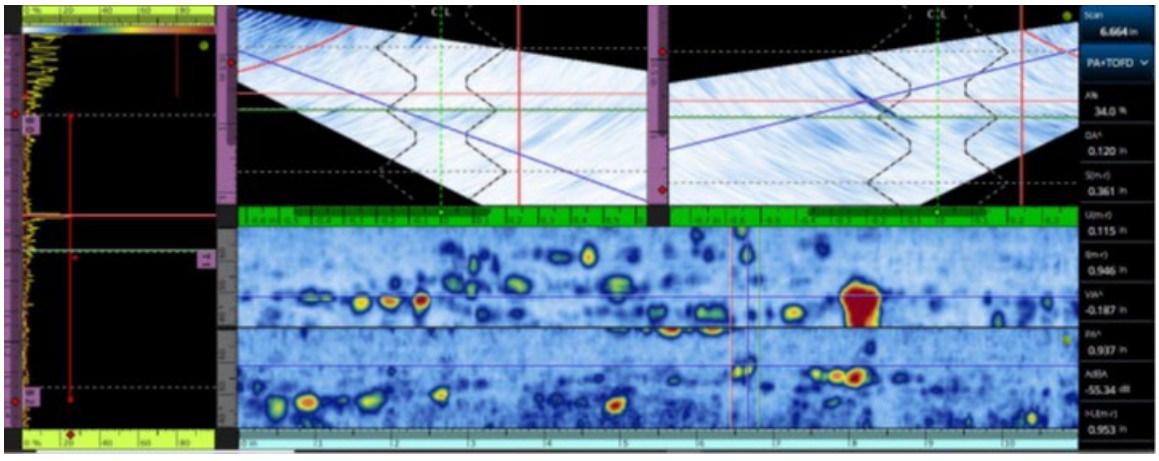

Figure 156. PAUT defect sizing at Location 2 in test panel MG-16 from OD-raster scan

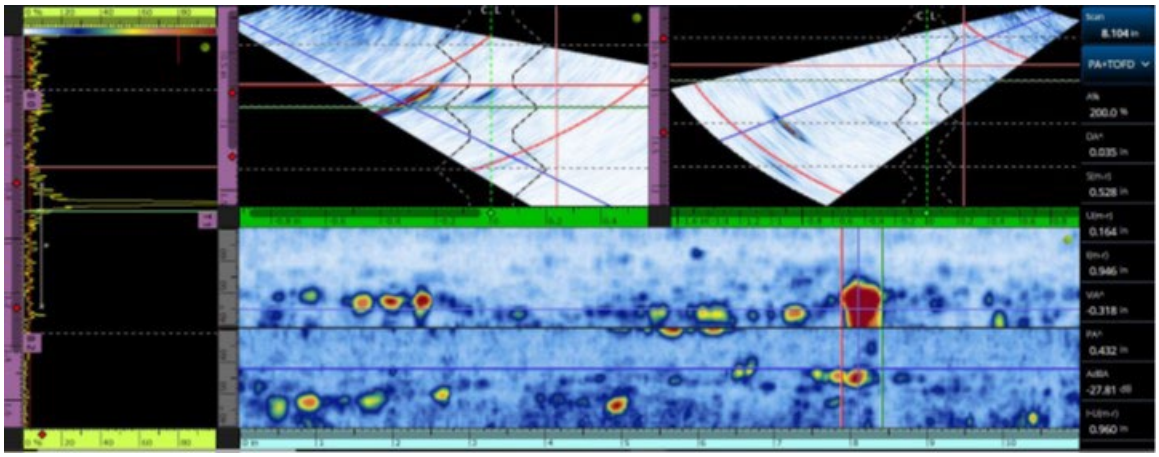

Figure 157. PAUT defect sizing at Location 3 in test panel MG-16 from OD-raster scan

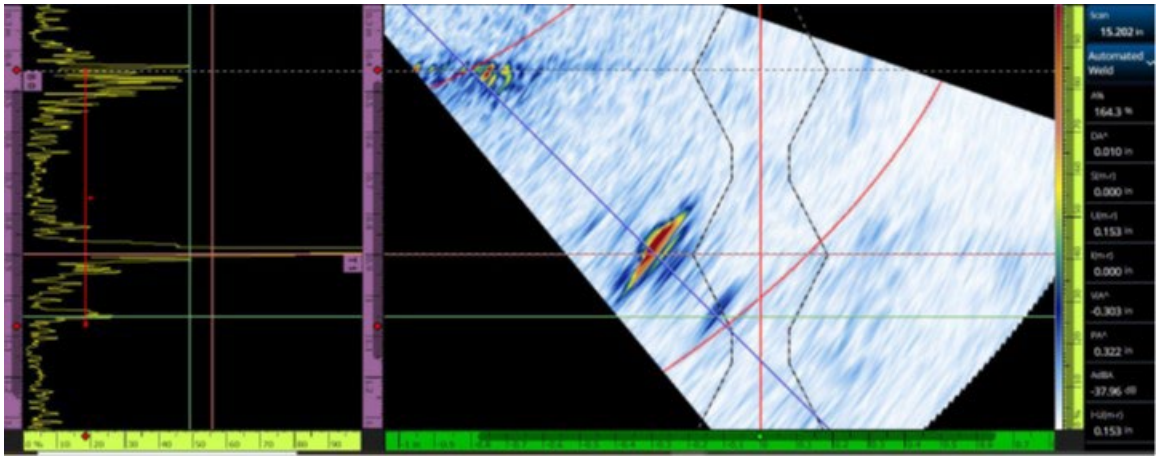

Figure 158. PAUT defect indication at Location 1 in test panel MG-16 from OD-raster scan

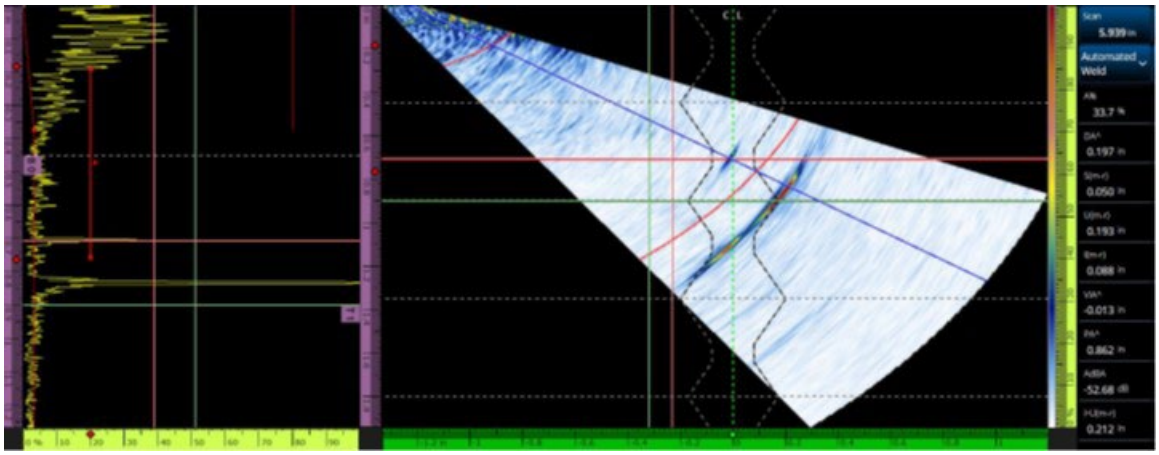

Figure 159. PAUT defect indication at Location 2 in test panel MG-16 from OD-raster scan

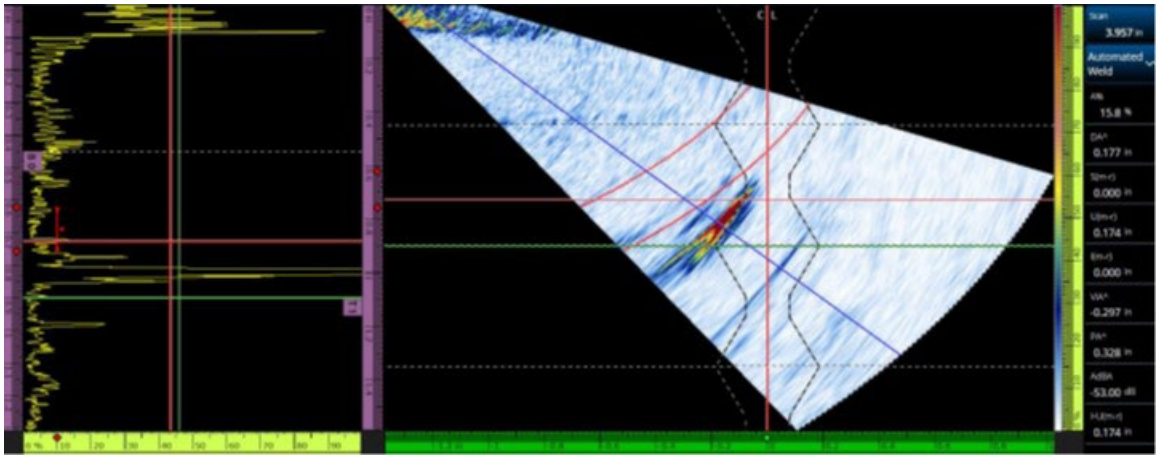

Figure 160. PAUT defect indication at Location 3 in test panel MG-16 from OD-raster scan

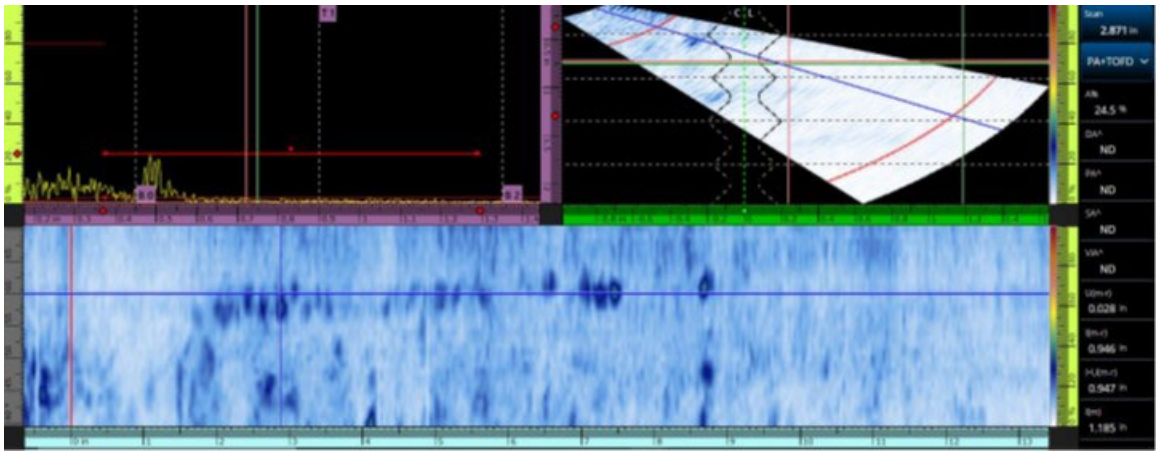

Figure 161. PAUT indication of defects at Locations A and B in fillet weld test panel TTCI-P2 from ID-encoded scan

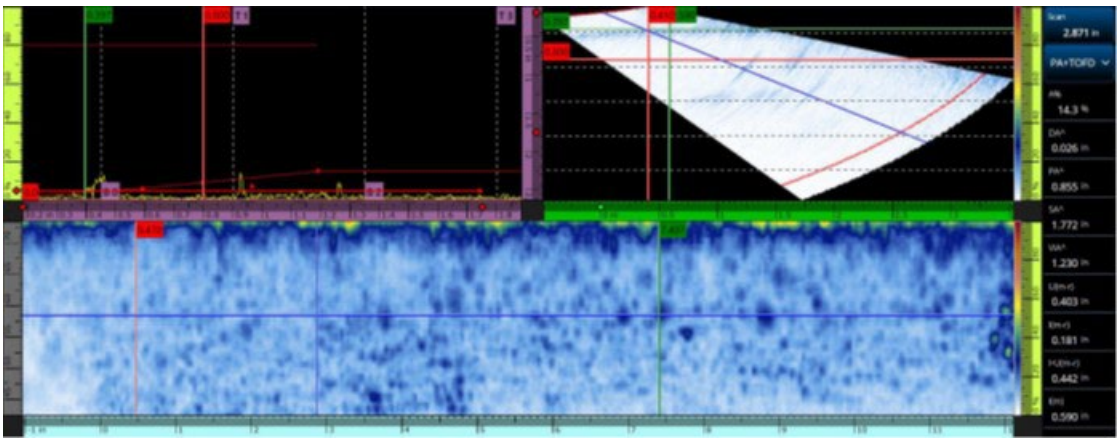

Figure 162. PAUT indication of defects at Locations A and B in fillet weld test panel TTCI-P2 from OD-encoded scan

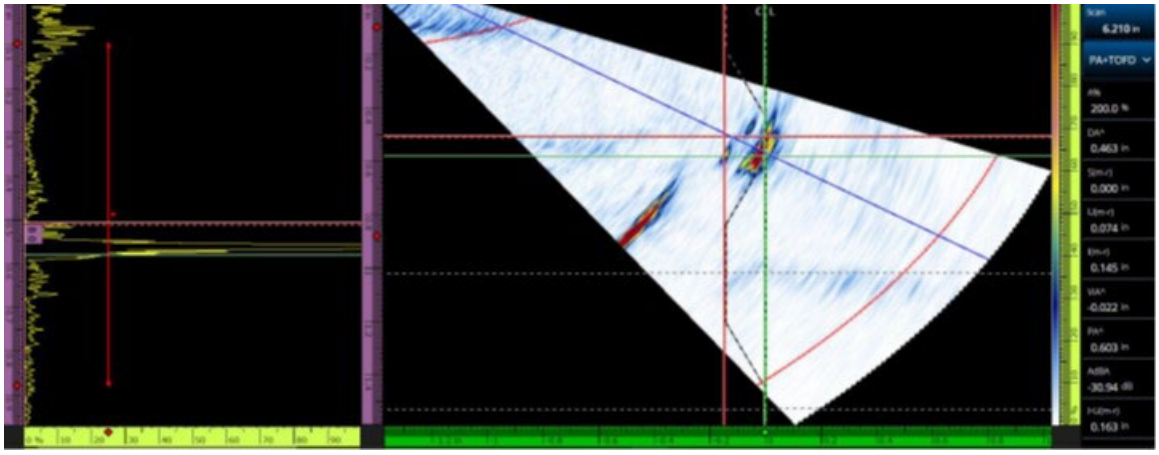

Figure 163. PAUT indication of defect at Location A in test panel TTCI-P2 from Repad-raster scan

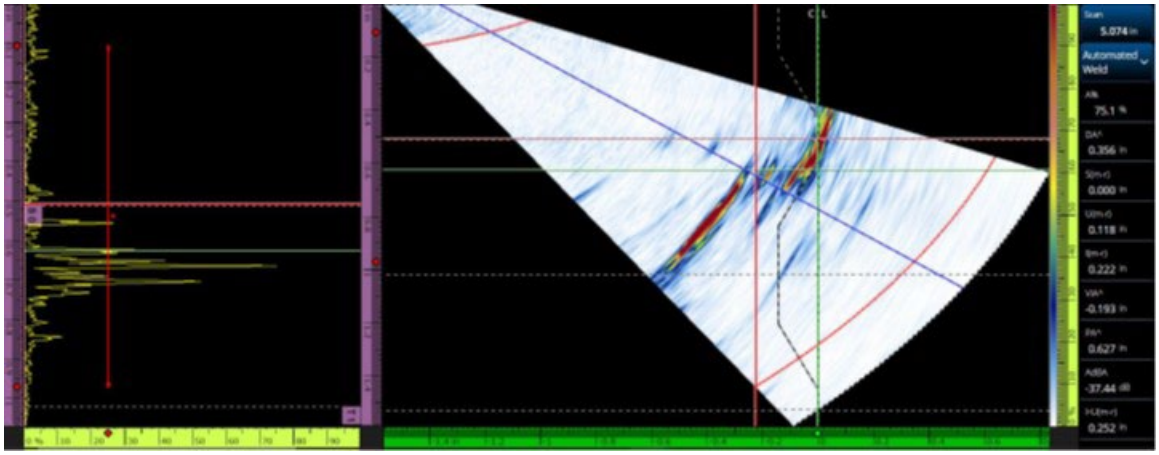

Figure 164. PAUT indication of defect at Location B in test panel TTCI-P2 from Repad-raster scan

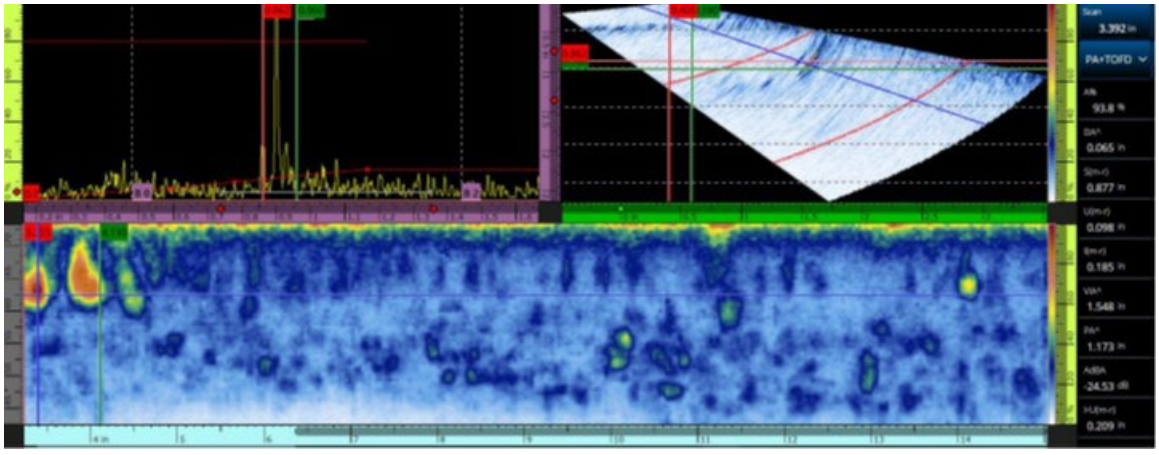

Figure 165. PAUT indication of defect at Location A in fillet weld test panel MGL-3 from OD-raster scan

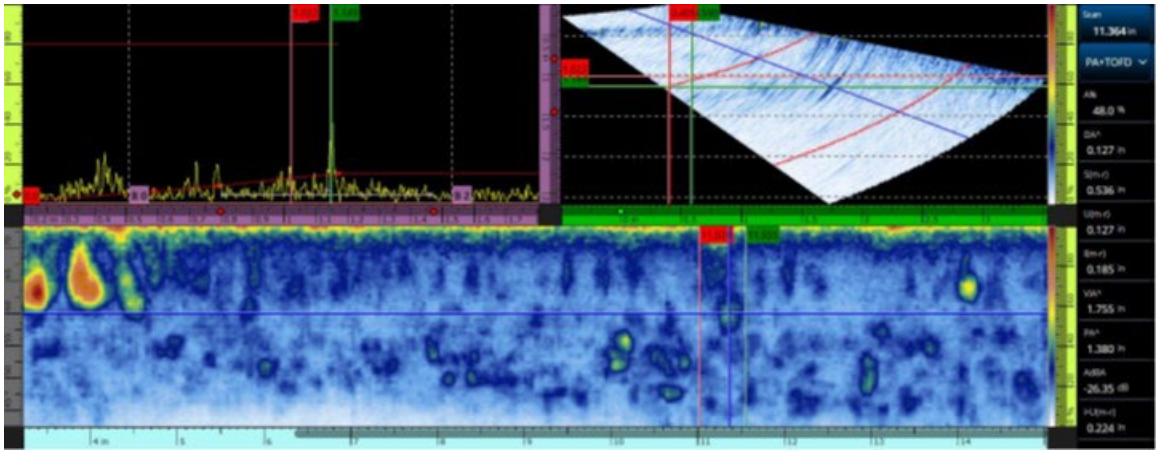

Figure 166. PAUT indication of defect at Location B in fillet weld test panel MGL-3 from OD-raster scan

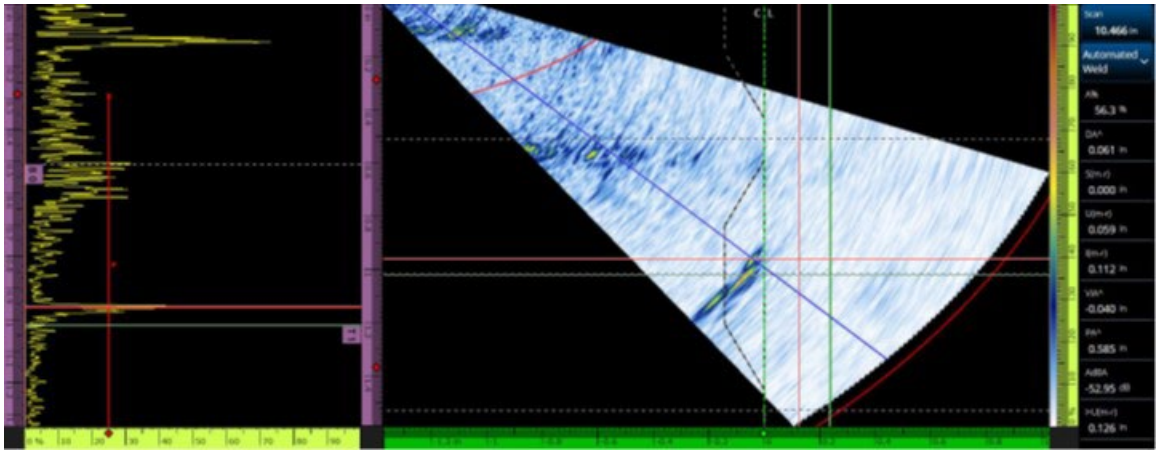

Figure 167. PAUT indication of defect at Location A in fillet weld test panel MGL-3 from OD-raster scan

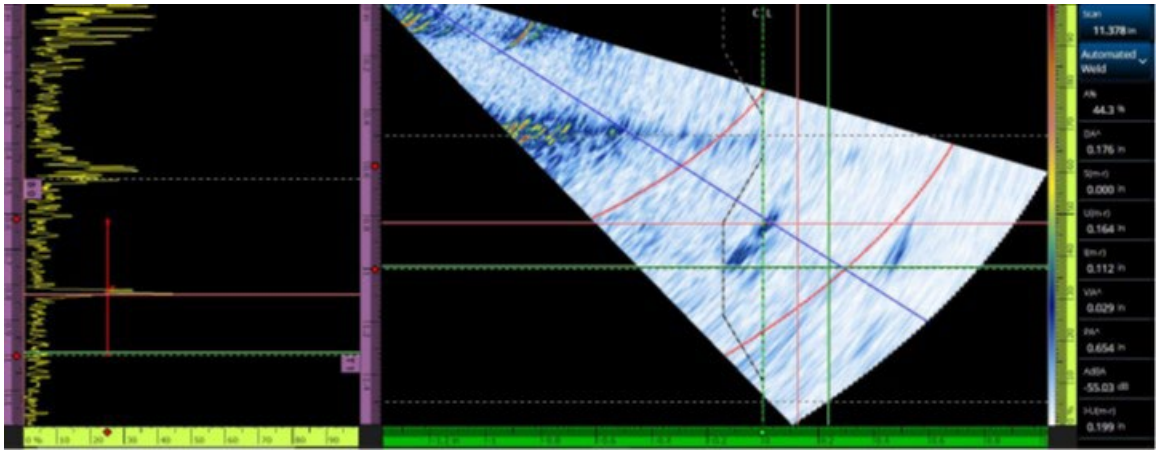

Figure 168. PAUT indication of defect at Location B in fillet weld test panel MGL-3 from OD-raster scan

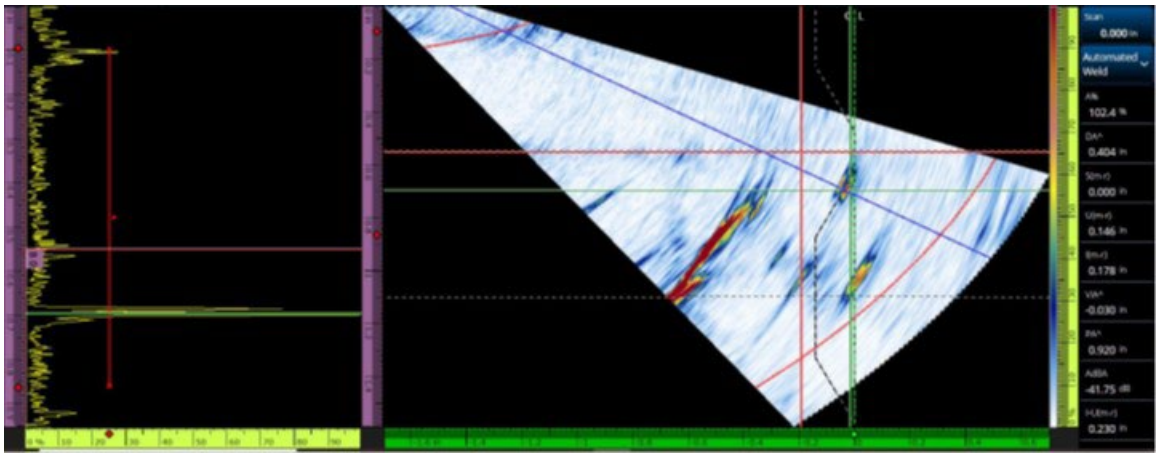

Figure 169. PAUT indication of defect at Location A in fillet weld test panel MGL-3 from Repad-raster scan

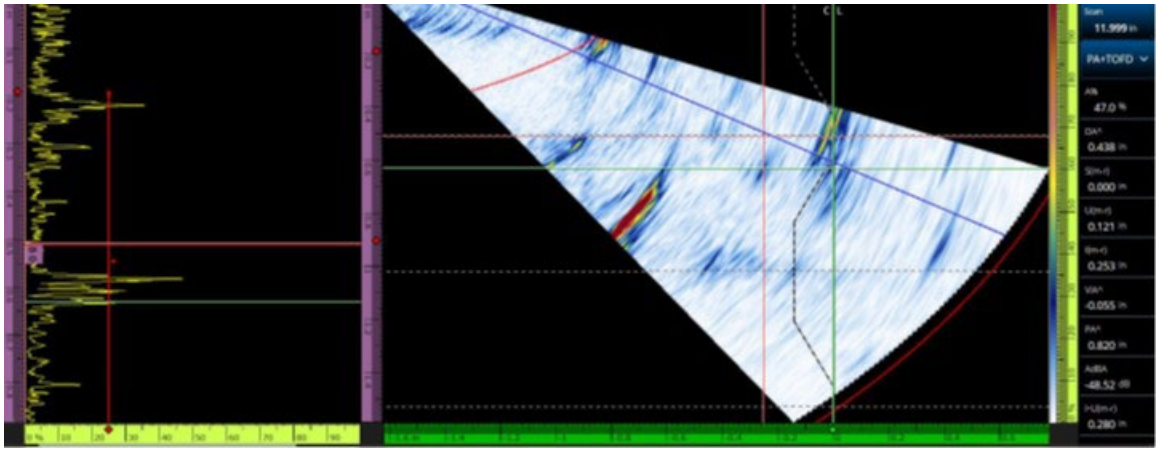

Figure 170. PAUT indication of defect at Location B in fillet weld test panel MGL-3 from Repad-raster scan

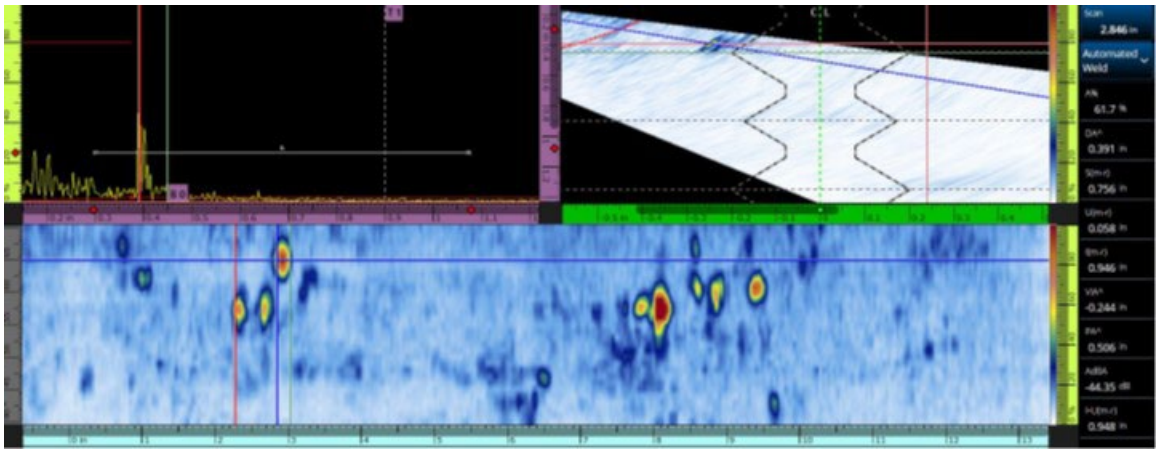

Figure 171. PAUT indication of defect at Location A in fillet weld test panel MGL-9 from ID-raster scan

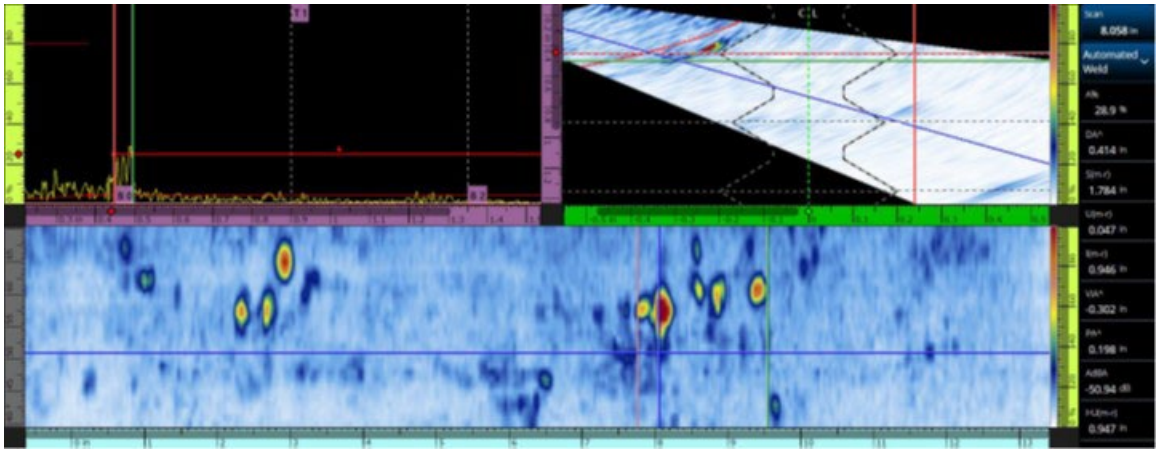

Figure 172. PAUT indication of defect at Location B in fillet weld test panel MGL-9 from ID-raster scan

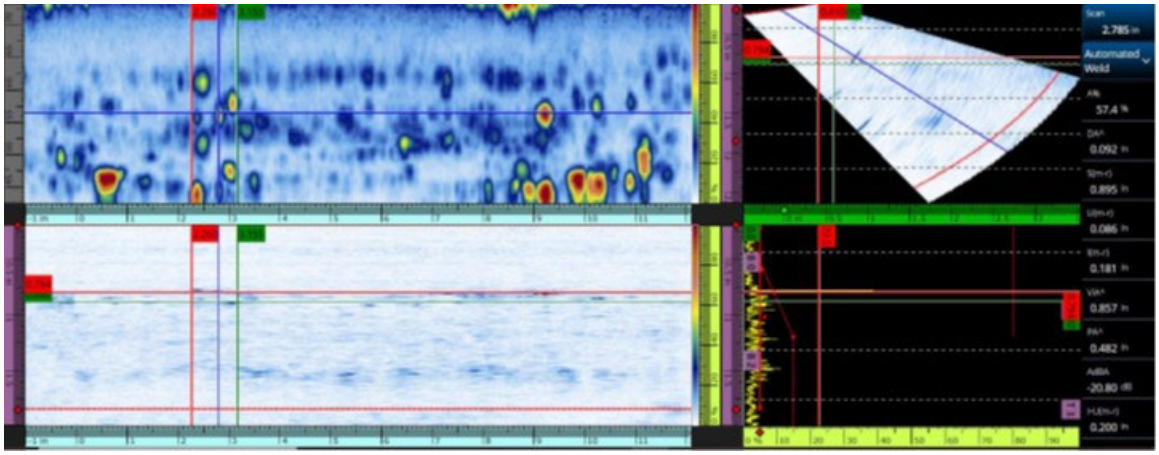

Figure 173. PAUT indication of defect at Location A in fillet weld test panel MGL-9 from OD-raster scan

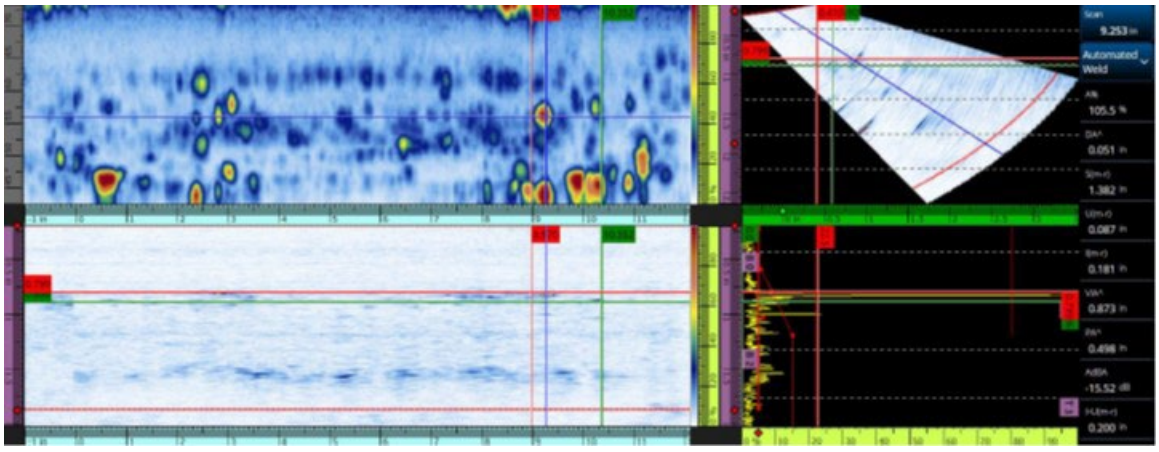

Figure 174. PAUT indication of defect at Location B in fillet weld test panel MGL-9 from OD-raster scan

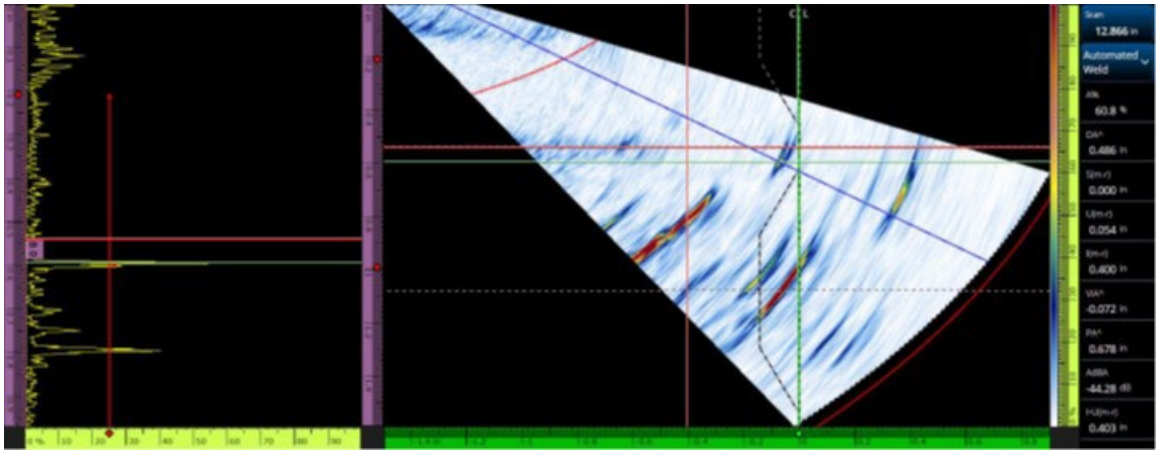

Figure 175. PAUT indication of defect at Location A in fillet weld test panel MGL-9 from Repad-raster scan

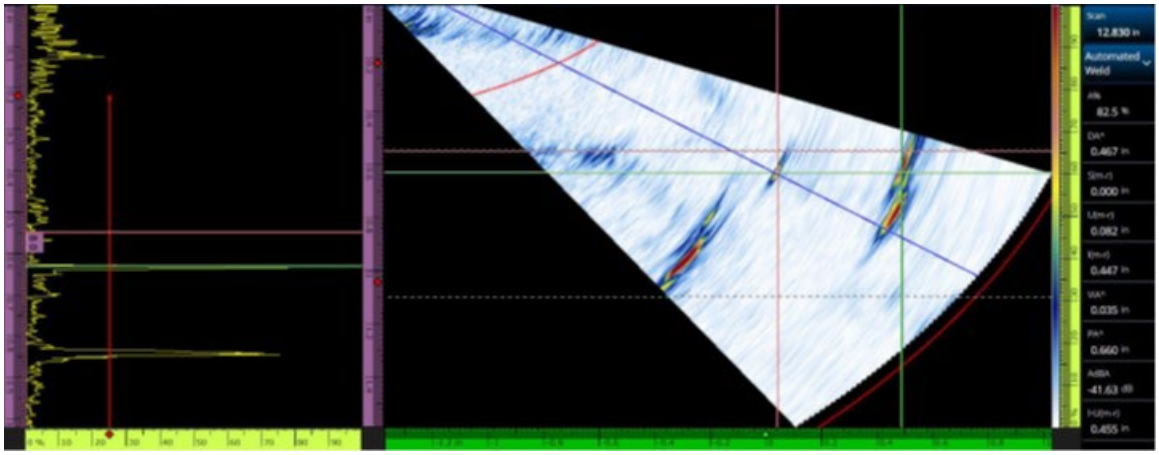

Figure 176. PAUT indication of defect at Location B in fillet weld test panel MGL-9 from Repad-raster scan

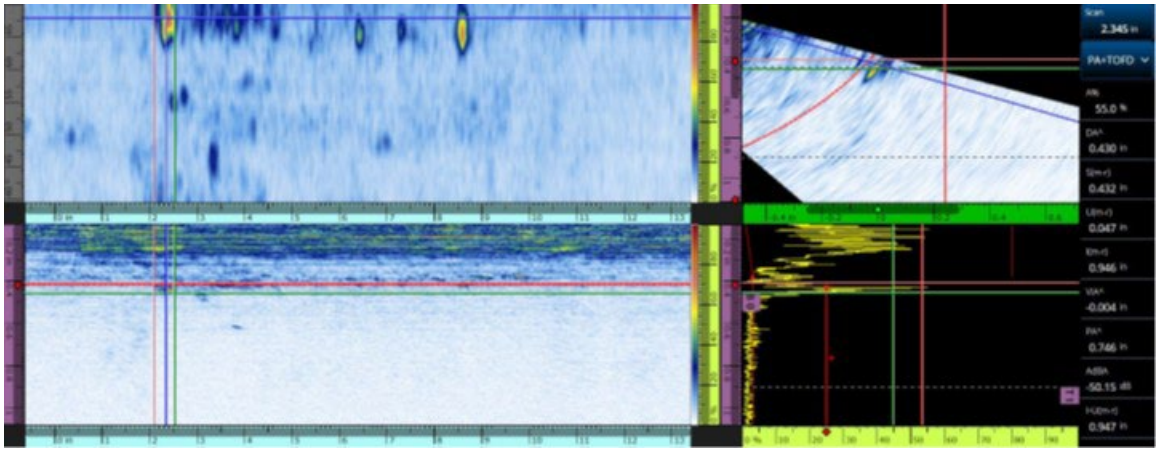

Figure 177. PAUT indication of defect at Location C in fillet weld test panel MGL-10 from ID-raster scan

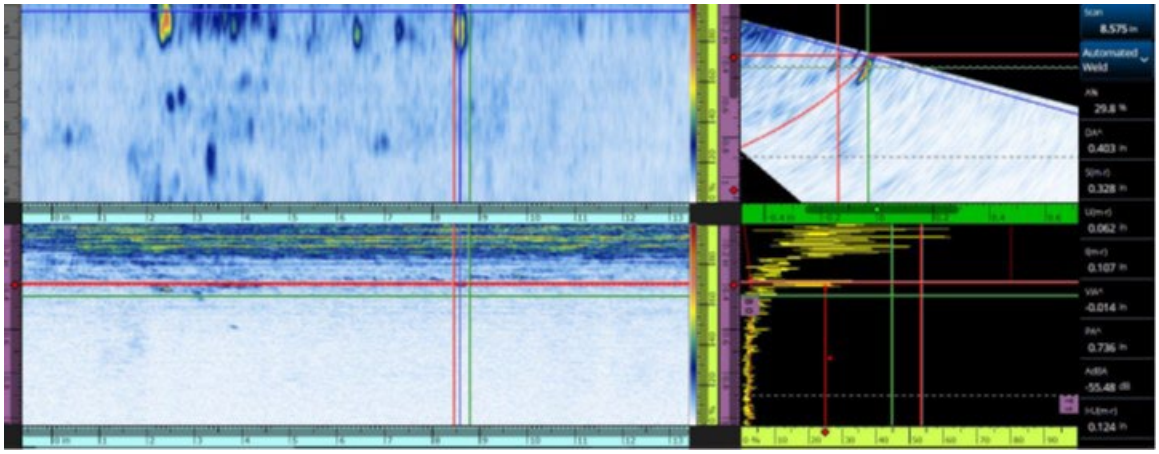

Figure 178. PAUT indication of defect at Location D in fillet weld test panel MGL-10 from ID-raster scan

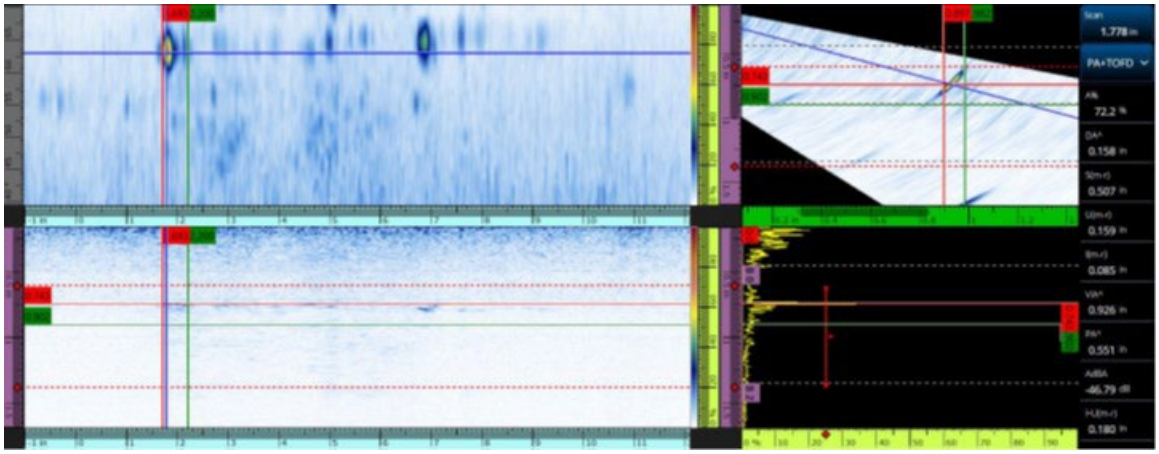

Figure 179. PAUT indication of defect at Location C in filler weld test panel MGL-10 from OD-raster scan

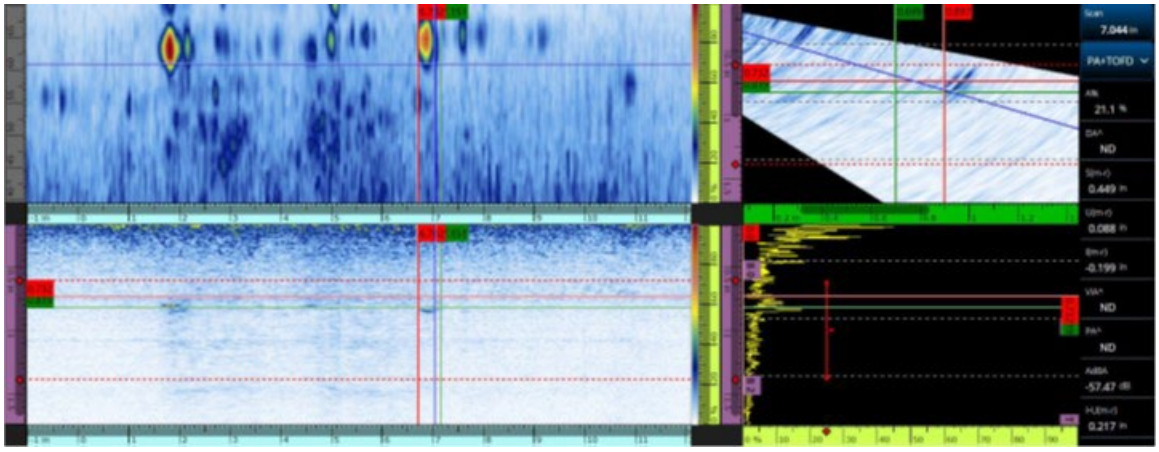

Figure 180. PAUT indication of defect at Location D in fillet weld test panel MGL-10 from OD-raster scan

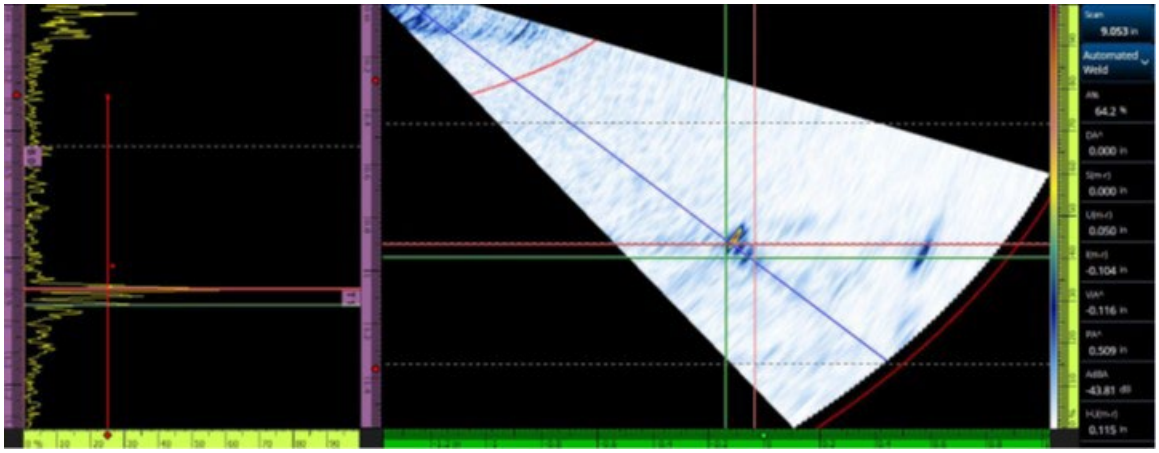

Figure 181. PAUT indication of defect at Location C in fillet weld test panel MGL-10 from OD-raster scan

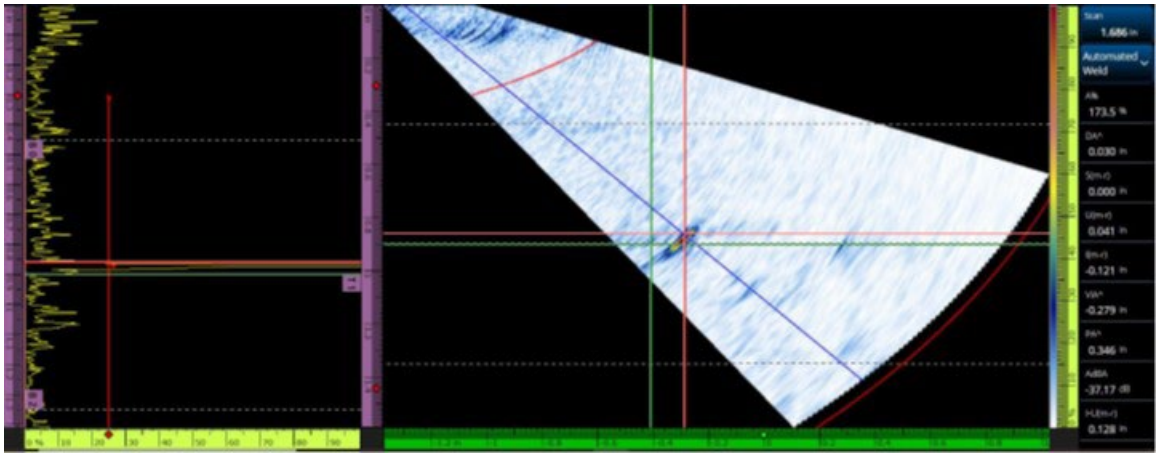

Figure 182. PAUT indication of defect at Location D in fillet weld test panel MGL-10 from OD-raster scan

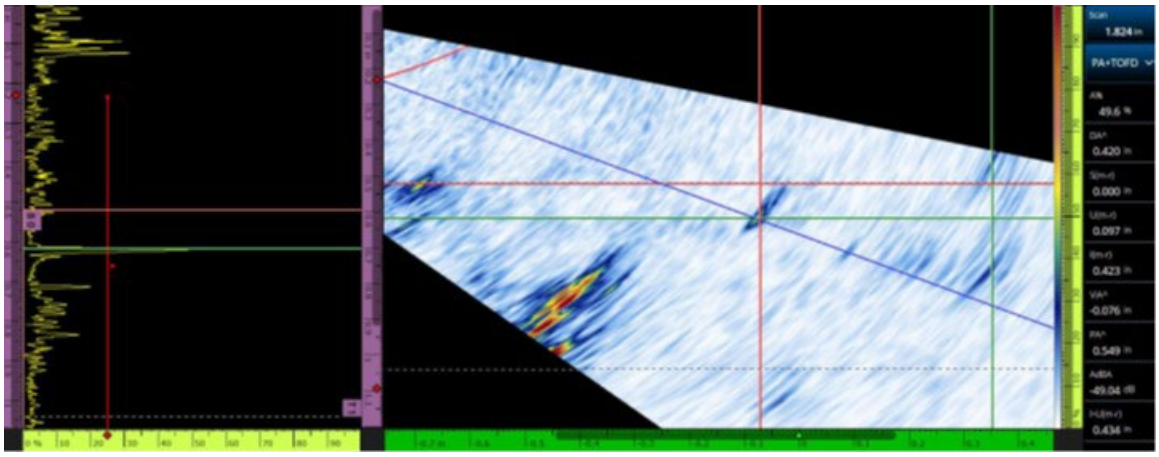

Figure 183. PAUT indication of defect at Location C in fillet weld test panel MGL-10 from Repad-raster scan

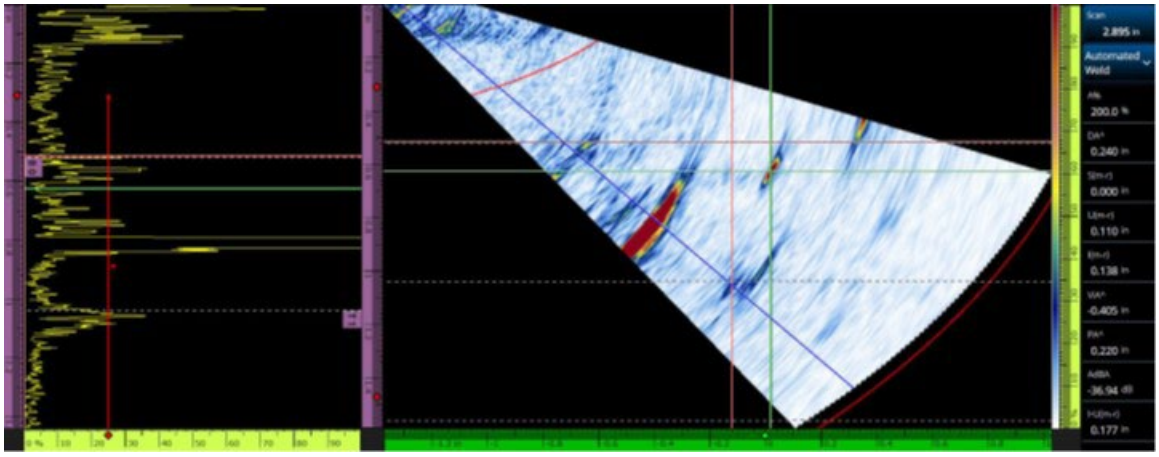

Figure 184. PAUT indication of defect at Location D in fillet weld test panel MGL-10 from Repad-raster scan

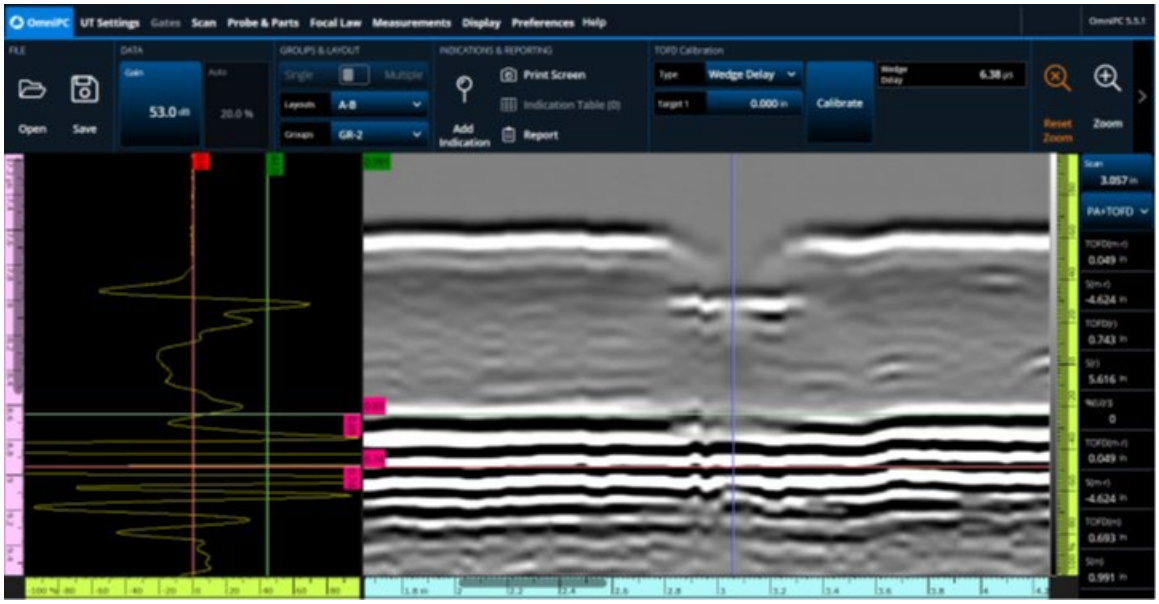

Figure 185. TOFD indication of defect at Location A in test panel TTCI-2

Figure 186. TOFD indication of defect at Location B in test panel TTCI-2

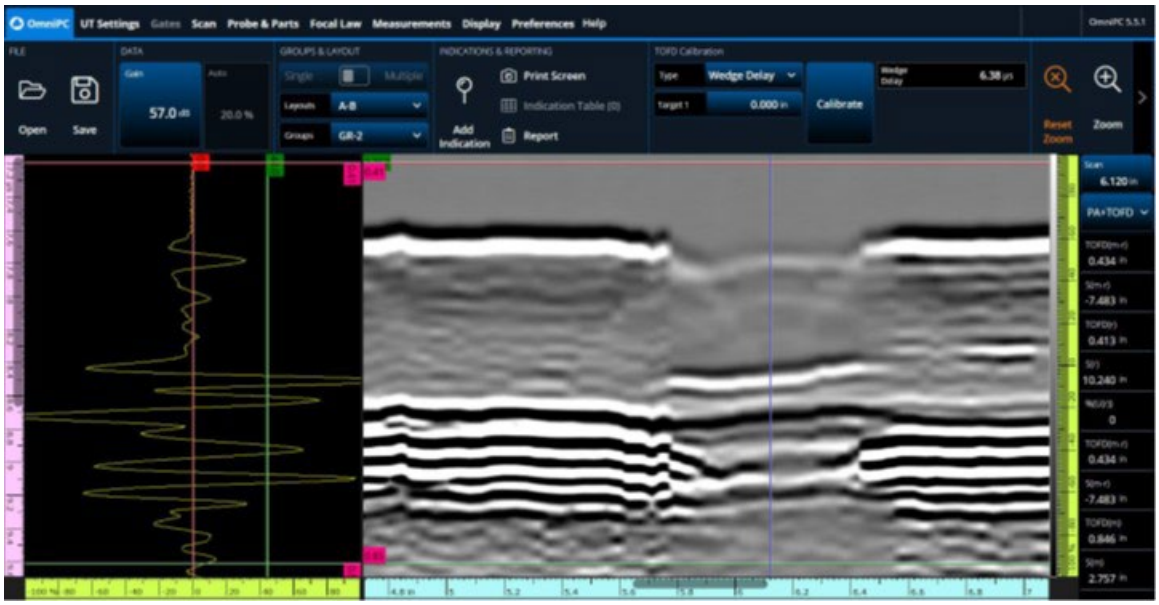

Figure 187. TOFD indication of defect at Location C in test panel TTCI-2

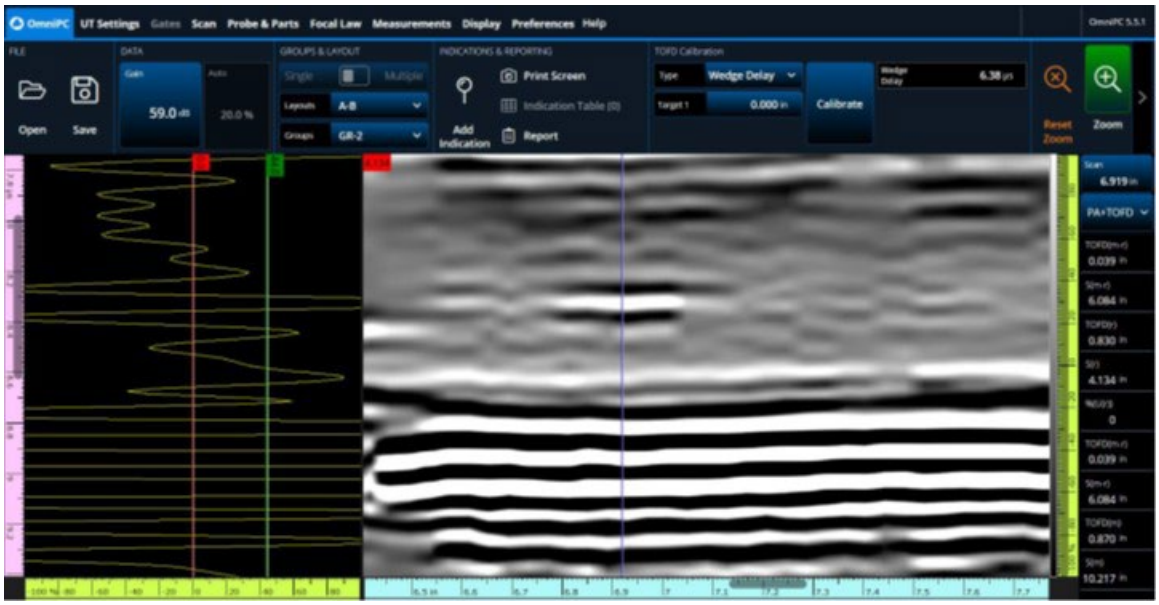

Figure 188. TOFD indication of defect at Location D in test panel TTCI-2

Figure 189. TOFD indication of defect at Location E in test panel TTCI-2

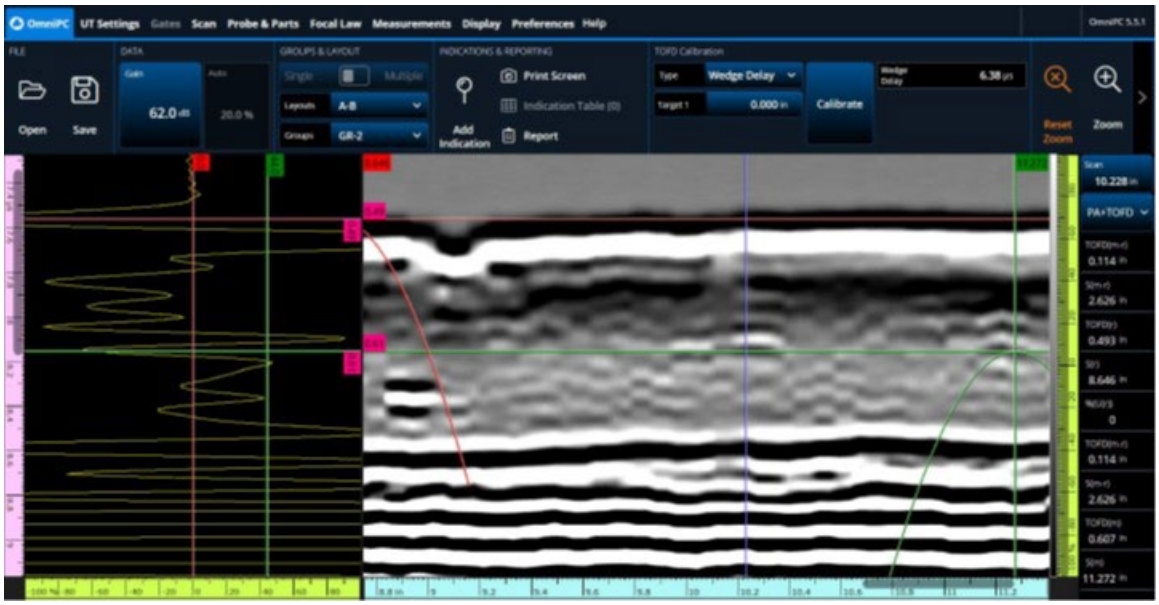

Figure 190. TOFD indication of defect at Location F in test panel TTCI-2

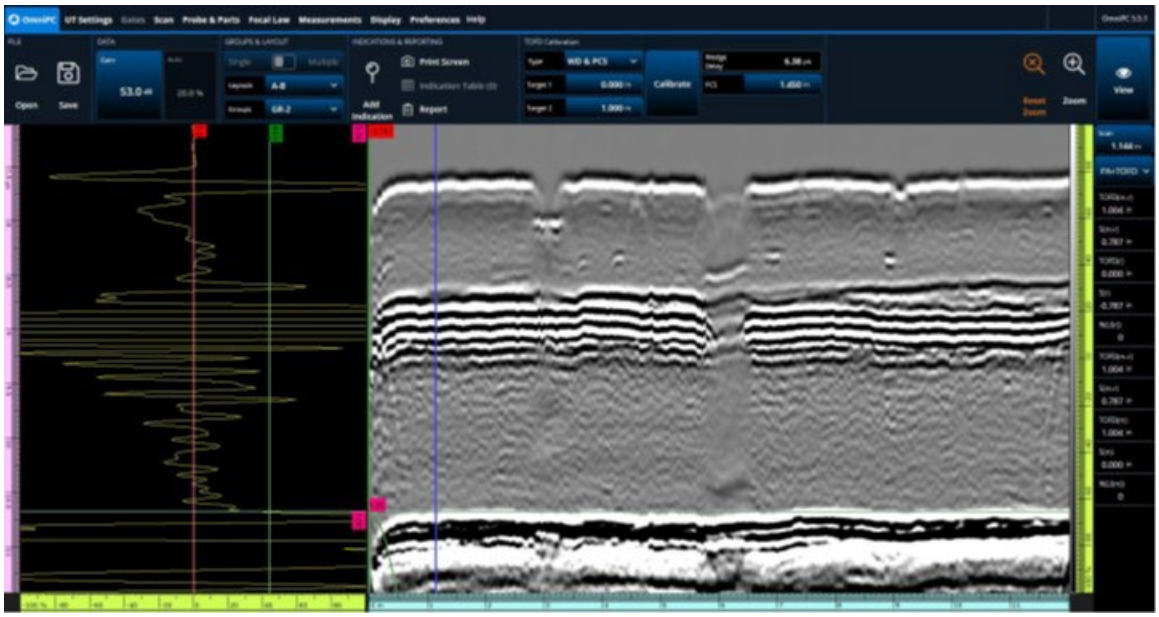

Figure 191. TOFD indication of defect at Location G in test panel TTCI-2

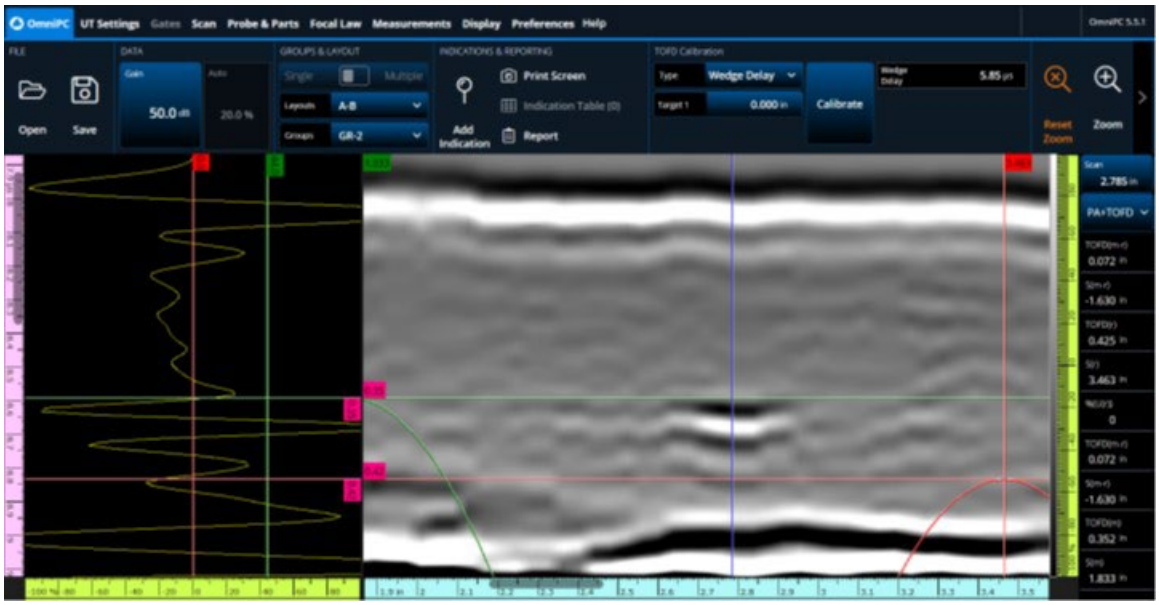

Figure 192. TOFD indication of defect at Location 1 in test panel MG-6

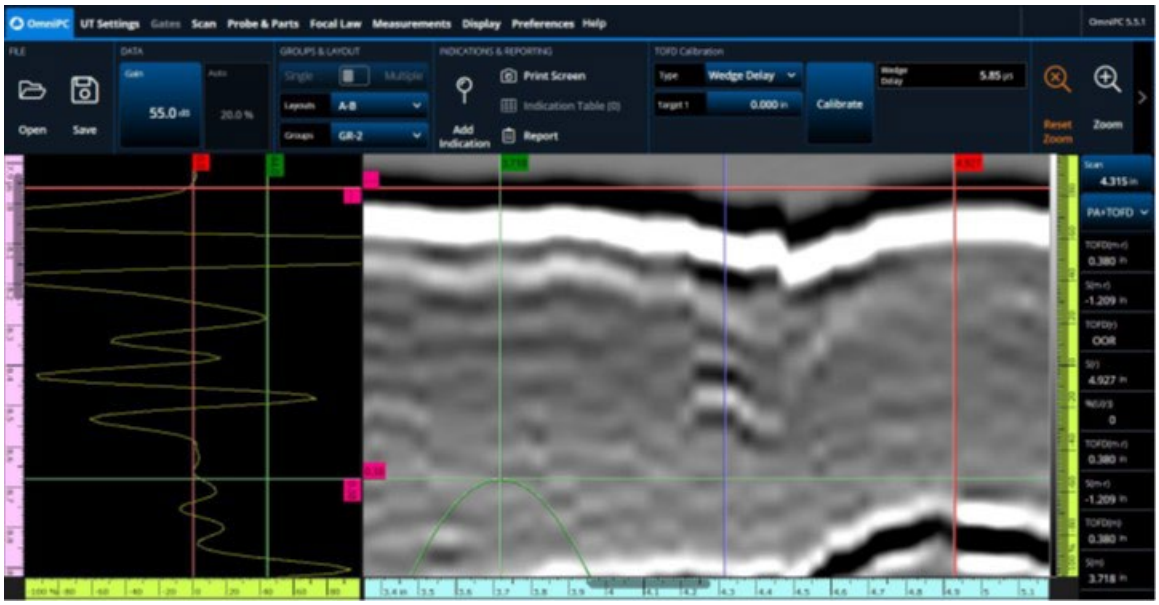

Figure 193. TOFD indication of defect at Location 2 in test panel MG-6

Figure 194. TOFD indication of defect at Location 3 in test panel MG-6

Figure 195. TOFD full scan of the test panel MG-6

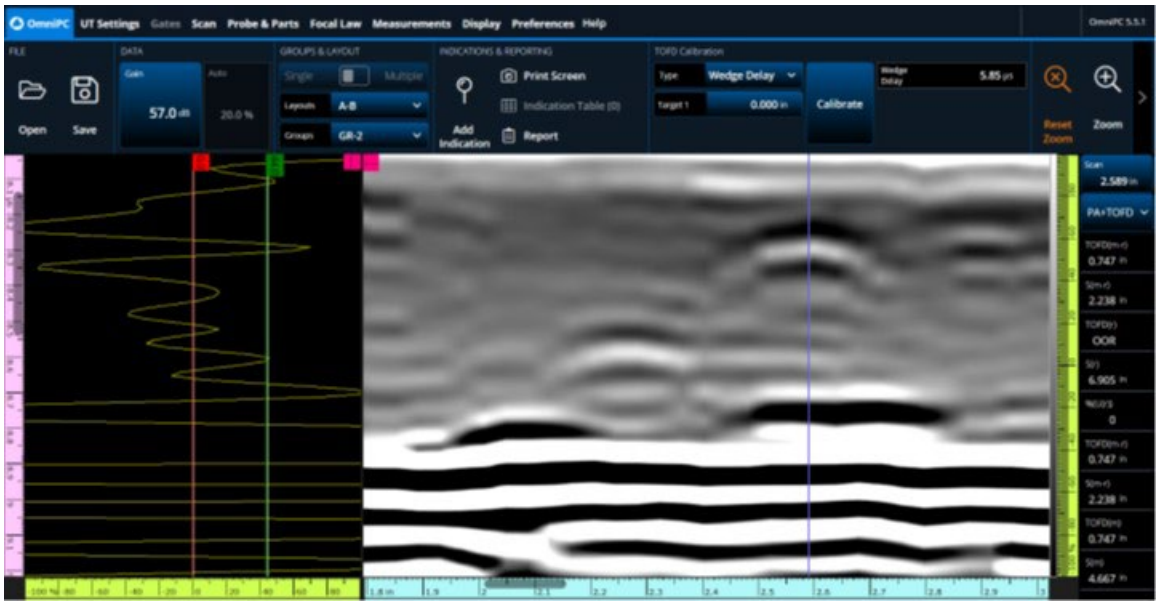

Figure 196. TOFD indication of defect at Location 1 in test panel MG-13

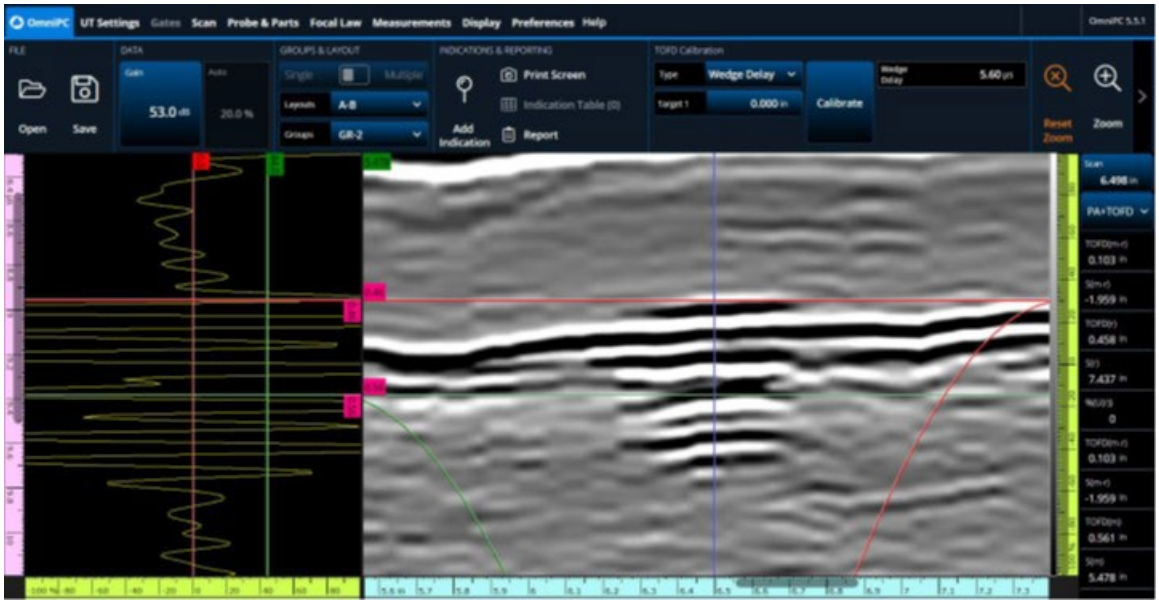

Figure 197. TOFD indication of defect at Location 2 in test panel MG-13

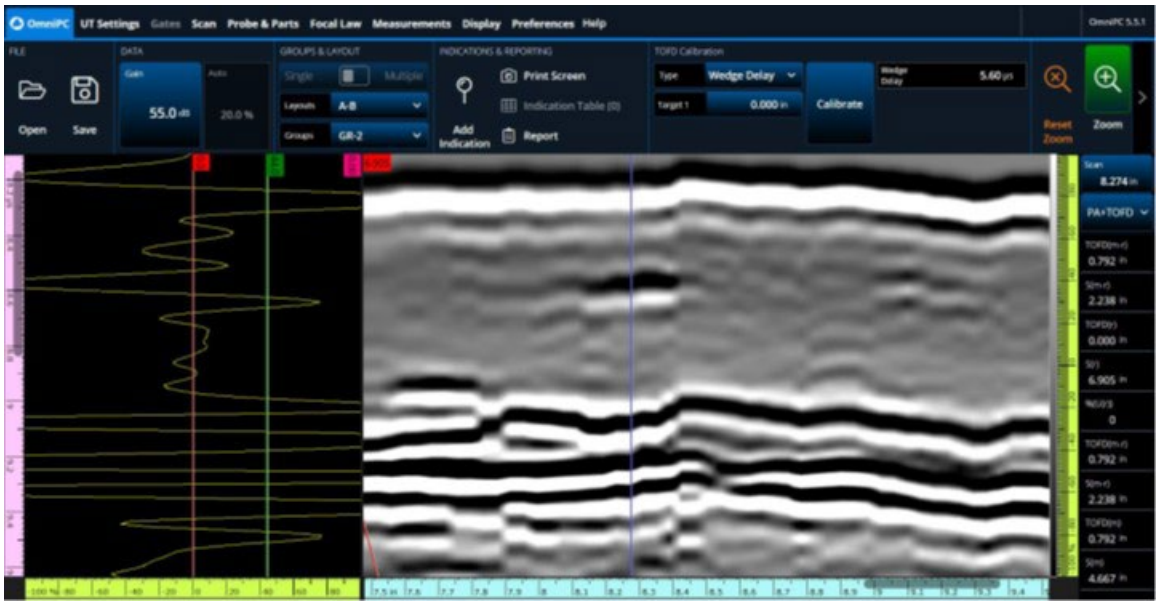

Figure 198. TOFD indication of defect at Location 3 in test panel MG-13

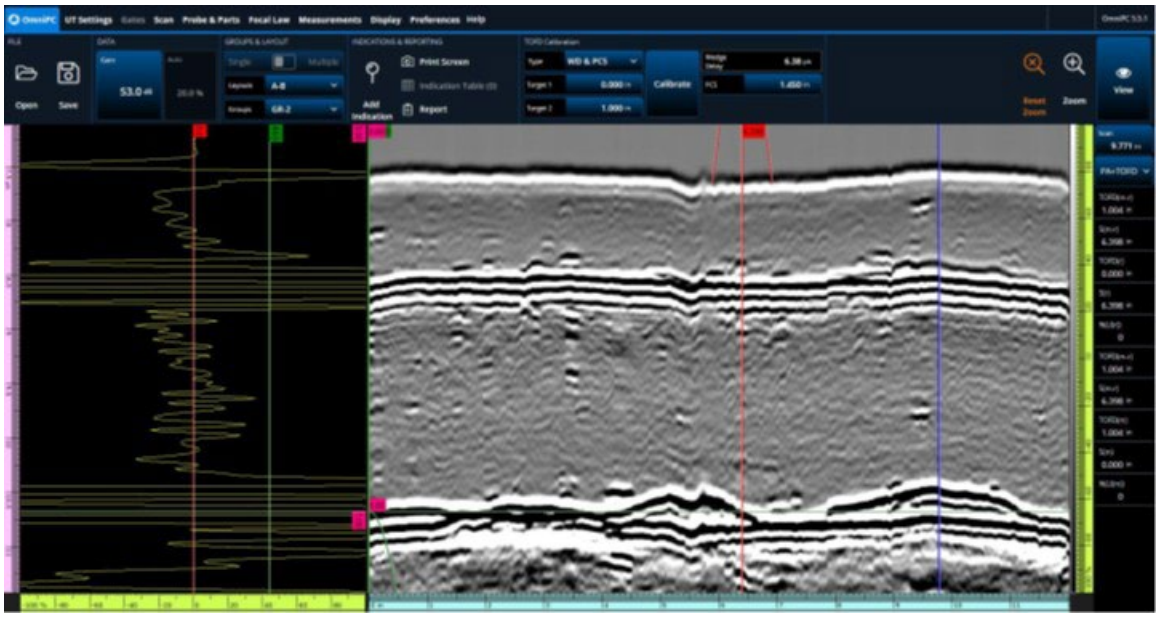

Figure 199. TOFD full scan of the test panel MG-13

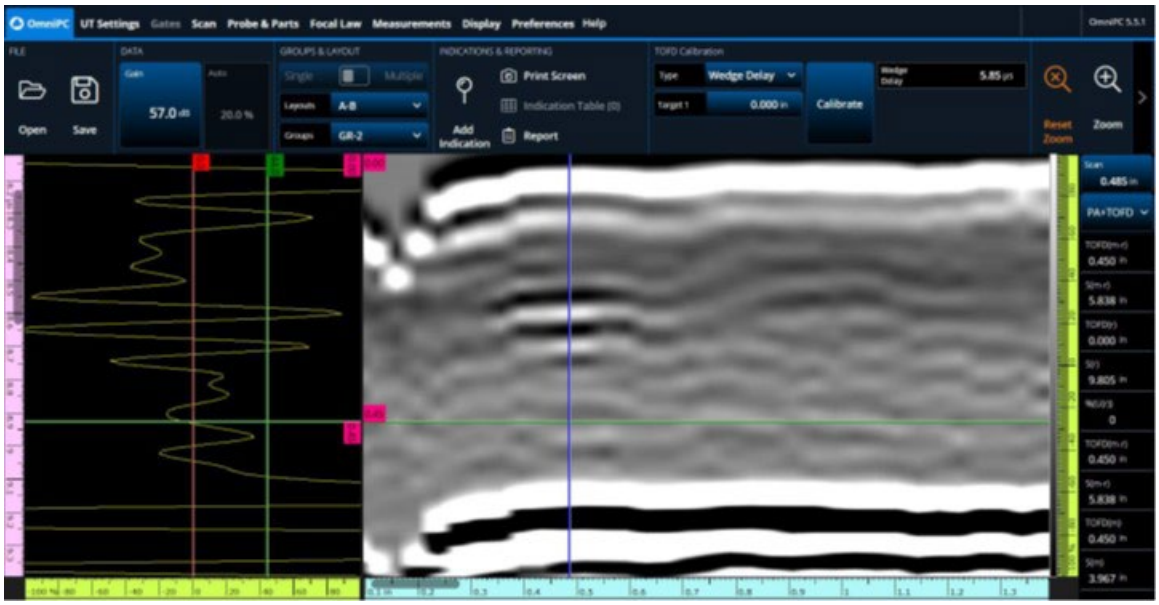

Figure 200. TOFD indication of defect at Location 1 in test panel MG-16

Figure 201. TOFD indication of defect at Location 2 in test panel MG-16

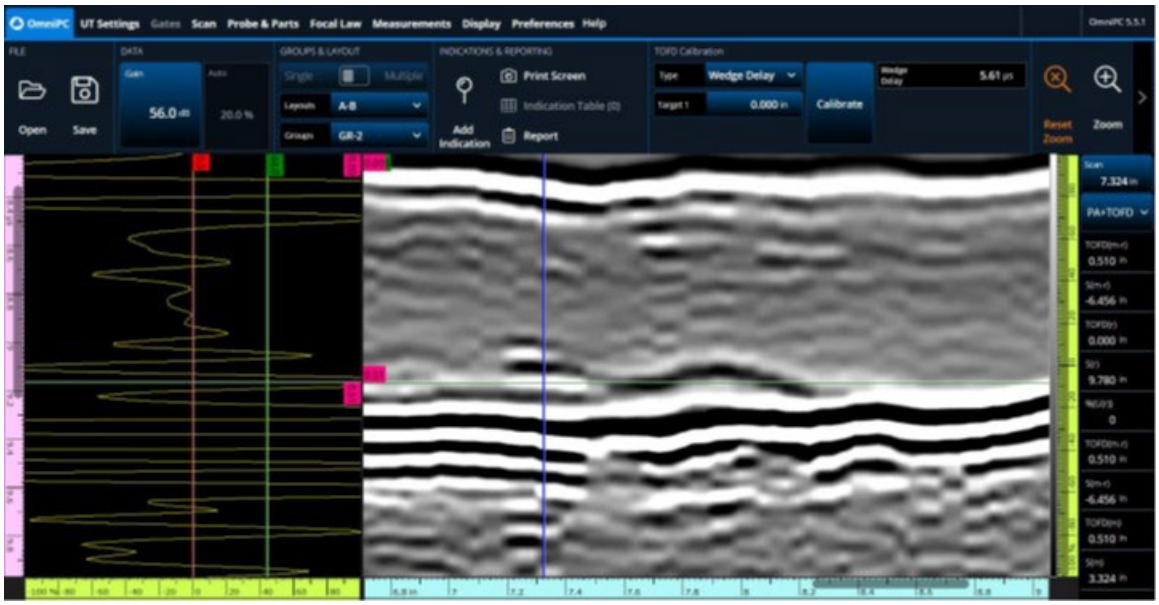

Figure 202. TOFD indication of defect at Location 3 in test panel MG-16

Figure 203. TOFD full scan of the test panel MG-16

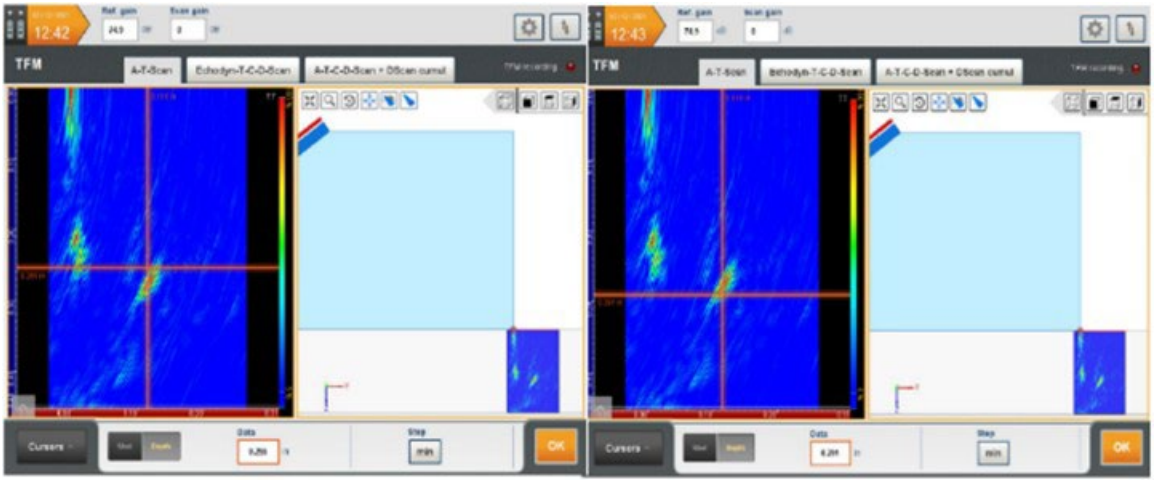

Figure 204. FMC/TFM indication of defect at Location A in test panel TTCI-2

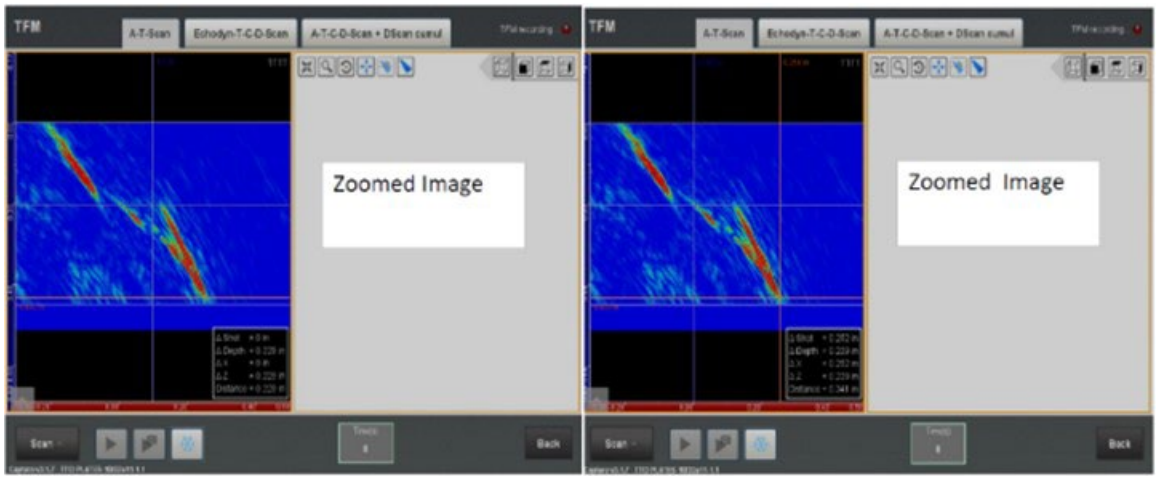

Figure 205. FMC/TFM indication of defect at Location B in test panel TTCI-2

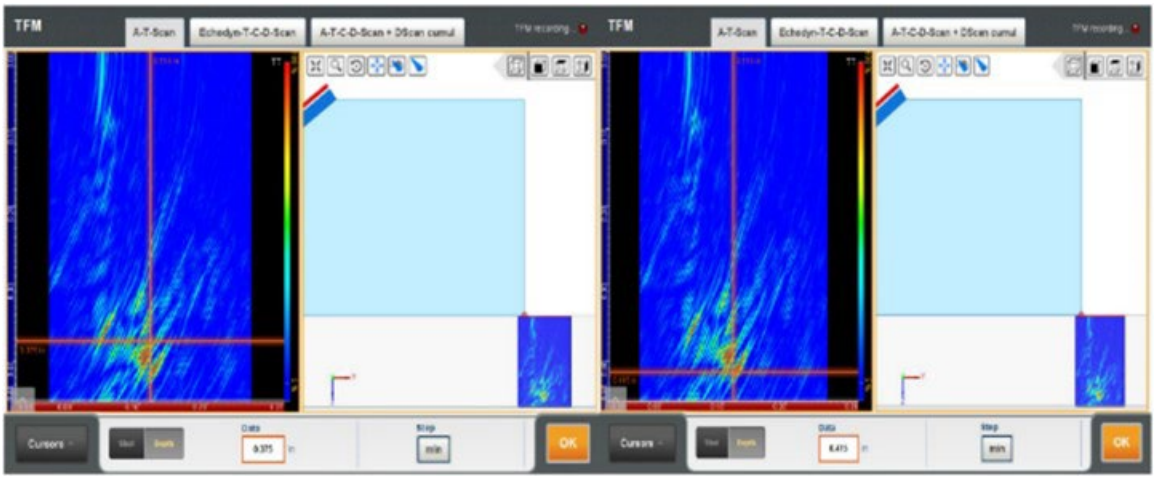

Figure 206. FMC/TFM indication of defect at Location C in test panel TTCI-2

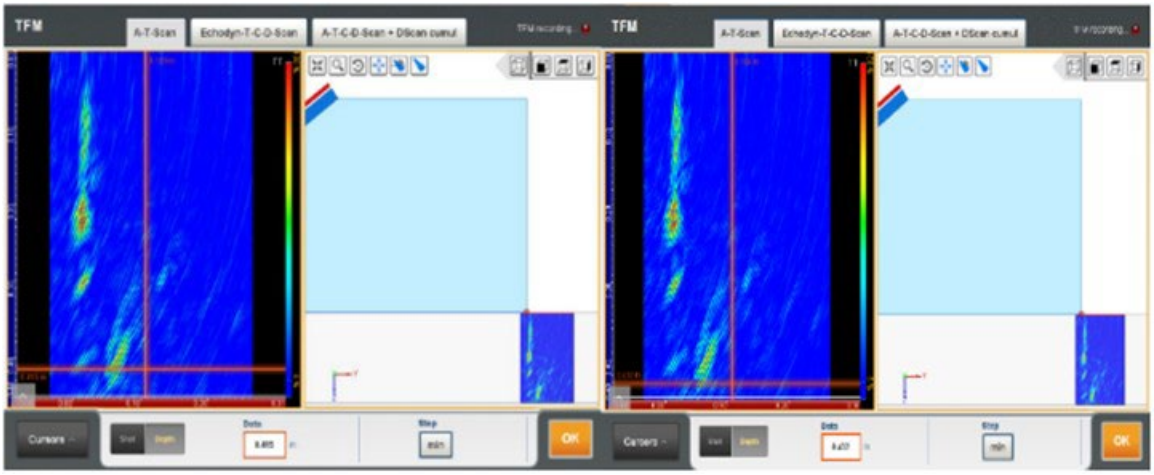

Figure 207. FMC/TFM indication of defect at Location D in test panel TTCI-2

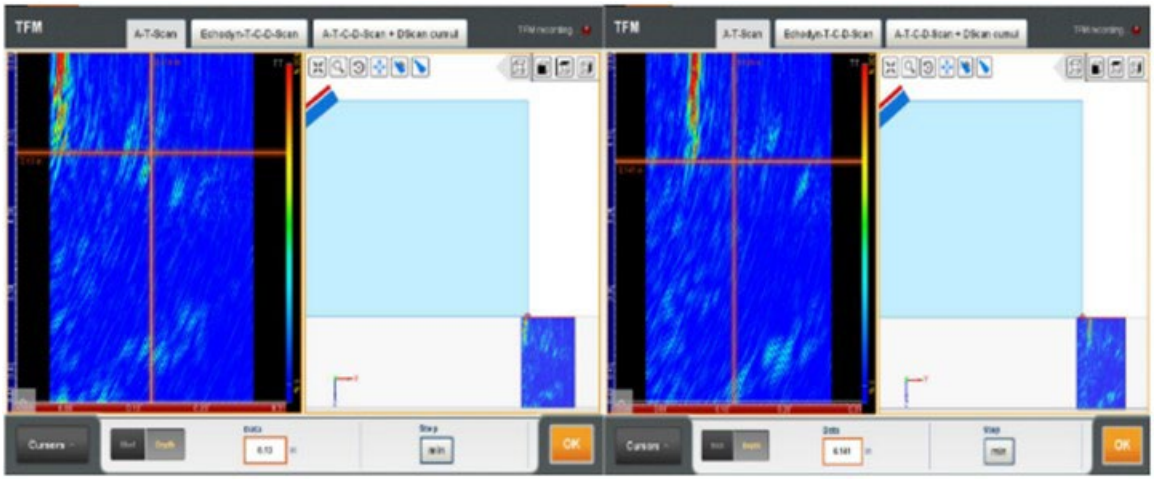

Figure 208. FMC/TFM indication of defect at Location E in test panel TTCI-2

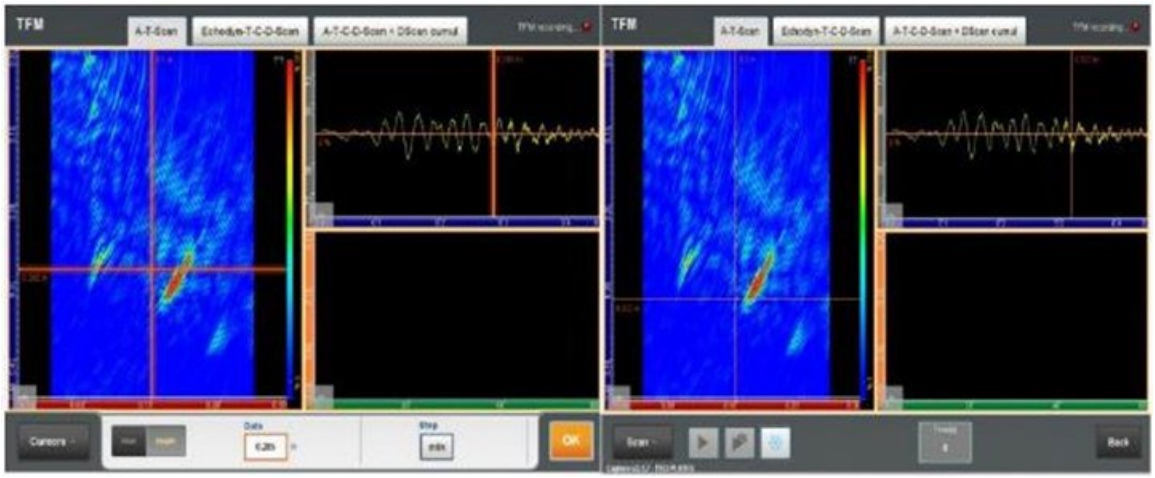

Figure 209. FMC/TFM indication of defect at Location F in test panel TTCI-2

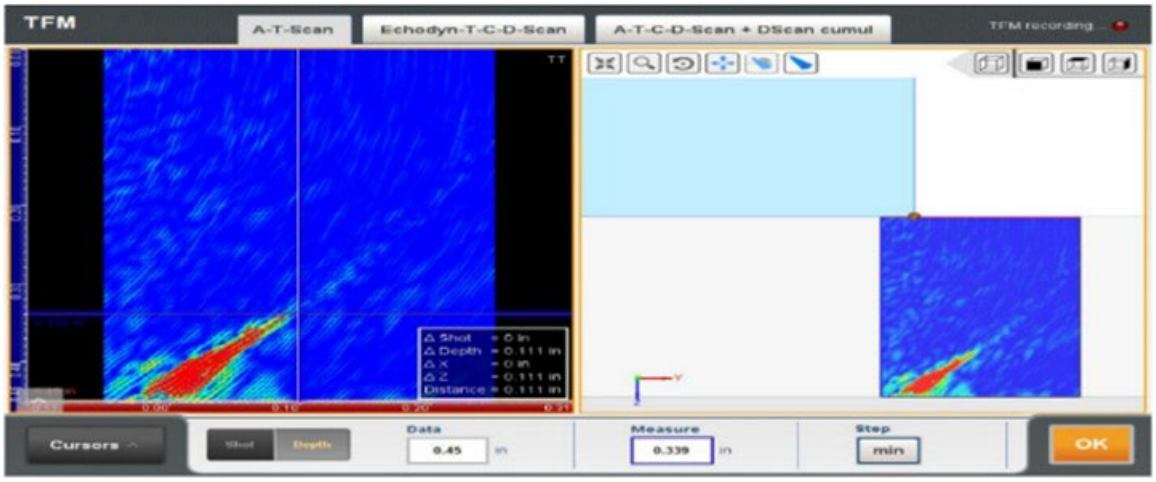

Figure 210. FMC/TFM indication of defect at Location 1 in test panel MG-6

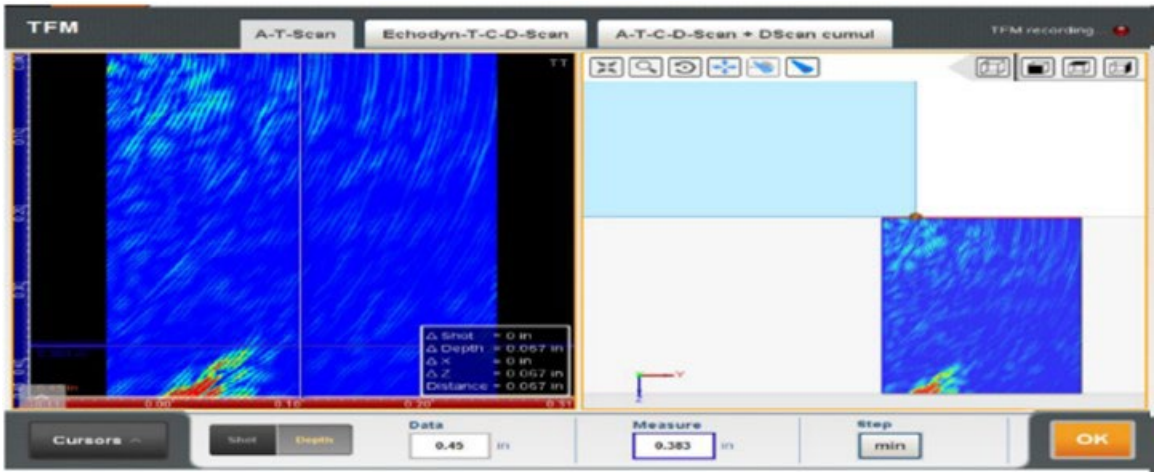

Figure 211. FMC/TFM indication of defect at Location 2 in test panel MG-6

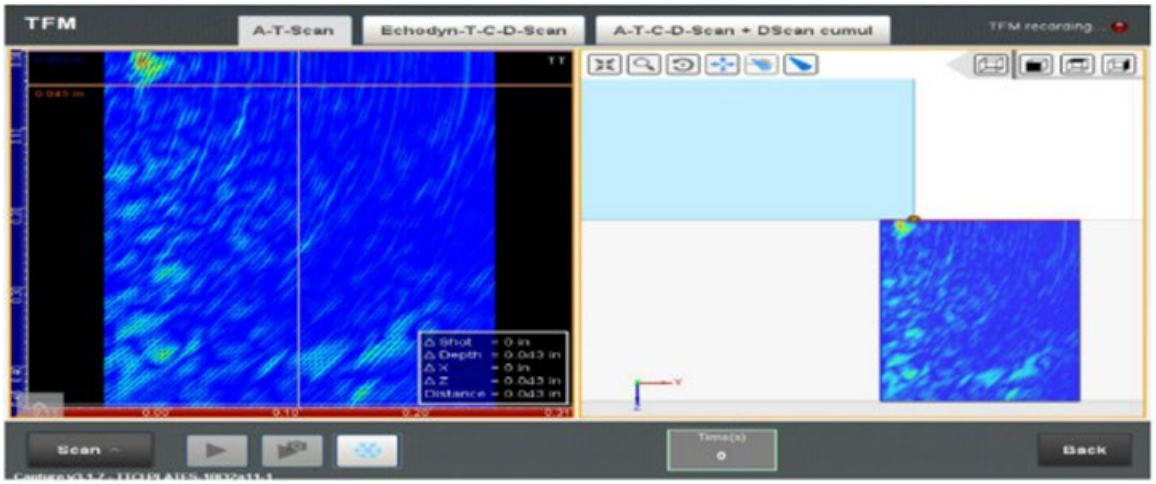

Figure 212. FMC/TFM indication of defect at Location 3 in test panel MG-6

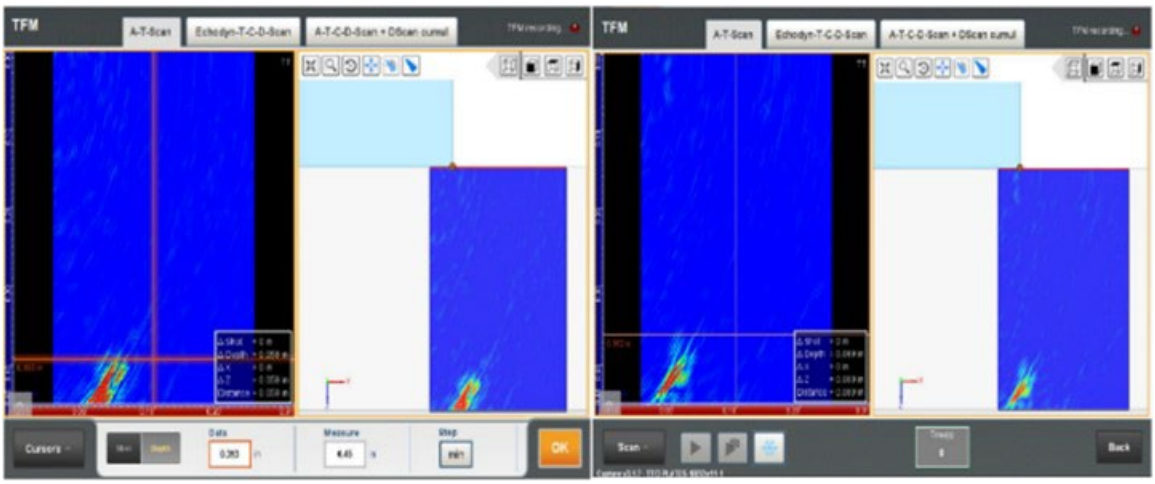

Figure 213. FMC/TFM indication of defect at Location 1 in test panel MG-13

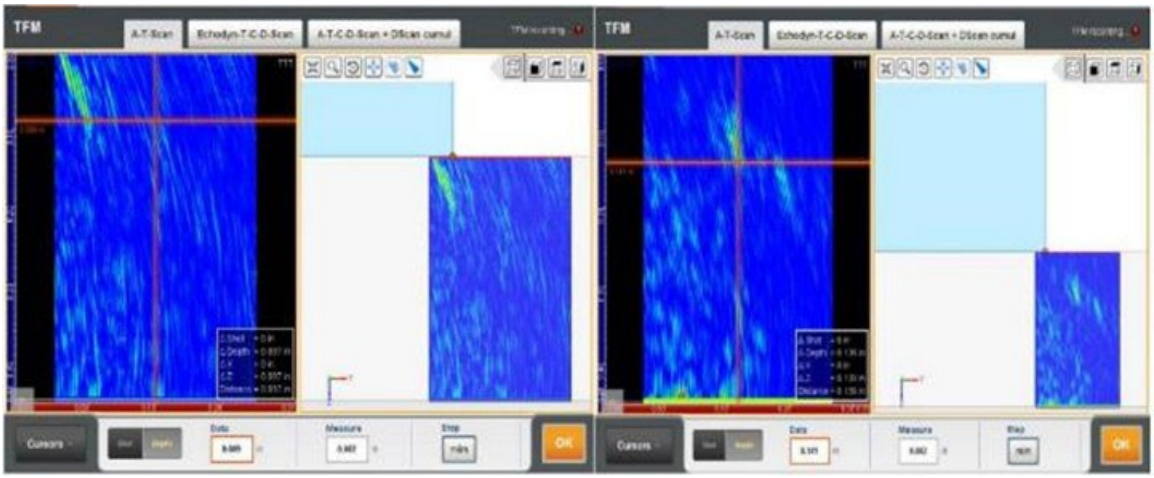

Figure 214. FMC/TFM indication of defect at Location 2 in test panel MG-13

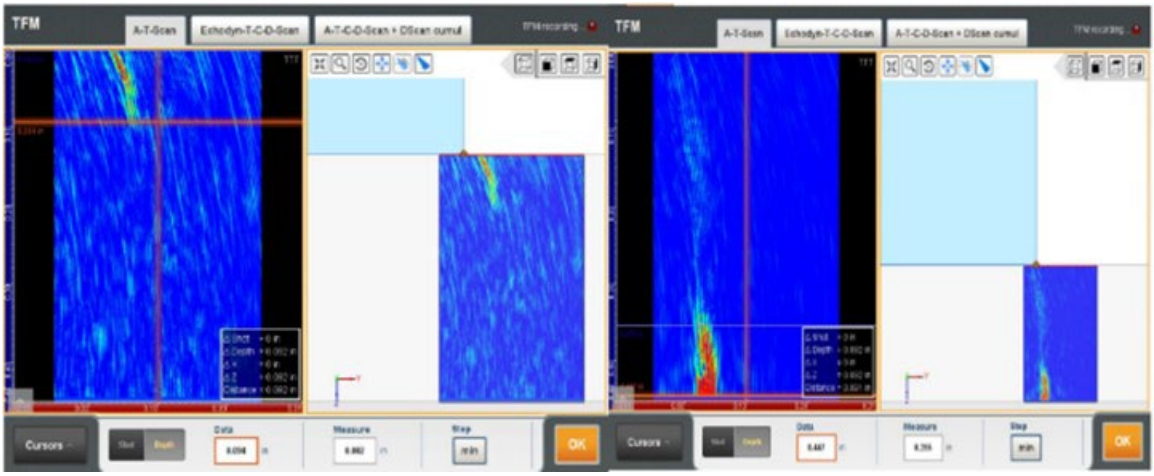

Figure 215. FMC/TFM indication of defect at Location 3 in test panel MG-13

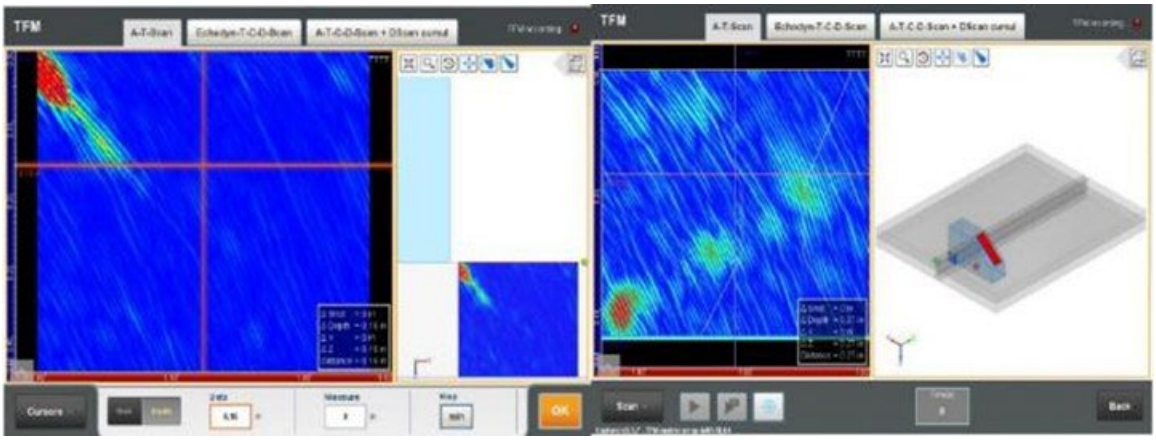

Figure 216. FMC/TFM indication of defect at Location 1 in test panel MG-16

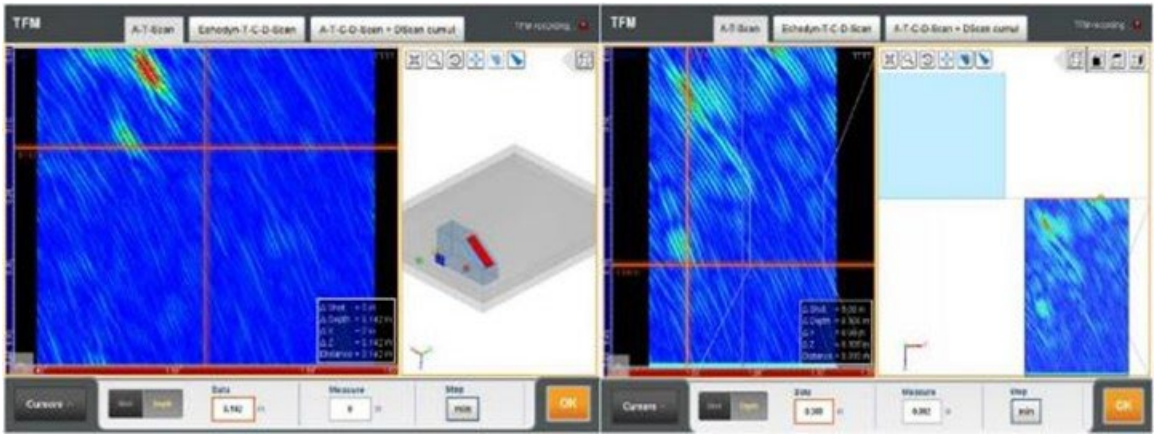

Figure 217. FMC/TFM indication of defect at Location 2 in test panel MG-16

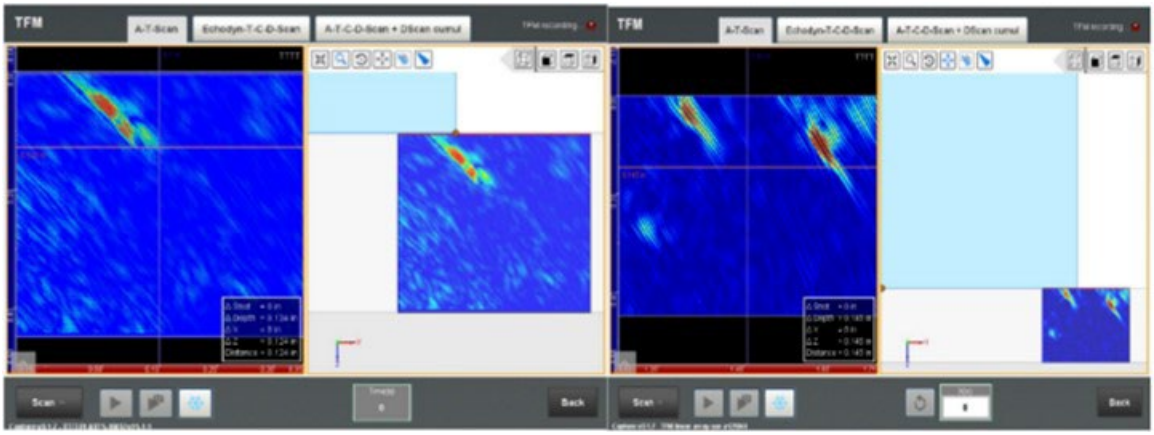

Figure 218. FMC/TFM indication of defect at Location 3 in test panel MG-16

Participant F

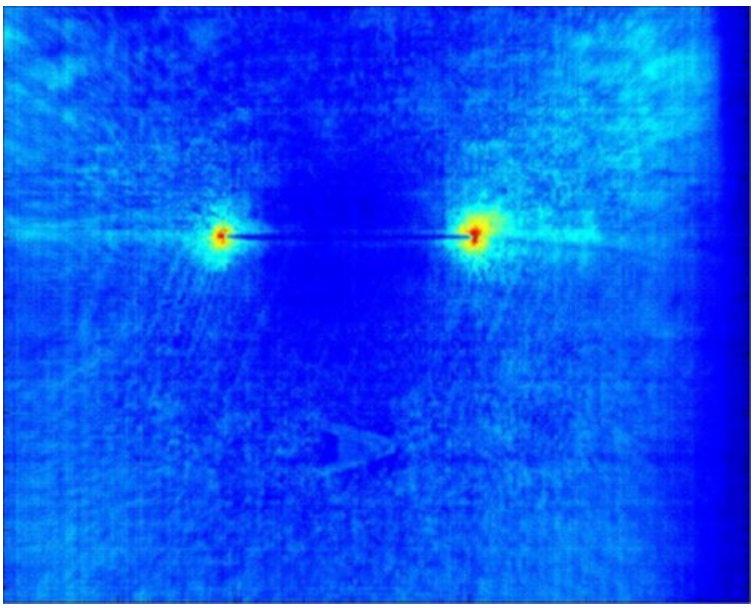

Figure 219. PECT indications of EDM notch 1in test panel TTCI-2

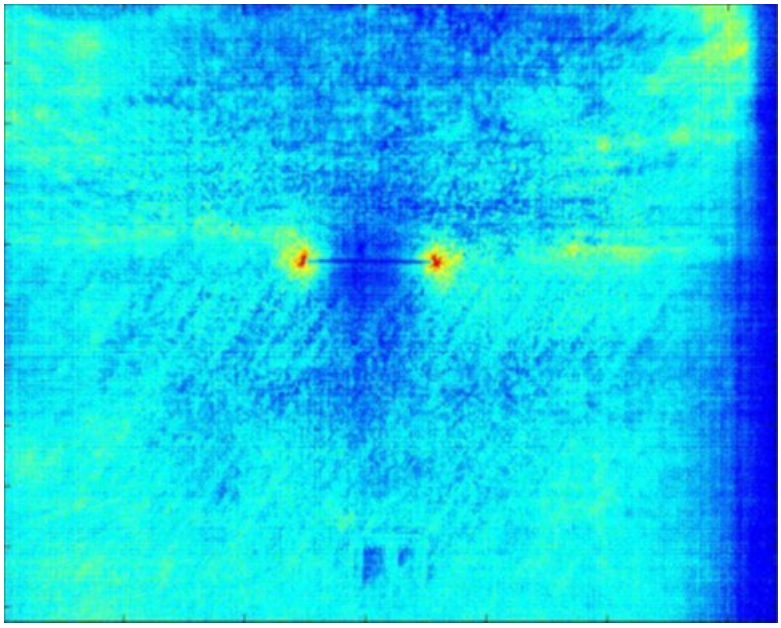

Figure 220. PECT indication of EDM notch 2in test panel TTCI-2

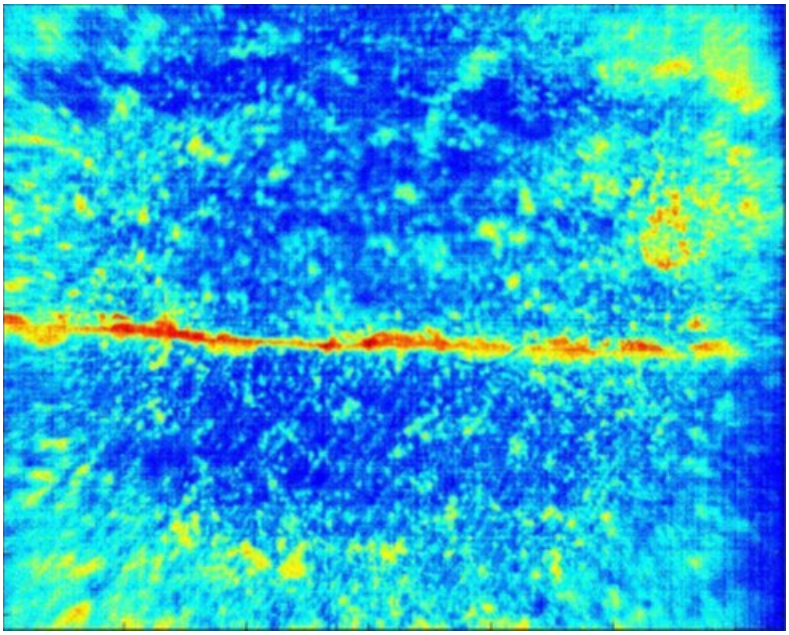

Figure 221. PECT indication of defect at Location 1 in test panel MG-6

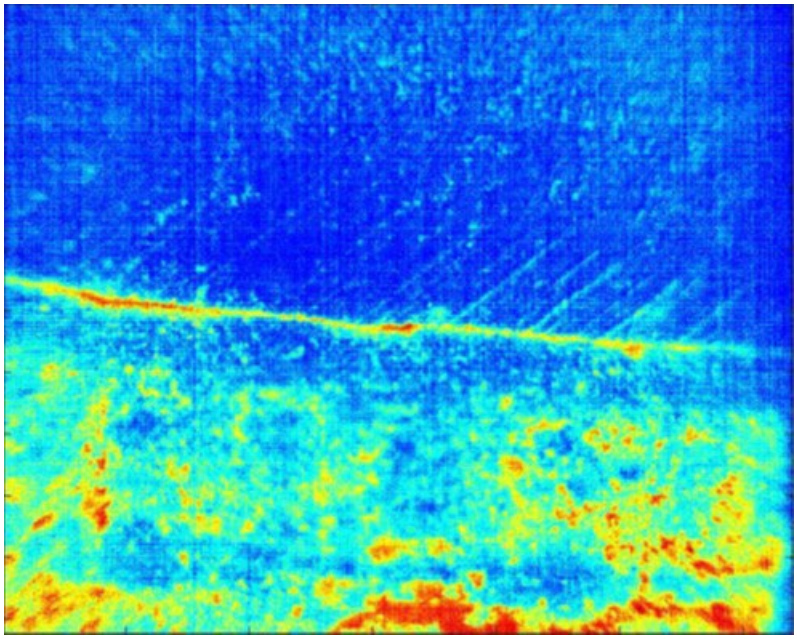

Figure 222. PECT indication of defect at Location 2 in test panel MG-6

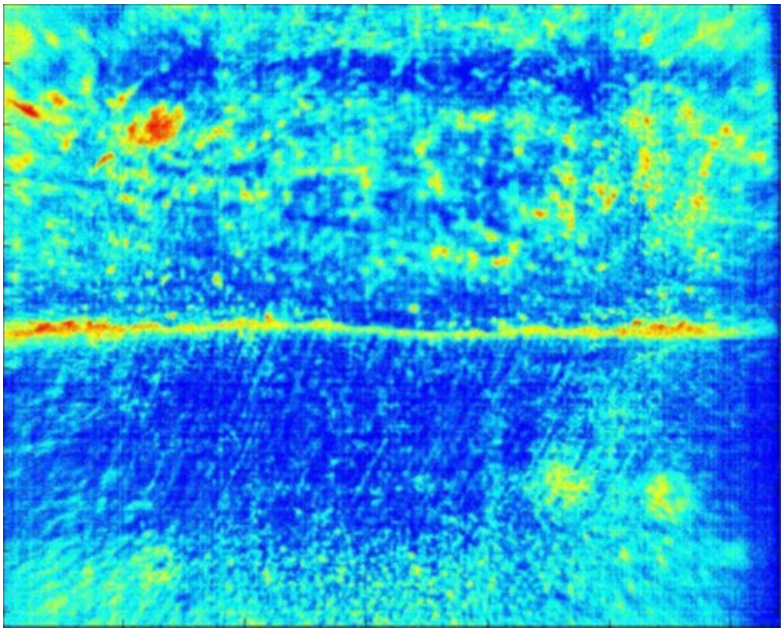

Figure 223. PECT indication of defect at Location 3 in test panel MG-6

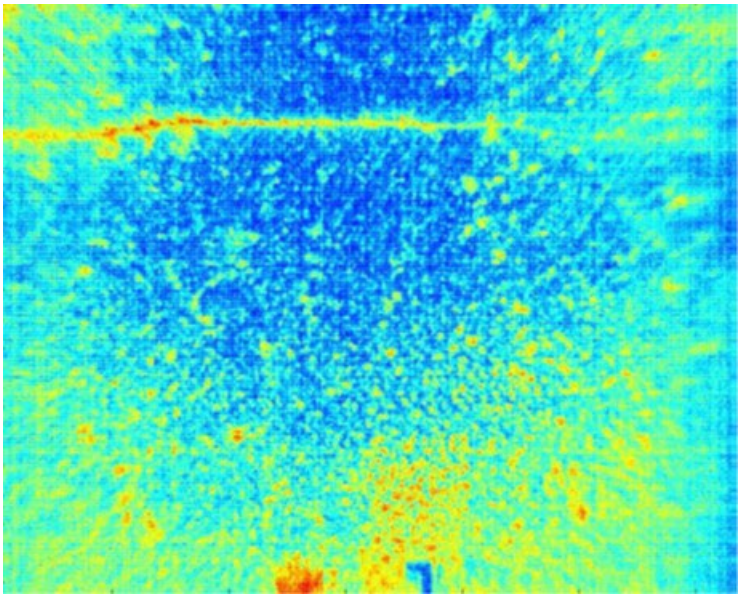

Figure 224. PECT indication of defect at Location 1 in test panel MG-13

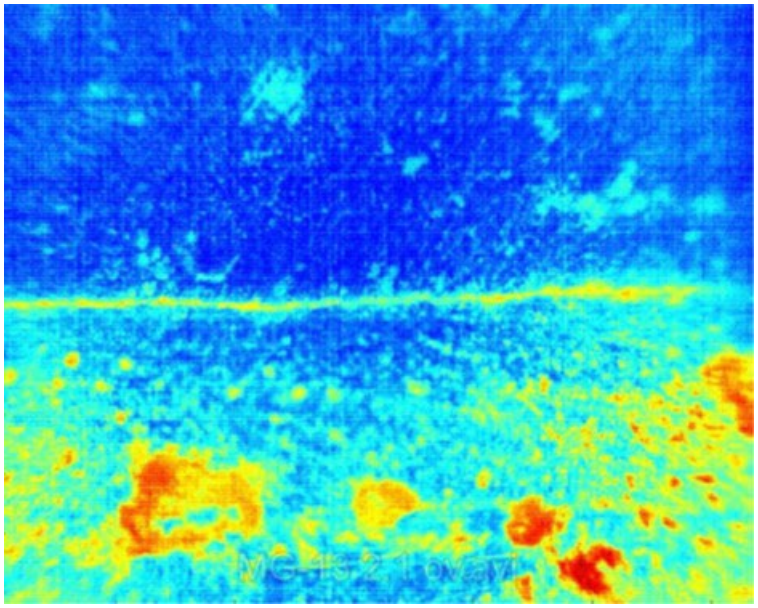

Figure 225. PECT indication of defect at Location 2 in test panel MG-13

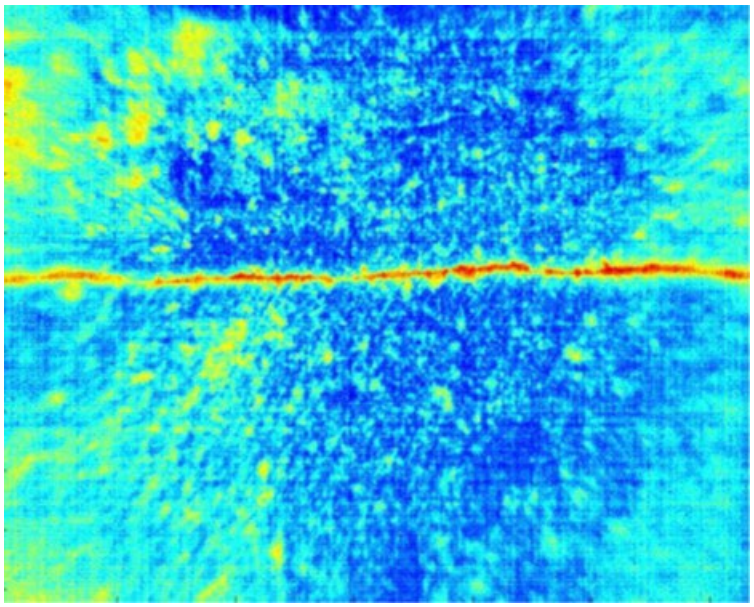

Figure 226. PECT indication of defect at Location 3 in test panel MG-13

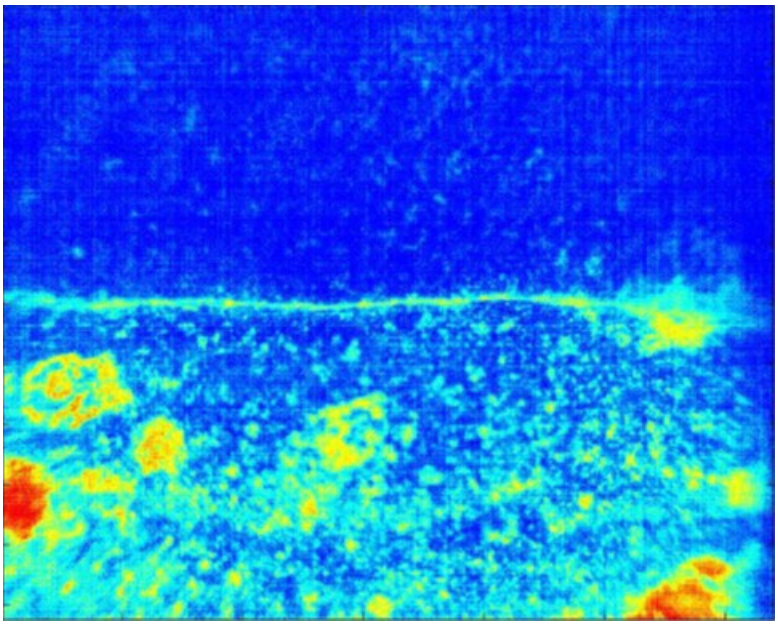

Figure 227. PECT indication of defect at Location 1 in test panel MG-16

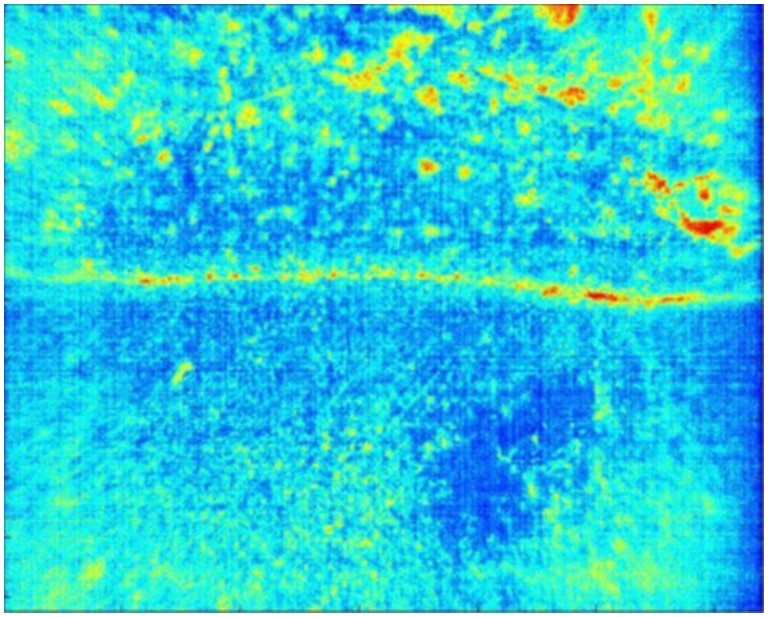

Figure 228. PECT indication of defect at Location 2 in test panel MG-16

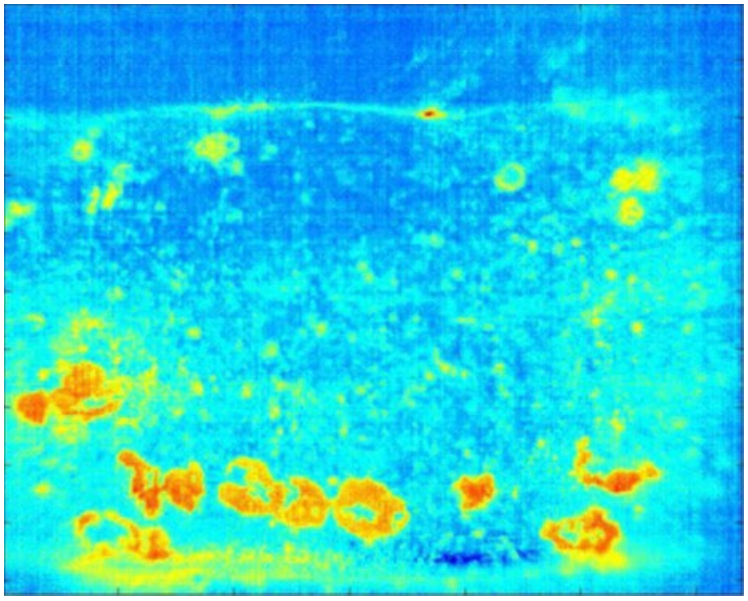

Figure 229. PECT indication of defect at Location 3 in test panel MG-16

Abbreviations and Acronyms

Acronym	Definition
AAR	Association of American Railroads
AC	Alternating Current
ACFM	Alternating Current Field Measurements
AE	Acoustic Emissions
BW	Butt Weld
CFR	Code of Federal Regulation
DC	Direct Current
DOT	Department of Transportation
EC	Eddy Current
ECA	Eddy Current Array
ECT	Eddy Current Thermography
ECTM	Eddy Current Thermography Methods
EDM	Electrical Discharge Machining
ET	Eddy Current Testing
FMC	Full Matrix Capture
FR	Federal Register
FRA	Federal Railroad Administration
GMR	Giant Magneto Resistance/ Resistive
HMR	Hazardous Materials Regulations
LPT	Liquid Penetrant Testing
MG	Master Gauge
MT	Magnetic particle Testing
NDE	Nondestructive Evaluation
NDI	Nondestructive Inspection
NDT	Nondestructive Testing
OEM	Original Equipment Manufacturer

Acronym	Definition
PAUT	Phased Array Ultrasonic Testing
PECA	Pulsed Eddy Current Array
PECT	Pulsed Eddy Current Thermography
POD	Probability of Detection
PT	Liquid Penetrant Testing
QAP	Quality Assurance Program
RT	Radiographic Testing
SAFT	Synthetic Aperture Focus Technique
SNR	Signal-to-Noise-Ratio
TECA	Tangential Eddy Current Array
TFM	Total Focusing Method
TTC	Transportation Technology Center
TTCI	Transportation Technology Center, Inc.
TOFD	Time of Flight Diffraction
USDOT	United States Department of Transportation
UT	Ultrasonic Testing
VT	Visual Testing